GAS-LIQUID PHASE EQUILIBRIA IN THE HYDROGEN-CARBON TETRAFLUORIDE AND HYDROGEN-CHLOROTRIFLUOROMETHANE SYSTEMS AT LOW TEMPERATURES AND 20 - 120 ATMOSPHERES

A THESIS

Presented to

The Faculty of the Graduate Division

by

Ju Fu Shiau

In Partial Fulfillment

of the Requirements for the Degree

Doctor of Philosophy

In the School of Chemical Engineering

Georgia Institute of Technology

September, 1973

GAS-LIQUID PHASE EQUILIBRIA IN THE HYDROGEN-CARBON TETRAFLUORIDE AND HYDROGEN-CHLOROTRIFLUOROMETHANE SYSTEMS AT LOW TEMPERATURES AND 20 - 120 ATMOSPHERES

Approved:

Chairman

Date Approved by Chairman 9/26/73

DEDICATION

To my mother and father

ACKNOWLEDGMENTS

I wish to express my sincere thanks and appreciation to Dr. W. T. Ziegler, my thesis advisor, for his guidance and advice during the course of this work. He helped me to improve my knowledge in thermodynamics and to develop attitudes necessary for a researcher. It was his guidance, his advice and his constant help that made this work possible.

I wish to thank Dr. J. T. Sommerfeld for his interest in this work, and Dr. H. C. Ward and Dr. R. A. Pierotti for serving on the Reading Committee. Their constructive criticisms and valuable suggestions are greatly appreciated. I also wish to thank Dr. G. L. Bridger for providing financial support throughout the period of this work. I am grateful to DuPont Corporation for the fellowship during the summer quarter of 1973.

I wish to thank Dr. B. S. Kirk, who built the equipment, and Dr. Y. K. Yoon, who helped me in learning the operation of the equipment. The suggestions and corrections in my English writing provided by Dr. K. A. Rogers and Dr. M. G. Klett are acknowledged. My appreciation is due Mr. R. Reich, Mr. N. Wei and Mr. R. C. Chu for their friendship and their interest in this work. My appreciation is due the graduate students, Ms. H. W. Tsou and Mr. W. T. Hui for their help in making checks on computer programs and typing the thesis draft. My appreciation is also due Ms. N. H. Price for typing this thesis.

Finally, I wish to thank my parents, my sister and my brothers for their encouragement and continuous love which made the work a reality.

TABLE OF CONTENTS

TABLE OF CONTENTS (Continued)

LIST OF TABLES

LIST OF TABLES (Continued)

LIST OF FIGURES

LIST OF FIGURES (Continued)

LIST OF FIGURES (Continued)

LIST OF FIGURES (Continued)

NOMENCLATURE

A = constant in Equation (VI-21)

$\overset{o}{A}$ = Angstrom unit, 1×10^{-8} cm.

A_o = empirical parameter in the BWR equation.

a = empirical parameter in the BWR equation; also used as Kihara core radius.

a_i = hard sphere diameter for molecule.

a_{12} = average hard sphere diameter.

B = second virial coefficient.

B_{12} = interaction second virial coefficient.

B^*_{CL} = reduced classical second virial coefficient from classical Lennard-Jones (6-12) intermolecular potential function (also written as $B^*_{CL}(T^*)$).

B_K = second virial coefficient calculated from classical Kihara (6-12) intermolecular potential function.

B_o = empirical parameter in the BWR equation.

B^*_o = reduced translational quantum second virial coefficient for an ideal gas.

BWR = Benedict-Webb-Rubin equation of state.

B^*_I, B^*_{II} = first and second reduced translational quantum corrections for the second virial coefficient from the Lennard-Jones (6-12) potential function.

b = empirical parameter in the BWR equation.

b_o = volumetric parameter in the Lennard-Jones (6-12) intermolecular potential function, Equation (IV-22)

$b^{(j)}$ = coefficients for series representation of $B^*_{CL}(T^*)$, Equation (IV-25).

NOMENCLATURE (Continued)

$b_s^{(j)}$ = coefficients for series representation of F_s, Equation (IV-37).

C = third virial coefficient.

$\bar{C}$ = dispersion constant.

C^*_{CL} = reduced classical third virial coefficient from Lennard-Jones (6-12) intermolecular potential function (also written as $C^*_{CL}(T^*)$).

C_o = empirical parameter in BWR equation.

ΔC = non-additivity correction to the third virial coefficient, Equation (IV-54).

C^{add} = classical contribution to the third virial coefficient, Equation (IV-54).

c = empirical parameter in BWR equation.

$c^{(j)}$ = coefficient for series representation of $C^*_{CL}(T^*)$, Equation (IV-61).

d = parameter in correlation of Chueh and Prausnitz; see Equation (IV-65).

$\bar{E}_i$ = partial molar internal energy.

exp = raise 2.71828 to the power to the number in parentheses.

F_1, F_2, F_3 = reduced functions for second virial coefficient from Kihara core model (6-12); Equation (IV-37).

f = fugacity and also used in Equation (IV-64).

$\bar{G}_c$ = partial molar Gibbs free energy for creation of a cavity.

$\bar{G}_i$ = partial molar Gibbs free energy for interaction.

g^o = Gibbs' molar free energy of an ideal gas at one atmosphere pressure.

H = Henry's law constant.

H^o = Henry's law constant at zero polarizability.

NOMENCLATURE (Continued)

ΔH_2^s = molar heat of solution of component 2 at infinite dilution.

H_2^v = molar enthalpy of component 2 in the vapor phase.

$\bar{H}_2^{L^\infty}$ = partial molar enthalpy of component 2 in liquid solution at infinite dilution.

$\bar{H}_c$ = partial molar enthalpy for creation of a cavity.

$\bar{H}_i$ = partial molar enthalpy for interaction.

h = Planck's constant = 6.6256×10^{-27} erg-sec; also used as peak height on chromatogram.

I = ionization potential.

i = summation index integer.

j = summation index integer.

KIH = Kihara core model (6-12).

KIHCK12 = Kihara core model (6-12) with correction applied to the geometric mixing rule using K_{12} calculated from Equation (V-5).

KIHEK12 = Kihara core model (6-12) with correction applied to the geometric mixing rule using experimental K_{12}.

$\bar{K}$ = Henry's law constant using consistency method.

K_i = K value; $K_i = y_i/x_i$.

K_{12} = constant representing the deviation from the Kihara potential geometric mean of the characteristic energy parameters of components i and j; see Equation(IV-51).

K_{LJ} = constant representing the deivation from the Lennard-Jones potential geometric mean of the characteristic energy parameters i and j; see Equation (VI-47).

k = Boltzmann constant = 1.38054×10^{-16} erg/K molecule.

k_i = Reiss function; see Equation (VI-29).

NOMENCLATURE (Continued)

LJCL = Lennard-Jones classical model.

ℓn = natural (base e) logarithm.

log = common (base 10) logarithm.

M = molecular weight.

M_o = core parameter in Kihara (6-12) core model.

m = mass of molecule, M/N_A.

N = a dummy quantity used to represent various equation of state parameters in writing mixture rules.

N_A = Avogadro's number 6.023×10^{23} molecules/gm mole.

n = number of gm moles and also used in the generalized correlation given by Chueh and Prausnitz; see Equation (IV-10).

n_i = number of moles of component i.

P = total absolute pressure.

P_c = critical pressure.

P_{ol} = vapor pressure of condensible component.

R = gas law constant = 82.0560 atm-cc/gm mole K or 0.0820537 atm-liter/gm mole K.

r = intermolecular distance between centers of molecules.

S_o = core parameter in Kihara (6-12) core model.

T = temperature, K (formerly ^oK).

T^* = kT/ϵ.

T_c^o = classical critical temperature at high temperature for quantum gases.

T_c = critical temperature.

NOMENCLATURE (Continued)

T_{Ri} = reduced temperature, T/T_c, of component i.

t = temperature, ^oC.

U = intermolecular potential energy.

U_o = minimum energy of the Kihara potential function.

U_o/k = energy parameter in Kihara (6-12) model.

V = total volume of gas.

V_c^o = classical critical volume at high temperature for the quantum gases.

V_c = critical molar volume.

$\bar{V}_c$ = partial molar volume change upon cavity formation.

$\bar{V}_I$ = partial molar volume change upon charging.

V_m = molar volume of gas mixture.

V_o = core parameter in Kihara core model.

V_{o1} = molar volume of component 1 gas at its vapor pressure.

V_1 = molar volume of component 1 gas.

V_2 = molar volume of component 2 gas.

$\bar{V}_i$ = partial molar volume of component i.

v_1 = molar volume of the compressed liquid phase.

v_{o1} = saturated liquid molar volume of the condensible component.

x = mole fraction in the condensed phase.

y_i = mole fraction of component i in the gas phase.

y_i^o = ideal mole fraction in the gas phase, P_{o1}/P.

Z = compressibility factor, PV/nRT; also U_o/kT in Kihara core model.

NOMENCLATURE (Continued)

GREEK LETTERS

α = parameter in BWR equation.

α_p = coefficient of thermal expansion for the pure component.

β^s = isothermal compressibility for the pure component at saturation.

β_T = isothermal compressibility for the pure component.

Γ = gamma function.

γ = empirical parameter in BWR equation.

γ_i' = activity coefficient of component i in liquid solutions referred to the pure liquid component at the system temperature and pressure.

ϵ = energy parameter in Lennard-Jones (6-12) intermolecular potential function.

ϵ/k = energy parameter in Lennard-Jones (6-12) intermolecular potential function.

Λ^* = translational quantum mechanical parameter.

μ = chemical potential.

μ^o = chemical potential of ideal gas at 1 atmosphere.

μ^* = chemical potential of pure component.

π = pi = 3.14159265.

ρ = distance between molecular cores in the Kihara model.

$\bar{\rho}$ = number density of fluid molecules, N_A / v_{ol}.

ρ_o = shortest distance between molecular cores at minimum potential energy.

ξ = see Equation (VI-21).

σ = length parameter in LJCL (6-12) intermolecular potential.

NOMENCLATURE (Continued)

ω	= Pitzer's acentric factor, Equation (IV-12).
ϕ	= enhancement factor.

SUBSCRIPTS

1	= condensible component.
01	= gas at its normal vapor pressure (i.e. saturated vapor).
2	= hydrogen.
c	= condensible component.
m	= gas mixture.
i, j, k	= 1, 2, or m.
v	= volatile component.

SUPERSCRIPTS

G	= gas.
L	= liquid.
∞	= refer to infinite dilution.
'	= used to distinguish BWR parameters from virial equation parameters; Equation (IV-74).

SUMMARY

The purpose of this work was to determine the experimental gas-liquid phase equilibrium data of the hydrogen-carbon tetrafluoride and the hydrogen-chlorotrifluoromethane systems at low temperatures and pressures up to 120 atmospheres. Two hydrogen binary systems (61, 87) and six helium binary systems (35, 73, 87, 132) have been studied previously in this laboratory. In order to contribute more data for hydrogen binary systems and to extend the limited phase equilibrium data available for binary fluorocarbon systems, the hydrogen-carbon tetrafluoride and the hydrogen-chlorotrifluoromethane systems were selected for study.

A single-pass, continuous flow type, phase equilibrium apparatus designed by Kirk (61), and used by the previous investigators (35, 61, 73, 87, 132), was also used in this work to determine the gas-liquid phase equilibrium compositions.

The gas-liquid phase equilibrium compositions in the hydrogen-carbon tetrafluoride system were measured at six isotherms, 94.94, 105.01, 119.94, 135.01, 149.98, and 164.99 K. In the hydrogen-chlorotrifluoromethane system, seven isotherms of 134.97, 145.02, 160.02, 175.02, 189.97, 205.03 and 219.99 K were studied. Six pressure points from 20 to 120 atmospheres with an interval of 20 atmospheres were measured along each isotherm of the two systems. The uncertainty of the gas phase analysis is believed to be $\pm$ 2.5 percent for the hydrogen-carbon tetrafluoride system and $\pm$ 3.0 percent for the hydrogen-chlorotrifluoro-

methane system. The liquid phase analysis for these two systems is believed to be accurate to ± 2.0 percent of hydrogen. These uncertainties are determined with the consideration of the temperature uncertainty (± 0.03 K), the pressure gauge uncertainty (± 0.5 percent) and the uncertainty of the chromatograph calibration curves.

The gas phase compositions of these systems were described in terms of the enhancement factor $\phi = \frac{Py_1}{P_{o1}}$. An exact thermodynamic expression was derived for the evaluation of the enhancement factor by assuming that the liquid phase was an ideal solution, and using the virial equation of state truncated after the third virial coefficient and the Benedict-Webb-Rubin equation of state to describe the gas phase behavior. For the hydrogen-chlorofluoromethane system, only the virial equation of state was used.

Two theoretical models describing the interaction potential between molecules were used to calculate the second virial coefficient of the virial equation of state. These two models are the Lennard-Jones (6-12) potential and the Kihara core potential. In the calculation of the third virial coefficients, the Lennard-Jones model and the method of Chueh and Prausnitz (16) were used. For the evaluation of $(B_o)_{12}$ in the Benedict-Webb-Rubin equation of state, both the Lorentz and linear averages were used.

The experimental enhancement factors of the two systems of this work were compared with the enhancement factors predicted by the theoretical models. Generally, the Lennard-Jones classical model predicts high values of enhancement factors at low temperatures and shows better agreement with the experimental values at high temperatures. At low

temperatures the Kihara core model represents the experimental data better than any of the other models examined. The Benedict-Webb-Rubin equation of state with $(B_o)_{12}$ computed using the Lorentz average always predicts higher values than that based on the linear average, and also shows better agreement with the experimental values than that based on the linear average. Although none of the theoretical models satisfactorily represent the experimental data over the entire temperature range, the theoretical predictions show the same trends as the experimental data.

The interaction second virial coefficient B_{12} were extracted from the phase equilibrium data. The theoretical B_{12} values were also calculated from the models described in the previous section for comparison. In general, the Kihara model best represents the experimental B_{12} values; this model also represents experimental enhancement factors better than the other theoretical models.

Many investigators (18, 35, 49, 54, 55, 87, 111) have shown that the geometric mixing rule for the energy parameter of the potential function is not adequate for the Kihara model to predict the correct interaction second virial coefficients. The correction factor K_{12} associated with the Kihara energy parameter in the prediction of the B_{12} values was experimentally determined for each of the two systems studied in this work. The K_{12} values found for these two systems were less than 0.02.

The phase equilibrium data for the hydrogen-argon (87), hydrogen-methane (61), hydrogen-ethane (52), and hydrogen-ethylene (51) systems, as well as the hydrogen-carbon tetrafluoride and hydrogen-chlorotri-

fluoromethane systems of this work, are summarized and compared with the corresponding helium binary systems (35, 44, 50, 87, 132) available in the literature. The comparison was made at the same pressure and the same reduced temperature of the condensed components. From this comparison, the helium systems and the hydrogen systems show two similar trends. Thus, 1) at the same reduced temperature of the condensed components, the B_{12} values tend to increase as the molecules of the condensed components become less spherical 2) at the same pressure and the same reduced temperature of the condensed components, the enhancement factors tend to decrease as the molecules of the condensed components become less spherical. Some general differences between the hydrogen systems and the helium systems in the limited experimental temperature and pressure region are: 1) the majority of the B_{12} values of the helium systems fall in the positive region, while all the B_{12} values of the hydrogen systems fall in the negative region, 2) in the liquid-gas region, the composition y_1 of the helium systems at a given temperature always decreases as pressure increases; a minimum of y_1 is shown on the composition isotherm of the hydrogen systems at low temperatures, 3) the enhancement factors of the helium systems are usually less than three at pressure up to 120 atm; the enhancement factors of the hydrogen systems may go up to twenty, 4) a minimum is shown on each enhancement factors isobar for a number of helium systems; the enhancement factors of the hydrogen systems decrease monotonously as temperature increases, 5) at a given temperature the enhancement factor of the hydrogen systems increases more rapidly than those of the helium systems as pressure increases, 6) the correction factors for the geometric

mixing rule of the Kihara potential for the helium systems are larger than those for the hydrogen systems and the K_{12} corrections for the hydrogen systems are usually quite small. Since the different trends between the hydrogen systems and the helium systems also appear in their theoretical models, analyses of the theoretical models were also made in this work.

The phase equilibrium data of the liquid phase of the hydrogen systems and the helium systems are also summarized for comparison, the solubility of hydrogen is always higher than the solubility of helium in the same liquid at the same temperature and pressure. In the comparison of the solubility of hydrogen in various liquid components at the same pressure and the same reduced temperature of the liquid components, it appears that the system which shows larger values of enhancement factor in the gas phase tends to have higher solubility of hydrogen in the liquid phase. But this rule is not followed in the helium systems; the solubility of helium in liquid argon and liquid methane is relatively lower than expected.

By means of a thermodynamic equation derived by Krichevsky-Kasarnovsky (68), the thermodynamic Henry's law constant H_2^{∞}, the partial molar volume $\bar{V}_2^{\infty}$, and the heat of solution ΔH_2^s are determined from the phase equilibrium data. The fugacity of hydrogen in the gas phase was evaluated using the virial equation of state.

The method of Pierotti (92, 93, 94) is used in this work to predict the theoretical values of H_2^{∞}, $\bar{V}_2^{\infty}$, ΔH_2^s for the hydrogen-carbon tetrafluoride and the hydrogen-chlorotrifluoromethane systems. The phase equilibrium data of the corresponding helium systems obtained by

Yoon (132) are used in this work to extract the parameters required for this calculation. For the hydrogen-carbon tetrafluoride system, the method of Pierotti (92, 93, 94) predicts H_2^∞ values which are too low by a factor of 4 at low temperatures; the prediction shows better agreement with experiment at higher temperatures. For the hydrogen-chlorotrifluoromethane system, the predicted H_2^∞ values are about 10 percent lower than the experimental values.

Pierotti (92) has suggested that the prediction may be considered to be satisfactory, if the predicted H_2^∞ is within a factor of two of the observed H_2^∞. Pierotti (92) has also suggested that the agreement between the experimental and theoretical H_2^∞ values might be improved by using a correction to the geometric mixing rule for the interaction energy.

The disagreement between the predicted and experimental H_2^∞ for the hydrogen-carbon tetrafluoride system may also be caused by the uncertainty of the LJCL parameters used in this calculation and the method of obtaining the a_1 values.

CHAPTER I

INTRODUCTION

From a technical viewpoint, all separation processes in chemical engineering are dependent upon the principles of phase equilibria, while from a theoretical point of view, the phase equilibrium behavior of a system is characterized by the properties of its components. The efforts of phase equilibrium studies have always been to generalize the phenomenon of phase equilibrium and to establish relations between theoretical predictions and technical applications by means of experimental values. Whenever a theoretical model is developed, extensive experimental data are needed to demonstrate the validity of the developed model and prove the utility for technical applications.

The purpose of this study was to examine the behavior of binary systems at low temperatures and high pressures, mainly, the experimental work was to test the theoretical equations developed from thermodynamic relations for prediction of gas-liquid equilibria for binary systems. It was also desired to study the relation between the behavior of binary systems and the molecular species involved. The character of the systems studied in this work is that one component, referred to as component 1 in this study, is below its critical temperature, the other component, referred to as component 2, is well above its critical temperature. The liquid mixture is always assumed to be an ideal solution.

A single pass, continuous-flow phase equilibrium apparatus designed by Kirk (61) and used by Kirk (61), Mullins (87), Liu (73), Garber (35) and Yoon (132) was used in this investigation to experimentally determine phase equilibrium compositions.

The construction and operation of this apparatus was described in detail by Kirk (61), Kirk and Ziegler (62) and will be briefly described in the following chapter. Binary systems with helium as component 2 previously studied in this laboratory are helium-argon by Mullins (87), helium-carbon dioxide by Liu (73), helium-ethylene and helium-propylene by Garber (35), helium-carbon tetrafluoride and helium-chlorotrifluoromethane by Yoon (132). Those with hydrogen as component 2 which have been previously studied are hydrogen-methane by Kirk (61) and hydrogen-argon by Mullins (87). In order to contribute more data for hydrogen systems for the purpose of comparison with helium systems, and to extend the limited available phase equilibrium data for binary fluorocarbon systems, the hydrogen-carbon tetrafluoride and hydrogen chlorotrifluoromethane systems were selected for this study.

From a thermodynamic point of view, it is required that the chemical potential of each component in each phase must be the same for a system at equilibrium. For a two-phase binary system, the following two relations must be met:

$$\mu_1^L(x_1, P, T) = \mu_1^G(y_1, P, T)$$

$$\mu_2^L(x_2, P, T) = \mu_2^G(y_2, P, T)$$

From the phase rule, the number of degrees of freedom is two for

a two phase binary system in equilibrium. If the temperature and pressure of a system are fixed, all the intensive properties of the system are fixed. Then the compositions of two phases could be theoretically obtained by solving the following two independent equations simultaneously at the given temperature and pressure.

$$\mu_1^L(x_1) = \mu_1^G(y_1)$$

$$\mu_2^L(x_2) = \mu_2^G(y_2)$$

Since some theoretical parameters in these equations are not available, experimental liquid and vapor compositions obtained from this work were used to extract those parameters.

Based on the criterion that the chemical potential of component 1 must be equal in both phases, exact thermodynamic expressions for the enhancement factor in terms of measurable quantities have been derived by Dokoupil et al. (27), Kirk (61), Kirk and Ziegler (62), Kirk et al. (63), Mullins (87), Liu (73), Garber (35), Smith et al. (116), Prausnitz et al. (97), Prausnitz and Chueh (96), Chiu and Canfield (15), Heck (43), and Yoon (132). The enhancement factor is defined as the ratio of the actual mole fraction to the ideal mole fraction of component 1 in the gas phase at the system pressure and temperature. The ideal mole fraction of component 1 in the gas phase is P_{o1}/P, where P_{o1} is the vapor pressure of component 1 and P is the total pressure of the system. Thus, the enhancement factor is $\phi = Py_1/P_{o1}$. The enhancement factor has long been used by many investigators to describe the composition of the gas phase and to indicate the nonideality of a gas mixture.

To express the enhancement factor explicitly in terms of measurable quantities, one must have an adequate equation of state to represent the behavior of the gases involved. The equation of state for an ideal gas was derived from kinetic theory based on the assumptions that the volume of the molecules is negligible and the interaction force between molecules is zero. Actually, all gases can be converted into liquid and eventually solidified to a finite volume, thus the two assumptions above are not acceptable for real gases.

The van der Waals equation was the first to include considerations of the volume and interaction force of the molecules. But the over-simplified form of van der Waals equation limited its use for practical applications and it is chiefly of theoretical interest. A good summary of equations of state for cryogenic purposes has been presented by Tsonopoulos and Prausnitz (124). Those equations are the virial equation of state (107), Beattie-Bridgeman equation (3), Benedict-Webb-Rubin equation (5,6,7), Strobridge equation (120), Hirschfelder-Buehler-McGee-Sutton equation (47), Martin-Hou equation (76), Redlich-Kwong equation (103). Among those equations, the virial equation of state is particularly important due to its firm theoretical foundation and was selected for use in this investigation. The Benedict-Webb-Rubin equation was also selected for use, because it represents a wider range of density for both gas and liquid phases, and the mixture rules for this equation are fully developed.

The virial equation of state, which was originally proposed as an empirical equation, was later derived from statistical mechanics (23, 48). It has been possible to show by statistical mechanics (78)

or the kinetic theory (25) of gases that the virial coefficients of the equation are related to intermolecular potential functions describing the force between molecules. If a model of the intermolecular potential is defined, the second and third virial coefficients can be described exactly by two and three body interactions of the intermolecular potential. Due to the limited knowledge of higher virial coefficients, the virial equation of state is limited to use at moderate densities.

Two intermolecular potential functions are used in this work to calculate the second virial coefficients, the Lennard-Jones model which describes the intermolecular potential between compressible spheres and the Kihara model which describes the intermolecular potential between molecules with impenetrable cores. The third virial coefficients used in this work are calculated from the Lennard-Jones model or from the semi-empirical equation derived by Chueh and Prausnitz (16). For a gas mixture, the mixture virial coefficients are expressed in terms of mole fractions, and pure and interaction virial coefficients as were given by Mayer (77).

Mullins (87), Hiza (49), Chueh and Prausnitz (16) and Hiza and Duncan (50) found that the interaction second virial coefficients calculated from the Kihara model do not agree with experiment for many helium systems. They also demonstrated that the introduction of a correction term $(1-K_{12})$ to the geometric mixing rule for the Kihara energy parameter would give a better fit between the theoretical and the experimental interaction second virial coefficients for the helium systems. Hiza and Duncan (50) and Hiza, Heck and Kidnay (51, 52) demonstrated that such a correction for hydrogen binary systems is

usually quite small. The correction term $(1-K_{12})$ for the mixing rule of the Kihara energy parameters are also experimentally determined for the two systems studied.

Based on the thermodynamic criterion for phase equilibrium, that is, the chemical potential of component 2 must be the same for both phases, the Krichevsky and Kasarnovsky equation (68) was derived (35, 132). From the Krichevsky and Kasarnovsky equation, the thermodynamic Henry's law constant and partial molar volume were extracted by using the experimental phase equilibrium data obtained in this work. Because of the complex nature of liquid mixtures, many theories (46, 92, 101, 105, 118) have been developed from various points of view to correlate gas solubility data. Pierotti's method (92, 93, 94) which is based on the scaled particle theory was used in this work to predict the theoretical Henry's law constants, partial molar volumes at infinite dilution, and heat of solution of the two systems studied.

A summary of binary systems studied by others has been given by Hiza (49). Many helium binary systems were summarized and analyzed by Liu (73), Garber (35), and Yoon (132). They concluded that most helium systems have enhancement factors less than three and the enhancement factors show a minimum on each isobar. The hydrogen systems including hydrogen-methane by Kirk (61), hydrogen-argon by Mullins (87), hydrogen-ethane by Hiza, Heck and Kidnay (52), hydrogen-ethylene by Hiza, Heck and Kidnay (51), hydrogen-carbon tetrafluoride and hydrogen-chlorotrifluoromethane obtained in this work are summarized for comparison.

CHAPTER II

EXPERIMENTAL APPARATUS

Description of Apparatus

In general, three types of apparatus are used to determine phase equilibrium compositions: the static apparatus, the closed circulation apparatus and the flow-type apparatus.

A single-pass flow type apparatus designed by Kirk (61), shown schematically in Figure 1, was used in this investigation to measure the phase equilibrium compositions. This apparatus has been described in detail by Kirk and Ziegler (62), and also by Mullins (87), Liu (73), Garber (35) and Yoon (132). The apparatus is designed mainly for phase equilibrium measurements at temperatures between 65 K and room temperature and pressures up to 120 atm. The limiting factors of selecting a proper range for a system to be studied are the sensitivity of the gas chromatographs and the evaporation rate of the condensed phase.

The basic concept of phase equilibria requires that all intensive properties of a system be fixed. A cryostat is used for the purpose of maintaining a constant temperature in the system to be studied. The cryostat designed for this purpose in this investigation will be described briefly in terms of its use. An equilibrium cell, in which phase equilibrium is established, is located in a copper block cryostat. The equilibrium cell consists primarily of a nine pound copper body with an internal volume of 40 cc. Both ends of the cell are closed with threaded monel plugs sealed with soft solder. The lower section

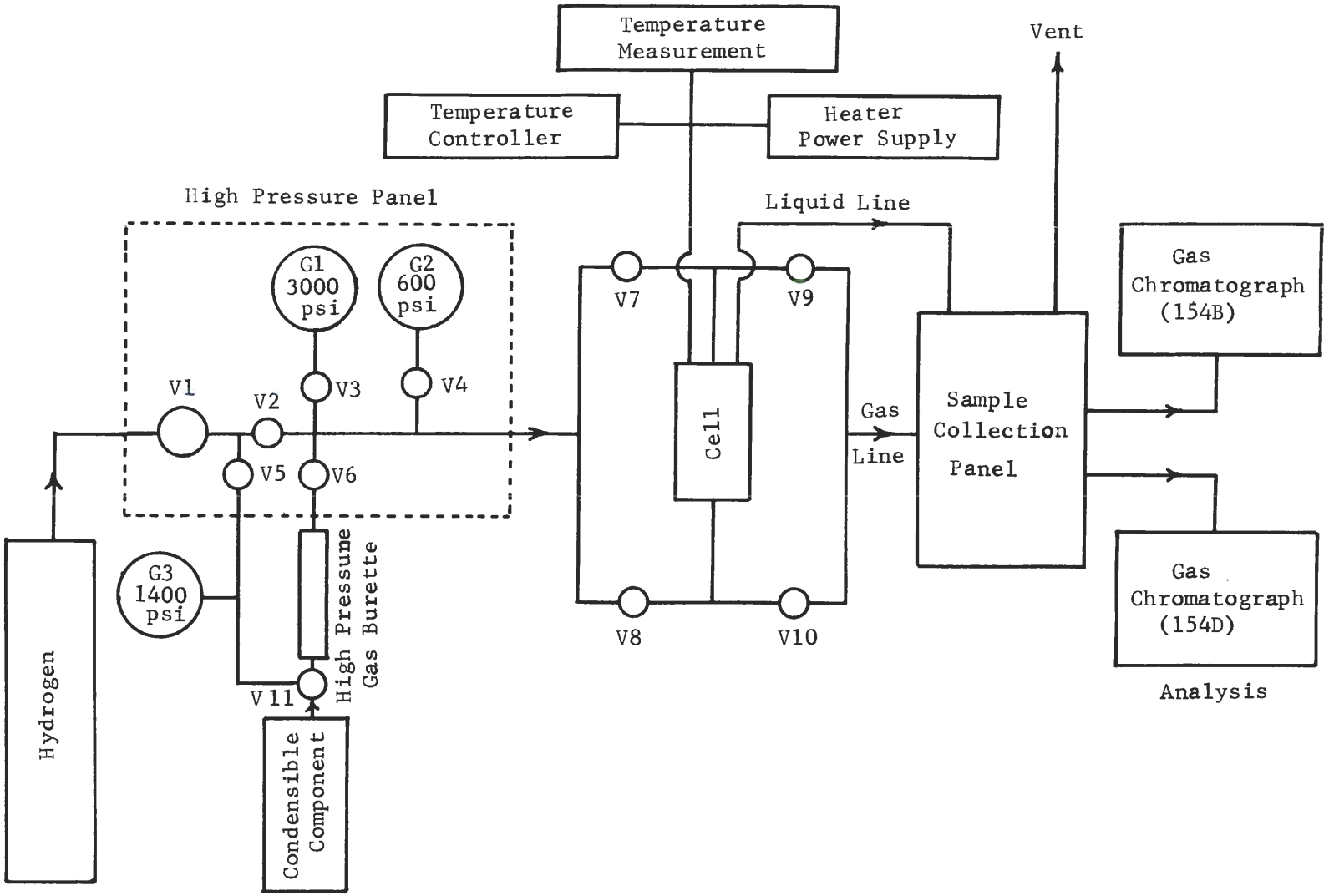

Figure 1. Schematic Diagram of Phase Equilibrium Apparatus.

contains a copper spiral for the purpose of increasing the contact time of the two phases; the upper section is packed with copper shavings. A liquid nitrogen container is connected to the copper-block by two tubes through which the refrigerant may be injected into the copper-block. To be thermally isolated from the environment, the copper-block and the refrigerant container are suspended inside an evacuated container filled with powder insulation which contains metal flakes (Linde CS-5 powder). The vacuum is maintained by a mechanical pump. The desired temperature of the equilibrium cell was adjusted by means of a slight excess of liquid nitrogen and balancing the cooling rate by an automatically controlled electric heater wrapped on the external jacket. The energy input to the heater was controlled by a photoelectric proportional sensing device. The pressure in the nitrogen container was maintained slightly higher than atmospheric pressure by a differential regulator. The flow rate of liquid nitrogen was controlled by a flow meter as well. A galvanometer light, which deflects proportionally to the temperature differences, was adjusted such that as it strikes the photocell, there is an increase of energy supplied to the equilibrium cell. With this control the temperature could be maintained within $\pm$ 0.03 K of the set temperature.

The system temperature was measured by a capsule-type platinum reistance thermometer mounted in a well within the cell. The resistance thermometer was manufactured by Leeds and Northrup company and has been calibrated by the National Bureau of Standards on the temperature scale of 1948 (IPTS-48) above 90.18 K. The temperatures reported in this work have been corrected to 1968 scale (IPTS-68) as discussed

in Appendix A . The temperature gradients along the equilibrum cell were measured by several thermocouples and thermopiles mounted on the cell. The thermocouples also serve to monitor the cell temperature. The pressure of the system was regulated by a self-contained pressure device and measured by two Bourdon pressure gauges having different pressure ranges. The high pressure gauge G1 covers the range from 0 to 3000 psig. The low pressure gauge G2, covers the range from 0 to 600 psig. Attached to it was a 570 psig cut-off unit to protect the gauge from excess pressure. The uncertainty of the pressure measurement is believed to be less than 0.5 percent of the indicated pressure. (See Appendix A).

The sample collection panel includes a mercury-filled glass burette to collect the vaporized liquid sample for analysis. A Perkin-Elmer Vapor Fractometer Model 154 B was used to analyze the liquid sample. The gas sample flows continuously from the cell to a copper burette attached to the analyzer. The gas sample collected in the copper burette can be isolated from the flowing gas stream. The flow rate of the gas was measured by a wet-test meter. A gas sample collected in the copper burette is analyzed by a Perkin-Elmer Vapor Fractometer Model 154D.

The operating conditions, the selection of the separation columns and the calibration of the two gas chromatographs are described in Appendix C.

Experimental Procedure

Before the experiment is started, the equilibrium cell and the nitrogen container are flushed with dry hydrogen and nitrogen respective-

ly, until no air or any condensibles remained in the system. The junctions of the gas line are checked to assure that there is no leakage.

Good insulation of the copper block is necessary for precise temperature control. The space containing insulation powder was evacuated by a mechanical pump to maintain a vacuum of 0.07 torr at the top and about 0.05 torr at the bottom. When these preparations are completed, liquid nitrogen is added to the refrigerant container. While filling the liquid nitrogen, the throttle valve and the regulator are fully open. After the container is full, the filling line and the regulator are closed. With the throttle valve wide open, it takes about 5 hours and 3 liters of liquid nitrogen to cool the system from room temperature to the cryogenic region. Once the cell temperature approaches the desired temperature, the refrigeration rate and the heating rate are so adjusted that the refrigeration rate is slightly higher than the heating rate. Meanwhile the position of the galvanometer light of the automatic controller is adjusted so that whenever the cell temperature is lower than the temperature desired the light will hit a photo cell and cause an increase of energy to increase the system temperature. The cell temperature can be controlled automatically within $\pm$ 0.03 K by this automatic controller. Two liters of liquid nitrogen are sufficient for 20 hours operation.

While adjusting the temperature of the cell, the desired pressure of the equilibrium cell is set by the pressure regulating valve. The gas flow rate from the equilibrium cell is set at 100 cc/hr (at cell temperature and pressure) by adjusting the flow rate regulating valve and measured by the wet-test meter. During this stage, valves V_1, V_2,

V_3, V_8 and V_9 in Figure 1 are opened, and V_5, V_6, V_7 and V_{10} are closed. Valve V_4 is opened for the low pressure range only. With V_5, V_6 and V_{11} closed, the high pressure gas burette is evacuated by a mechanical vacuum pump and then filled with known amount of component 1. The gas pressure in the burette is measured by gauge G3. Approximately 11 cc of pure liquid component 1 is introduced into the cell by opening V_5, V_6 and closing V_2. About 5 cc of the liquid sample is above the end of the liquid sampling line. Too much liquid sample will cause undesirable entrainment of liquid in the gas phase.

Since the liquid level indicator was not working at the time of this work, the liquid level was estimated from the gas flow rates, compositions of the gas and the liquid phases and amount of liquid sample taken for analysis. The liquid level was also determined by withdrawing the liquid sample continuously and analyzing until a large amount of hydrogen was detected. Five cc of liquid was reintroduced after the liquid level was detected.

After the desired temperature and pressure of the system are established, the gas phase is analyzed by the 154D gas chromatograph at 15-minute intervals until the differences of the peak height are less than 2 percent. When equilibrium was established, three continuous gas samples were analyzed and recorded. The liquid sample is collected using the sample collecting panel and analyzed by the 154B gas chromatograph. At least two analyses were made for each gas sample so collected.

Throughout this work, the temperature gradients of the cell were measured at each experimental point and were always found to be less

than 0.03 K. It took approximately two hours for the measurement of each data point on an isotherm.

CHAPTER III

EXPERIMENTAL RESULTS AND DISCUSSION

Experimental compositions of the equilibrium gas and liquid phases of hydrogen-carbon tetrafluoride and hydrogen-chlorotrifluoromethane system measured in this work are shown in Figure 2 through Figure 7. The gas phase compositions are presented in terms of enhancement factors. The detailed experimental data and smoothed values are presented in Appendix D and Appendix E, respectively. The experimental K values ($K_i = y_i/x_i$) are also shown in Appendix D.

Six isotherms for the hydrogen-carbon tetrafluoride system ranging from 94.94 to 164.99K and seven isotherms for the hydrogen-chlorotrifluoromethane system ranging from 134.97 to 219.99K were studied from 20 to 120 atm at intervals of 20 atm.

Since no other experimental data are available for hydrogen-carbon tetrafluoride and hydrogen-chlorotrifluoromethane systems, the results of this investigation are compared to those of the hydrogen-argon system investigated by Mullins (87), hydrogen-methane by Kirk (61), hydrogen-ethylene by Hiza, Heck and Kidnay (51) and hydrogen-ethane by Hiza, Heck and Kidnay (52). Comparisons are also made for the corresponding helium systems, which are helium-methane by Heck and Hiza (44), helium-argon by Mullins (87), helium-ethylene by Garber (35), helium-ethane by Hiza and Duncan (50) and Heck (43), helium-carbon tetrafluoride and helium-chlorotrifluoromethane by Yoon (132).

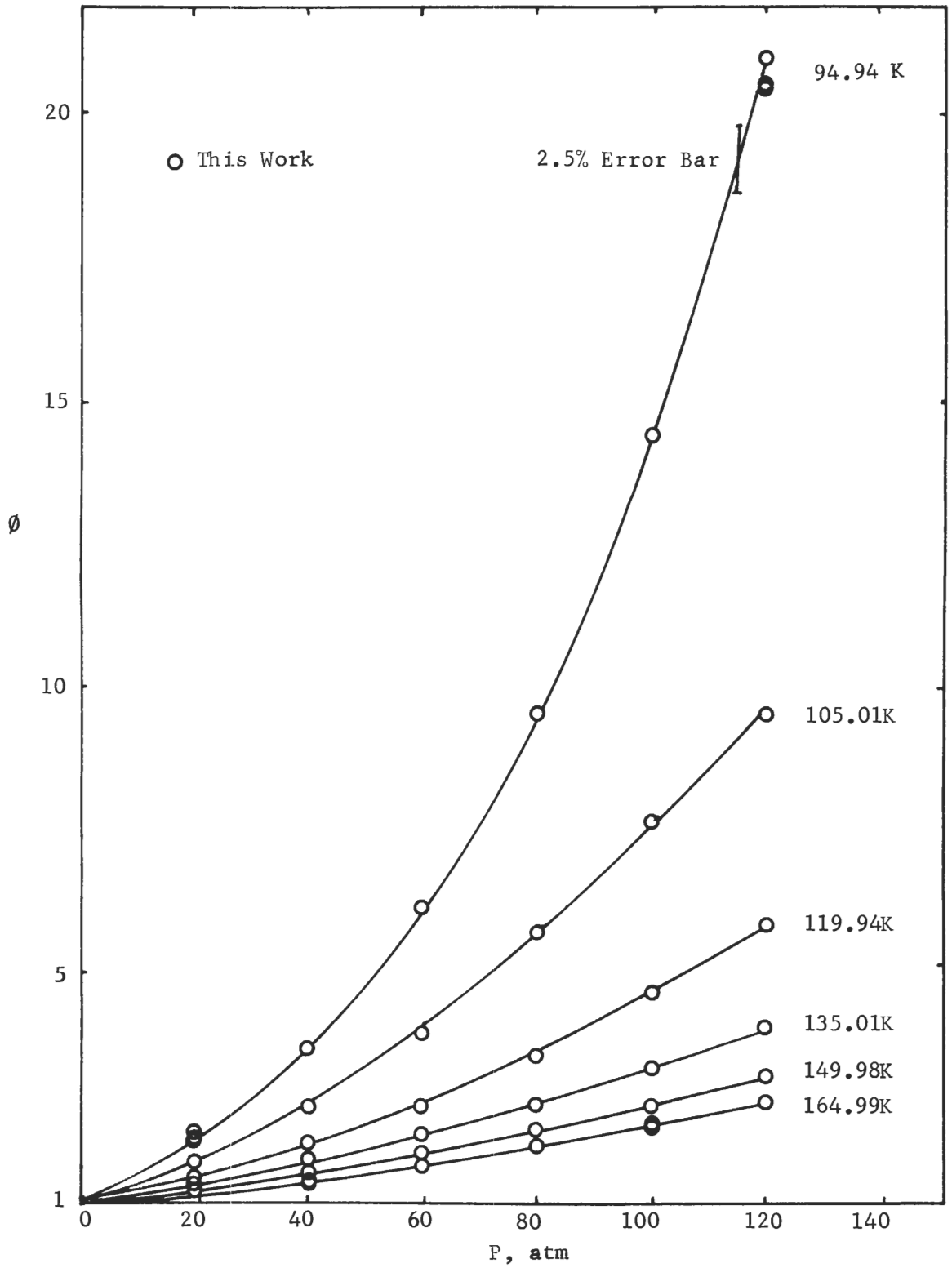

Figure 2. Experimental Enhancement Factors of Carbon Tetrafluoride in Hydrogen at 94.94, 105.01, 119.94, 135.01, 149.98 and 164.99K.

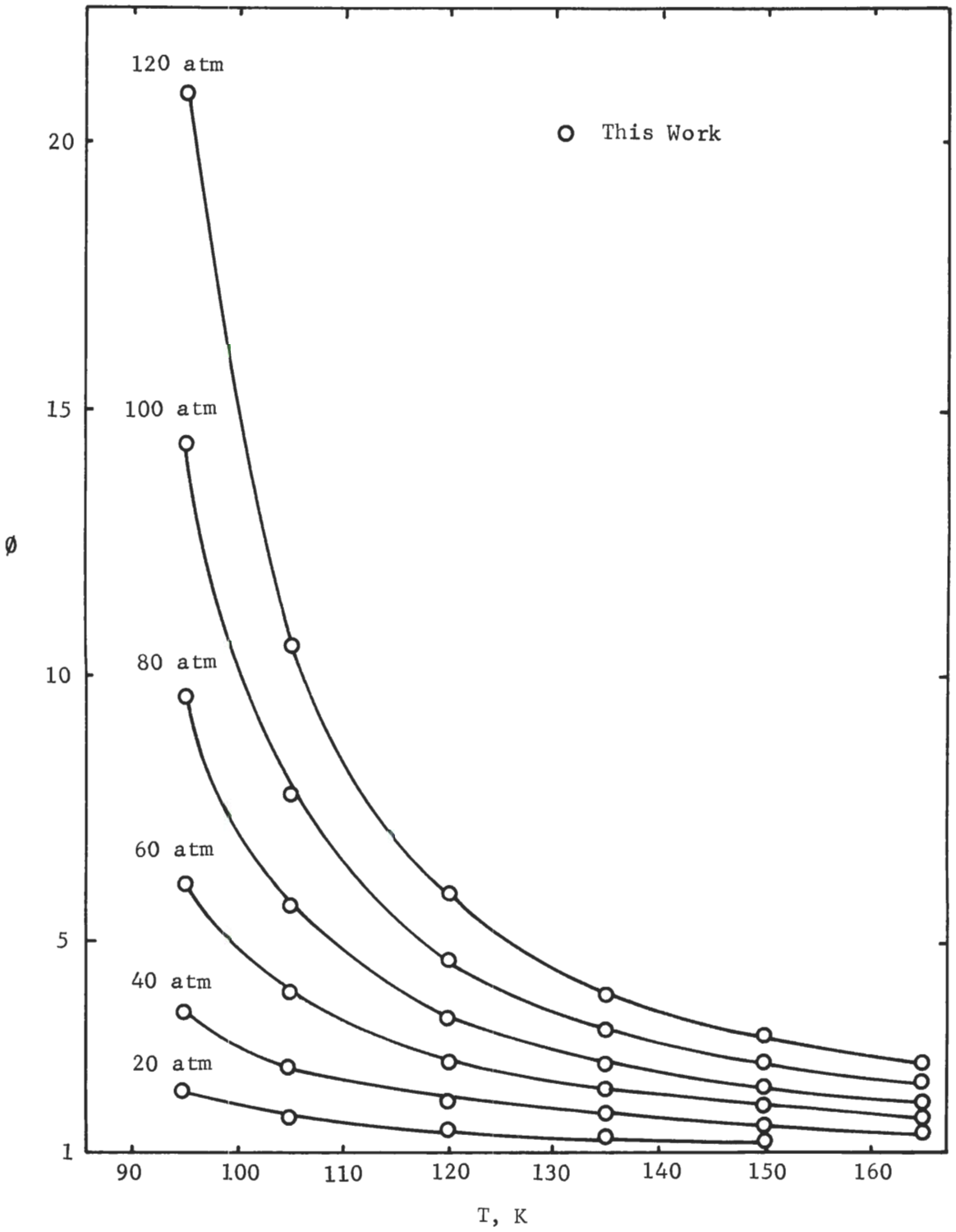

Figure 3. Experimental Enhancement Factors of Carbon Tetrafluoride in Hydrogen along Isobars.

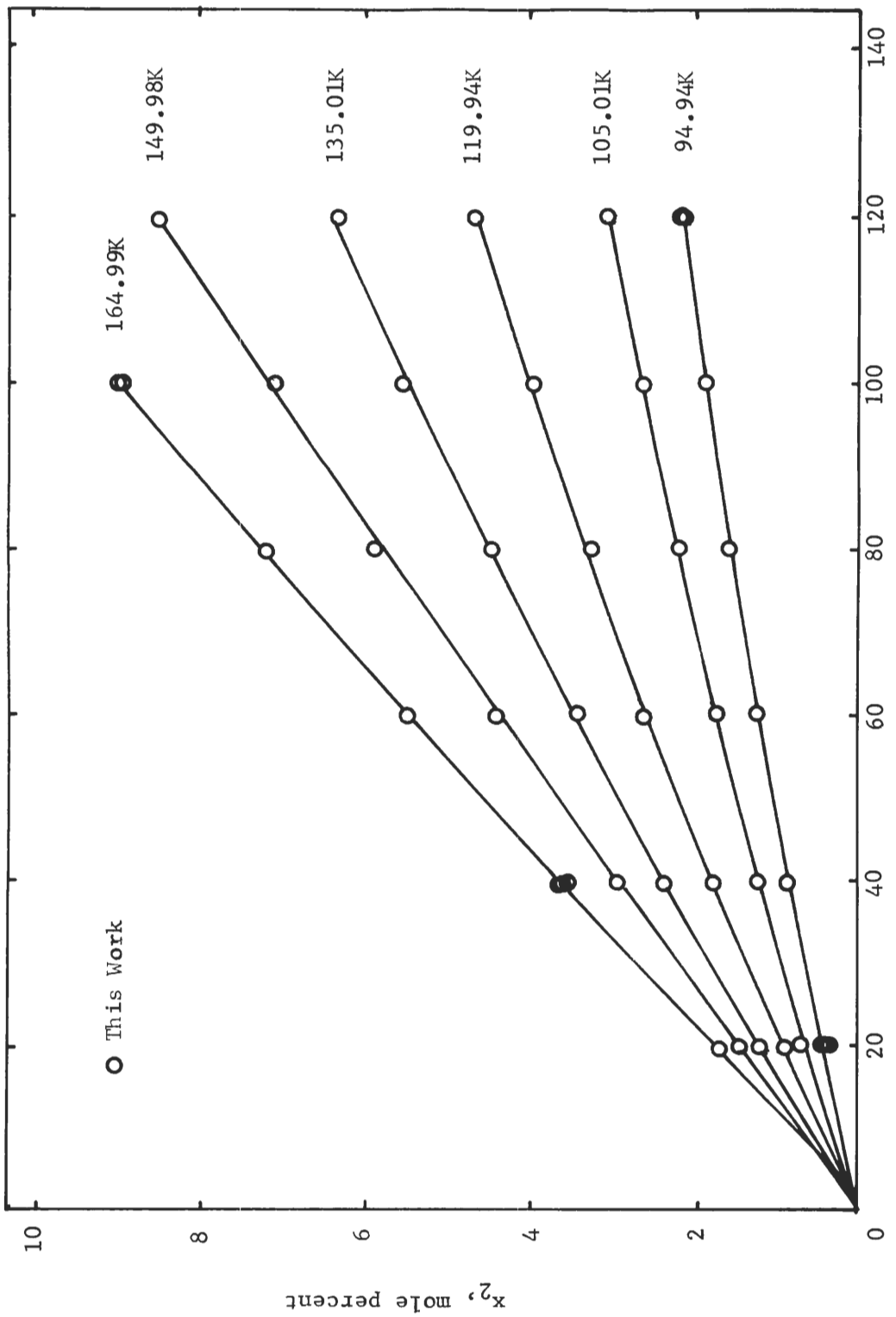

Figure 4. Experimental Solubility of Hydrogen in Liquid Carbon Tetrafluoride.

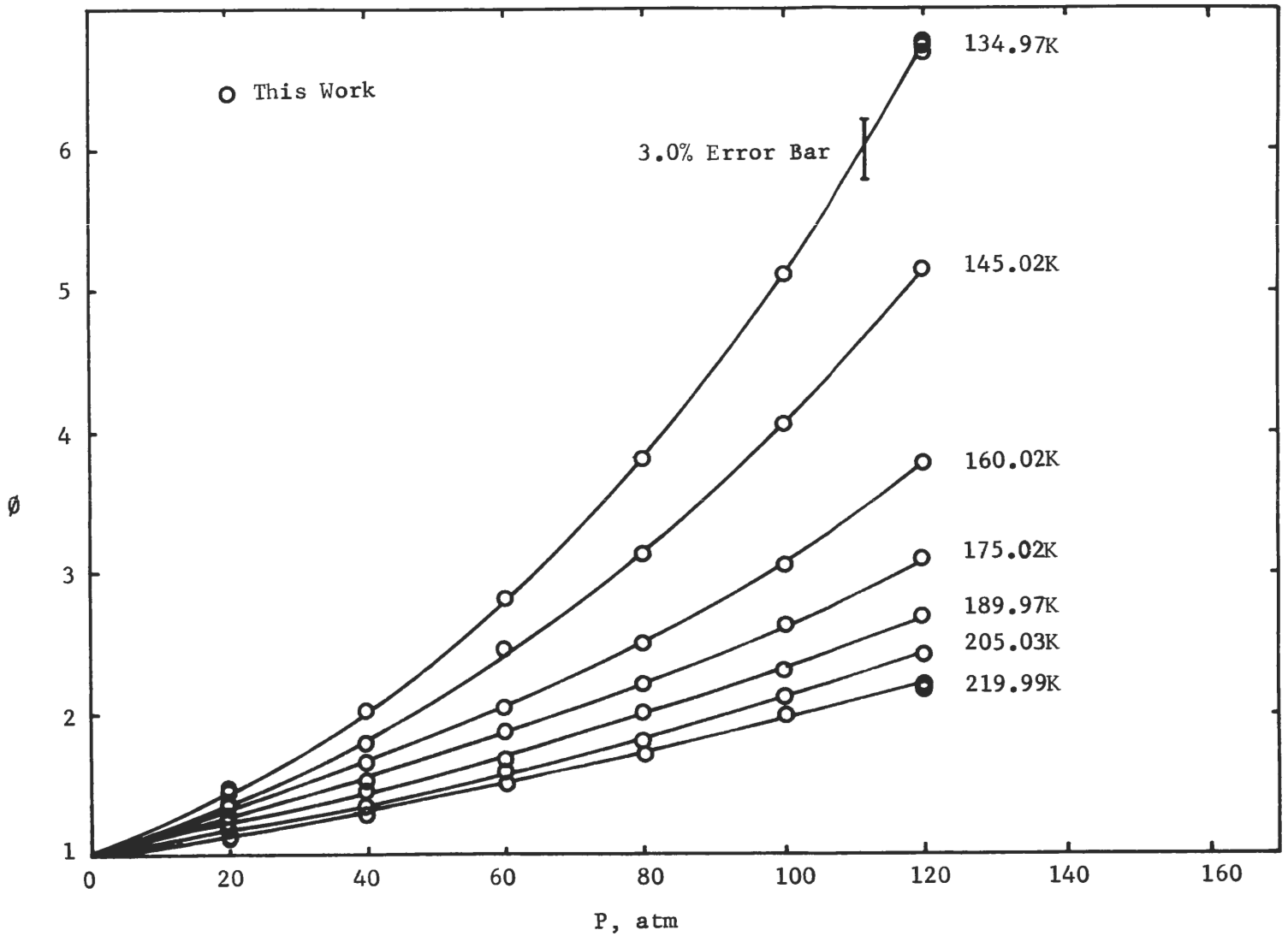

Figure 5. Experimental Enhancement Factors of Chlorotrifluoromethane in Hydrogen at 134.97, 145.02, 160.02, 175.02, 189.97, 205.03, and 219.99K.

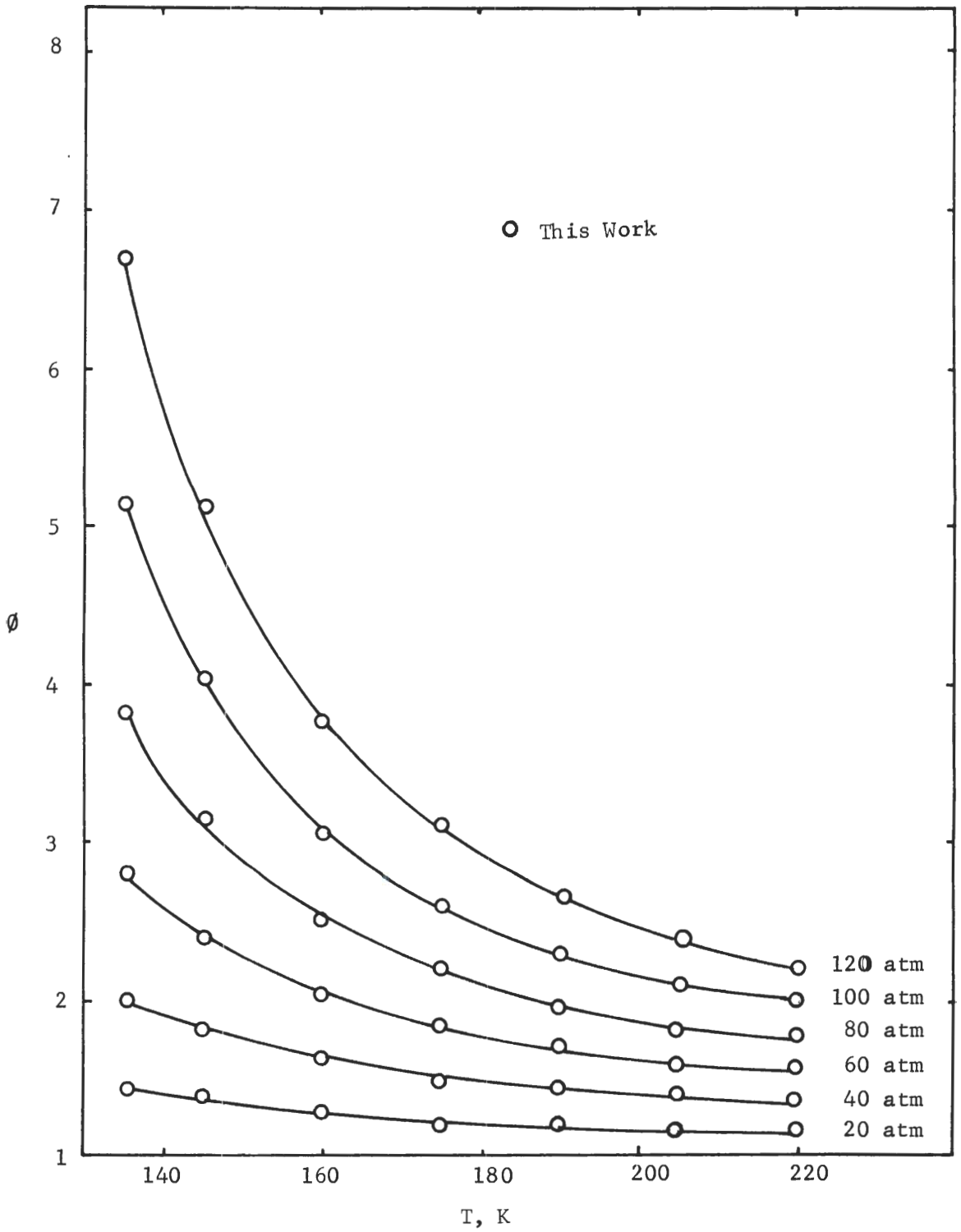

Figure 6. Experimental Enhancement Factors of Chlorotrifluoromethane in Hydrogen along Isobars.

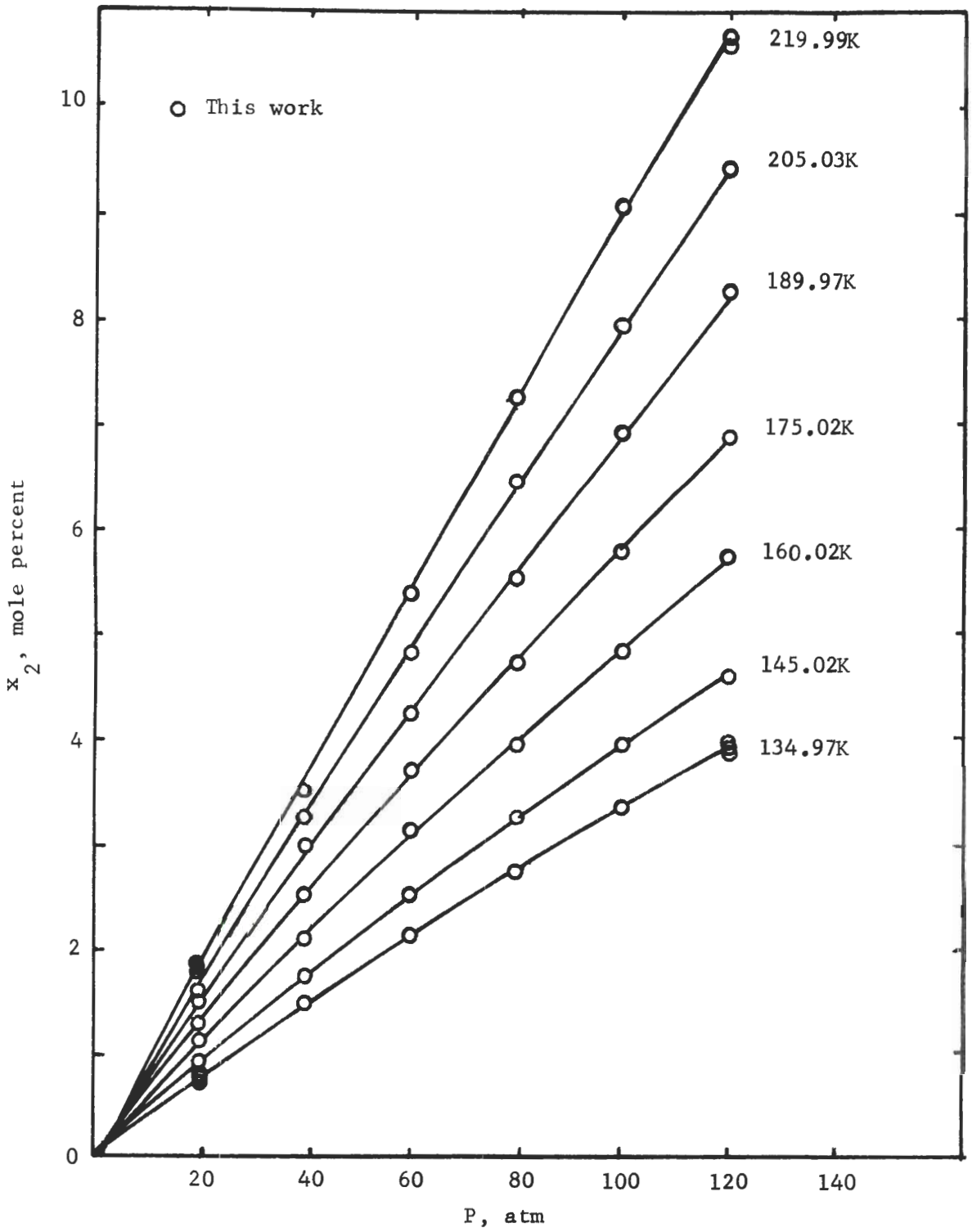

Figure 7. Experimental Solubility of Hydrogen in Liquid Chlorotrifluoromethane.

The comparisons are made at the same pressure and reduced temperature of component 1 in an attempt to give a clue to the fundamental relationship between the molecular species and interaction involved.

Experimental Results

The equilibrium gas phase compositions for the hydrogen-carbon tetrafluoride system measured along six isotherms of 94.94, 105.01, 119.94, 135.01, 149.98 and 164.99 K are shown in Figure 2 in terms of enhancement factors. The data points shown on the figures are the average values of three or more experimental points at the given temperature and pressure. The error of the enhancement factor measurement is believed to be less than 2.5 percent. Each smoothed curve is obtained by the method of least squares to fit the experimental data to a polynomial, except the low end is drawn by eye so that the curve intersects the abscissa at the vapor pressure of carbon tetrafluoride. Deviations of the experimental data from the values on the smoothed curve are always less than 2 percent which is consistent with the 2.5 percent error claimed above. Figure 3 shows six isobars of the enhancement factors which were obtained from the fitted polynomials at smoothed pressures.

The liquid phase compositions measured at corresponding temperatures and pressures are shown in Figure 4. These smoothed curves were also obtained by the least-squares fitting method. The experimental error of liquid phase compositions is believed to be less than 2 percent and the deviation of experimental points from the smoothed curve is always less than 2 percent. The smoothed experimental values are shown

in Table 13 in Appendix E.

Similar treatments of data are applied to the experimental data of the hydrogen-chlorotrifluoromethane system. Seven isotherms of the enhancement factors measured at 134.97, 145.02, 160.02, 175.02, 189.97, 205.03 and 219.99 K are shown in Figure 5. Six isobars are shown in Figure 6 at six smoothed pressures. The liquid phase compositions plotted isothermally against pressure are shown in Figure 7. The experimental error in composition measurement is believed to be less than 3 percent for the vapor phase and 2 percent for the liquid phase. The deviation of data points from the smoothed curve is always less than 2 percent. The smoothed experimental data are shown in Table 14 in Appendix E.

The uncertainty of the experimental results was estimated from the scatter in the chromatograph calibration curves, the pressure gauge uncertainty of 0.5 percent and the uncertainty of temperature measurement at $\pm$ 0.03 K. The experimental points scatter along an isotherm within the estimated uncertainty expected.

Discussion of Results

The six isotherms and six isobars of the hydrogen-carbon tetrafluoride system presented in Figure 2 and Figure 3 show the general trends of the system. The enhancement factors range from 1.26 to 20.86 and the gas phase compositions range from 0.0282 to 12.20 mole percent of carbon tetrafluoride. The enhancement factors of this system decrease monotonously as temperature increases. Figure 5 and Figure 6 present seven isotherms and six isobars of the hydrogen-chlorotrifluo-

romethane system. The enhancement factors of this system range from 1.18 to 6.73 and the gas phase compositions range from 0.0587 to 21.69 mole percent of chlorotrifluoromethane.

The solubility of hydrogen in carbon tetrafluoride ranges from 0.466 to 8.97 mole percent. The solubility of hydrogen in chlorotrifluoromethane ranges from 0.740 to 10.54 mole percent. From Figure 4 and Figure 7 it is seen that the solubility of hydrogen for these two systems increases as temperature increases and the solubility curves bend downward at high pressures. Both systems show reverse solubility effect and negative deviation from Henry's law. These are characteristics of hydrogen and helium solubility exhibited by most cryogenic fluids.

Since a flow type phase equilibrium apparatus was used in this work, the composition measured may be a steady state composition and not an equilibrium composition if the gas flow rate from the equilibrium cell is too fast. Kirk (61), Mullins (87), Liu (73), Garber (35), and Yoon (132) have all verified that a flow rate of 100 cc/hr at the cell temperature and pressure is sufficient to establish equilibrium for the He-X(X=Ar(87), CO_2(73), C_2H_6(35), C_2H_4(35), CF_4(132), $CClF_3$(132)) and H_2-X (X=Ar(87), CH_4(61)) systems studied by them. In order to assure that the same flow rate is adequate for the systems studied here, four data points of each system were repeated at various flow rates. In the hydrogen-carbon tetrafluoride system, two points at 20 atm and 120 atm on the lowest isotherm, 94.94 K, were rerun at twice the normal flow rate, and at one-half the normal flow rate. The datum point at 100 atm on the highest isotherm, 164.99 K, was repeated at one-half the normal

flow rate. The point at 40 atm of the highest isotherm was run at the normal flow rate, and equilibrium was reached by increasing the pressure from 20 atm to the equilibrium pressure. This was repeated twice at flow rates of 200 cc/hr and 50 cc/hr respectively, but equilibrium was reached by decreasing the pressure from 60 atm to the equilibrium pressure. All of these data points fell within the estimated uncertainty. This experiment not only demonstrated that the recommended flow rate is adequate for this work, but also proved that the compositions are not changed when equilibrium is reached from the low or high pressure side. In the hydrogen-chlorotrifluoromethane system, four points at 20 atm and 120 atm on the lowest and the highest isotherm were repeated. Each point was rerun at three different flow rates. The data points also fell within the estimated uncertainties.

For purposes of comparison of the hydrogen and helium systems, the experimental vapor phase compositions of six helium systems at 60 and 120 atm, and the corresponding six hydrogen systems are summarized in Figure 8 through Figure 11. The liquid phase compositions are also shown in Figure 12 through Figure 15. The experimental data are plotted against the reduced temperature of component 1. The helium systems include helium-argon (87), helium-methane (44), helium-ethane (43, 50), helium-ethylene (35,50), helium-carbon tetrafluoride and helium-chlorotrifluoromethane (132). The experimental data of the helium systems as smoothed by Liu (73), Garber (35), and Yoon (132) were used in this comparison. The corresponding hydrogen systems are hydrogen-argon (87), hydrogen-methane (61), hydrogen-ethane (52), hydrogen-ethylene (51), and hydrogen-carbon tetrafluoride and hydrogen-

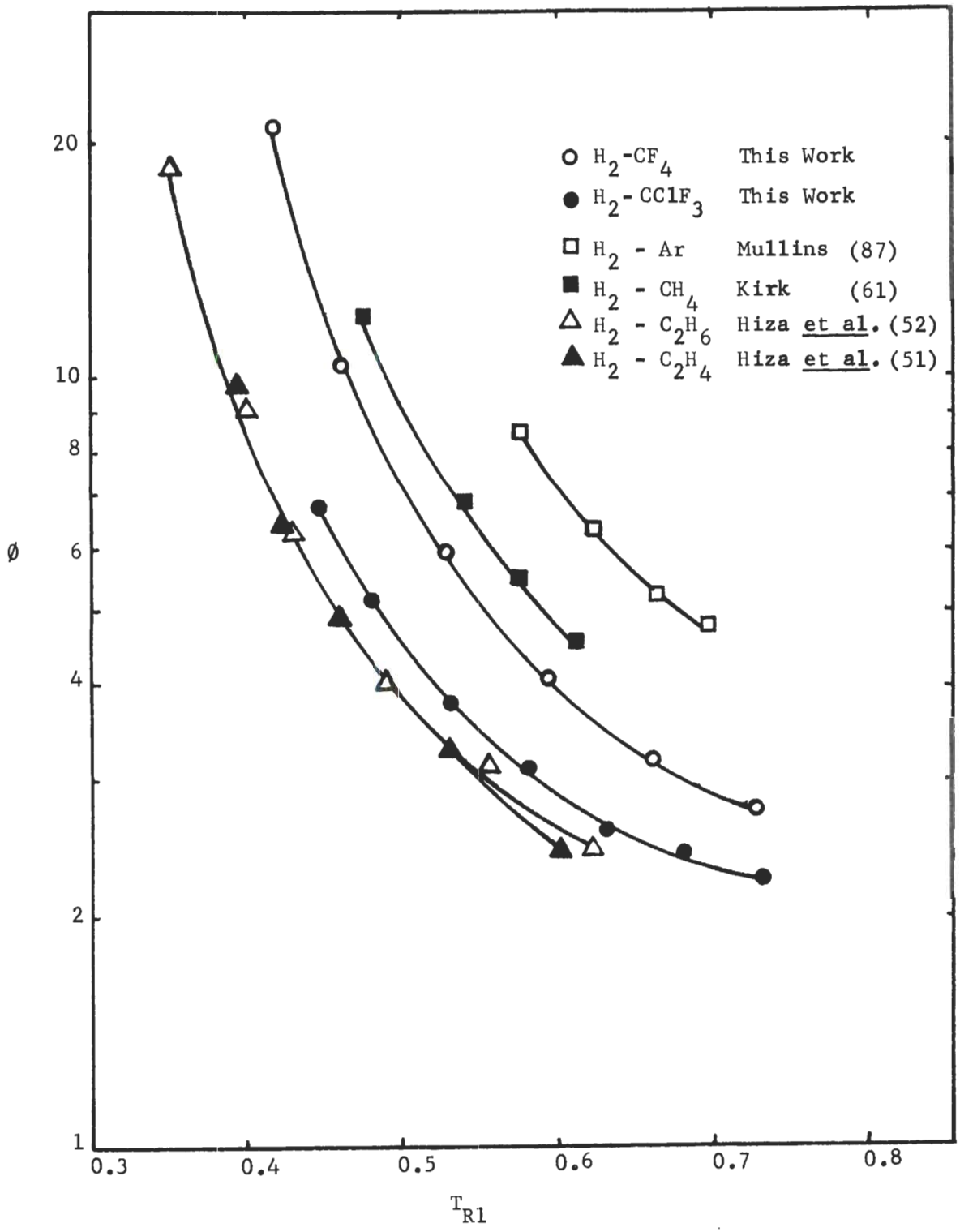

Figure 8. Experimental Enhancement Factors of Six Hydrogen Systems at 120 atm.

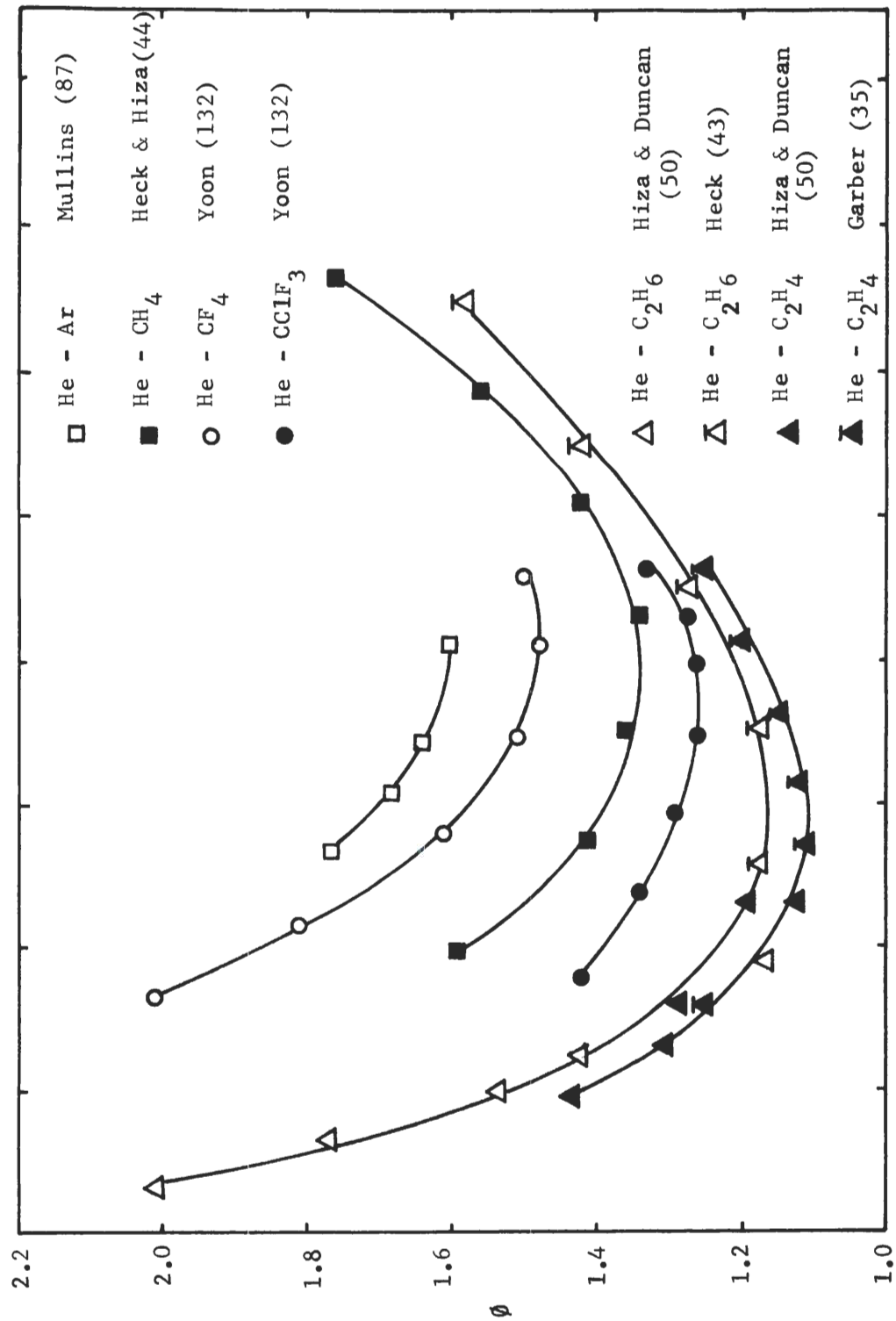

Figure 9. Experimental Enhancement Factors of Six Helium Systems at 120 atm.

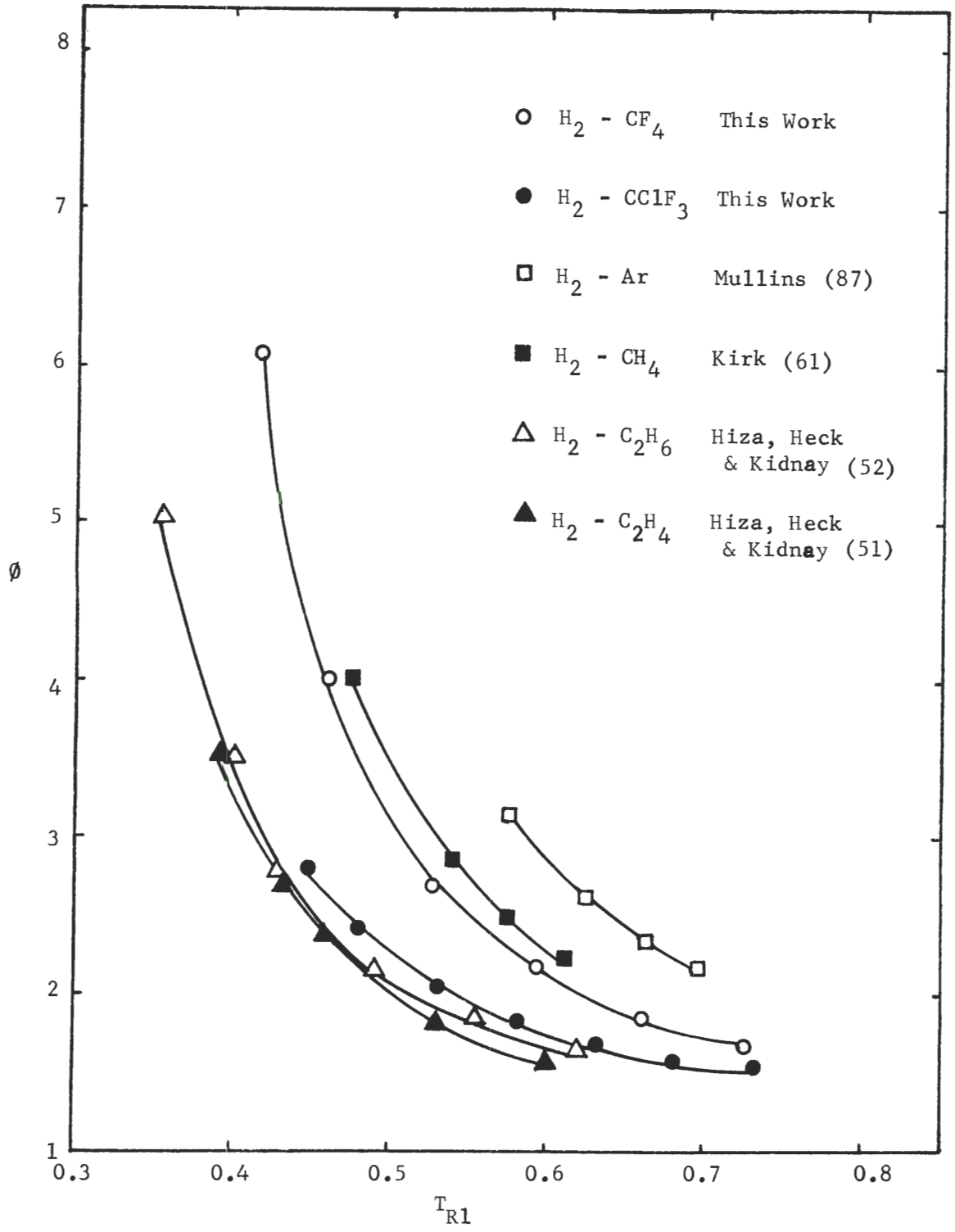

Figure 10. Experimental Enhancement Factors of Six Hydrogen Systems at 60 atm.

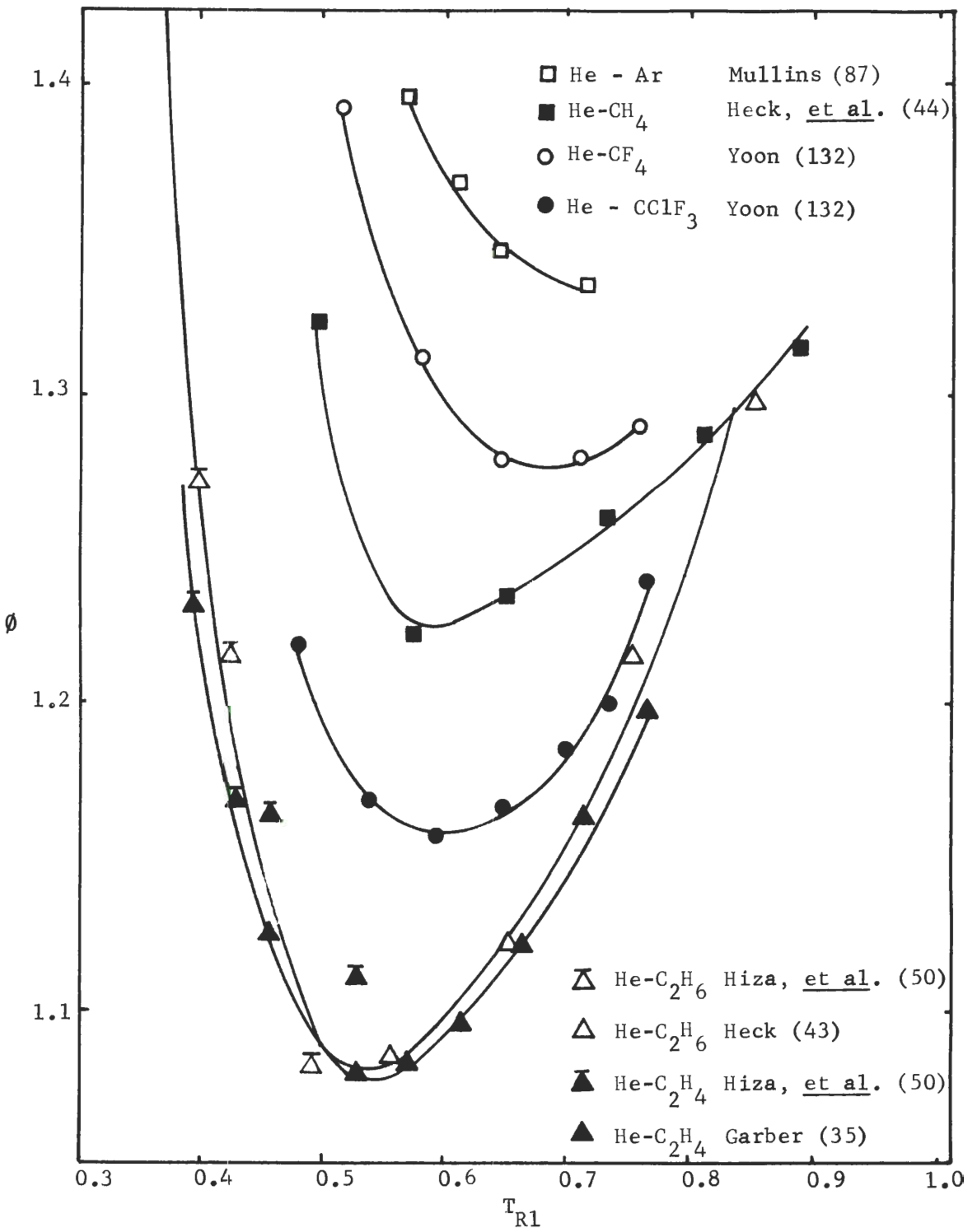

Figure 11. Experimental Enhancement Factors of Six Helium Systems at 60 atm.

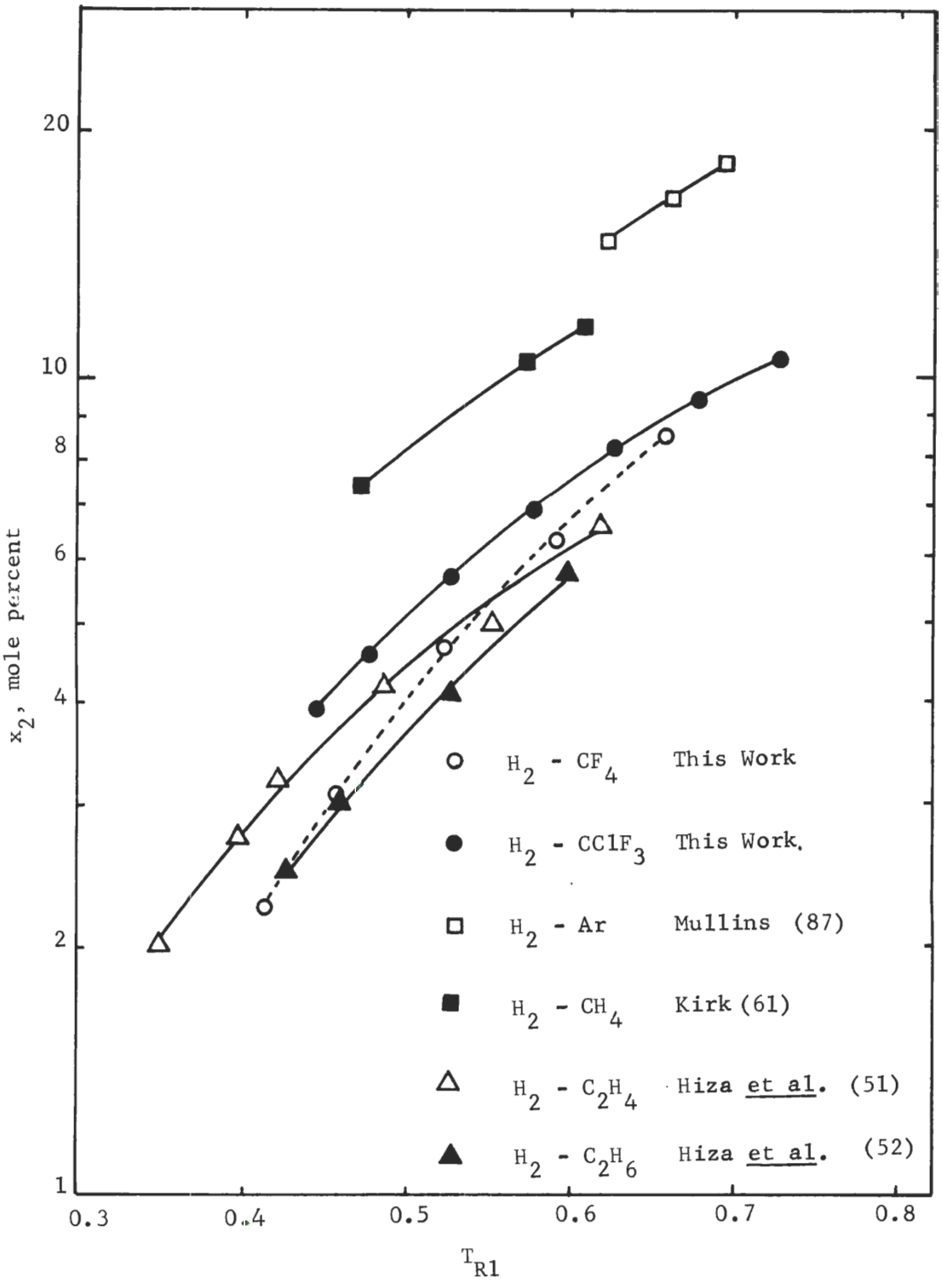

Figure 12. Experimental Solubility of Hydrogen at 120 atm.

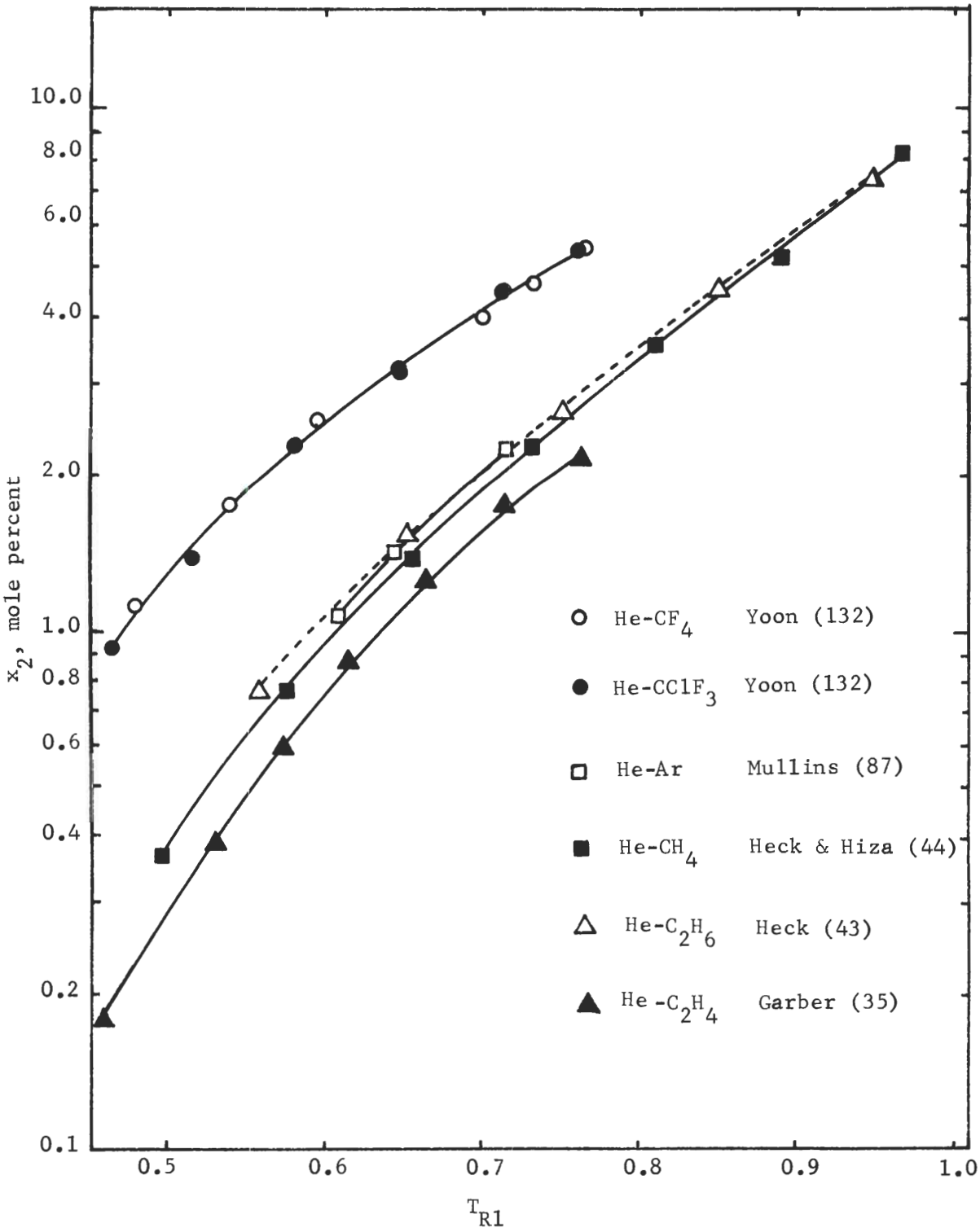

Figure 13. Experimental Solubility of Helium at 120 atm.

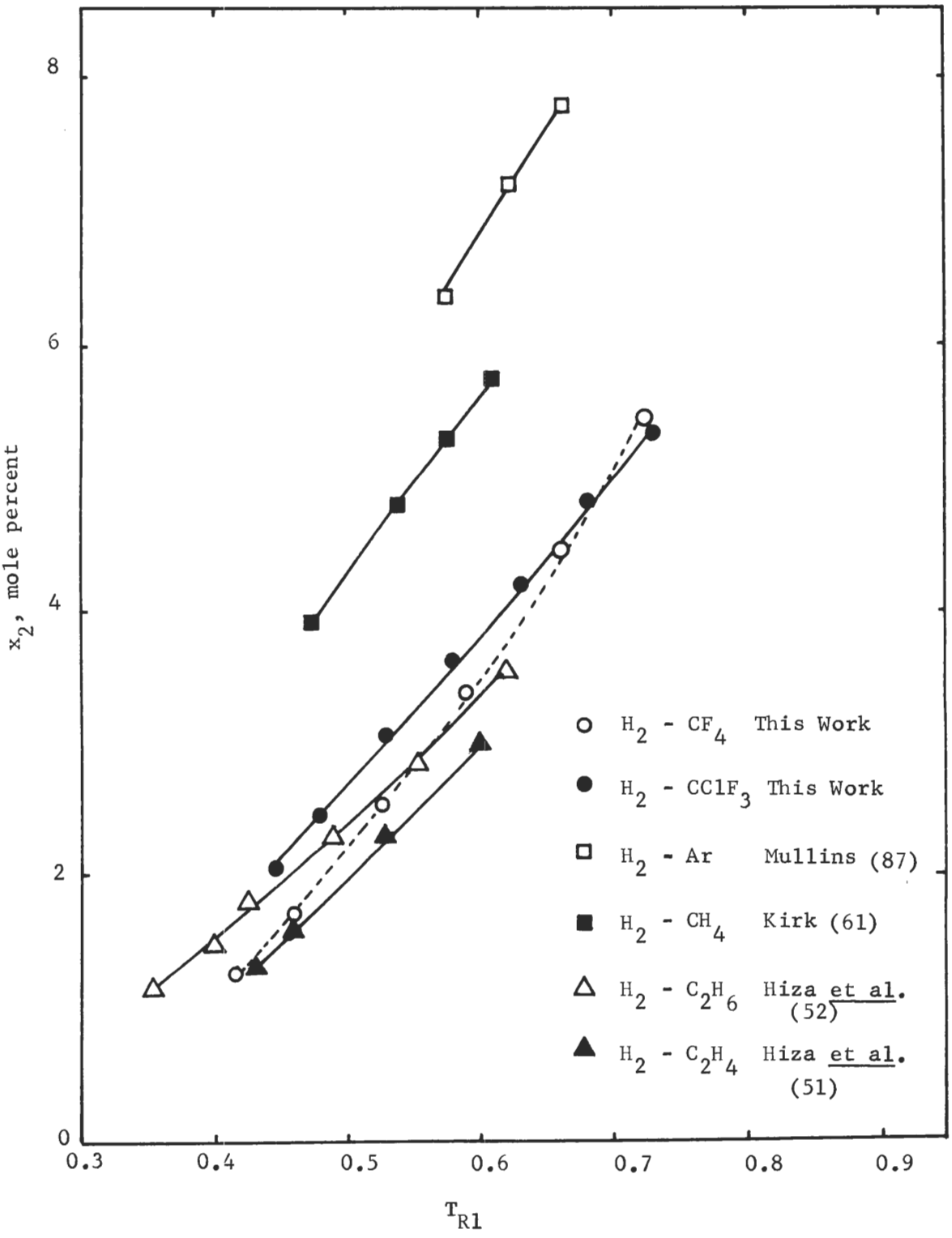

Figure 14. Experimental Solubility of Hydrogen at 60 atm.

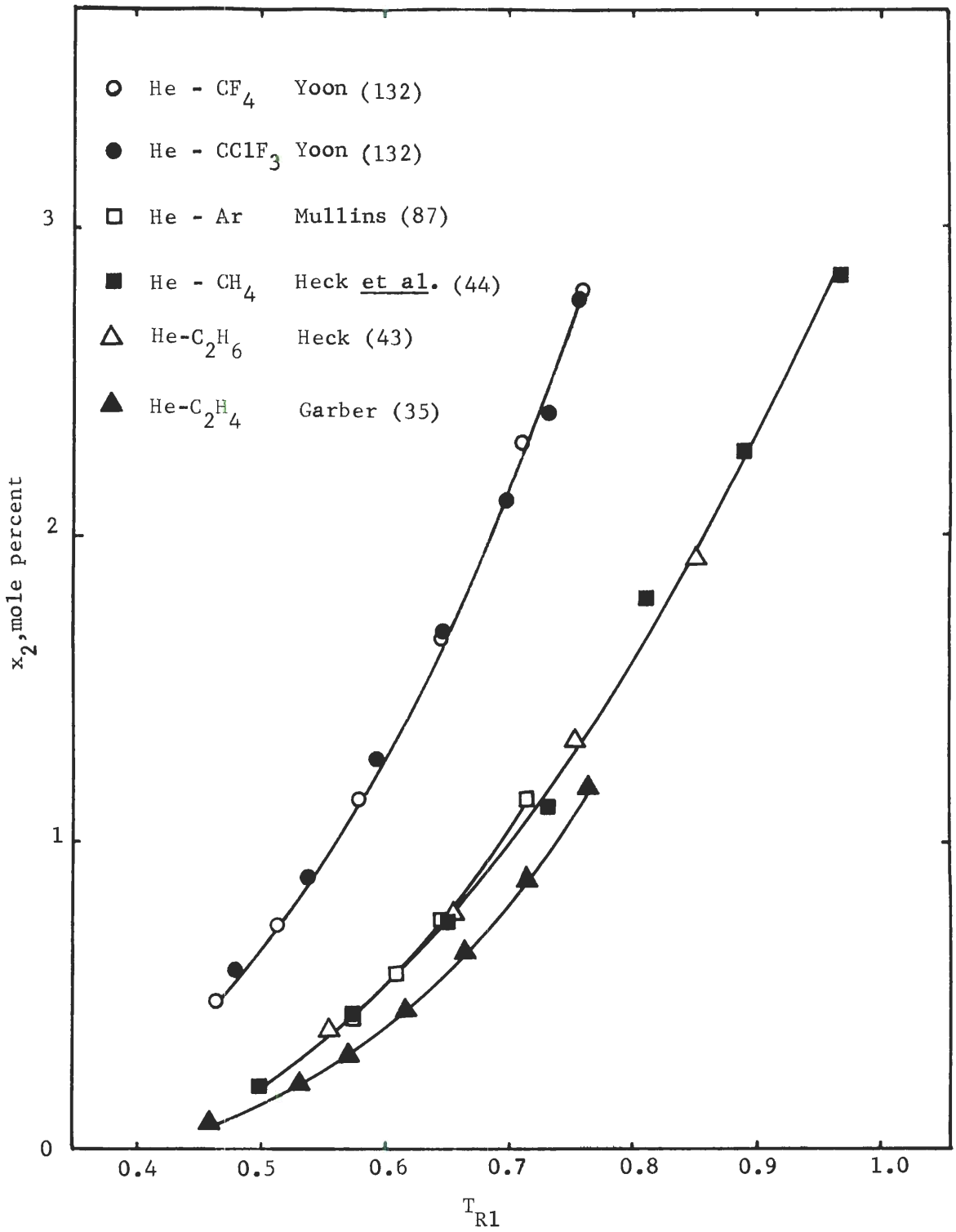

Figure 15. Experimental Solubility of Helium at 60 atm.

chlorotrifluoromethane from this work. The experimental phase equilibrium data of the hydrogen systems have been smoothed in this work as shown in Table 15 through Table 18 in Appendix E. The comparisons are made at 60 and 120 atm; the phase equilibrium data for all the systems considered here are not available at lower pressure.

Hiza (50), Garber (35), and Yoon (132) pointed out that a plot of the enhancement factor of helium systems usually shows a minimum on the isobar and that the values of the enhancement factor usually range between one and three in the liquid-vapor region at pressures up to 120 atm. These two interesting phenomena are demonstrated in Figure 9 and 11. The corresponding plot for the hydrogen systems in Figure 8 and 10 show that the enhancement factors for the hydrogen system are much higher than the corresponding helium system at the same reduced temperature, and that the enhancement factors decrease monotonously as temperature increases. The relative position of each isobar of the hydrogen systems is quite similar to that of the helium systems, except that the positions of the isobar of the hydrogen-methane and the hydrogen-carbon tetrafluoride are reversed. Although it is a complicated matter to give a conclusion for this phenomenon, two facts pointed out by Yoon (132) for the helium systems still hold for the hydrogen systems. Thus, at the same pressure and reduced temperature, T_{R1}, the hydrogen-saturated hydrocarbon system shows a greater enhancement factor than the hydrogen-unsaturated hydrocarbon system, and the hydrogen binary system with spherical molecules gives a greater enhancement factor than that with less spherical molecules.

Comparison of the six helium systems at the same pressure and

reduced temperature, T_{R1}, shows (see Table 2) that the helium system with the larger ionization potential of component 1 exhibits the larger enhancement factors. This phenomenon is also true for the six hydrogen system summarized, except the order of the hydrogen-carbon tetrafluoride and hydrogen-methane systems is reversed. In comparison of the liquid phases at the same pressure and reduced temperature, T_{R1}, Figures 12 and 14 show that a hydrogen system which has larger values of enhancement factors tends to have higher solubility of hydrogen in the liquid phase. Figures 13 and 15 show that the solubility of helium in argon and methane is relatively lower, while the solubility of hydrogen in argon and methane is relatively higher than the others.

From the limited phase equilibrium data summarized in this work, the information is not sufficient to give a more specific conclusion on the observed phenomena. It may be interesting to compare the phase equilibrium data of some other binary systems, and hopefully, a clearer picture can be seen. Perhaps, both the ionization potential and the polarizability of different species must be taken into consideration in this kind of comparison, since the two quantities are related to the interaction forces of the species involved.

CHAPTER IV

CALCULATION OF ENHANCEMENT FACTOR*

Introduction

From the phase rule, it is known that the number of degrees of freedom is two for a binary system with two phases in equilibrium. If the temperature and pressure of the system are fixed then the other intensive variables are fixed and the condition of the system at equilibrium can be defined.

From a thermodynamic point of view, the chemical potential of a component must have the same value in every phase for a system in equilibrium at a given temperature and pressure. Therefore the following relations of the condensible component 1 and the more volatile component 2 for a binary system will hold.

$$\mu_1^L(P,T,x_1) = \mu_1^G(P,T,y_1) \qquad \text{(IV-1)}$$

$$\mu_2^L(P,T,x_2) = \mu_2^G(P,T,y_2) \qquad \text{(IV-2)}$$

These two equations can be expressed in terms of measurable quantities and will be discussed separately later. If all theoretical parameters in these two equations are available, the theoretical vapor and liquid composition at a given temperature and pressure can be ob-

---

* The development given in this chapter follows closely that given by Yoon (132).

tained by solving these two equations simultaneously. Since none of the theoretical parameters are available, several assumptions must be made or some theoretical parameters must be extracted from the experimental data of other investigators. While no attempt was made in this study to solve these two equations simultaneously, certain of the theoretical parameters were extracted from the experimental data of this investigation through the use of these equations. An expression of Equation (IV-1) in terms of measurable quantities will be derived and discussed in this chapter. The extraction of the interaction second virial coefficient from Equation (IV-1) and of the thermodynamic Henry's law constant and the partial molar volume from Equation (IV-2) will be discussed in Chapter V and Chapter VI respectively.

The chemical potential of component 1 in the liquid mixture can be expressed by the relation

$$\mu_1^L(P,T,x_1) = \mu_1^{*L}(P,T) + RT \ln (\gamma_1' x_1) \qquad \text{(IV-3)}$$

where $\mu_1^{*L}(P,T)$ is the chemical potential of pure component 1 at the same temperature and pressure, and γ_1' is the activity coefficient which approaches unity as x_1 approaches unity.

From the criteria for phase equilibrium, the chemical potential of the pure gas must be equal to that of the pure liquid at its saturation pressure P_{o1}.

$$\mu_1^{*L}(P_{o1},T) = \mu_1^{*G}(P_{o1},T) \qquad \text{(IV-4)}$$

The chemical potential of a pure liquid at temperature T and

pressure P is related to its chemical potential at the saturation pressure P_{o1} by:

$$\mu_1^{*L}(P,T) = \mu_1^{*L}(P_{o1},T) + \int_{P_{o1}}^{P} v_1 dP \qquad \text{(IV-5)}$$

By combining Equations (IV-3), (IV-4) and (IV-5) the chemical potential of the liquid mixture becomes:

$$\mu_1^{L}(P,T,x_1) = \mu_1^{*G}(P_{o1},T) + \int_{P_{o1}}^{P} v_1 dP + RT \ln (\gamma_1' x_1) \qquad \text{(IV-6)}$$

where

$$\mu_1^{*G}(P_{o1},T) = \int_{V_{o1}}^{\infty} [(\frac{\partial P_1}{\partial n_1})_{V_1,T} - \frac{RT}{V_1}] dV_1 - RT \ln \frac{V_{o1}}{RT} + g_1^o \qquad \text{(IV-7)}$$

The chemical potential of component 1 in a binary gas mixture is

$$\mu_1^{G}(P,T,y_1) = \int_{V_m}^{\infty} [(\frac{\partial P}{\partial n_1})_{V_m,T,n_2} - \frac{RT}{V_m}] dV_m - RT \ln \frac{V_m}{RT}$$

$$+ RT \ln y_1 + g_1^o \qquad \text{(IV-8)}$$

Combining Equation (IV-1), (IV-6), (IV-7) and (IV-8) the following equation is obtained.

$$\ln \phi = \ln \frac{Py_1}{P_{o1}} = \ln \frac{PV_m}{P_{o1}V_{o1}} + \frac{1}{RT} \int_{P_{o1}}^{P} v_1 \, dP$$

$$+ \frac{1}{RT} \int_{V_{o1}}^{\infty} [(\frac{\partial P_1}{\partial n_1})_{V_1,T} - \frac{RT}{V_1}] dV_1 - \frac{1}{RT} \int_{V_m}^{\infty} [(\frac{\partial P}{\partial n_1})_{V_m,T,n_2}$$

$$- \frac{RT}{V_m}] dV_m + \ln (\gamma_1') + \ln(x_1) \qquad \text{(IV-9)}$$

where $\phi = Py_1/P_{o1}$ is defined as the enhancement factor of component 1 in the gas mixture in equilibrium with the liquid phase. Equation (IV-9) has been reported by several investigators(35, 61, 62, 63, 73, 87, 132).

To calculate the theoretical enhancement factor from Equation (IV-9), the following information is required.

1. Composition of liquid phase.
2. Experimental data or an assumption for γ_1'.
3. Molar volume of pure liquid component 1 as a function of temperature and pressure.
4. Vapor pressure of component 1.
5. Equation of state for the gas mixture and the gas phase of pure component 1.

In the absence of a satisfactory theoretical model for the liquid phase, the liquid phase compositions cannot be obtained by solving Equation (IV-1) and Equation (IV-2). The experimental liquid compositions measured in this work were used in the calculation of the theoretical enhancement factors. It may be noted that since the solubility of hydrogen in the liquid phase for the hydrogen-carbon tetrafluoride and hydrogen-chlorotrifluoromethane system is less than 10 percent, elimination of $\ell n\ x_1$ term in Equation(IV-9) would have caused a maximum error of 10 percent in the enhancement factor calculation. Since the liquid compositions are always less than 10 percent, an ideal solution can be assumed without great error and γ_1' becomes unity in this calculation. From the analysis of the phase equilibrium data of this work (see Appendix H), it is quite satisfactory to assume an ideal solution model in this calculation.

To express the molar volume of the condensed phase as a function of pressure, a generalized correlation for the compressibilities of normal liquids derived by Chueh and Prausnitz (19) has been used for this purpose. The molar volume of liquid at a given temperature is expressed as a function of pressure as follows:

$$v_1 = v_{o1} \left[1 + n\beta^s (P - P_{o1})\right]^{-1/n} \qquad \text{(IV-10)}$$

where v_{o1} and P_{o1} are the saturated liquid molar volume and the vapor pressure of the condensed phase, β^s is the isothermal compressibility of the saturated liquid and n is an empirical constant.

The isothermal compressibility of the saturated liquid is given as

$$\beta^s = \frac{V_{c1}}{RT_{c1}} (1.0 - 0.89\omega^{\frac{1}{2}}) \left[\exp (6.9547 - 76.2853T_{R1} + 191.3060T_{R1}^2 - 203.5472T_{R1}^3 + 82.7361T_{R1}^4)\right] \qquad \text{(IV-11)}$$

where ω is Pitzer's acentric factor and is given by

$$\omega = - \log P_{R1} - 1.0 \qquad \text{(IV-12)}$$

and P_{R1} is the reduced vapor pressure of the component 1 evaluated at a reduced temperature of 0.7. Chueh and Prausnitz (19) have suggested use of a value of n in Equation (IV-10) of 9 for normal liquids. This value has been used in the present work. Equation (IV-11) is good for the temperature interval $0.4 \leq T_{R1} \leq 0.98$, which covers the temperature range of this work. Using Equation (IV-10), the first integral in Equation (IV-9) can be evaluated as:

$$\frac{1}{RT}\int_{P_{o1}}^{P} v_1\, dP = \frac{v_{o1}}{8\beta^s RT}\left[\left\{1 + 9\beta^s(P - P_{o1})\right\}^{8/9} - 1\right] \qquad \text{(IV-13)}$$

The evaluation of the remaining integrals in Equation (IV-9) requires an equation of state for the pure component and the gas mixture. The theoretical virial equation of state and the empirical Benedict-Webb-Rubin equation of state used in this work are described in the following section.

Virial Equation of State

The virial equation of state, originally proposed as an empirical equation of state, was later derived from statistical mechanics (23, 48). This equation truncated after the third virial coefficient is used in this work.

$$\frac{PV}{nRT} = 1 + \frac{nB}{V} + \frac{n^2C}{V^2} \qquad \text{(IV-14)}$$

The virial coefficient B and C in Equation (IV-14) are temperature dependent. These coefficients for a binary mixture are

$$B_m = y_1^2 B_{11} + 2y_1y_2B_{12} + y_2^2B_{22} \qquad \text{(IV-15)}$$

$$C_m = y_1^3 C_{111} + 3y_1^2y_2C_{112} + 3y_1y_2^2\, C_{122} + y_2^3C_{222} \qquad \text{(IV-16)}$$

By substituting Equation (IV-13), (IV-14), (IV-15) and (IV-16) into Equation (IV-9), one obtains the enhancement factor:

$$\ell n\ \phi = \frac{v_{o1}}{8\beta^s RT}\left[\{1 + 9\beta^s(P - P_{o1})\}^{8/9} - 1\right] + \frac{2B_{11}}{V_{o1}}$$

$$+ \frac{3C_{111}}{2V_{o1}^2} - \ell n\ Z_{o1} - \frac{2(y_1 B_{11} + y_2 B_{12})}{V_m}$$

$$- \frac{3(y_1^2 C_{111} + 2y_1 y_2 C_{112} + y_2^2 C_{122})}{2V_m^2} + \ell n\ Z_m + \ell n\ x_1 \qquad \text{(IV-17)}$$

This equation can be used for solid-gas equilibrium where solubility of component 2 in the solid phase and the compressibility of the solid are negligible. With these assumptions, the value of x_1 becomes unity and the first integral of Equation (IV-9) is simplified to

$$\frac{1}{RT}\int_{P_{o1}}^{P} v_1\, dP = \frac{v_1}{RT}(P - P_{o1}) \qquad \text{(IV-18)}$$

Calculation of Virial Coefficients

Second Virial Coefficient

Exact relationships between the virial coefficient and the intermolecular potential function have been established from statistical mechanics (23,48). If the intermolecular potential function is known, the second virial coefficients can be calculated from the following equation.

$$B(T) = \int_{r=o}^{r=\infty} \left(1 - \exp\left(-\frac{U(r)}{kT}\right)\right) d\, b_o\,(r) \qquad \text{(IV-19)}$$

where

$$b_o(r) = \frac{2\pi N_A}{3} r^3 \qquad \text{(IV-20)}$$

The Lennard-Jones (6-12) potential (48) and the Kihara core potential (59, 60) are used in the present work to calculate the second virial coefficients.

Lennard-Jones (6-12) Classical Model (LJCL)

The Lennard-Jones potential function (48) is given as

$$U(r) = 4\epsilon \left[\left(\frac{\sigma}{r}\right)^{12} - \left(\frac{\sigma}{r}\right)^{6} \right] \qquad \text{(IV-21)}$$

This function describes the attraction and repulsion energy between two spherical molecules with point masses and negligible volume. The variable r represents the distance between the two point masses, σ corresponds to the value of r at $U(r) = 0$, and ϵ is the minimum potential which occurs at $r = 2^{1/6}\,\sigma$.

Based on Equation (IV-19), Hirschfelder et al. (48) have expressed the second virial coefficients between molecules i and j as follows.

$$B_{ij} = (b_o)_{ij}\, B^{*}_{CL}\, (T^{*}_{ij}) \qquad \text{(IV-22)}$$

where

$$T^{*}_{ij} = \frac{T}{(\epsilon/k)_{ij}} \qquad \text{(IV-23)}$$

$$(b_o)_{ij} = \frac{2\pi N_A \sigma^{3}_{ij}}{3} \qquad \text{(IV-24)}$$

and the reduced second virial coefficient is given as

$$B^{*}_{CL}(T^{*}_{ij}) = \sum_{j=0}^{\infty} b^{(j)} (T^{*}_{ij})^{-(1+2j)/4} \qquad \text{(IV-25)}$$

where

$$b^{(j)} = -\left(\frac{2^{j+\frac{1}{2}}}{4\ j!}\right)\ \Gamma\left(\frac{2j-1}{4}\right) \qquad \text{(IV-26)}$$

Kirk (61) has calculated the values of $b^{(j)}$ up to 41 terms. The values were in good agreement with those of Hirschfelder et al. (48), except that $b^{(16)}$ was determined to be $-0.3386316 \times 10^{-5}$ as compared to $-0.33872440 \times 10^{-5}$ given by Hirschfelder et al. (48). The values of $b^{(j)}$ developed by Kirk have been used in this work.

The mixture rules for $(b_o)_{ij}$ and $(\varepsilon/k)_{ij}$ in Equation (IV-23) and (IV-24) are

$$(b_o)_{ij} = \frac{1}{8}\ (b_{oi}^{1/3} + b_{oj}^{1/3})^3 \quad \text{(Lorentz average)} \qquad \text{(IV-27)}$$

and

$$\left(\frac{\varepsilon}{k}\right)_{ij} = \left(\frac{\varepsilon}{k}\right)_i^{\frac{1}{2}}\ \left(\frac{\varepsilon}{k}\right)_j^{\frac{1}{2}} \quad \text{(geometric average)} \qquad \text{(IV-28)}$$

The selected parameters for the Lennard-Jones potential function to calculate the second virial coefficient in this work are shown in Table 19 of Appendix F.

Kihara Core Model (KIH)

The Kihara core potential (59,60) is given by the relation

$$U(\rho) = U_o\ \left[\left(\frac{\rho_o}{\rho}\right)^{12} - 2\ \left(\frac{\rho_o}{\rho}\right)^6\right] \qquad \text{(IV-29)}$$

This function takes into consideration the size and the shape of the molecules with an impenetrable core. The quantity ρ is the shortest distance between the cores, and ρ_o is the value of ρ when $U(\rho)$ is at its minimum.

In the Kihara core model, the molecular cores are described in terms of three parameters M_o, S_o, V_o. The carbon tetrafluoride and chlorotrifluoromethane molecules are assumed to have spherical cores (59, 98) in this work. The above parameters are related to the spherical core by the expressions

$$M_o = 4\pi a \tag{IV-30}$$

$$S_o = 4\pi a^2 \tag{IV-31}$$

$$V_o = (4/3)\pi a^3 \tag{IV-32}$$

where a is the radius of the core.

The hydrogen molecule is assumed to be a thin rod (59) in this work and the parameters are

$$M_o = \pi L \tag{IV-33}$$

$$S_o = 0 \tag{IV-34}$$

$$V_o = 0 \tag{IV-35}$$

where L is the length of the rod.

Taking into consideration the shape and the size of molecular cores, Kihara (59,60) has used Equations (IV-19) and (IV-29) to derive an expression of the pure and mixed second virial coefficients.

$$\frac{(B_k)_{ij}}{N_A} = \frac{2\pi}{3}(\rho_o)_{ij}^3 F_3 + \frac{M_{oi} + M_{oj}}{2}(\rho_o)_{ij}^2 F_2 + \left[\frac{S_{oi} + S_{oj}}{2} + \frac{M_{oi}M_{oj}}{4\pi}\right](\rho_o)_{ij} F_1 + \frac{M_{oi}S_{oj} + M_{oj}S_{oi}}{8\pi} + \frac{V_{oi} + V_{oj}}{2} \tag{IV-36}$$

where F_1, F_2, F_3 are functions of Z ($Z = (U_o)_{ij}/kT$) and can be calculated from the relations given by Kihara (59).

$$F_s = \sum_{j=0}^{\infty} b_s^{(j)} Z^{(6j+s)/12} \qquad \text{(IV-37)}$$

$$b_s^{(j)} = -\left(\frac{s}{12}\right)\left(\frac{2^j}{j!}\right)\Gamma\left(\frac{6j - s}{12}\right) \qquad \text{(IV-38)}$$

The first 40 values of $b_s^{(j)}$ for s = 1, 2, and 3 have been calculated by Mullins (87) and presented by Kirk (61). These values have been used in this work. The mixture rules assumed for the interaction parameters are

$$(\rho_o)_{ij} = \frac{(\rho_o)_i + (\rho_o)_j}{2} \qquad \text{(IV-39)}$$

$$(U_o)_{ij} = U_{oi}^{\frac{1}{2}} U_{oj}^{\frac{1}{2}} \qquad \text{(IV-40)}$$

DeBoer and Michels (24) have presented the following equation for the second virial coefficient with quantum corrections

$$B_{ij} = (B_k)_{ij} + (b_o)_{ij} \left[\Lambda_{ij}^{*2} B_I^* + \Lambda_{ij}^{*4} B_{II}^* - \Lambda_{ij}^{*3} B_o^* \right] \qquad \text{(IV-41)}$$

Prausnitz and Myers (98) pointed out that the quantum corrections in the calculation of the second virial coefficient are essential for light gases like helium, hydrogen, and neon, and the corrections are still necessary for mixtures of quantum and non-quantum gases. The correction terms in Equation (IV-41) are originally proposed for the Lennard-Jones model which is similar to the Kihara model with a

vanishing core. The reduced quantum mechanical parameter applied to the Kihara core potential is given as

$$\Lambda_{ij}^{*2} = \frac{h^2}{2k\sigma_{ij}^2 \, m_{ij} \, (U_o/k)_{ij}} \tag{IV-42}$$

where

$$\sigma_{ij} = 2^{-1/6} \, (\rho_o)_{ij} + \frac{M_{oi} + M_{oj}}{4\pi} \tag{IV-43}$$

$$m_{ij} = \frac{M_{ij}}{N_A} \tag{IV-44}$$

and

$$\frac{1}{M_{ij}} = \frac{1}{M_i} + \frac{1}{M_j} \tag{IV-45}$$

The two translational quantum correction terms B_I^* and B_{II}^* are given (48) as

$$B_I^* = \sum_{j=o}^{\infty} b_I^{(j)} (T^*)^{-(6j+13)/12} \tag{IV-46}$$

$$B_{II}^* = \sum_{j=o}^{\infty} b_{II}^{(j)} (T^*)^{-(6j+23)/12} \tag{IV-47}$$

where

$$b_I^{(j)} = -\left(\frac{11-36j}{768\pi^2}\right) \left(\frac{2^{(6j+13)/6}}{j!}\right) \Gamma\left(\frac{6j-1}{12}\right) \tag{IV-48}$$

$$b_{II}^{(j)} = -\left(\frac{3024j^2 + 4728j + 767}{491520\pi^4}\right)\left(\frac{2^{(6j+23)/6}}{j!}\right)$$

(continued)

$$\times \Gamma \left(\frac{6j + 1}{12} \right) \qquad \text{(IV-49)}$$

The values for the first 42 terms of $b_I^{(j)}$ and $b_{II}^{(j)}$ have been computed by Kirk (61). The values used differ only slightly from those given by Hirschfelder et al. (48). These values are used in this work. The ideal gas quantum correction B_o^* in Equation (IV-4) is given as

$$B_o^* = \frac{3}{32\pi^{5/2}(T^*)^{3/2}} \qquad \text{(IV-50)}$$

Kihara Core Model with K_{12} (KIHCK12 and KIHEK12)

Prausnitz et al.(16, 17, 31) have shown that a better representation of the interaction second virial coefficient data can be obtained if the geometric mixing rule for the Kihara energy parameter is corrected by a factor of $(1 - K_{12})$ in the mixing rule for $(U_o)_{12}$ as:

$$(U_o)_{12} = (1 - K_{12}) (U_o)_{12G} \qquad \text{(IV-51)}$$

where

$$(U_o)_{12G} = U_{o1}^{1/2} \; U_{o2}^{1/2} \qquad \text{(IV-52)}$$

Hiza and Duncan (50) have presented an experimental correlation of K_{12} as a function of ionization potential. The Kihara core model using a value of K_{12} based on the correlation of Hiza and Duncan is called KIHCK12 in this work. The Kihara core model using a value of K_{12} obtained by fitting the experimental interaction second virial coefficients, is called KIHEK12.

Third Virial Coefficient

The third virial coefficient is concerned with three-body interactions. By assuming pairwise additivity of potentials, the potential function can be written as:

$$U_{ijk} = U_{ij} + U_{ik} + U_{jk} + \Delta U_{ijk} \tag{IV-53}$$

where ΔU_{ijk} is a correction to the assumption of pairwise additivity of potentials.

Using this potential function, the classical third virial coefficient is written by Sherwood and Prausnitz (109) as

$$C = C^{add} + \Delta C \tag{IV-54}$$

where

$$C^{add} = -\frac{8\pi^2 N_A^2}{3} \iiint f_{12} f_{13} f_{23}\, r_{12} r_{13} r_{23}\, dr_{12} dr_{13} dr_{23}$$

$$\Delta C = -\frac{8\pi^2 N_A^2}{3} \iiint \exp\left[-\frac{\Sigma U_{ij}}{kT} \left\{ \exp\left(-\frac{\Delta U}{kT}\right) - 1 \right\} \right] \times r_{12} r_{13} r_{23}\, dr_{12} dr_{13} dr_{23} \tag{IV-55}$$

and

$$f_{ij} = \exp\left(-\frac{U_{ij}}{kT} \right) - 1 \tag{IV-56}$$

$$\Sigma U_{ij} = U_{12} + U_{13} + U_{23} \tag{IV-57}$$

If ΔU in Equation (IV-55) is zero, the non-additive term vanishes. The

numerical values of C^{add} have been calculated by Bird et al.(10), Bergeon (9), Kihara (57), Rowlinson et al. (107) and Sherwood and Prausnitz (109) using the Lennard-Jones potentials. Assuming a spherical core for the Kihara core potential, Sherwood and Prausnitz (109) have obtained values of C^{add}.

The non-additivity term ΔC is the sum of a dispersion and an overlap portion. Therefore

$$C = C^{add} + \Delta C(\text{overlap}) + \Delta C(\text{dispersion}) \qquad \text{(IV-58)}$$

The quantity ΔC(dispersion) has been calculated for the Lennard-Jones (6-12) potential by Fowler and Graben (34), Graben and Present (37), and Sherwood and Prausnitz (109). Similar calculations were performed by Sherwood and Prausnitz on the Kihara (6-12) potential. Sherwood and Prausnitz have demonstrated that ΔC(dispersion) is always positive and that its contribution becomes more significant at low temperatures.

The repulsive portion of the non-additivity contribution is ΔC (overlap). Graben et al.(38) and Sherwood et al.(108) have made calculations for the Lennard-Jones (6-12) potential. From their calculations, it is found that ΔC(overlap) is negative and its magnitude is nearly the same as that of ΔC(dispersion). Thus the net contribution of ΔC to the third virial coefficient is small and the usual expression for the third virial coefficient was used, namely,

$$C = C^{add} \qquad \text{(IV-59)}$$

Lennard-Jones (6-12) Classical Model (LJCL)

Using the Lennard-Jones model, the expression for the third virial

virial coefficient has been developed by Hirschfelder, et al.(48) as

$$C_{ijk} = C_{ijk}^{add} = (b_o)_{ijk}^2 \, C_{CL}^*(T_{ijk}^*) \qquad \text{(IV-60)}$$

where

$$C_{CL}^* \; (T_{ijk}^*) = \sum_{j=o}^{\infty} c^{(j)} \; (T_{ijk}^*)^{-(j+1)/2} \qquad \text{(IV-61)}$$

The above third virial coefficient does not include any non-additivity correction. The $c^{(j)}$ values used in this work have been computed by several investigators (9 , 10, 59, 107). Yoon (132) has calculated the values of $C_{CL}^*(T^*)$ based on different sets of $c^{(j)}$ values. He found that the $C_{CL}^*(T^*)$ values calculated from the Kihara's first 18 values of $c^{(j)}$ are in good agreement with those calculated by Bird et al.(10). The $c^{(j)}$ values given by Kihara (59) were used in this work. For mixtures the following mixing rules were used:

$$\left(\frac{\varepsilon}{k}\right)_{ijk} = \left(\frac{\varepsilon}{k}\right)_i^{1/3} \left(\frac{\varepsilon}{k}\right)_j^{1/3} \left(\frac{\varepsilon}{k}\right)_k^{1/3} \qquad \text{(IV-62)}$$

and

$$(b_o)_{ijk} = \frac{1}{27} \left[(b_o)_i^{1/3} + (b_o)_j^{1/3} + (b_o)_k^{1/3}\right]^3 \qquad \text{(IV-63)}$$

Method of Chueh and Prausnitz

A generalized corresponding states correlation has been presented by Chueh and Prausnitz (16) for estimating the third virial coefficient of pure and mixed non-polar gases. It is expressed as a function of reduced temperature and an empirical parameter d

$$\frac{C}{V_c^2} = f(T_R, d) \qquad \text{(IV-64)}$$

These authors presented the following empirical expression

$$\frac{C}{V_c^2} = (0.232\ T_R^{-0.25} + 0.468\ T_R^{-5}) \times (1 - e^{(1-1.89\ T_R^2)}) + de^{-(2.49-2.30\ T_R+2.70\ T_R^2)} \qquad \text{(IV-65)}$$

The parameter d is Equation (IV-64) is related to the size, shape and polarizability of the molecule. The value of d becomes important at reduced temperatures below 1.75. Some values of the parameter d have been presented by Chueh and Prausnitz (16). The values of d for methane, ethane, ethylene, carbon tetrafluoride, and chlorotrifluoromethane were obtained by Garber (35) and Yoon (132) using the experimental third virial coefficients available in the literature. The values obtained by Garber (35) and Yoon (132) were used in this work.

For the quantum gases, effective critical constants are used instead of the experimental critical constants. This is because of the configurational properties of these gases. Chueh and Prausnitz (16) used the following equations given by Gunn, Chueh and Prausnitz (39) to obtain the effective critical constants for light gases such as helium, neon, and hydrogen.

$$T_c = \frac{T_c^\circ}{1 + \frac{21.8}{MT}} \qquad \text{(IV-66)}$$

$$V_c = \frac{V_c^\circ}{1 - \frac{9.91}{MT}} \qquad \text{(IV-67)}$$

where T_c° = 43.6 K and V_c° = 51.5 cc/gm mole for hydrogen. In these equations M is the molecular weight.

The effective critical constants calculated from Equations (IV-65) and (IV-66) are used in Equation (IV-64) to calculate the third virial coefficients for light gases. For gas mixtures, Chueh and Prausnitz (16) recommended the following mixture rules to calculate the third virial coefficients.

$$C_{ijk} = (C_{ij}\, C_{ik}\, C_{jk})^{1/3} \tag{IV-68}$$

where

$$C_{ij} = (V_c)_{ij}^2\, f\left(\frac{T}{(T_c)_{ij}}, d_{ij}\right) \tag{IV-69}$$

For a binary mixture containing a classical gas 1 and a quantum gas 2, the binary critical constants are

$$(T_c)_{12} = \frac{(1 - K_{12})\, T_{c_1}^{\circ\frac{1}{2}}\, T_{c_2}^{\circ\frac{1}{2}}}{\left(1 + \frac{21.8}{M_{12}T}\right)} \tag{IV-70}$$

$$(V_c)_{12} = \frac{\left(V_{c_1}^{\circ 1/3} + V_{c_2}^{\circ 1/3}\right)^3}{8\left(1 - \frac{9.91}{M_{12}T}\right)} \tag{IV-71}$$

In this case,

$$d_{12} = \frac{d_1 + d_2}{2} \tag{IV-72}$$

and

$$M_{12} = \frac{2M_1 M_2}{M_1 + M_2} \qquad \text{(IV-73)}$$

The K_{12} used in Equation (IV-70) is the correction to the geometric mixing rule and is obtained from experimental interaction second virial coefficient data. The method of Chueh and Prausnitz (16) has been used to calculate all the third virial coefficients in the Kihara enhancement factor programs. Because of the large uncertainty of the third virial coefficient at $T_R < 0.8$, Equation (IV-65) is useful only for $T_R > 0.8$ as recommended by Chueh and Prausnitz (16). The values of C_{111}, C_{112} and C_{122} are set equal to zero when the effective reduced temperature is less than 0.8.

Benedict-Webb-Rubin Equation of State (BWR)

The Benedict-Webb-Rubin equation of state was originally developed for use with hydrocarbons and hydrocarbon mixtures. This equation of state is an empirical equation with eight parameters which can be adjusted to fit the volumetric properties of fluids. The BWR equation has also been used to predict phase equilibrium data of binary systems (43, 61, 62, 79, 87, 116, 117). The BWR equation for mixtures can be written as

$$P = \frac{RT}{V_m} + \frac{RTB'_m}{V_m^2} + \frac{RTC'_m}{V_m^3} + \frac{a_m \alpha_m}{V_m^6} + \frac{c_m (1+\frac{\gamma_m}{V_m^2}) \exp(-\frac{\gamma_m}{V_m^2})}{V_m^3 T^2} \qquad \text{(IV-74)}$$

The parameters B'_m and C'_m are defined as

$$B'_m = (B_o)_m - \frac{(A_o)_m}{RT} - \frac{(C_o)_m}{RT^3} \qquad \text{(IV-75)}$$

and

$$C'_m = b_m - \frac{a_m}{RT} \tag{IV-76}$$

The mixture rules used are

$$N_m = y_1^2 N_{11} + 2y_1y_2N_{12} + y_2^2 N_{22} \tag{IV-77}$$

for N = A_o, B_o, C_o, and γ. Values of N_{12} are given by

$$N_{12} = (N_1 N_2)^{\frac{1}{2}} \tag{IV-78}$$

for A_o, C_o, and γ. Values of $(B_o)_{12}$ are given by

$$(B_o)_{12} = \frac{B_{o1} + B_{o2}}{2} \text{ (linear)} \tag{IV-79}$$

$$(B_o)_{12} = \frac{1}{8} (B_{o1}^{1/3} + B_{o2}^{1/3})^3 \text{ (Lorentz)} \tag{IV-80}$$

The BWR equations using the linear average and the Lorentz average of $(B_o)_{12}$ are called BWR (LINEAR) and BWR(LORENTZ) respectively.

The mixture rules for a, b, c, and α are

$$N_m = y_1^3N_{111} + 3y_1^2y_2N_{112} + 3y_1y_2^2N_{122} + y_2^3N_{222} \tag{IV-81}$$

where

$$N_{ijk} = (N_iN_jN_k)^{1/3}. \tag{IV-82}$$

Combining Equation (IV-9), (IV-13) and (IV-74) for mixture and pure components, the enhancement factor is given as follows:

$$\ln \phi = \ln \frac{PV_m}{P_{o1}V_{o1}} + \frac{v_{o1}}{8\beta^s RT}\left[\{1 + 9\beta^s(P-P_{o1})\}^{8/9} - 1\right] \qquad \text{(IV-83)}$$

$$+ \frac{2B'_{11}}{V_{o1}} + \frac{3C'_{111}}{2V_{o1}^2} + \frac{6a_1\alpha_1}{5RTV_{o1}^5} + \frac{c_1}{RT^3\gamma_1} + \frac{c_1}{RT^3}$$

$$\times \exp\left(-\frac{\gamma_1}{V_{o1}^2}\right)\left[\frac{\gamma_1}{V_{o1}^4} + \frac{1}{2V_{o1}^2} - \frac{1}{\gamma_1}\right] - \frac{2[y_1(B'_{11}-B'_{12})+B'_{12}]}{V_m}$$

$$- \frac{3[y_1^2(C'_{111} - 2C'_{112} + C'_{122}) + 2y_1(C'_{112} - C'_{122}) + C'_{122}]}{2V_m^2}$$

$$- \frac{3(a_m\alpha_{1mm} + \alpha_m a_{1mm})}{5RTV_m^5} - \frac{3c_{1mm}}{RT^3\gamma_m} + \frac{2c_m\gamma_{1m}}{RT^3\gamma_m^2} + \frac{\exp(-\frac{\gamma_m}{V_m^2})}{RT^3}$$

$$\times \left(\frac{3c_{1mm}}{\gamma_m} - \frac{2c_m\gamma_{1m}}{\gamma_m^2} + \frac{3c_{1mm}}{2V_m^2} - \frac{2c_m\gamma_{1m}}{\gamma_m V_m^2} - \frac{c_m\gamma_{1m}}{V_m^4}\right)$$

$$+ \ln(\gamma'_1 x_1)$$

The mixing rules for α, a and c in Equation (IV-83) are

$$N_{1mm} = (N_1 N_m^2)^{1/3} \qquad \text{(IV-84)}$$

where N_m is given by Equation (IV-81).

For γ_{1m}, the mixing rule

$$N_{lm} = (N_l\ N_m)^{\frac{1}{2}} \tag{IV-85}$$

is used, where N_m is given by Equation (IV-77).

By expanding the exponential term in Equation (IV-74) and rearranging this equation into a virial form, the second and third virial coefficients can be expressed in terms of the parameters of the BWR equation as follows (61).

$$B_{ij} = (B_o)_{ij} - \frac{(A_o)_{ij}}{RT} - \frac{(C_o)_{ij}}{RT^3} \tag{IV-86}$$

$$C_{ijk} = b_{ijk} - \frac{a_{ijk}}{RT} + \frac{c_{ijk}}{RT^3} \tag{IV-87}$$

The second and third virial coefficients of hydrogen calculated from these equations are shown in Appendix F. The parameters of the BWR equation for the gases considered in this work are shown in Table 20 of Appendix F.

CHAPTER V

COMPARISON OF PREDICTED AND EXPERIMENTAL GAS PHASE EQUILIBRIUM DATA

Interaction Second Virial Coefficient

If sufficient P-V-T data are available for a pure gas, the interaction potential between the molecules can be determined. For gas mixtures, the interaction potential between dissimilar molecules is usually obtained by using the mixing rules to combine the potential energies of the pure gases.

The interaction second virial coefficient, which is related to the interaction potential between dissimilar molecules, plays a very important role in the calculation of thermodynamic properties of gas mixtures. Therefore, it is necessary to experimentally determine the interaction second virial coefficient and to test the mixing rules used to combine the potentials of pure gases, and to compare with the theoretical interaction second virial coefficients.

Various methods (12, 13, 20, 21, 125, 129) have been presented to obtain experimental values of the interaction second virial coefficient. The indirect method for the extraction of the interaction second virial coefficients from experimental phase equilibrium data used by Reuss and Beenakker (106), Chiu and Canfield (15), Mullins (87), Liu (73), Garber (35), and Yoon (132) is also used in this work.

Extraction of B_{12} from Phase Equilibrium Data

The enhancement factor equation (IV-17) can be rearranged to give the expression of B_{12} as

$$B_{12} = \frac{V_m}{2y_2}\left[\frac{2B_{11}}{V_{o1}} + \frac{3C_{111}}{2V_{o1}^2} - \ell n\ Z_{o1} - \frac{3}{2V_m^2}\left(y_1^2 C_{111} + 2y_1 y_2 C_{112} + y_2^2 C_{122}\right) + \frac{V_{o1}}{8\beta^s RT}\left\{(1 + 9\ \beta^s(P-P_{o1}))^{8/9} - 1\right\} - \frac{2y_1 B_{11}}{V_m} + \ell n\ Z_m + \ell n\ x_1 - \ell n\ \frac{Py_1}{P_{o1}}\right] \qquad (V\text{-}1)$$

To calculate the experimental values of B_{12}, the experimental gas and liquid compositions obtained in this work were used. Selection of the value of β^s and P_{o1} is discussed in Appendix F. Besides the mentioned quantities, the virial coefficients B_{11}, B_{22}, C_{111}, C_{222}, C_{112} and C_{122} are required for the calculation of B_{12}. Of these virial coefficients, B_{22} and C_{222} are implicitly involved in the V_m term. The second virial coefficients of the condensed phase B_{11} evaluated by the Lennard-Jones model and Kihara model have been used in this calculation for comparison. The second virial coefficient of hydrogen, B_{22}, was calculated from the Lennard-Jones parameters which were extracted from the experimental B_{22} of White and Johnston (128) and Michels *et al*. (81).

From Figure 50 in Appendix F the experimental C_{222} data of Michels *et al*. (81) and those of White and Johnston (128) are discrete from each other. The data of White and Johnston (128) are better described by the Lennard-Jones model, and the data of Michels *et al*. (81) are better described by the equation of Chueh and Prausnitz (16). Both the Lennard-

Jones model and the method of Chueh and Prausnitz (16) were used to calculate the values of C_{222}. Garber (35) and Yoon (132) showed that the method of Chueh and Prausnitz (16) fits the experimental values of C_{111} best for the condensed phases considered in this work. Therefore this method was used for the calculation of C_{111}, C_{122}, C_{112} when estimating the experimental B_{12} value. Since the interaction second virial coefficient is also implicitly involved in the V_m term, Equation (V-1) must be solved by an iterative scheme. The initial guess of the B_{12} value was calculated from the Kihara model. In this calculation, an initial estimate of the K_{12} value is also required. Since most hydrogen binary systems show very small values of K_{12}, $K_{12} = 0$ was used as the initial value for this calculation. The final values of B_{12} obtained at each experimental pressure were plotted isothermally against $(P - P_{o1})$. The actual value of B_{12} at the given temperature was taken to be the intercept of B_{12} at $(P - P_{o1}) = 0$. This was done by extrapolating the curve to $(P - P_{o1}) = 0$. The actual values of B_{12} obtained in this way at the experimental temperatures were then plotted on a set of theoretical B_{12} values calculated from the Kihara model as a function of temperature at the values of K_{12} from 0 to 1. A new value of K_{12} was obtained and used to calculate new values of B_{12}. This method has been described by Mullins (87), Liu (73),Garber(35) and Yoon(132). Since the K_{12} values of hydrogen systems are small, two iterations of the B_{12} program were sufficient to obtain the value of K_{12} which gave the best fit of the experimental B_{12} data.

Results of B_{12} Extraction from Phase Equilibrium Data

Two sets of experimental values of B_{12} were obtained for each of

the hydrogen-carbon tetrafluoride and the hydrogen-chlorotrifluoromethane systems. The first set of B_{12} values was obtained by using B_{11} and C_{222} calculated from the Lennard-Jones model. The second set was obtained by using the B_{11} values of the Kihara model and the C_{222} from the method of Chueh and Prausnitz (16).

Several other phase equilibrium data for hydrogen systems from the literature were used in this work to extract the experimental values of B_{12}. The B_{11} and C_{222} values of these systems are calculated from the Lennard-Jones model in the extraction of B_{12}.

The experimental B_{12} and the theoretical B_{12} from several theoretical models are presented from Figure 16 through Figure 20. The theoretical model used are LJCL, KIH, KIHCK12, BWR(LINEAR), BWR (LORENTZ). These models have been described in Chapter IV. The experimental B_{12} values of these systems obtained from this work are shown in Table 1 with the corresponding error range. The error range was estimated by varying the input values of $\emptyset$ and x_2 by the error assigned to these quantities for each system. The estimated data agreed with the experimental data to within the uncertainty shown.

B_{12} for Hydrogen-Carbon Tetrafluoride System and Hydrogen-Chlorotrifluoromethane System

No experimental data of B_{12} for the hydrogen-carbon tetrafluoride and the hydrogen-chlorotrifluoromethane systems have been found in the literature. The phase equilibrium data obtained in this work are the only source available for the extraction of B_{12} data of these two systems. The smoothed experimental data of $\emptyset$ and x_2 presented in Table

Table 1. Values of B_{12} for Hydrogen Binary Systems

System	T, K	B_{12}, cc/gm mole
H_2 - CF_4	94.94	-118.0 ± 4.0
	105.01	- 88.3 ± 4.0
	119.94	- 64.8 ± 4.0
	135.01	- 49.4 ± 4.0
	149.98	- 34.9 ± 4.0
	164.99	- 26.7 ± 4.0
H_2 - $CClF_3$	134.97	- 69.9 ± 3.0
	145.02	- 60.2 ± 3.0
	160.02	- 50.7 ± 3.0
	175.02	- 42.2 ± 3.0
	189.97	- 32.5 ± 3.0
	205.03	- 22.7 ± 3.0
	219.99	- 16.8 ± 3.0
H_2 - C_2H_4	122.00	- 59.3 ± 3.0
	130.00	- 51.0 ± 3.0
	149.70	- 31.2 ± 3.0
	169.75	- 18.0 ± 3.0

Table 1. (Continued)

System	T, K	B_{12}, cc/gm mole
H_2 - C_2H_6	108.00	-105.4 ± 4.0
	122.00	- 86.2 ± 4.0
	130.00	- 75.4 ± 4.0
	149.60	- 54.8 ± 4.0
	169.40	- 43.6 ± 4.0
	189.57	- 33.3 ± 4.0
H_2 - CH_4	90.74	- 79.5 ± 5.0
	103.07	- 60.5 ± 5.0
	109.98	- 54.8 ± 5.0
	116.53	- 48.0 ± 5.0
H_2 - Ar (87)	86.95	- 58.9
	94.21	- 49.5
	99.95	- 44.1
	105.01	- 40.1

13 and Table 14 of Appendix E were used to extract the B_{12} values of the systems. The uncertainty for the liquid compositions is 2 percent for both systems. The uncertainty for the enhancement factor is 2.5 percent for the hydrogen-carbon tetrafluoride system and 3 percent for the hydrogen-chlorotrifluoromethane. The experimental data of B_{12} and the theoretical values of B_{12} are shown on Figure 16 and Figure 17 for the hydrogen-carbon tetrafluoride system and the hydrogen-chlorotrifluoromethane system respectively. Since the constants of the BWR equation are not available for chlorotrifluoromethane, only the theoretical curve of the Lennard-Jones model and Kihara model are shown for the hydrogen-chlorotrifluoromethane system. The input data for the theoretical calculation are presented in Appendix F.

B_{12} for Hydrogen-Ethane System and Hydrogen-Ethylene System

The phase equilibrium data of Hiza, Heck and Kidnay (51, 52) were smoothed and used to extract the experimental B_{12} of the hydrogen-ethane and the hydrogen-ethylene systems. The physical properties of ethane and ethylene selected for use are presented in Appendix F. The input values of enhancement factor and liquid composition are shown in Table 15 and Table 16 in Appendix E for the hydrogen-ethane system and the hydrogen-ethylene system respectively. The experimental B_{12} and the theoretical B_{12} of these two systems are shown on Figure 18 and Figure 19. The uncertainties of $\emptyset$ and x_2 are 2 percent for both systems.

B_{12} for Hydrogen-Methane System

The phase equilibrium data of Kirk (61) have been used by Chiu and Canfield (15) to extract experimental values of B_{12}. Liu (73)

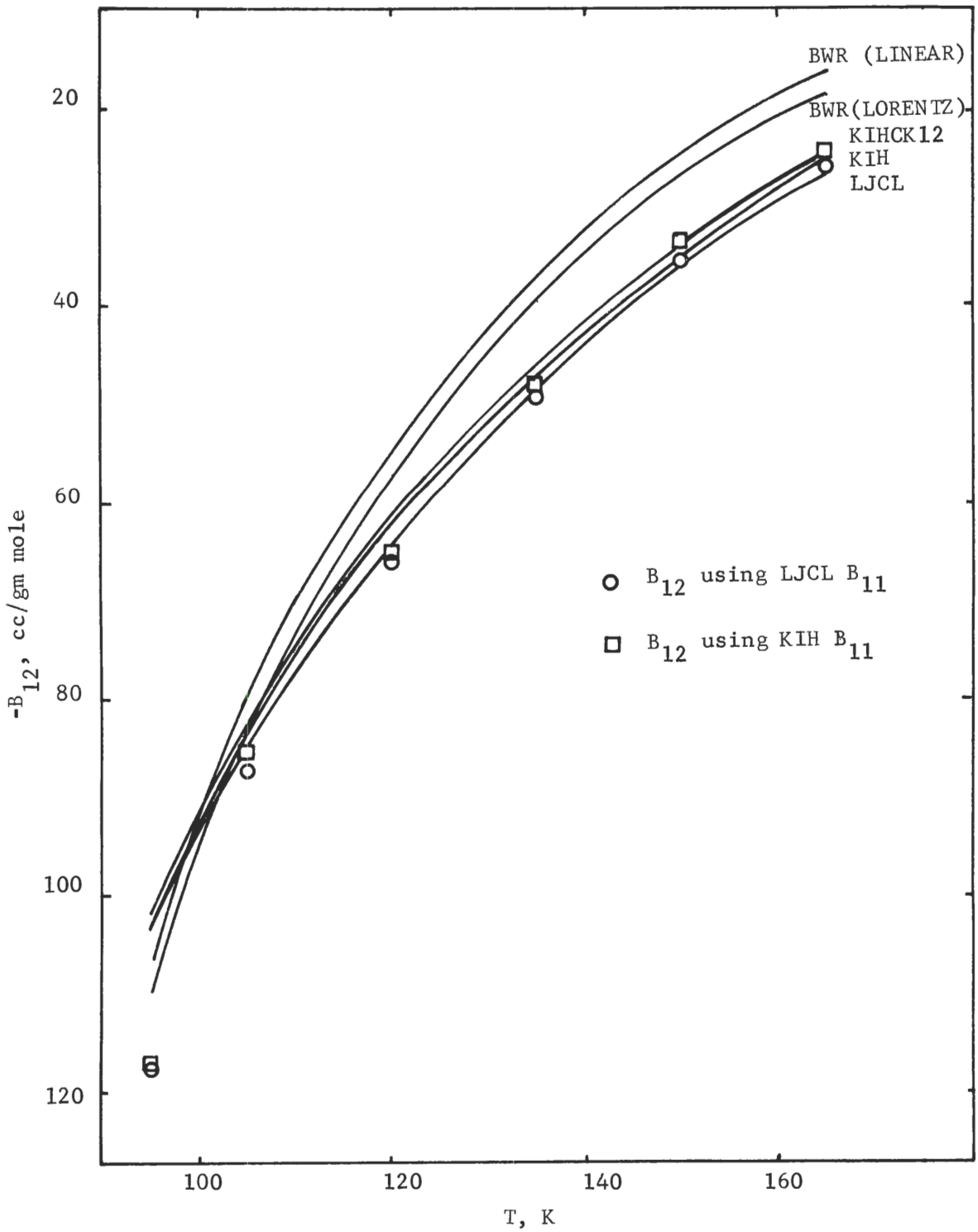

Figure 16. Predicted and Experimental B_{12} for the Hydrogen-Carbon Tetrafluoride System at Temperature Between 95 to 165 K.

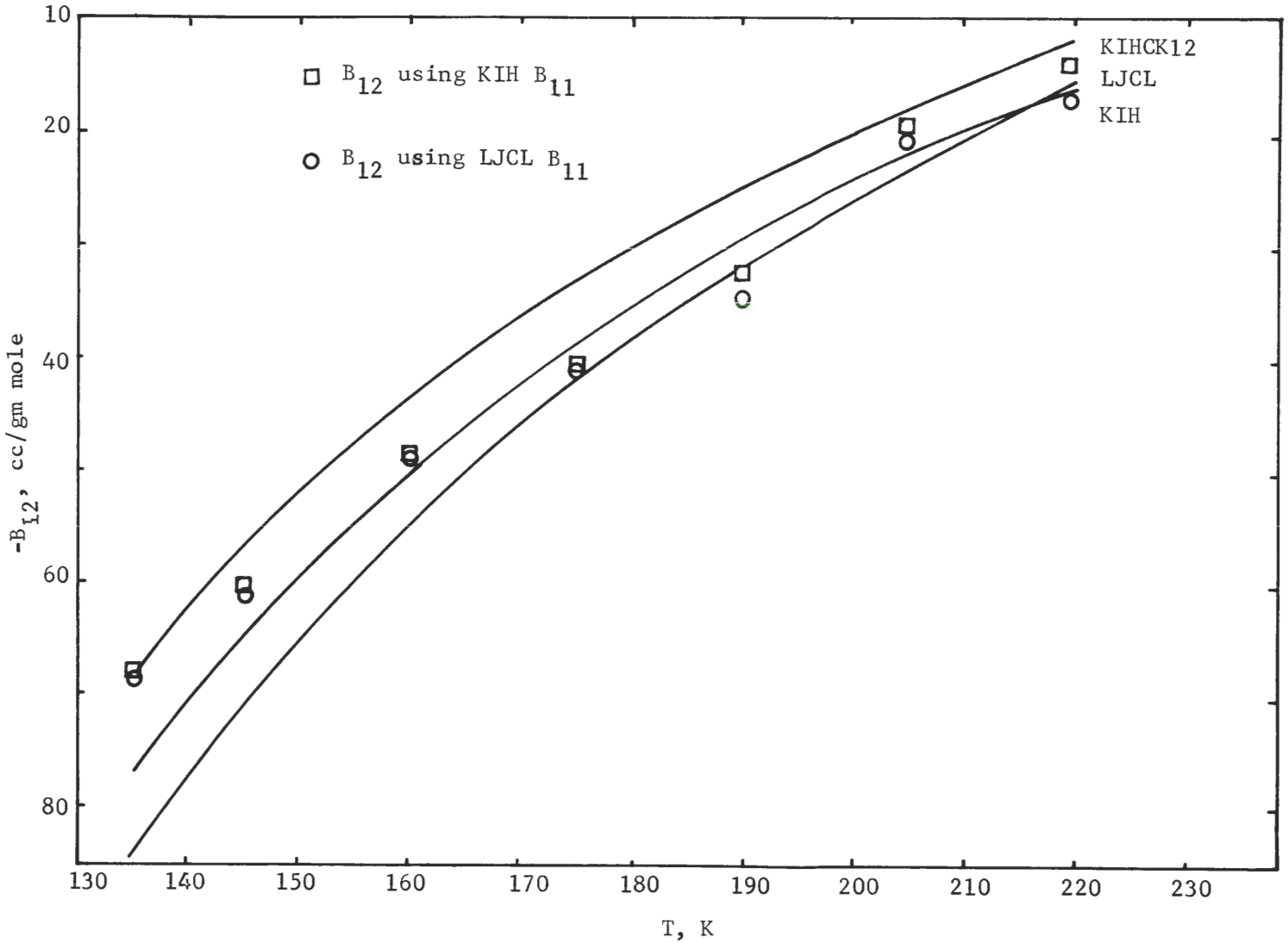

Figure 17. Predicted and Experimental B_{12} for the Hydrogen-Chlorotrifluoromethane System at Temperature Between 135 to 220 K.

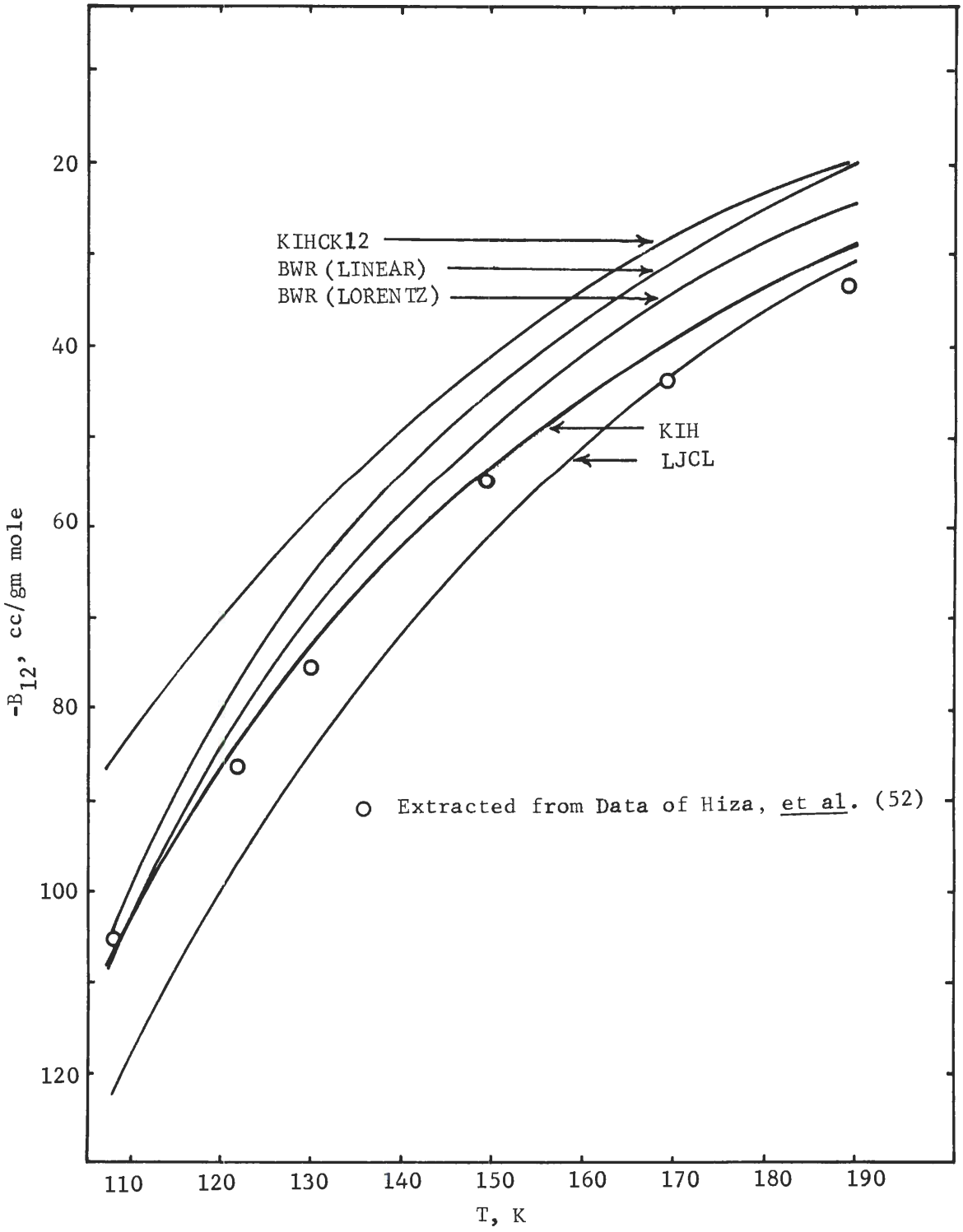

Figure 18. Predicted and Experimental B_{12} for the Hydrogen-Ethane System at Temperature Between 108 to 190 K

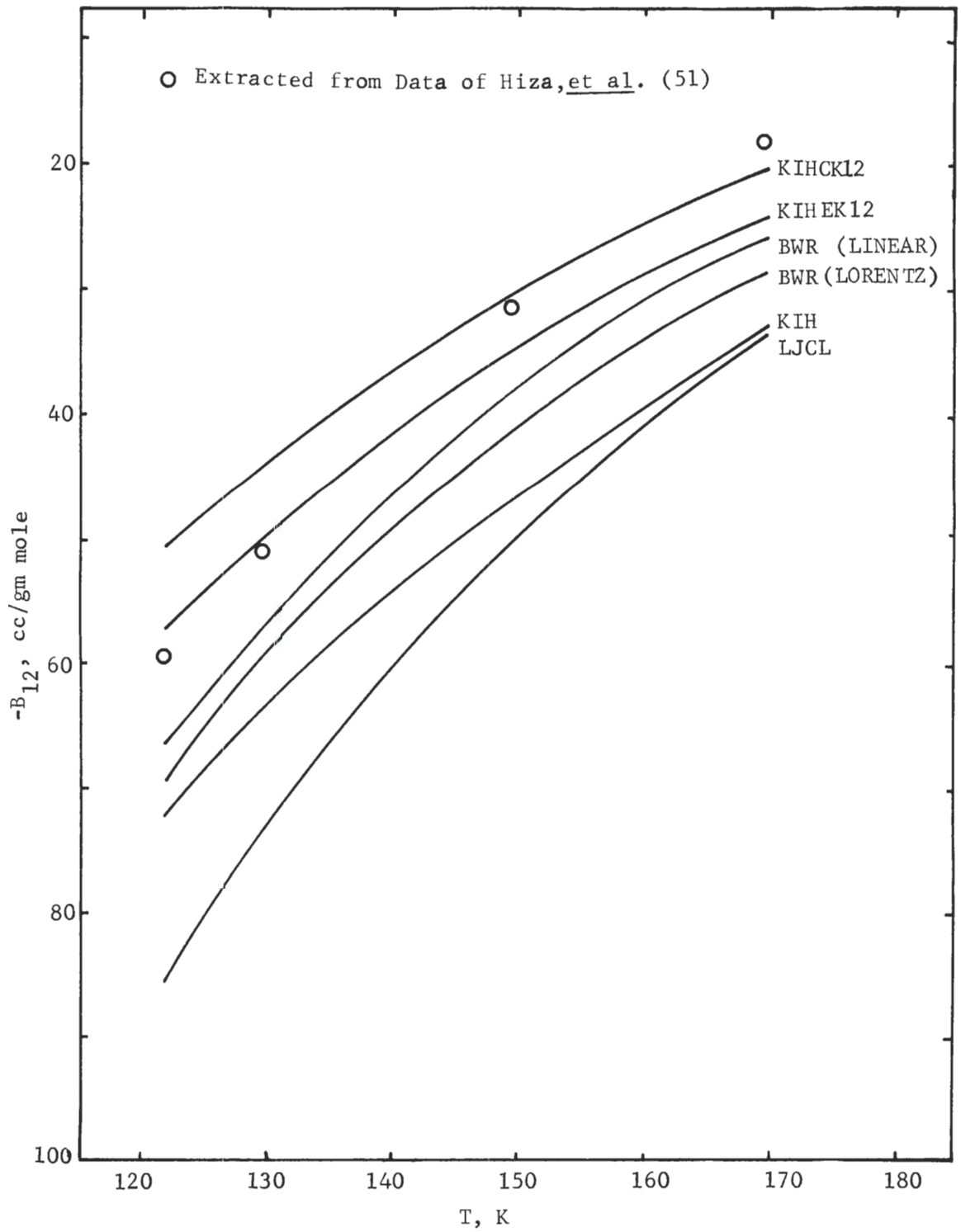

Figure 19. Predicted and Experimental B_{12} for the Hydrogen-Ethylene System at Temperature Between 122 to 170 K

also used these data to obtain the experimental B_{12} value at the highest temperature 116.53 K and the lowest temperature 66.88 K. Kirk's data are also used in this work to extract the B_{12} value at 90.74, 103.07, 109.98, 116.53 K. The method used in this work to extract the experimental B_{12} values is similar to the method used by Liu (73), except that the effect of pressure on the liquid molar volume and the input parameters for the potential function of hydrogen are different from those used by Liu (73). The physical properties selected are presented in Appendix F, and the smoothed $\emptyset$ and x_2 used in this calculation are shown in Table 17 of Appendix E. The uncertainty of the experimental $\emptyset$ and x_2 is 2 percent.

The B_{12} values extracted in this work agreed well with those of Chiu and Canfield (15) and Liu (73). The experimental B_{12} and theoretical B_{12} of this system are shown in Figure 20.

Discussion of Results

The experimental values of B_{12} for many helium systems have been summarized and analyzed by Liu (73), Garber (35), and Yoon (132). They pointed out that most experimental values of B_{12} for helium systems fall in the positive range, and a helium system with a condensed component of a less spherical molecule always show a larger value of B_{12} at the same reduced temperature T_{R1}. A plot of B_{12} values versus T_{R1} for six helium binary systems is shown in Figure 21.

The experimental values of B_{12} of the five hydrogen systems obtained in this work together with those of the hydrogen-argon system given by Mullins (87) are shown in Figure 22. For the six hydrogen systems summarized here, it was found that all the experimental B_{12}

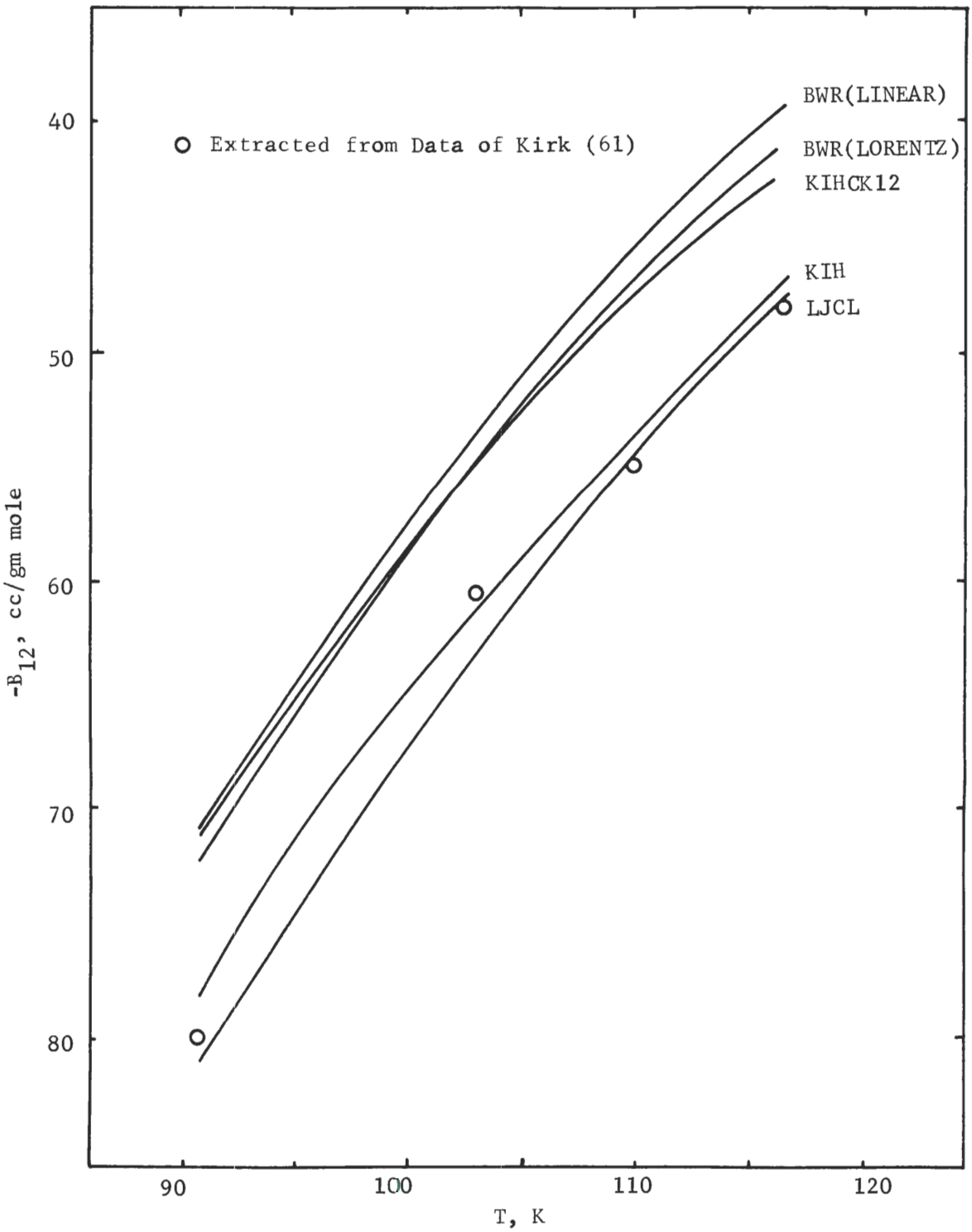

Figure 20. Predicted and Experimental B_{12} for the Hydrogen-Methane System at Temperature Between 90 to 116 K

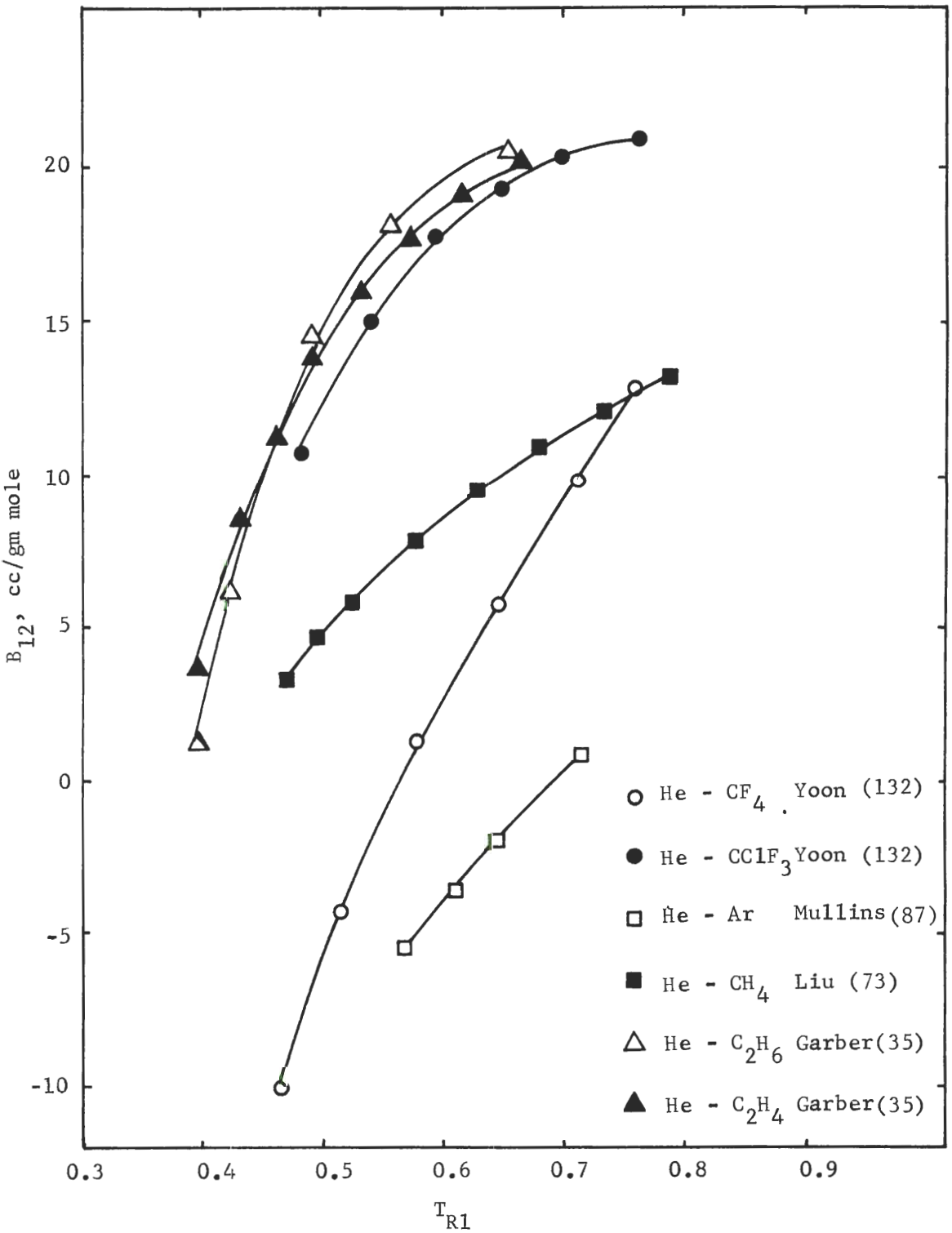

Figure 21. Experimental B_{12} for Six Helium Binary Systems.

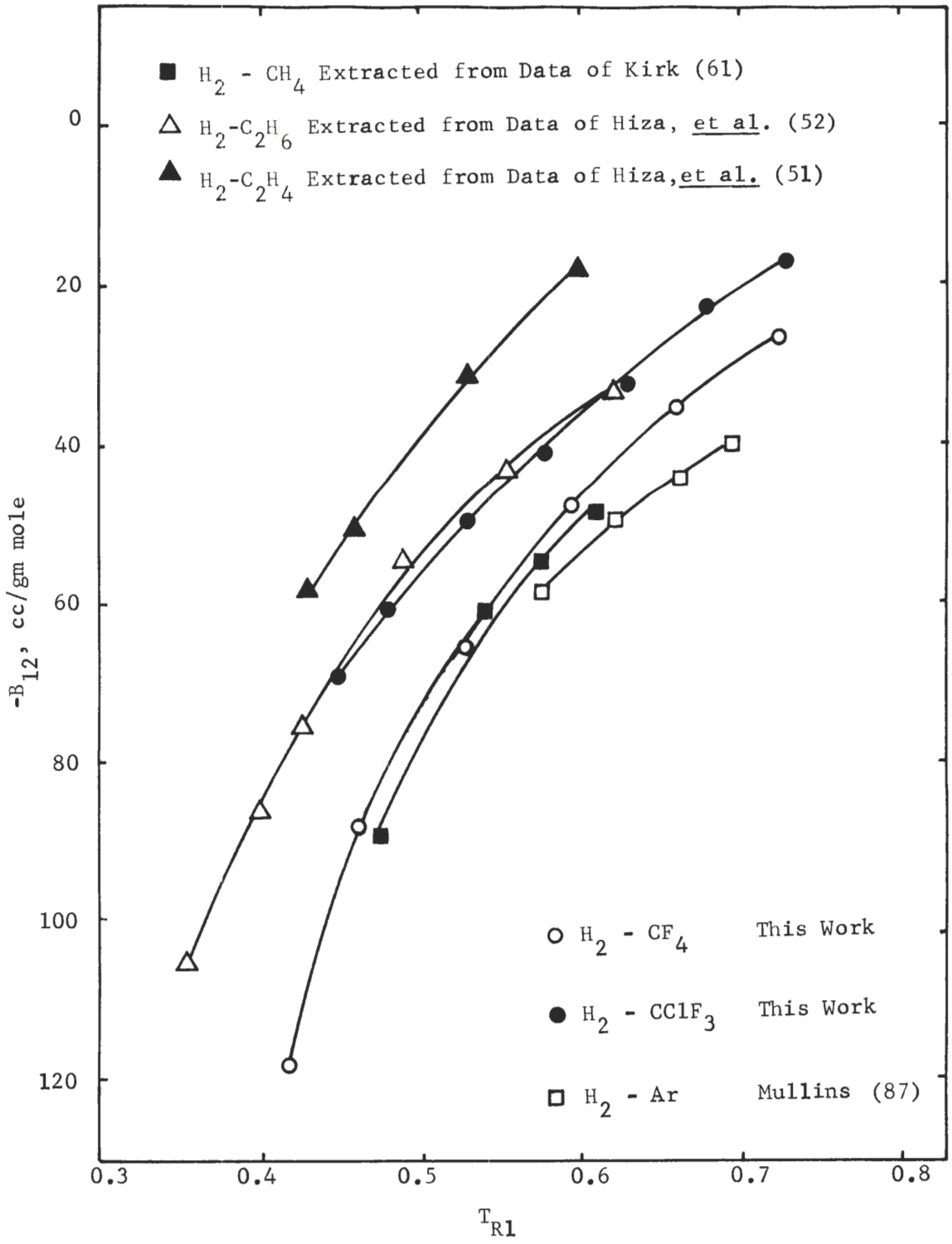

Figure 22. Experimental B_{12} for Six Hydrogen Binary Systems.

values fall in the negative range. Although the relative positions of the B_{12} curves for the various hydrogen systems are not identical with those of the corresponding helium systems, the B_{12} values of the hydrogen systems also show a tendency to increase as the molecule of the condensed component becomes less spherical.

In a comparison of a hydrogen system with a helium system for the same condensed component, the hydrogen system usually shows a more negative value of B_{12} than the helium system at the same temperature; and this accounts for the fact that the enhancement factors of a hydrogen system are higher than the corresponding helium system. The contribution of B_{12} to the enhancement factors will be discussed later in this chapter.

In Chapter III, it has been pointed out that at a given pressure and a reduced temperature T_{R1}, the enhancement factors of the helium systems and the hydrogen systems tend to decrease as the molecules of the condensed components become less spherical. In the comparison of the helium systems, the magnitude of the enhancement factors seems to be reflected by the magnitude of the B_{12} values. This is also true for the hydrogen systems.

Garber (35) also pointed out that the maxima in the B_{12} curves are not unusual in helium systems. The second virial coefficient curve for pure substances has been analyzed by Hirschfelder et al. (48). They pointed out these curves should pass through a maximum at high temperatures. A summary of the approximate temperature maximum for various helium binary systems has been presented by Garber (35). From the second virial coefficient curve, it shows that the slope of the

second virial coefficient versus temperature in the negative region of the second virial coefficients is much higher than the slope at the positive region of the second virial coefficients. The second virial coefficients always increase very rapidly as temperature increases in the negative region of the second virial coefficient. The experimental data of B_{12} of the hydrogen systems summarized here also show the same trend, and no maximum is expected in this temperature region.

In a comparison of the experimental B_{12} with those calculated from various theoretical models, the Kihara model usually represents the experimental values best whereas the BWR equation predicts higher values of B_{12}.

Deviation from Geometric Mixing Rule

To calculate the property data of a mixture, geometric mixing rules have been used to combine the energy parameters of the pure components of the mixture. Numerous investigators (18, 35, 49, 50, 54, 55, 87, 110) have shown that the mixture data for many binary systems cannot be satisfactorily represented using the geometric rules to combine the energy parameter of the pure components. Mullins (87), Garber (35), Chueh and Prausnitz (16), Eckert, et al. (31), Hiza and Duncan (49), Hiza (50) and Yoon (132) have shown that better mixture data can be obtained by empirical adjustment of the mixture energy parameter. They used the following mixing rule to calculate the interaction energy parameter for the Kihara core potential.

$$(U_o)_{12} = (1-K_{12})(U_{o1}\, U_{o2})^{1/2} \qquad \text{(V-2)}$$

where K_{12} is a correction factor for the mixing rule.

A similar mixing rule was used by Liu (73) for the calculation of the interaction energy parameter for the Lennard-Jones potential, that is,

$$\epsilon_{12} = (1-K_{LJ})(\epsilon_1 \quad \epsilon_2)^{1/2} \tag{V-3}$$

Since the Lennard-Jones parameters are very sensitive to temperature as stated by Lin and Robinson (72) and Hanley and Klein (42), it is of less interest to have the correction for the interaction energy parameters of this model. The parameters of the Kihara core potential function have less temperature dependency. Therefore, the correction of the interaction energy parameter of this model has attracted much attention and has been proved to be more meaningful.

From the following equation derived by Hudson and McCoubrey (54) for the energy parameter of the Lennard-Jones (6-12) potential function,

$$\epsilon_{12} = \left[\frac{2(I_1 I_2)^{1/2}}{I_1 + I_2}\right] \quad \left[\frac{2^6 \sigma_1^3 \quad \sigma_2^3}{(\sigma_1 + \sigma_2)^6}\right] \quad (\epsilon_1 \epsilon_2)^{1/2} \tag{V-4}$$

it can be seen that the product of the ionization potential and the collision diameter terms is related to the $(1-K_{LJ})$ term in Equation (V-3). Equation (V-3) is a reduced form of Equation (IV-27) with K_{LJ} = 0 which is equivalent to Equation (V-4) of two components with the same values of ionization potential and the same values of collision diameter.

Hiza (49) has proposed an empirical relation for computing K_{12} of Equation (V-2) which involves the ionization potential of the

interacting species as follows,

$$K_{12} = 0.17\ (I_2-I_1)^{1/2}\ \ln\ (I_2/I_1) \qquad (V\text{-}5)$$

This correlation was developed by empirically fitting the experimental values of B_{12} for a number of helium,hydrogen and neon binary systems (49).

The K_{12} values for the Kihara core potential of several helium binary systems have been experimentally determined by Hiza and Duncan (50), Hiza (49), Garber (35), and Yoon (132). The experimental results were compared with the values calculated from Equation (V-5). In spite of the temperature dependency of K_{12} as pointed by Hiza and Duncan (50), the results of helium-hydrocarbon systems are in good agreement. The experimental K_{12} values for the helium-halogen-substituted-methane systems are lower than the values predicted from Equation (V-5). This may be due to the uncertainty in the ionization potential I_1.

The K_{12} values for several hydrogen systems have also been presented by Mullins (87), Hiza (49),and Hiza, Heck and Kidnay(51,52). They found that the K_{12} values of the hydrogen system are quite small and are independent of temperature. The corrections for the two hydrogen-halogen-substituted-methane systems found in this work are negligibly small and independent of temperature. The K_{12} values of several hydrogen binary systems obtained from this work are shown in Table 2. The K_{12} values calculated from Equation (V-5) are also shown in the same table.

The method used to extract the K_{12} values from experimental data have been given in the early part of this chapter. The experimental results of this work are in good agreement with those obtained by other

investigators. The average values of the experimental K_{12} determined for each of the H_2 - X (X = Ar, CH_4, CF_4, $CClF_3$, C_2H_6) systems are always less than 0.02 and K_{12} = 0 is selected for these systems. The calculated K_{12} for the hydrogen systems, except the H_2 - C_2H_6 and H_2 - C_2H_4 systems, are also small. This reveals that the correction to the geometric mixing rule for these systems is negligible.

Table 2. Values of K_{12} for Hydrogen Systems

Gas	I	Calculated from Equation (V-5)	Experimental (This Work)	
H_2	15.426 (127)			
CF_4	15.00 (64)	0.003	0.0	
$CClF_3$	12.91 (127)	0.048	0.0	
Ar	15.76 (104)	0.000		0.00(87)
CH_4	12.98 (127)	0.046	0.0	0.03(49)
C_2H_6	11.65 (127)	0.093	0.0	0.02(50)
C_2H_4	10.52 (127)	0.144	0.1	0.07(49)

Enhancement Factor

The enhancement factors for the hydrogen-carbon tetrafluoride system have been predicted by using the theoretical models designated as LJCL, KIH, KIHCK12, BWR(LINEAR), and BWR(LORENTZ). Because BWR parameters were not available for the hydrogen-chlorotrifluoromethane system, only LJCL, KIH, and KIHCK12 models were used to calculate the enhancement factors for this system. These models have been

discussed in Chapter IV. Since the experimental values of K_{12} for these two systems were found to be zero, the KIHEK12 model is identical to the KIH model. The predicted enhancement factors using these models are presented in Table 13 and Table 14 of Appendix E, where they are compared with smoothed experimental values.

Among the six theoretical models, the LJCL, KIH, KIHCK12, KIHEK12 models are calculated by using the virial equation of state with different potential functions and different mixing rules; the BWR(LINEAR) and BWR(LORENTZ) models are calculated from the BWR equation with a different mixing rule for B_o. The Lennard-Jones (6-12) potential is used to evaluate all the virial coefficient for the LJCL model. For the KIH, KIHCK12, KIHEK12 models, Kihara potential was used to calculate the virial coefficients. These three models differ only in the calculation of B_{12}, C_{112} and C_{122}. The BWR(LINEAR) and the BWR(LORENTZ) model differ only in the combination of B_{o1} and B_{o2}.

Two representative isotherms of each system are presented in Figure 23 through Figure 26 for comparison. For the hydrogen-carbon tetrafluoride system, none of the theoretical models can represent the experimental data for the entire temperature range. The KIH and KIHCK12 models always predict values of the enhancement factor higher than those experimentally determined. In the low temperature region, the KIHCK12 model represents the experimental values better than the other models. As the temperature increases the BWR(LINEAR) and BWR (LORENTZ) models are better able to predict the experimental data. At the high temperature region, the LJCL model represents the experimental data best, the other models predict the enhancement factor to be

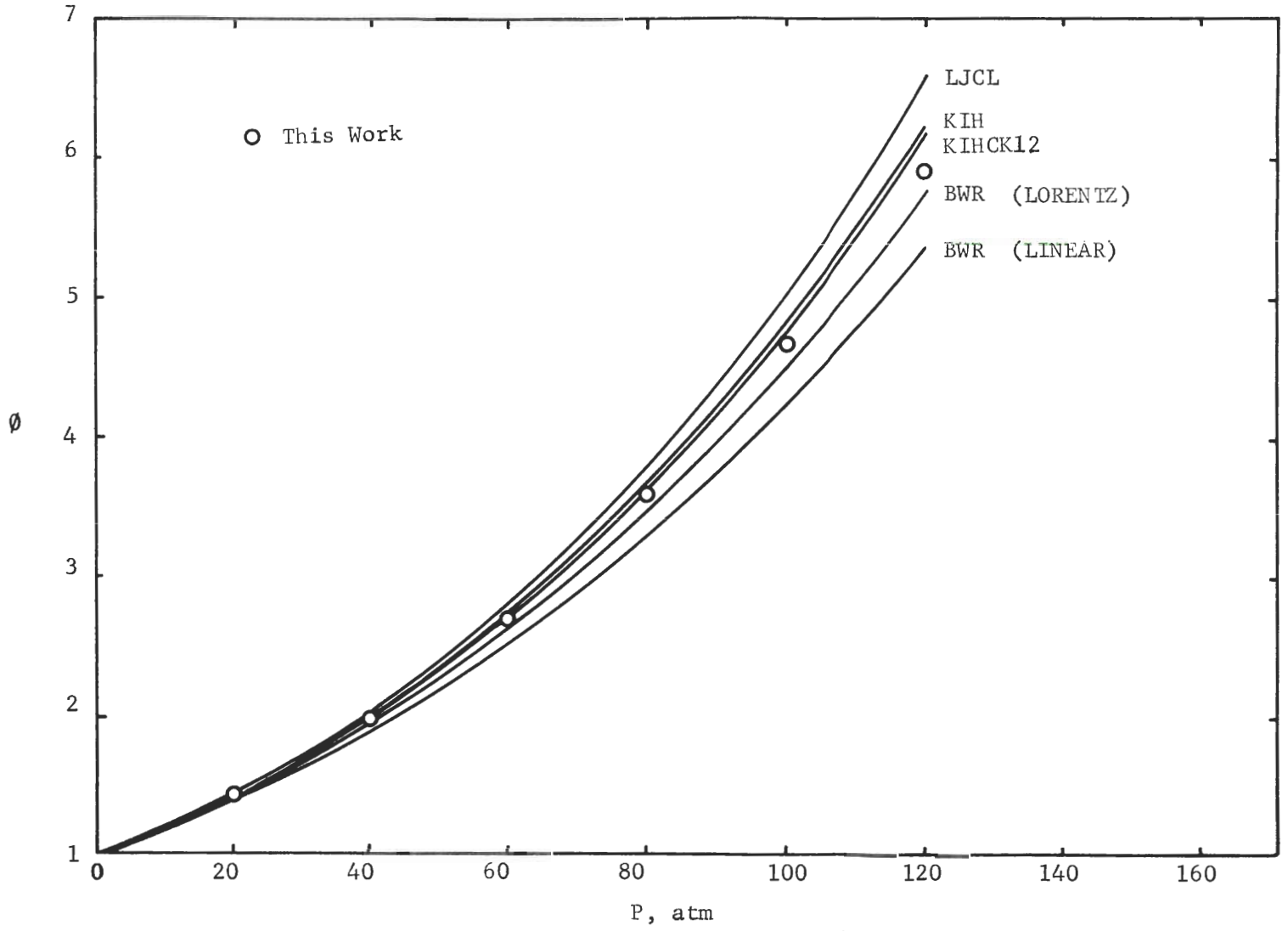

Figure 23. Theoretical and Experimental Enhancement Factors in the Hydrogen-Carbon Tetrafluoride System at 119.94 K

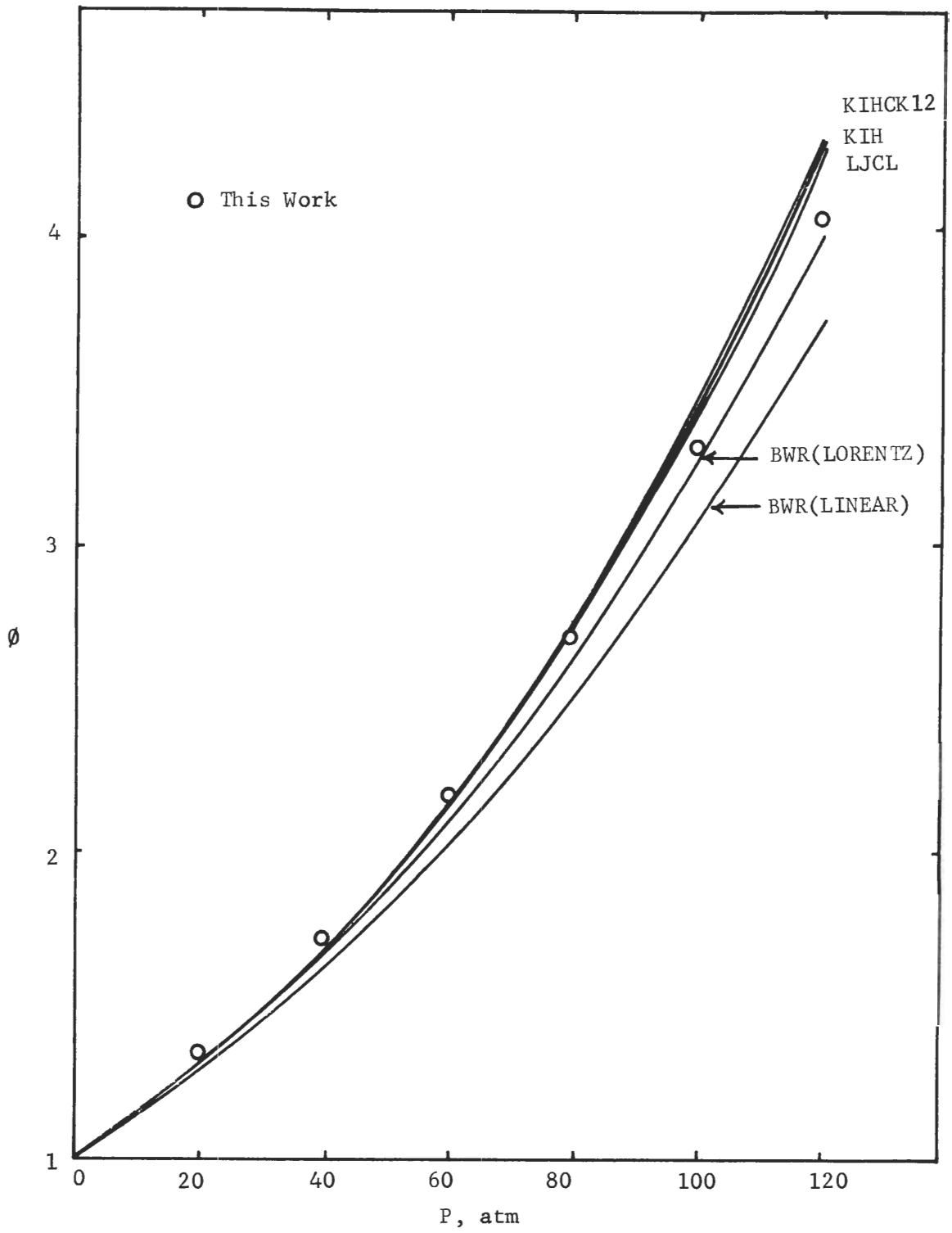

Figure 24. Theoretical and Experimental Enhancement Factors in the Hydrogen-Carbon Tetrafluoride System at 135.01 K.

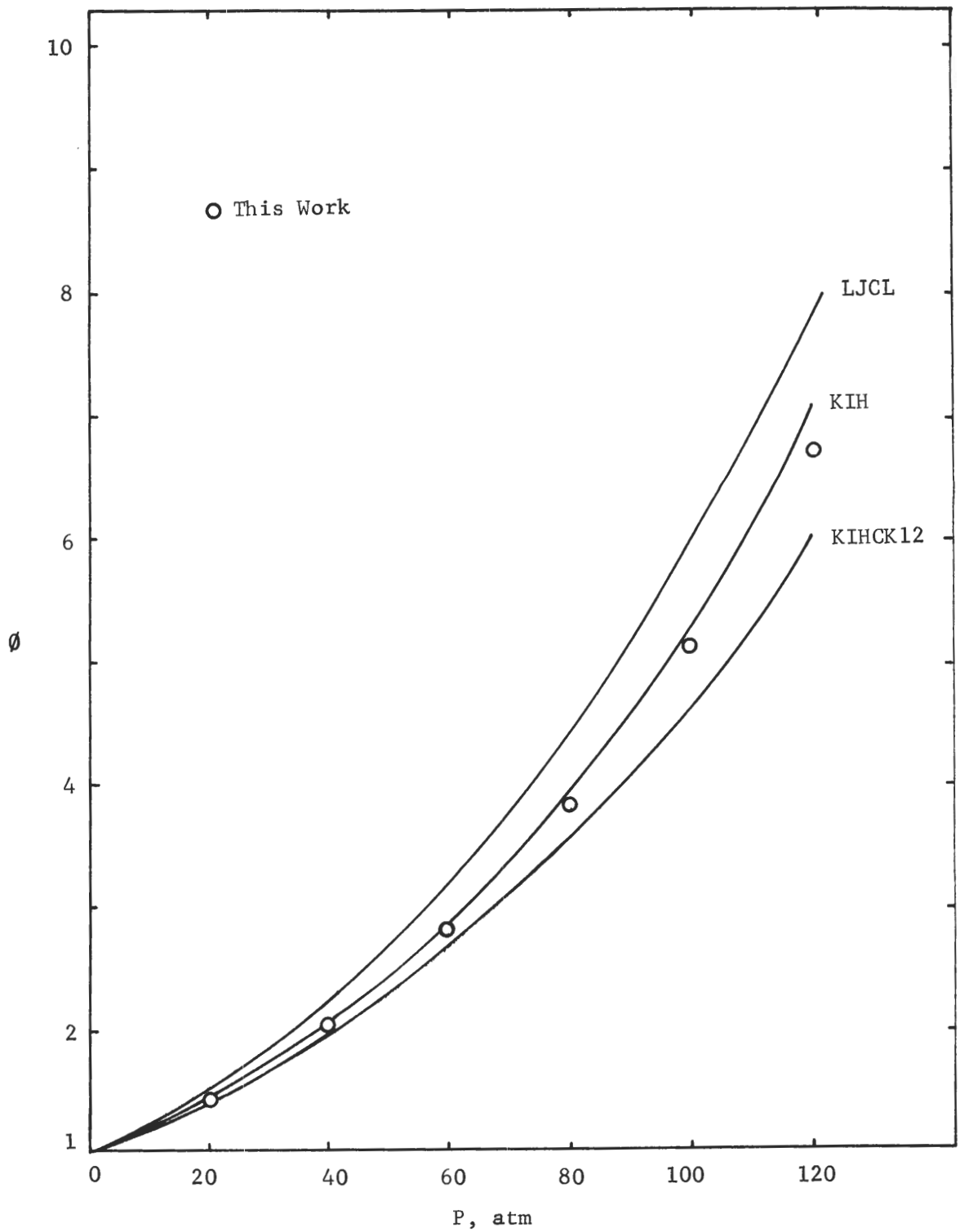

Figure 25. Theoretical and Experimental Enhancement Factors in the Hydrogen-Chlorotrifluoromethane System at 134.97 K.

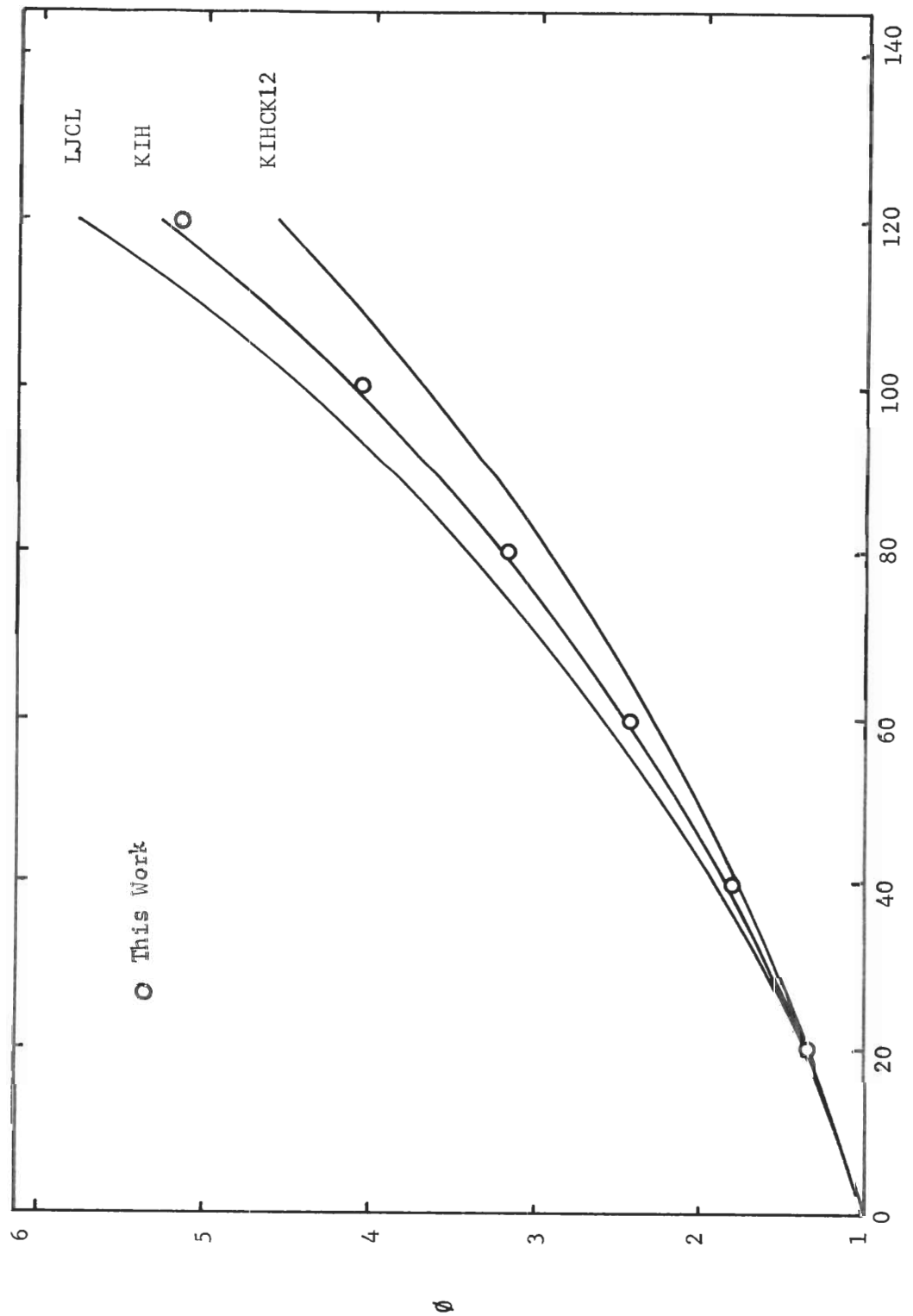

Figure 26. Theoretical and Experimental Enhancement Factors in the Hydrogen-Chlorotrifluoromethane System at 145.02 K.

higher than the experimental values in the high temperature region. In the low temperature region, the LJCL model predicts the experimental values too high by 35 percent. For the hydrogen-chlorotrifluoromethane system the experimental enhancement factors usually fall between the predicted values of the KIH model and the KIHCK12 model. The LJCL model predicts values of the enhancement factor higher than the experimentally determined values in the low temperature region but becomes a better model to represent the experimental data in the high temperature region. The LJCL model predicts values of enhancement factor too high by 20 percent in the low temperature region.

Representative isotherms of the hydrogen-ethane system (52) and the hydrogen-ethylene system (51) are shown in Figure 27 and Figure 28, respectively. The predicted values for these and other isotherms are presented in Table 15 and Table 16 of Appendix E. It is to be noted that, although none of the theoretical models predict the enhancement factor too well, all theoretical values follow the same trends as the experimental values. This is also found in the helium systems (35, 44, 50, 87, 132). Therefore, it seemed interesting to compare the helium systems with the hydrogen systems in terms of their theoretical models.

The helium carbon tetrafluoride system studied by Yoon (132) and the hydrogen-carbon tetrafluoride system of this work are selected for this comparison. Figures 29, 30, 31, 32 and 33 show the differences between the two systems. The theoretical curves of the two systems shown in these figures are calculated from the KIH model. These figures show that the experimental data follow the same trends as the

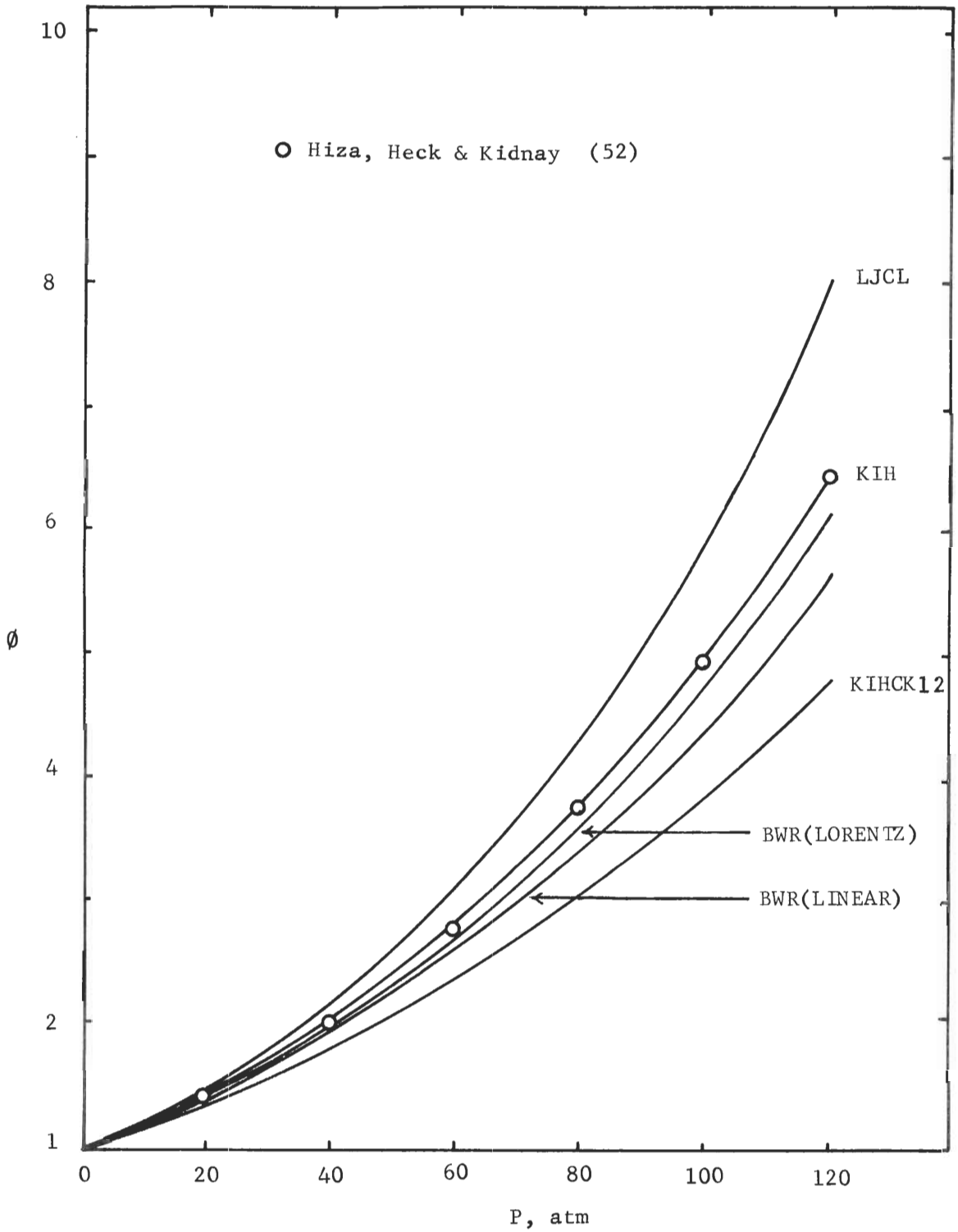

Figure 27. Theoretical and Experimental Enhancement Factors in the Hydrogen-Ethane System at 130.00 K.

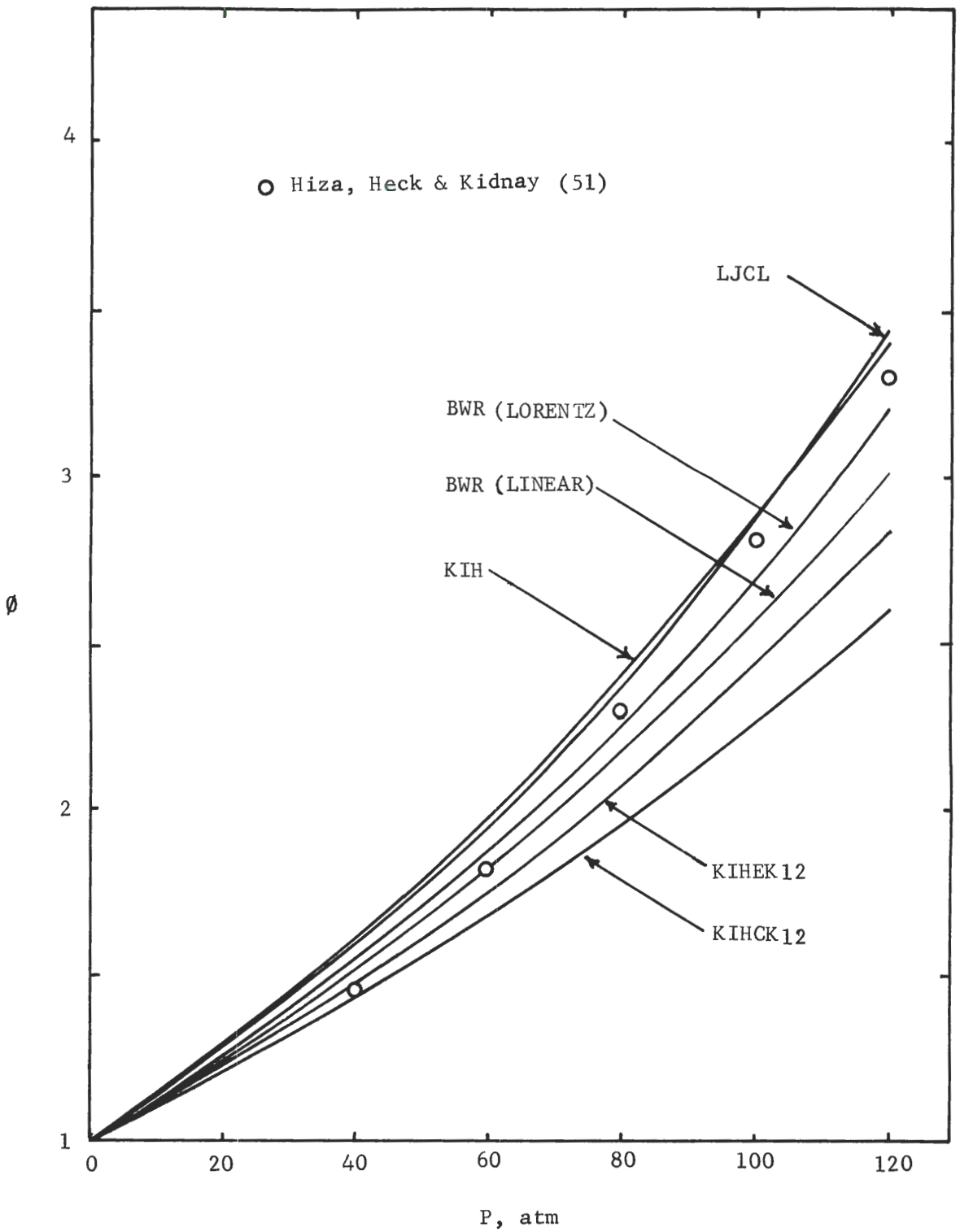

Figure 28. Theoretical and Experimental Enhancement Factors in the Hydrogen-Ethylene System at 149.70 K.

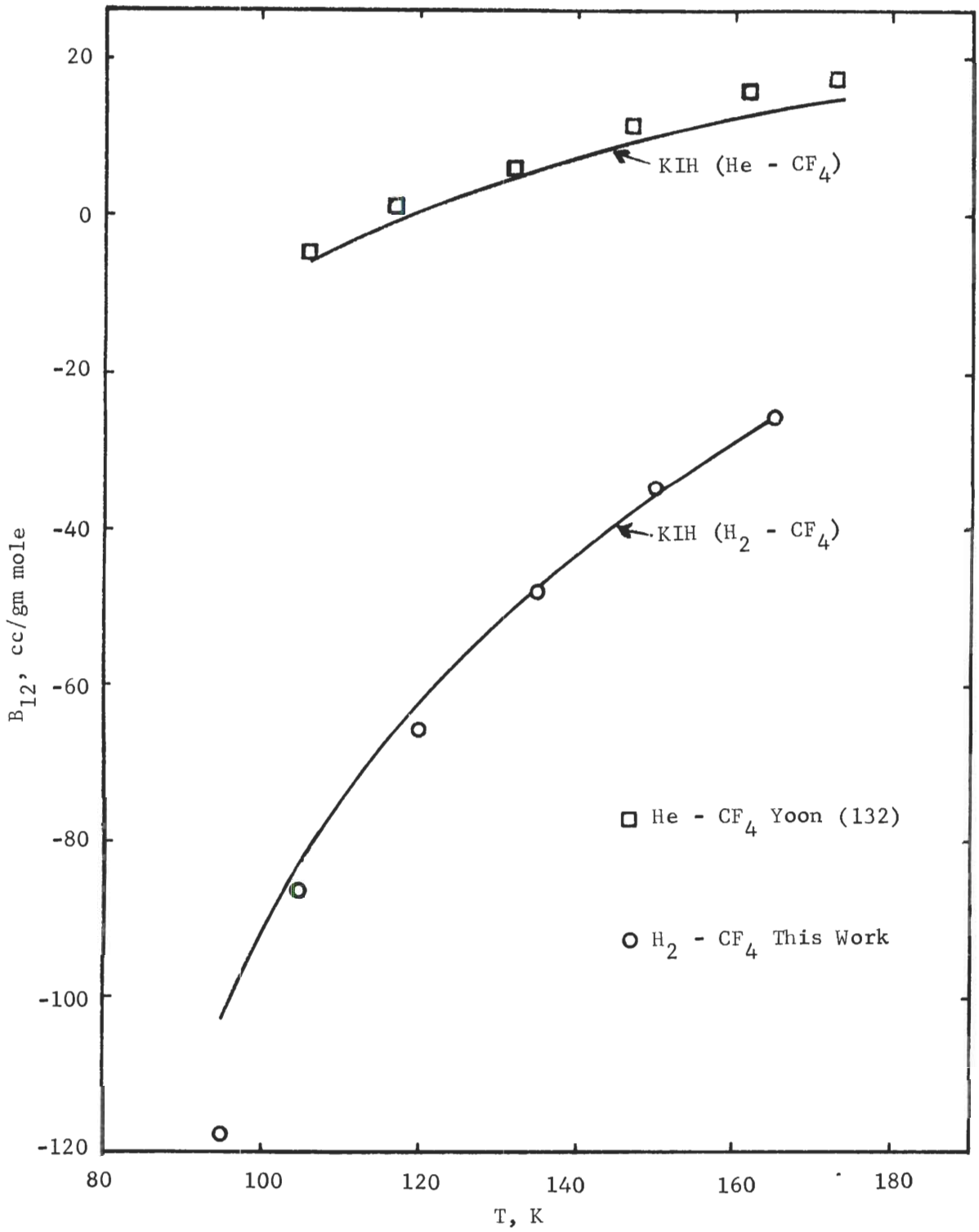

Figure 29. Comparison of B_{12} for the Hydrogen-Carbon Tetrafluoride and Helium-Carbon Tetrafluoride Systems.

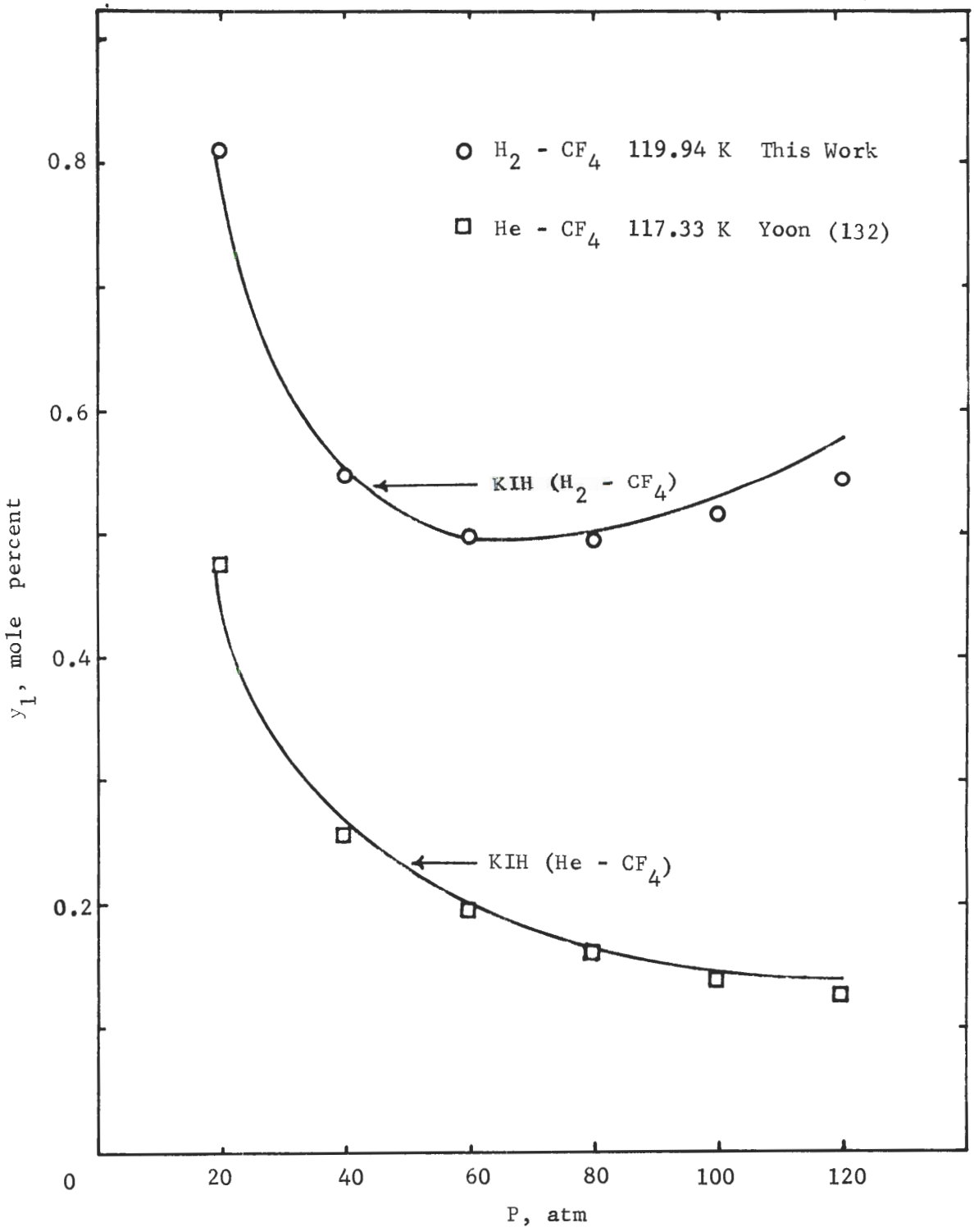

Figure 30. Comparison of the Gas Phase Compositions of the Hydrogen-Carbon Tetrafluoride and Helium-Carbon Tetrafluoride Systems.

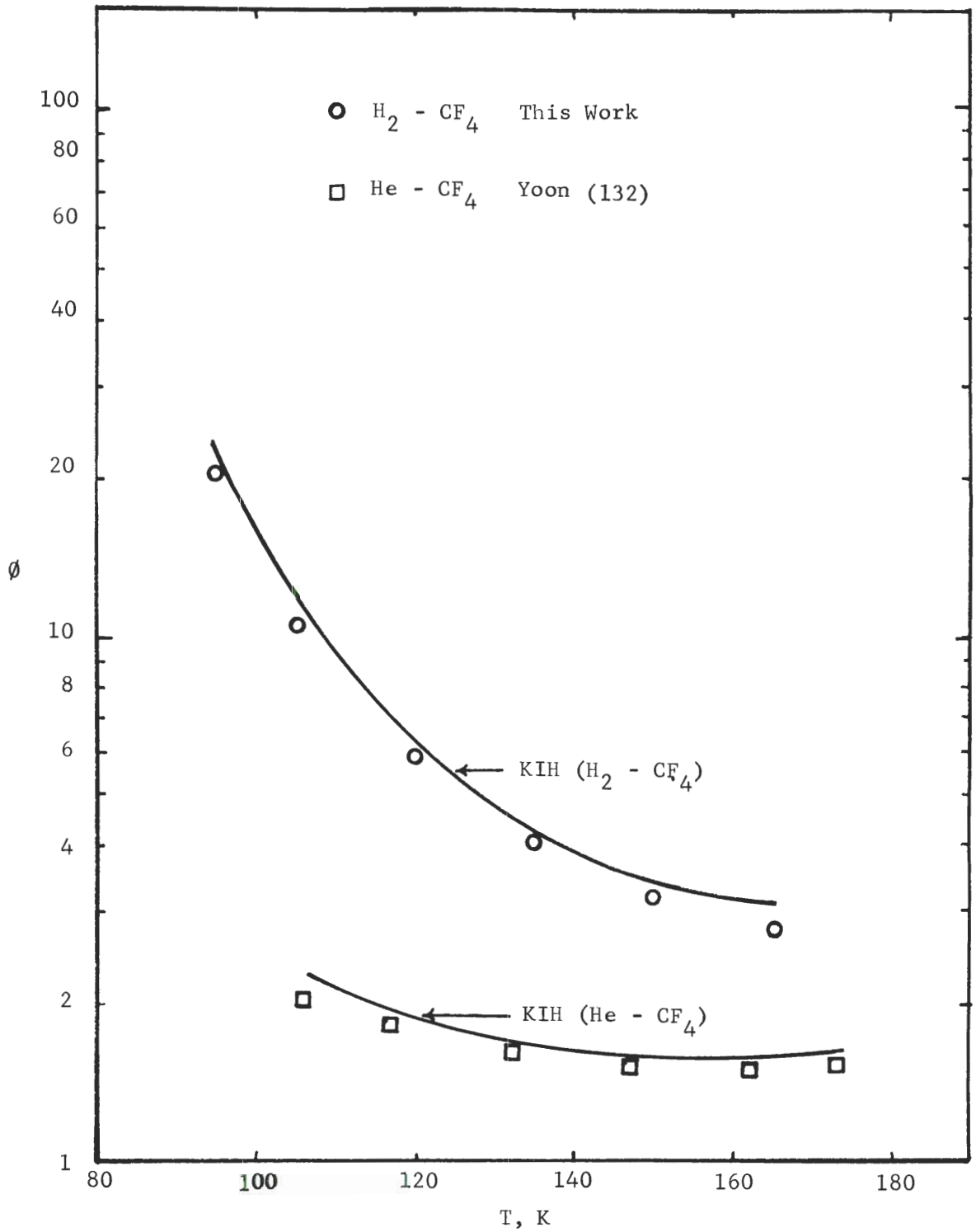

Figure 31. Comparison of the Enhancement Factors at 120 atm for the Hydrogen-Carbon Tetrafluoride and Helium-Carbon Tetrafluoride Systems.

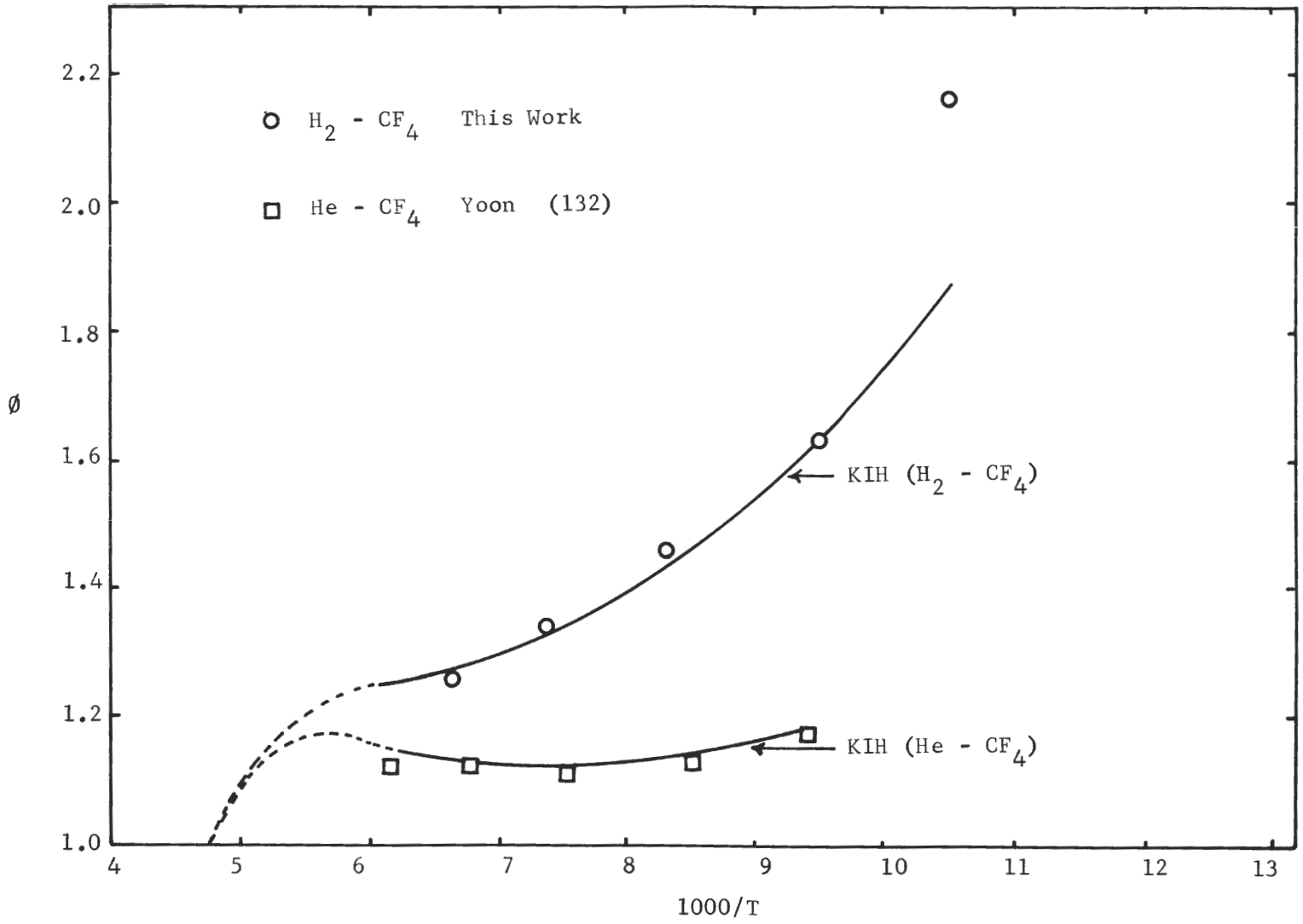

Figure 32. Comparison of the Enhancement Factors at 20 atm for the Hydrogen-Carbon Tetrafluoride and Helium-Carbon Tetrafluoride Systems.

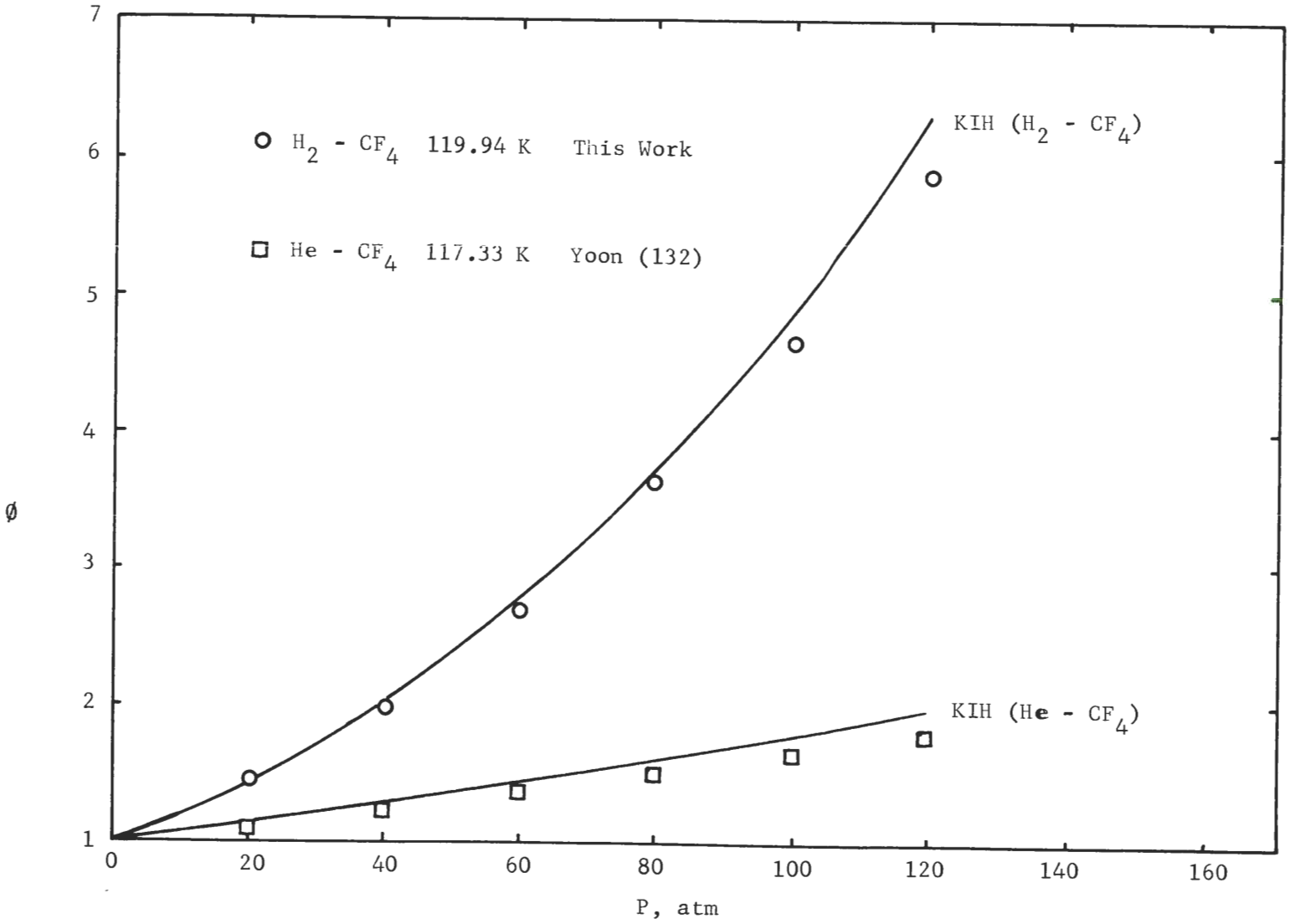

Figure 33. Comparison of the Enhancement Factor Isotherm of the Hydrogen-Carbon Tetrafluoride and Helium-Carbon Tetrafluoride Systems.

theoretical curves and that the theoretical model has the ability to predict the minimum on the y_1 isotherm of the hydrogen system, the minimum on the enhancement factor isobar of the helium system, and the maximum on the enhancement isobar of the helium system at 20 atm. Liu (73) first became aware of the ability of the LJCL and KIH models to predict those minima and maxima for helium systems. Garber (35) has also shown that the BWR equation is capable of reproducing the same trends as well. The same phenomena are also found for hydrogen systems and were pointed out earlier in this chapter.

Figure 29 shows that the majority of the B_{12} values of the helium-carbon tetrafluoride system are positive while those of the hydrogen-carbon tetrafluoride system are negative. From the fact that the hydrogen system has larger negative B_{12} values, it can be expected that the interaction between the hydrogen and carbon tetrafluoride molecules is more pronounced than that between the helium and carbon tetrafluoride molecules.

Figure 30 shows that the hydrogen system exhibits a minimum in y_1 on its composition isotherm, and that y_1 values of the helium system decrease monotonously with increasing pressure. (Note that the point of intersection of the curves at $y_1 = 1$ will be the vapor pressure of carbon tetrafluoride). This phenomenon is probably due to the stronger attractive force between the hydrogen and carbon tetrafluoride molecules. In the low pressure region, the mole fraction of carbon tetrafluoride in the gas phase for both systems decreases as pressure increases. As the pressure is further increased, the two different molecules of the system are brought closer together. The attractive

force between the hydrogen and carbon tetrafluoride molecules in the gas phase becomes large enough to overcome the attraction between the carbon tetrafluoride molecules in the liquid phase. Therefore the amount of carbon tetrafluoride found in the gas phase becomes larger as pressure on the hydrogen system increases, and a y_1 minimum might be expected if the pressure of the helium system is large enough to bring the molecules together. A y_1 minimum has been observed in the helium-oxygen system investigated by Herring and Barrick (45).

Figures 31 and 32 show that the enhancement factor of the hydrogen system is considerably higher than that of the helium system at the same temperature and pressure. Also, the enhancement factor isobar of the helium system exhibits a slight minimum as the temperature decreases while the enhancement factor of the hydrogen system always decreases as the temperature increases. Figure 32 shows that a relative maximum is expected for the helium system if the enhancement factor isobar is extended to the temperature where the vapor pressure of carbon tetrafluoride is equal to the total pressure of the system. Note that the total pressure is less than the critical pressure of carbon tetrafluoride.

Although the experimental and theoretical enhancement factors for the hydrogen system show a monotonously decreasing trend, one cannot conclude that there will be no maximum in the low pressure region. From Table 13 of Appendix E it is to be noted that at 20 atm the enhancement factor predicted from BWR equation at 164.99K is greater than that at 149.98K. To illustrate the phenomena shown in Figures 31 and 32, Equation(IV-17)is selected for this purpose. Garber (35) has also used this equation to compare the helium systems at low pressure. For

simplicity, the comparison of the helium and the hydrogen systems is made at low pressure, because the contribution of the third virial coefficients to the enhancement factor calculation is negligible in the low pressure region. At low pressures Equation (IV-17) is reduced to:

$$\ell n\ \phi = \frac{V_{o1}}{8\beta^s RT}\left[\{\ 1 + 9\beta^s(P - P_{o1})\}^{8/9} - 1\right] + \frac{2\ B_{11}}{V_{o1}} - \ell n\ Z_{o1} - \frac{2(y_1\ B_{11} + y_2\ B_{12})}{V_m} + \ell n\ Z_m + \ell n\ x_1 \qquad (V\text{-}6)$$

Since this comparison is made for two systems with the same condensed component, the terms that are responsible for the different phenomena of the two systems are $-\frac{2}{V_m}(y_1\ B_{11} + y_2\ B_{12})$, $\ell n\ (Z_m)$ and $\ell n\ (x_1)$. As a matter of fact, the contributions of $\ell n\ (Z_m)$ and $\ell n\ (x_1)$ are relatively small. Thus the term $-\frac{2}{V_m}(y_1\ B_{11} + y_2\ B_{12})$ plays a major role in representing the shape of the enhancement factor curves and the magnitude of the enhancement factors for the two systems in the low pressure region. The main difference between the helium and the hydrogen system is that large negative values of B_{12} are found in the hydrogen system while small positive values are found in the helium system at the same temperature. Since the B_{11} values of carbon tetrafluoride are negative, the term $-\frac{2}{V_m}(y_1\ B_{11} + y_2\ B_{12})$ is the sum of two positive numbers for the hydrogen system and is the difference of two positive numbers for the helium system. Owing to this fact, the hydrogen system always shows a larger enhancement factor than the helium system.

It was found for both systems that a plot of $-\frac{2}{V_m}(y_1 B_{11} + y_2 B_{12})$ versus temperature at constant pressure shows a minimum on the curve. If the sum of $-\frac{2}{V_m}(y_1 B_{11} + y_2 B_{12})$ and the other terms involved in the enhancement factor calculation is plotted against temperature, the location of the minimum of each system is switched to the higher temperature. Therefore, showing a minimum on the enhancement factor isobar is not characteristic solely for helium systems. A minimum on the enhancement factor isobar of a hydrogen system might be observed in the temperature region where the hydrogen system shows positive values of B_{12}.

Figure 33 shows that the enhancement factors of hydrogen systems increase more rapidly than those of helium systems as pressure is increased. Mathematically, the value of $(\frac{\partial^2 \phi}{\partial P^2})_T$ for a hydrogen system is much greater than that of the corresponding helium system. From the previous discussion, the $\frac{-2}{V_m}(y_1 B_{11} + y_2 B_{12})$ term is the only different term for the hydrogen and helium system with the same condensed component. Therefore, the magnitude of $(\frac{\partial^2 \phi}{\partial P^2})_T$ for the two systems is different because the contribution of $[\frac{\partial^2}{\partial P^2}{}^2 (\frac{-2}{V_m}(y_1 B_{11} + y_2 B_{12}))]_T$ is different.

CHAPTER VI

COMPARISON OF PREDICTED AND EXPERIMENTAL LIQUID PHASE EQUILIBRIUM DATA

Experimental Henry's Law Constant and Partial Molar Volume at Infinite Dilution

Introduction

The influence of pressure on the solubility of a gas in a liquid phase at constant temperature was expressed by William Henry (1803). In modern form, Henry's law is

$$Py_2 = Hx_2 \qquad \text{(VI-1)}$$

where H is known as the Henry's law constant. Henry's law is a special case of a general thermodynamic formulation involving the assumptions: the liquid phase is an ideal solution, the effect of pressure on the condensed phase is neglected, and the gas phase is an ideal gas.

The thermodynamic derivation of the Henry's law constant is based on the criterion for phase equilibrium*, that is, the chemical potential of component 2 must be the same in both phases. The following relation is established

$$\mu_2^L(P,T,x_2) = \mu_2^G(P,T,y_2) \qquad \text{(VI-2)}$$

* The derivation given here follows closely that given by Garber (35) and Yoon (132).

This equation can be expressed in terms of measurable quantities, if the standard states of component 2 in both phases are suitably defined.

The chemical potential of component 2 in the liquid phase is defined as

$$\mu_2^L (P,T, x_2) = \mu_2^{*L} (P,T) + RT \ln (\gamma_2' x_2) \qquad \text{(VI-3)}$$

where the standard state μ_2^* (P,T) is a hypothetical liquid of pure component 2 at the given temperature and pressure. For a binary solution γ_2' is specified as

$$\gamma_2' (P,T,x_2) \rightarrow 1 \qquad \text{as } x_2 \rightarrow 0 \qquad \text{and } P \rightarrow P_{ol}$$

The chemical potential of the gas phase can be defined as

$$\mu_2^G (P,T,y_2) = \mu_2^o (P = 1, T) + RT \ln \frac{f_2^G (P,T,y_2)}{f_2^\circ (P=1, T)} \qquad \text{(VI-4)}$$

where the standard state μ_2° (P=1,T) is an ideal gas of pure component 2 at one atmosphere and the temperature in question, and f_2° is unity for an ideal gas at one atmosphere.

Substitution of Equation (VI-3) and Equation (VI-4) into Equation (VI-2) gives

$$\ln \frac{f_2^G (P,T,y_2)}{x_2} = \ln H_2 (P,T) + \ln \gamma_2' \qquad \text{(VI-5)}$$

where

$$\ell n\ H_2\ (P,T) = \frac{\mu_2^{*L}\ (P,T) - \mu_2^{o}\ (P=1,T)}{RT} \qquad \text{(VI-6)}$$

is the definition of the thermodynamic Henry's law constant $H_2(P,T)$ with the unit of atmosphere, (Note that the left hand side of this equation should have been written as $\ell n\ (H_2(P,T)/f^{o}(P=1,T))$ where $f_2^{o}\ (P=1,T)=1$).

Differentiation of Equation (VI-3) with respect to pressure at constant temperature and composition gives

$$\left(\frac{\partial \mu_2^{L}}{\partial P}\right)_{T,x_2} = \bar{V}_2 = \left(\frac{\partial \mu_2^{*L}\ (P,T)}{\partial P}\right)_{T} + RT\left(\frac{\partial(\ell n\ \gamma_2')}{\partial P}\right)_{T,x_2} \qquad \text{(VI-7)}$$

As x_2 approaches zero, γ_2' becomes unity, thus

$$\left(\frac{\partial \mu_2^{*L}\ (P,T)}{\partial P}\right)_{T} = \bar{V}_2^{\infty} \qquad \text{(VI-8)}$$

After differentiating Equation (VI-6) with respect to pressure at constant temperature, one obtains

$$\left(\frac{\partial\ \ell n\ H_2\ (P,T)}{\partial P}\right)_{T} = \frac{1}{RT}\left(\frac{\partial \mu_2^{*L}}{\partial P}\right)_{T} = \frac{\bar{V}_2^{\infty}}{RT} \qquad \text{(VI-9)}$$

Integrating Equation (VI-9), one obtains

$$\ell n\ H_2\ (P,T) = \ell n\ H_2^{\infty}\ (P_{o1},T) + \frac{1}{RT}\int_{P_{o1},T}^{P,\ T} \bar{V}_2^{\infty}\ dP \qquad \text{(VI-10)}$$

Substituting Equation (V-10) into Equation (VI-5) gives

$$\ell n \frac{f_2^G}{x_2} = \ell n H_2^{\infty} (P_{o1},T) + \frac{1}{RT} \int_{P_{o1},T}^{P,T} \bar{V}_2^{\infty} dP + \ell n \gamma_2' \qquad \text{(VI-11)}$$

This is an exact thermodynamic relation for the solubility of a gas in a liquid phase. This equation has been used by many investigators (91,119,123) to correlate the liquid solubility data.

If it is assumed that the change of $\bar{V}_2^{\infty}$ with respect to pressure is negligible and that the liquid phase is an ideal solution, then Equation (VI-4) is reduced to the form:

$$\ell n \frac{f_2^G}{x_2} = \ell n H_2^{\infty} (P_{o1},T) + \frac{\bar{V}_2^{\infty} (P - P_{o1})}{RT} \qquad \text{(VI-12)}$$

which is the Krichevsky-Kasarnovsky equation (68, 95, 113, 114). This equation can be further reduced to Henry's law Equation (VI-1) for a case where the system pressure is as low as the vapor pressure of component 1 and the gas phase behaves as an ideal gas.

With the assumption that $\bar{V}_2^{\infty}$ is independent of pressure, Equation (VI-12) suggests that a straight line would be obtained by plotting $\ell n(f_2^G/x_2)$ versus $(P-P_{o1})$. Thus the value of $\bar{V}_2^{\infty}$ can be calculated from the slope of the straight line and the value of H_2^{∞} can be obtained by extrapolating the straight line to $(P-P_{o1}) = 0$.

In order to make the calculation possible, an equation of state for the gas phase must be assumed to obtain the value of $f_2^G(P,T,y_2)$.

If the gas phase is assumed to be an ideal gas mixture then

$$f_2^G (P,T,y_2) = Py_2 = P-Py_1 \qquad \text{(VI-13)}$$

Replacing Py_1 by P_{o1} for the case where the total pressure and the solubility of component 2 in the liquid phase are small, Equation (V-13) becomes

$$f_2^G(P,T,y_2) = P-P_{o1} \qquad \text{(VI-14)}$$

If the gas phase follows the Lewis and Randall rule then

$$f_2^G(P,T,y_2) = f_2^G(P,T) \cdot y_2 \qquad \text{(VI-15)}$$

This equation takes into consideration the nonideality of the gas phase and was used by Sinor and Kurata (113) and Trust and Kurata (123) to extract the experimental values of H_2^∞ and $\overline{V}_2^\infty$.

An exact thermodynamic expression of $f_2^G(P,T,y_2)$ in terms of measurable quantities was derived as follows (35,95,132):

$$\ell n\ f_2^G = \frac{1}{RT} \int_V^\infty \left[\left(\frac{\partial P}{\partial n_2}\right)_{V,T,n_1} - \frac{RT}{V} \right] dV - \ell n \frac{V}{n_2 RT} \qquad \text{(VI-16)}$$

which requires an equation of state to carry out the integration. Solen et al.(117) used the Redlich-Kwong equation for the calculation of helium binary systems. The virial equation of state was used for this purpose in this work.

Using Equations (IV-14), (IV-15), and (IV-16) the integral in Equation (VI-16) can be evaluated. After some algebraic manipulation, the following expression is obtained for $\ell n(f_2^G/x_2)$ (35, 132), namely,

$$\ell n \frac{f_2^G}{x_2} = \frac{2(y_1 B_{12} + y_2 B_{22})}{V_m} + \frac{3(y_1^2 C_{112} + 2y_1 y_2 C_{122}}{2V_m^2}$$

$$\frac{+ y_2^2 C_{222})}{} + \ell n \frac{y_2 RT}{x_2 V_m} \qquad \text{(VI-17)}$$

The values of x_2 and y_1 used in Equation (VI-17) were the experimental values shown in Appendix E. The values of B_{12} were those experimental values obtained in Chapter V. All the third virial coefficients were calculated from the method of Chueh and Prausnitz (16). The K_{12} values required for the calculation of the third virial coefficients were those experimentally determined in Chapter V. The B_{11} values were calculated using the Kihara parameters. The B_{22} values were calculated from the Lennard-Jones parameters which were extracted from the experimental B_{22} values of Michels et al. (81) and White and Johnston (128).

With the known values of $\ell n(f_2^G/x_2)$ and $(P-P_{o1})$ calculated from the phase equilibrium data shown in Appendix E, the values of H_2^∞ and $\bar{V}_2^\infty$ at a certain temperature were then obtained by the least squares method. The values of $\ell n(f_2^G/x_2)$ and $(P-P_{o1})$ at a given temperature were fitted into a straight line according to Equation (VI-12). The values of H_2^∞ and $\bar{V}_2^\infty$ were calculated from the intercept and the slope of the fitted linear equation.

An approximate method to calculate the Henry's law constant is to assume the gas phase is an ideal gas mixture and combining Equation (VI-14) with Equation (VI-12) which gives

$$\ell n \left(\frac{P-P_{o1}}{x_2} \right) = \ell n\, H_2^\infty (P_{o1}, T) + \frac{\bar{V}_2^\infty (P-P_{o1})}{RT} \qquad \text{(VI-18)}$$

From Equation (VI-18), it can be seen that as $(P-P_{o1})$ approaches zero the equation becomes:

$$\lim_{\substack{P \to P_{o1} \\ x_2 \to 0}} \ell n \left(\frac{P-P_{o1}}{x_2} \right) = \ell n \, H_2^{\infty} (P_{o1}, T) \qquad \text{(VI-19)}$$

Eliminating the logarithms for both sides of Equation (VI-19) and defining the Henry's law constant calculated from this method as $\overline{K}_2^{\infty}$, one obtains

$$\overline{K}_2^{\infty} = \lim_{\substack{(P-P_{o1}) \to 0 \\ x_2 \to 0}} \frac{(P-P_{o1})}{x_2} \qquad \text{(VI-20)}$$

By fitting the experimental values of $\ell n((P-P_{o1})/x_2)$ and $(P-P_{o1})$ into a smooth curve according to Equation (VI-18), the value of $\ell n((P-P_{o1})/x_2)$ at $(P-P_{o1}) = 0$ can be obtained from the intercept of the fitted curve. The thus obtained value is the value of $\overline{K}_2^{\infty}$, which is defined by Equation (VI-20). This method is referred to as the consistency method in this work. This method has also been used by Mullins (87), Garber (35) and Yoon (132) to obtain $\overline{K}_2^{\infty}$ by a graphic scheme. The least squares method was used in this work to fit the experimental values of $\ell n((P-P_{o1})/x_2)$ and $(P-P_{o1})$ into a straight line for each isotherm. The value of $\overline{K}_2^{\infty}$ at a certain temperature was calculated from the intercept of the fitted equation. It must be noted that Equation (VI-18) is a special case of Equation (VI-12) with the assumption of an ideal gas mixture. A plot of $\ell n((P-P_{o1})/x_2)$ versus $(P-P_{o1})$ for a real gas mixture may not be a straight line. But the extrapolation of Equations (VI-12) and(VI-18)

will give the same intercept at $(P-P_{o1}) = 0$, if the value of P_{o1} is low enough and the gas mixture behaves like an ideal gas mixture. Thus, it is not surprising that the values of $\overline{K}_2^{\infty}$ from Equation (VI-18) and the values of H_2^{∞} from Equation (VI-12) show better agreement in low temperature regions where the P_{o1} values are relatively small.

The smoothed experimental phase equilibrium data for the hydrogen-carbon tetrafluoride and the hydrogen-chlorotrifluoromethane systems obtained in this work and those of hydrogen-argon (87), hydrogen-methane (61), hydrogen-ethane (52), and hydrogen-ethylene (51) systems were used to extract the experimental values of H_2^{∞} and $\overline{V}_2^{\infty}$ from Equations (VI-12) and (VI-17), and the values of $\overline{K}_2^{\infty}$ from Equation (VI-20). The smoothed phase equilibrium data of these systems are shown in Table 13 through Table 18 of Appendix E. The values of H_2^{∞}, $\overline{V}_2^{\infty}$ and $\overline{K}_2^{\infty}$ of these systems determined in this work are presented in the following sections. The error ranges of the results are determined by varying the input data of x_2 and y_1 by the corresponding experimental errors.

Experimental Values of H_2^{∞} and $\overline{V}_2^{\infty}$ for the Hydrogen-Carbon Tetrafluoride and Hydrogen-Chlorotrifluoromethane Systems

The smoothed experimental data of this work presented in Table 13 and Table 14 of Appendix E are used for the extraction of H_2^{∞} and $\overline{V}_2^{\infty}$. The experimental and the smoothed values of H_2^{∞} and $\overline{V}_2^{\infty}$ are shown in Table 3 and Table 4. No other experimental data are available for comparison; however, the values of $\overline{K}_2^{\infty}$ obtained from the consistency method agree well with the values of H_2^{∞} obtained from Equations (VI-12) and (VI-17) as shown in Figure 34 and Figure 35 for the two systems investigated. The uncertainty of $\overline{V}_2^{\infty}$ values is approximately 30 percent for both systems.

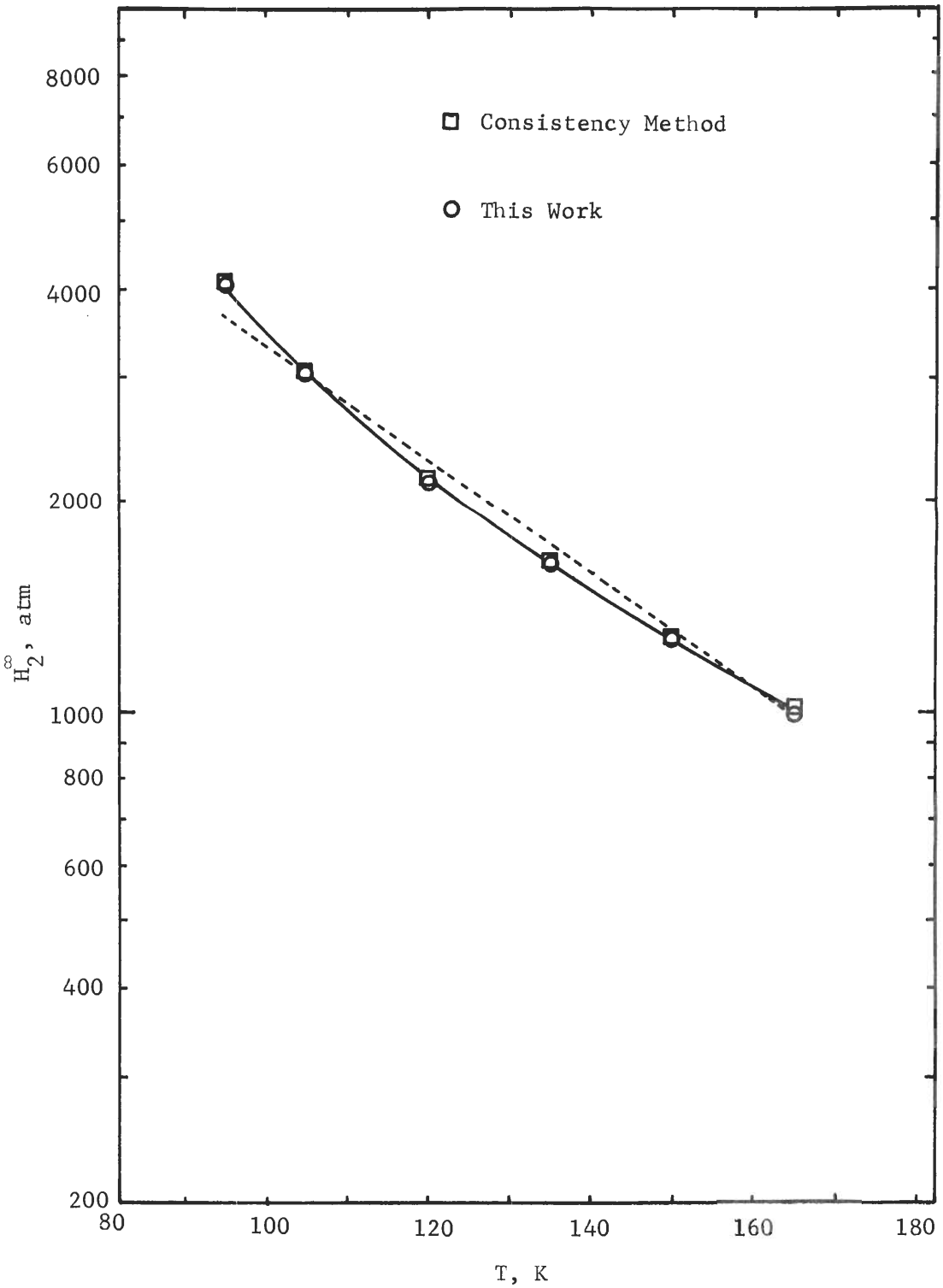

Figure 34. Experimentally Determined Henry's Law Constants for the Hydrogen-Carbon Tetrafluoride System.

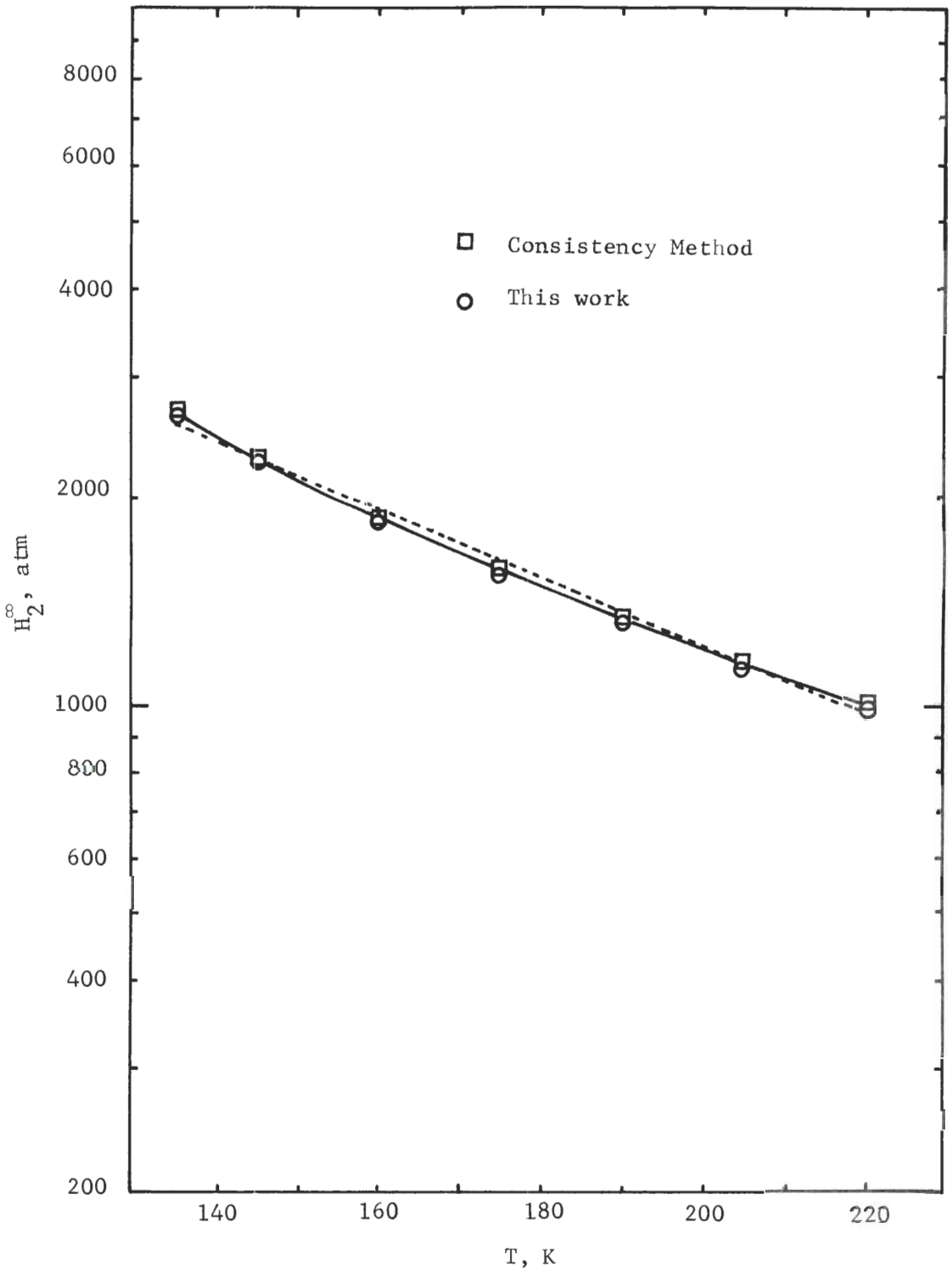

Figure 35. Experimentally Determined Henry's Law Constants for the Hydrogen-Chlorotrifluoromethane System.

Table 3. H_2^∞ and $\bar{V}_2^\infty$ for the Hydrogen-Carbon Tetrafluoride System

T, K	H_2^∞, atm Experimental	H_2^∞, atm Smoothed	$\bar{V}_2^\infty$ cc/gm mole Experimental	$\bar{V}_2^\infty$ cc/gm mole Smoothed
94.94	4,005 ± 110	4,003	22.6 ± 5.7	19.0
105.01	3,013 ± 81	3,018	22.2 ± 5.8	19.2
119.94	2,130 ± 43	2,120	20.9 ± 5.8	19.7
135.01	1,592 ± 32	1,601	21.2 ± 6.2	20.6
149.98	1,259 ± 25	1,254	18.1 ± 6.6	21.7
164.98	984 ± 19	980	18.0 ± 6.9	23.1

Table 4. H_2^∞ and $\bar{V}_2^\infty$ for the Hydrogen-Chlorotrifluoromethane System

T, K	H_2^∞, atm Experimental	H_2^∞, atm Smoothed	$\bar{V}_2^\infty$ cc/gm mole Experimental	$\bar{V}_2^\infty$ cc/gm mole Smoothed
134.97	2,658 ± 54	2,655	21.3 ± 6.7	22.4
145.02	2,254 ± 43	2,260	23.5 ± 6.7	22.5
160.02	1,853 ± 38	1,851	23.7 ± 6.7	22.8
175.02	1,575 ± 31	1,566	22.5 ± 7.4	23.1
189.97	1,328 ± 28	1,338	23.4 ± 7.4	23.5
205.03	1,149 ± 22	1,139	23.0 ± 7.4	23.9
219.99	987 ± 19	990	25.1 ± 7.7	24.4

The uncertainty is estimated by varying x_2 by ± 2 percent of the experimental quantity.

Experimental Values of H_2^∞ and $\bar{V}_2^\infty$ for the Hydrogen-Ethane and Hydrogen-Ethylene Systems

The phase equilibrium data obtained by Hiza, Heck and Kidnay (51,52)

were smoothed in this work as shown in Table 15 and Table 16 of Appendix E. The smoothed data were used for the extraction of the values of H_2^∞ and $\overline{V}_2^\infty$. The experimental and the smoothed values of H_2^∞ and $\overline{V}_2^\infty$ obtained from this work are shown in Table 5 and Table 6. The phase equilibrium data obtained by Williams and Katz (130) have been used by Orentlicher and Prausnitz (91) to extract H_2^∞ values. The values of H_2^∞ obtained in this work together with those obtained by Orentlicher and Prausnitz are shown in Figure 36 and Figure 37. The values of $\overline{K}_2^\infty$ obtained from the consistency method agree well with those of H_2^∞ obtained from Equations (VI-12) and (VI-17). The uncertainty of the $\overline{V}_2^\infty$ values is estimated to be 25 percent for the hydrogen-ethane system and 48 percent for the hydrogen-ethylene system.

Table 5. H_2^∞ and $\overline{V}_2^\infty$ for the Hydrogen-Ethane System

T, K	H_2^∞, atm		$\overline{V}_2^\infty$ cc/gm mole	
	Experimental	Smoothed	Experimental	Smoothed
108.00	4,556 ± 92	4,576	23.6 ± 6.6	25.5
122.00	3,701 ± 72	3,680	20.3 ± 6.6	25.6
130.00	2,946 ± 58	2,990	29.8 ± 6.7	25.8
149.62	2,451 ± 50	2,425	23.4 ± 6.9	26.4
169.40	1,880 ± 39	1,913	35.4 ± 7.5	28.2
189.57	1,545 ± 32	1,539	29.5 ± 7.9	32.9

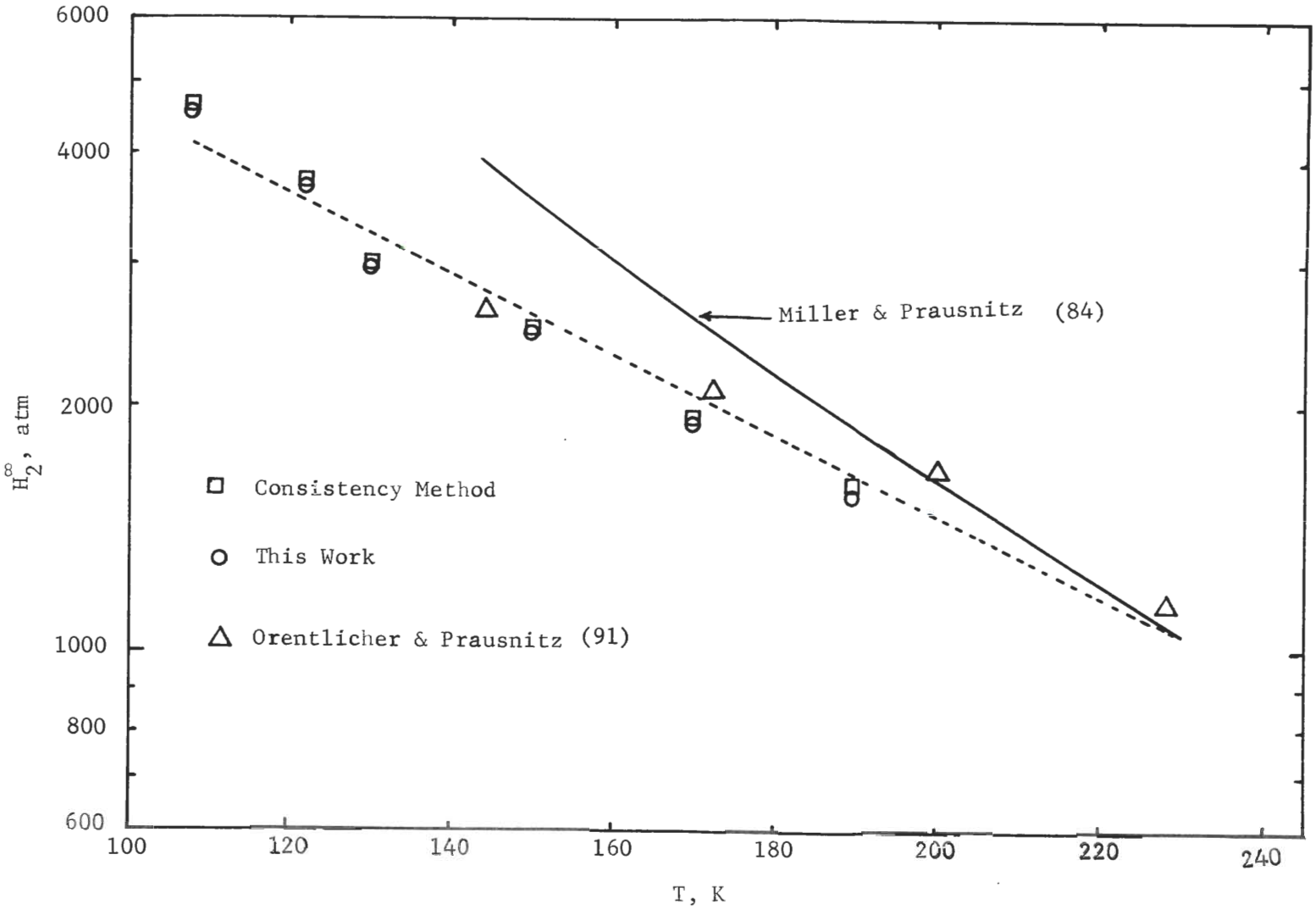

Figure 36. Experimentally Determined Henry's Law Constants for the Hydrogen-Ethane System.

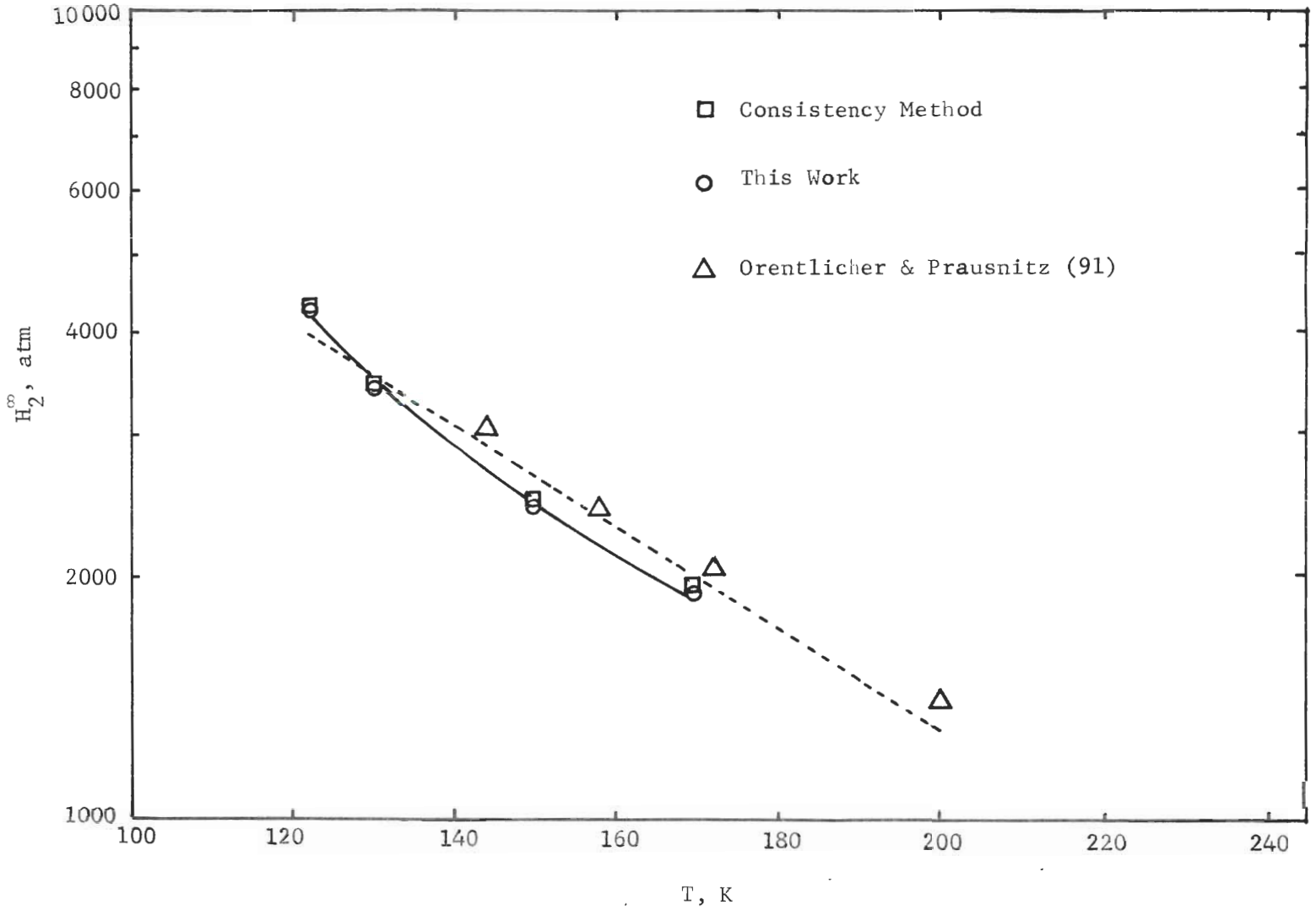

Figure 37. Experimentally Determined Henry's Law Constants for the Hydrogen-Ethylene System.

Table 6. H_2^∞ and $\overline{V}_2^\infty$ for the Hydrogen-Ethylene System

T, K	H_2^∞, atm		$\overline{V}_2^\infty$ cc/gm mole	
	Experimental	Smoothed	Experimental	Smoothed
122.00	4,290 ± 84	4,289	14.9 ± 8.7	18.0
130.00	3,407 ± 67	3,407	20.9 ± 8.7	18.1
149.70	2,463 ± 47	2,462	24.4 ± 8.8	18.7
169.75	1,916 ± 39	1,916	16.9 ± 9.6	20.6

Experimental Values of H_2^∞ and $\overline{V}_2^\infty$ for the Hydrogen-Methane and Hydrogen-Argon Systems

The phase equilibrium data of the hydrogen-methane system obtained by Kirk (61) and those of the hydrogen-argon system by Mullins (87) have been smoothed and presented in Table 17 and Table 18 in Appendix E. The smoothed phase equilibrium data were used to extract the values of H_2^∞ and $\overline{V}_2^\infty$. The experimental values of H_2^∞ and $\overline{V}_2^\infty$ obtained in this work are shown in Table 7 and Table 8.

The H_2^∞ values for these systems have also been extracted from the phase equilibrium data (8, 126) by Orentlicher and Prausnitz (91). The results of this work and those of Orentlicher and Prausnitz are shown in Figure 38 and Figure 39. The $\overline{K}_2^\infty$ values of the hydrogen-methane system agree with those of H_2^∞ obtained from Equations (VI-12) and (VI-17). For the hydrogen-argon system, the H_2^∞ values obtained from this work show better agreement with the values of $\hat{K}^o$ obtained by Mullins (87). The value of $\hat{K}^o$ is defined as $\hat{K}^o = \lim_{x_2 \to 0} (Py_2/x_2)$. The uncertainty of the $\overline{V}_2^\infty$ values is estimated to be 300 percent for the hydrogen-argon system and 55 percent for the hydrogen-methane system. The uncertainties are

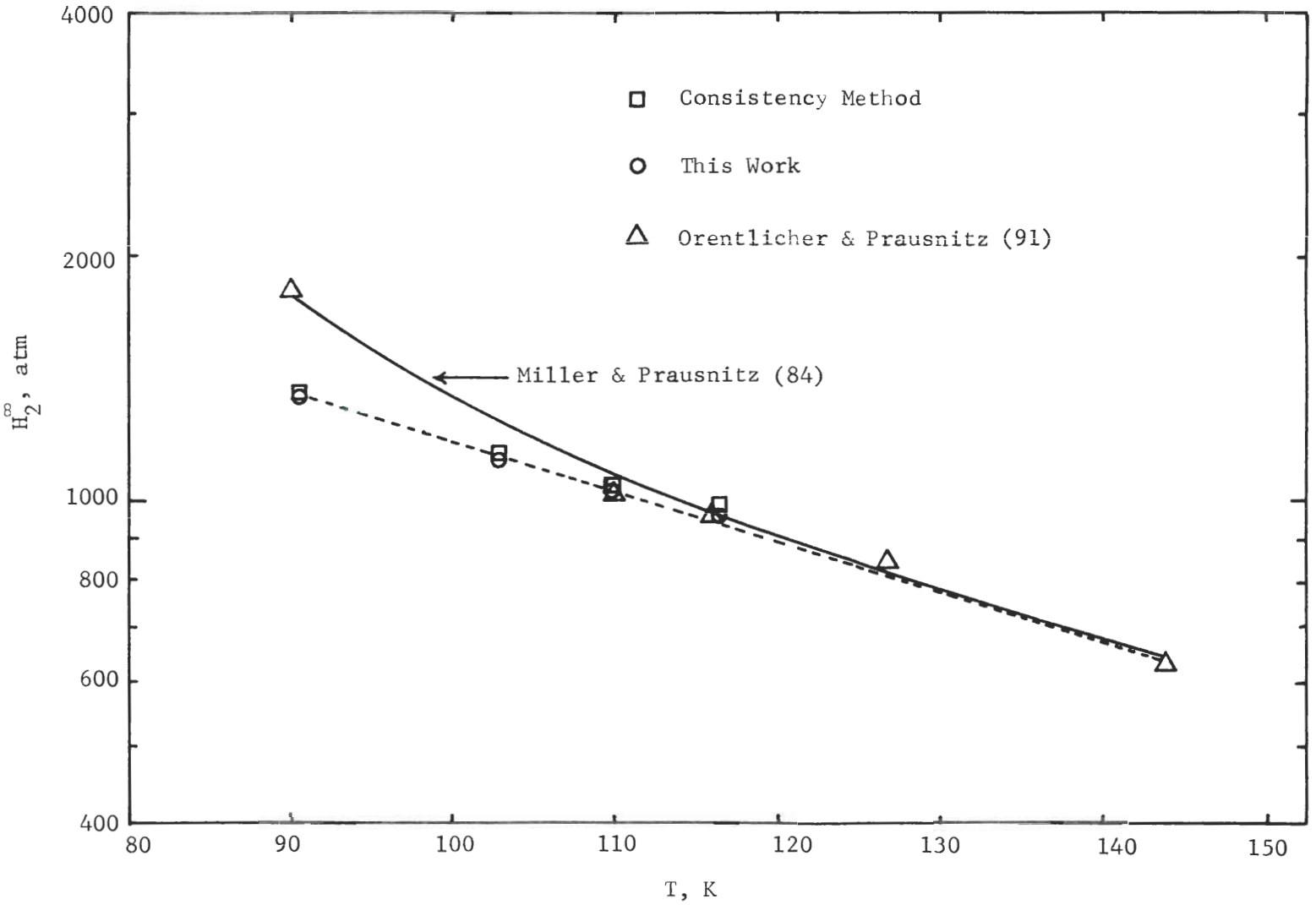

Figure 38. Experimentally Determined Henry's Law Constants for the Hydrogen-Methane System.

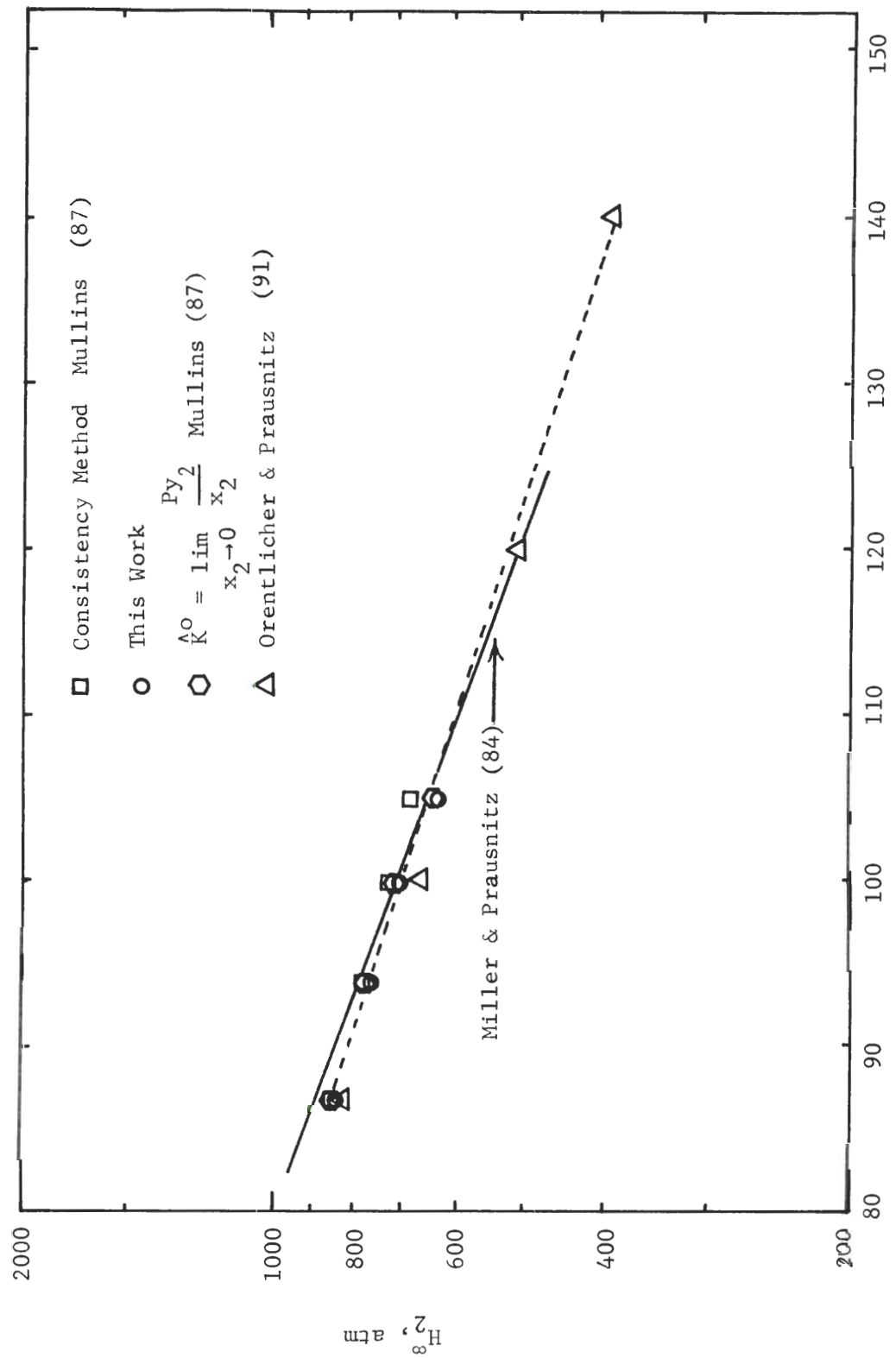

Figure 39. Experimentally Determined Henry's Law Constants for the Hydrogen-Argon System.

estimated by varying x_2 by ± 2 percent, the estimated uncertainty in the experimental quantity. With the large uncertainties for the $\overline{V}_2^\infty$ values of these two systems, no smoothed values of $\overline{V}_2^\infty$ are shown in Table 7 and Table 8.

Table 7. H_2^∞ and $\overline{V}_2^\infty$ for the Hydrogen-Methane System

T, K	H_2^∞, atm		$\overline{V}_2^\infty$ cc/gm mole
	Experimental	Smoothed	Experimental
90.74	1,338 ± 27	1,338	12.0
103.07	1,122 ± 24	1,120	11.2
109.98	1,021 ± 21	1,025	10.4
116.53	954 ± 19	953	8.4

Table 8. H_2^∞ and $\overline{V}_2^\infty$ for the Hydrogen-Argon System

T, K	H_2^∞, atm		$\overline{V}_2^\infty$ cc/gm mole
	Experimental	Smoothed	Experimental
86.95	844 ± 18	844	3.4
94.21	753 ± 16	756	1.0
99.95	691 ± 15	688	-1.7
105.01	627 ± 13	628	-1.9

Discussion of Results

From the experimental results of H_2^∞ shown in Figure 34 through 39 it is seen that the results from the consistency method give very good agreement with those extracted from Equation (VI-12). It has

been pointed out in the previous section that the consistency method is a form of Equation (VI-12) simplified by assuming the gas mixture is an ideal gas. In determining the experimental values of H_2^∞, the value of $(P-P_{o1})$ is extrapolated to $(P-P_{o1}) = 0$. The total pressure can reach a lower value for a lower isotherm. When the total pressure is lower, the gas phase is closer to an ideal gas. Thus, it is not surprising that the agreement of the results of Equation (VI-12) and those of the consistency method becomes better at lower temperatures.

From Figure 36 through Figure 39, it can be seen that the results of this work do not agree too well with those of Orentlicher and Prausnitz (91). The experimental results of this work were obtained by using Equation (VI-12) while the results of Orentlicher and Prausnitz were extracted by using the following equation:

$$\ln \frac{f_2^G}{x_2} = \ln H_2^\infty (P_{o1}, T) + [\bar{V}_2^\infty - \frac{2A}{(H_2^\infty/\xi) - P_{o1}}] (\frac{P-P_{o1}}{RT}) \quad \text{(VI-21)}$$

where

$$\xi = f_2^G (P_{o1}, T)/P_{o1}\, y_2 \quad \text{(VI-22)}$$

This takes into consideration the non-ideality of the liquid mixture. It should be pointed out that the experimental H_2^∞ obtained in both cases were extracted from a semilogarithmic plot of the ratio of (f_2^G/x_2) against $(P-P_{o1})$. No matter which equation is used, the results of H_2^∞ would be exactly the same provided the same sources of (f_2^G/x_2) and $(P-P_{o1})$ values were used for the two methods. The difference between these two results are directly caused by using different sources of

phase equilibrium data and different equations of state to calculate f_2^G. It can also be concluded that no matter how large the value of the constant A is, the experimental values of H_2^∞ obtained from Equation (VI-21) will be exactly the same as those from Equation (VI-12) if the same sources of phase equilibrium data and the same expression for fugacity are used. Since the values of $\overline{V}_2^\infty$ presented by Orentlicher and Prausnitz are not extracted from the phase equilibrium data but estimated with the help of an approximate theory, no comparison of the $\overline{V}_2^\infty$ values is made in this investigation.

Equation (VI-21) derived by Orentlicher and Prausnitz with the consideration of non-ideality of liquid mixture does not seem to help too much in the extraction of H_2^∞ and $\overline{V}_2^\infty$.

Analyzing the phase equilibrium data using the Gibbs-Duhem relation (see Appendix H) suggests that the ideal solution assumption is probably a good one.

Heat of Solution

By differentiating Equation (VI-6) with respect to temperature at constant pressure, an exact thermodynamic relation for the heat of solution of a gas at infinite dilution can be obtained

$$\left(\frac{\partial \ln H_2^\infty}{\partial T} \right)_p = - \frac{\Delta H_2^s}{RT^2} \qquad \text{(VI-23)}$$

where

$$\Delta H_2^s = \overline{H}_2^{L\infty} - H_2^V \qquad \text{(VI-24)}$$

If the volatility of the solvent is neglected, Equation (VI-23) becomes

$$\frac{d \ln H_2^{\infty}}{dT} = - \frac{\Delta H_2^s}{RT^2} \qquad \text{(VI-25)}$$

From the analyses given by Orentlicher and Prausnitz (91), it appears that a plot of $\ln(H_2^{\infty})$ versus temperature would give a straight line. The value of $\frac{d \ln H_2^{\infty}}{dT}$ for each system considered here is obtained by drawing a straight line through the experimental data as obtained by Orentlicher and Prausnitz (91) and from this work. The dotted lines shown on Figure 34 through Figure 39 are the straight lines selected to calculate the average values of $\frac{d \ln H_2^{\infty}}{dT}$. The calculated values are shown in Table 9 together with those obtained by Orentlicher and Prausnitz (91).

Table 9. Experimental Values of $(d \ln H_2^{\infty}/dT)$ for Hydrogen Systems

Liquid Component	$(d \ln H_2^{\infty}/dT) \times 10^2$, (K^{-1})	
	(This Work)	(91)
CF_4	-1.01	
$CClF_3$	-1.18	
Ar	-1.44	-1.54
CH_4	-1.45	-1.47
C_2H_4	-1.08	-1.04
C_2H_6	-1.39	-1.13

Using the values of Table 9 the heat of solution ΔH_2^s can be obtained

from Equation (VI-25). The average ΔH_2^s values for the hydrogen-carbon tetrafluoride and hydrogen-chlorotrifluoromethane systems in the temperature range considered are 343 cal/gm mole (1434 $\frac{\text{Joule}}{\text{gm mole}}$) and 744 cal/gm mole (3010 $\frac{\text{Joule}}{\text{gm mole}}$) respectively.

Theoretical Prediction of Henry's Law Constant and Partial Molar Volume at Infinite Dilution

Introduction

Because of the complexity of liquid mixtures, many theories have been developed from various points of view and used to correlate gas solubility data. For example, the cell theory (102) is used by Kobatake and Alder (66), the scaled particle theory (105) by Pierotti (92, 93, 94) and Snider and Herrington (118), the free volume theory (101) by Miller and Prausnitz (84) and Nakahara and Hirata (89), and the regular solution theory (46) by Prausnitz and Shair (99). At present, no theory gives complete and exact explanation of the behavior of liquid mixtures. The method of Pierotti (92, 93, 94) has been used by Heck (43) and Garber (35) for the prediction of the H_2^∞ and $\overline{V}_2^\infty$ values of several helium binary systems. This method is also used in the present work to predict the H_2^∞ and $\overline{V}_2^\infty$ values for the hydrogen-halogen-substituted-methane systems. The treatment given in this work follows closely that given by Garber (35).

Miller and Prausnitz (84) have predicted the theoretical H_2^∞ values for hydrogen in argon, methane and ethane. Their values are also shown in Figures 36, 38, and 39 for comparison.

Method of Pierotti

The equations developed by Pierotti for predicting the Henry's law constant, the partial molar volume at infinite dilution, and the heat of solution are based on the scaled particle theory presented by Reiss et al. (105). The reversible work required to introduce a hard sphere into a fluid can be calculated from the scaled particle theory (105). Pierotti considered that two steps are required to introduce a solute molecule into a solvent. First, a hole is created in the solvent to accommodate the solute. Second, the solute molecule and the solvent interact according to the Lennard-Jones (6-12) pairwise potential.

By equating the chemical potential of component 2 in both phases at the same temperature and pressure, Pierotti derived the following equations for calculating the Henry's law constant, the partial molar volume at infinite dilution and the heat of solution.

$$\ell n\ H_2^{\infty} = \frac{\bar{G}_i}{RT} + \frac{\bar{G}_c}{RT} + \ell n\ \left(\frac{RT}{v_1}\right) \qquad \text{(VI-26)}$$

$$\bar{V}_2^{\infty} = \bar{V}_I + \bar{V}_c + \beta_T RT \qquad \text{(VI-27)}$$

$$\Delta H_2^s = \left(\frac{\partial\ \ell n\ H_2^{\infty}}{\partial\ 1/RT}\right)_p = \bar{H}_i + \bar{H}_c - RT + \alpha_p RT^2 \qquad \text{(VI-28)}$$

where $\bar{G}_c$ is the partial molar free energy of creating a cavity in a fluid and is given by Reiss (105) as

$$\bar{G}_c = k_o + k_1 a_{12} + k_2 a_{12}^2 + k_3 a_{12}^3 \qquad \text{(VI-29)}$$

where

$$k_o = RT \left[- \ell n (1 - Y) + \left(\frac{9}{2}\right)\left(\frac{Y}{(1 - Y)}\right)^2 \right] - \frac{\pi P a_1^3}{6} \qquad \text{(VI-30)}$$

$$k_1 = - \left(\frac{RT}{a_1} \right) \left[\frac{6Y}{(1 - Y)} + 18 \left(\frac{Y}{(1 - Y)} \right)^2 \right] + \pi P a_1^2 \qquad \text{(VI-31)}$$

$$k_2 = \left(\frac{RT}{2}\right) \left[\left(\frac{12Y}{(1 - Y)} \right) + 18 \left(\frac{Y}{(1 - Y)} \right)^2 \right] - 2\pi P a_1 \qquad \text{(VI-32)}$$

$$k_3 = (4/3)\, \pi P \qquad \text{(VI-33)}$$

and where

$$Y = \frac{\pi a_1^3 \bar{\rho}}{6} \qquad \text{(VI-34)}$$

$$\bar{\rho} = N_A / v_{o1} \qquad \text{(VI-35)}$$

$$a_{12} = \frac{a_1 + a_2}{2} \qquad \text{(VI-36)}$$

and $\bar{G}_i$ is the partial molar Gibbs free energy for the interaction term. The contribution of $P\bar{V}_i$ and $\bar{S}_i T$ terms are negligible compared with the $\bar{E}_i$ term. Therefore, $\bar{G}_i$ can be approximated by the partial molar internal energy $\bar{E}_i$, where

$$\bar{E}_i = - \frac{5.33\, \pi \bar{\rho}\, \bar{C}}{6 a_{12}^3} \qquad \text{(VI-37)}$$

The dispersion constant, $\bar{C}$, can be evaluated in terms of the Lennard-Jones (6-12) parameters, and the relationship is as follows,

$$\bar{C} = 4(\epsilon_1 \epsilon_2)^{\frac{1}{2}} \left(\frac{a_1 + a_2}{2} \right)^6 \qquad \text{(VI-38)}$$

In the calculation of the heat of solution ΔH_2^s, $\bar{H}_i$ is the partial molar enthalpy for the interaction term. Since the $\bar{PV}_i$ term is negligible $\bar{H}_i$ is approximated by $\bar{E}_i$. $\bar{H}_c$ is the partial molar enthalpy for the cavity formation and is given by

$$\bar{H}_c = \left(\frac{\partial \bar{G}_c}{\partial \frac{1}{RT}} \right)_P = \alpha_P RT^2 Y \{[6/(1 - Y) +$$

$$6Y/(1 - Y)^2][2(a_{12}/a_1)^2 - (a_{12}/a_1)] +$$

$$[36Y/(1 - Y)^2 + 36Y^2/(1 - Y)^3][(a_{12}/a_1)^2 -$$

$$(a_{12}/a_1) + 1/4] + 1/(1 - Y)\} \qquad \text{(VI-39)}$$

In Equation (VI-27), $\bar{V}_I$ is the volume change upon charging and is negligible in this calculation. Thus, Equation (VI-27) is reduced to

$$\bar{V}_2^{\infty} = \bar{V}_c + \beta_T RT \qquad \text{(VI-40)}$$

The partial molar volume of cavity formation is given by

$$\bar{V}_c = 82.0560\ \beta_T\ TY \left\{ \left[\frac{6}{(1 - Y)} + \frac{6Y}{(1 - Y)^2} \right] \left[2\left(\frac{a_{12}}{a_1}\right)^2 \right.\right.$$

$$\left.\left. - \left(\frac{a_{12}}{a_1}\right) \right] + \left[\frac{36Y}{(1 - Y)^2} + \frac{36Y^2}{(1 - Y)^3} \right] \right.$$

(Continued)

$$\times \left[\left(\frac{a_{12}}{a_1}\right)^2 - \left(\frac{a_{12}}{a_1}\right) + \frac{1}{4}\right] + \frac{1}{(1 - Y)}\Big\} + \frac{\pi a_2^3 N_A}{6} \qquad \text{(VI-41)}$$

In the preceding equations, a_1 and a_2 are the hard sphere diameters of component 1 and 2 respectively. Pierotti (92) has shown that a plot of $\ell n\ (H_2^\infty)$ versus polarizability, α_2, for various solutes in a given solute might give a smooth curve. By extrapolating this curve to zero polarizability, a finite value of $\ell n(H_2^\infty)$ is obtained. This extrapolation is equivalent to determining the solubility of a hard sphere of diameter 2.58 Å. Since $\bar{C}$ in Equation (VI-37) is related to the polarizability of the solute, Equation (VI-26) can be reduced to the following form for the solubility of a hard sphere of zero polarization.

$$(\ell n\ H_2^\infty)_{\alpha_2=0} = \frac{\bar{G}_c}{RT} + \ell n\left(\frac{RT}{v_{o1}}\right) \qquad \text{(VI-42)}$$

Using the values of $\ell n\ H_2^\infty$ for $\alpha_2 = 0$ obtained as described above, the values of a_1 at various temperatures can be calculated from Equation (VI-42). The a_1 values of argon, methane, ethane, and ethylene have been obtained by Garber (35) to predict the theoretical values of H_2^∞ for helium systems. The a_1 values of carbon-tetrafluoride and chlorotrifluoromethane, shown in Figure 40, are extracted by using the experimental H_2^∞ values of the helium systems from Yoon (132) and the H_2^∞ values of the hydrogen systems of this work. These values are then used to calculate the H_2^∞, $\bar{V}_2^\infty$, and ΔH_2^s for the hydrogen systems of this work. The calculation of $\bar{V}_2^\infty$ and ΔH_2^s require accurate data of β_T and α_p of the solvent. They are defined as follows

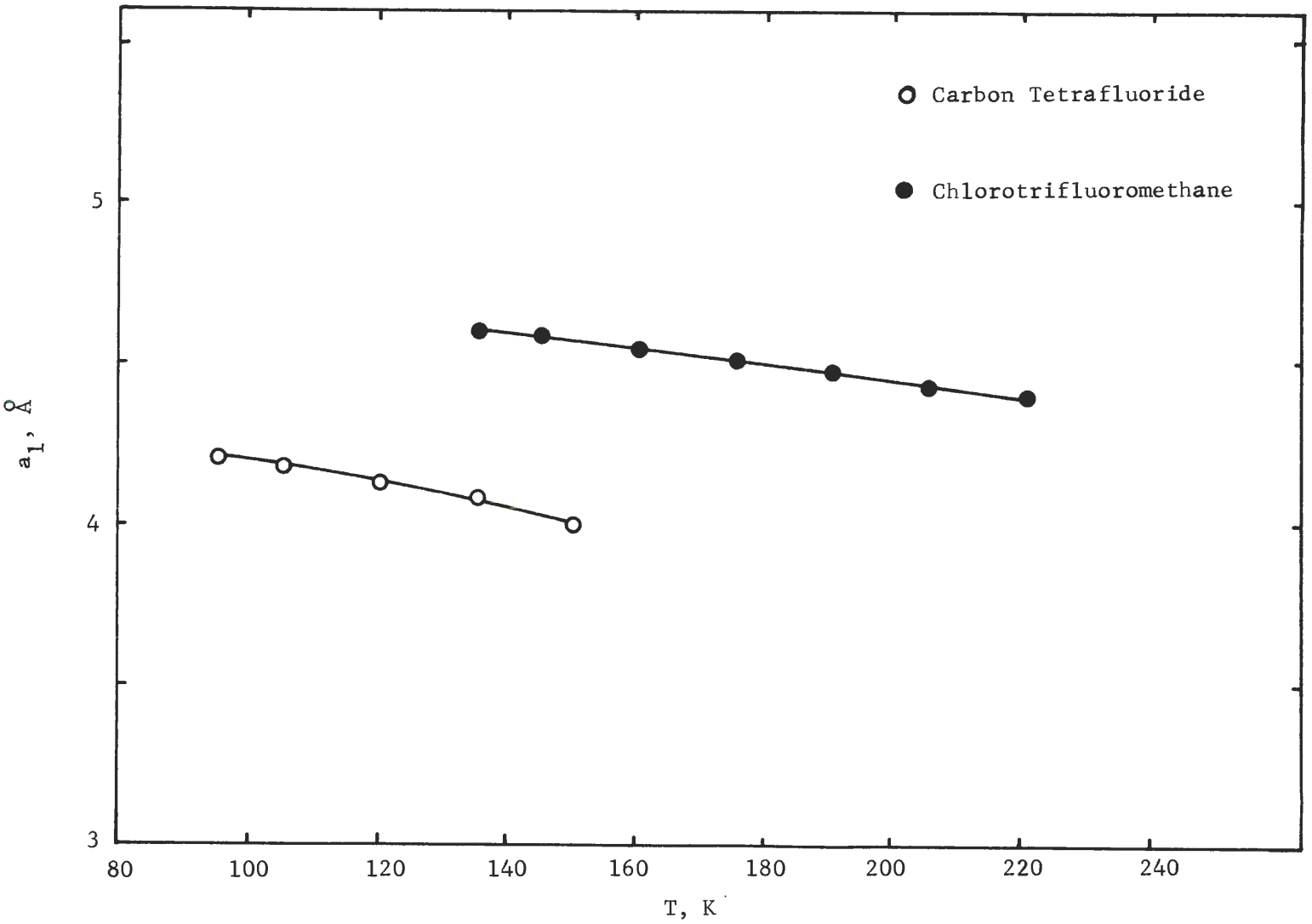

Figure 40. Variation of a_1 with Temperature for Carbon Tetrafluoride and Chlorotrifluoromethane.

$$\beta_T = -\frac{1}{V}\left(\frac{\partial V}{\partial p}\right)_T \qquad \text{(VI-43)}$$

$$\alpha_P = \frac{1}{V}\left(\frac{\partial V}{\partial T}\right)_T \qquad \text{(VI-44)}$$

Since no experimental β_T and α_P values are available for carbon tetrafluoride and chlorotrifluoromethane, the following expressions given by Reiss (105) were used to calculate β_T and α_P.

$$\beta_T = \frac{a_1^3 N_A (1 - Y)^4}{6RT\, Y(1 + 2Y)^2} \qquad \text{(VI-45)}$$

$$\alpha_P = \frac{1 - Y^3}{T(1 + 2Y)^2} \qquad \text{(VI-46)}$$

Garber (35) has shown that the predicted values of H_2^∞ for helium systems agree within a factor of two with experiment. He suggested an introduction of a correction factor $(1 - K_{LJ})$ before the geometric mixing rule in Equation (VI-38). This would give a better agreement between the predicted and experimental values.

Therefore, the following equation was used to obtain the theoretical H_2^∞ values.

$$\bar{C} = 4(1 - K_{LJ})\,(\epsilon_1\,\epsilon_2)^{\frac{1}{2}}\left(\frac{a_1 + a_2}{2}\right)^6 \qquad \text{(VI-47)}$$

The Lennard-Jones parameters required in this calculation are those shown in Table 19 of Appendix F. The K_{LJ} values determined from this work are 0.33 and 0.05 for the hydrogen-carbon tetrafluoride and the

hydrogen-chlorotrifluoromethane system respectively. The value of K_{LJ} for each system was obtained by varying the value of K_{LJ} in the theoretical calculation of H_2^∞, the value of K_{LJ} which gave the best fit of the experimental H_2^∞ was then selected.

The values of H_2^∞ predicted from Equation (VI-26) together with the experimental values of this work are shown in Figures 41 and 42. Figure 41 shows that the predicted values of H_2^∞ for the hydrogen-carbon tetrafluoride system are considerably lower than the experimental values, and a value of $K_{LJ} = 0.33$ is required in Equation (VI-37) to bring the theoretical values into agreement with the experimental values. Figure 42 shows that the predicted values of H_2^∞ for the hydrogen-chlorotrifluoromethane system are approximately ten percent lower than the experimental values, and the theoretical values calculated with $K_{LJ} = 0.05$ show better agreement with the experimental values.

The heat of solution ΔH_2^s can be calculated from Equation (VI-28) which is obtained by differentiating Equation (VI-26) with respect to temperature at constant pressure. From Figures 41 and 42, it is seen that the H_2^∞ values calculated from Equation (VI-26) with the adjusted value of K_{LJ} show a similar trend as the experimental H_2^∞. If an accurate α_p was used in Equation (VI-28) with the adjusted value of K_{LJ}, the predicted ΔH_2^s would show the similar trend with those estimated from the experimental H_2^∞. Unfortunately, the predicted ΔH_2^s values using α_p from Equation (VI-46) are negative while the ΔH_2^s estimated from the experimental H_2^∞ are positive. This reveals the fact that the expression of α_p from Equation (VI-46) is not adequate for the condensed components considered in this work. If an average value of α_p is roughly estimated from the

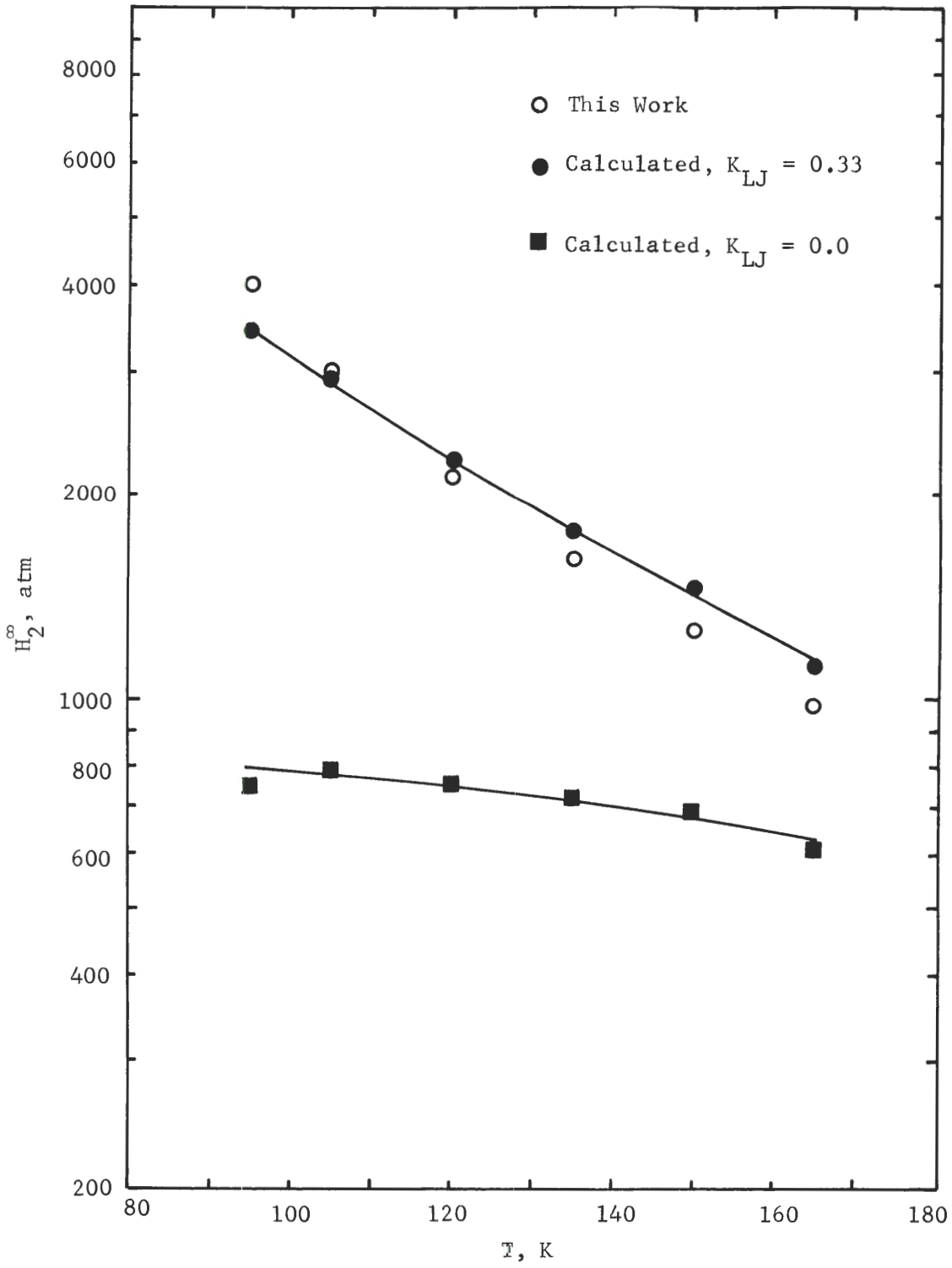

Figure 41. Comparison of Theoretical and Experimental H_2^{∞} for the Hydrogen-Carbon Tetrafluoride System.

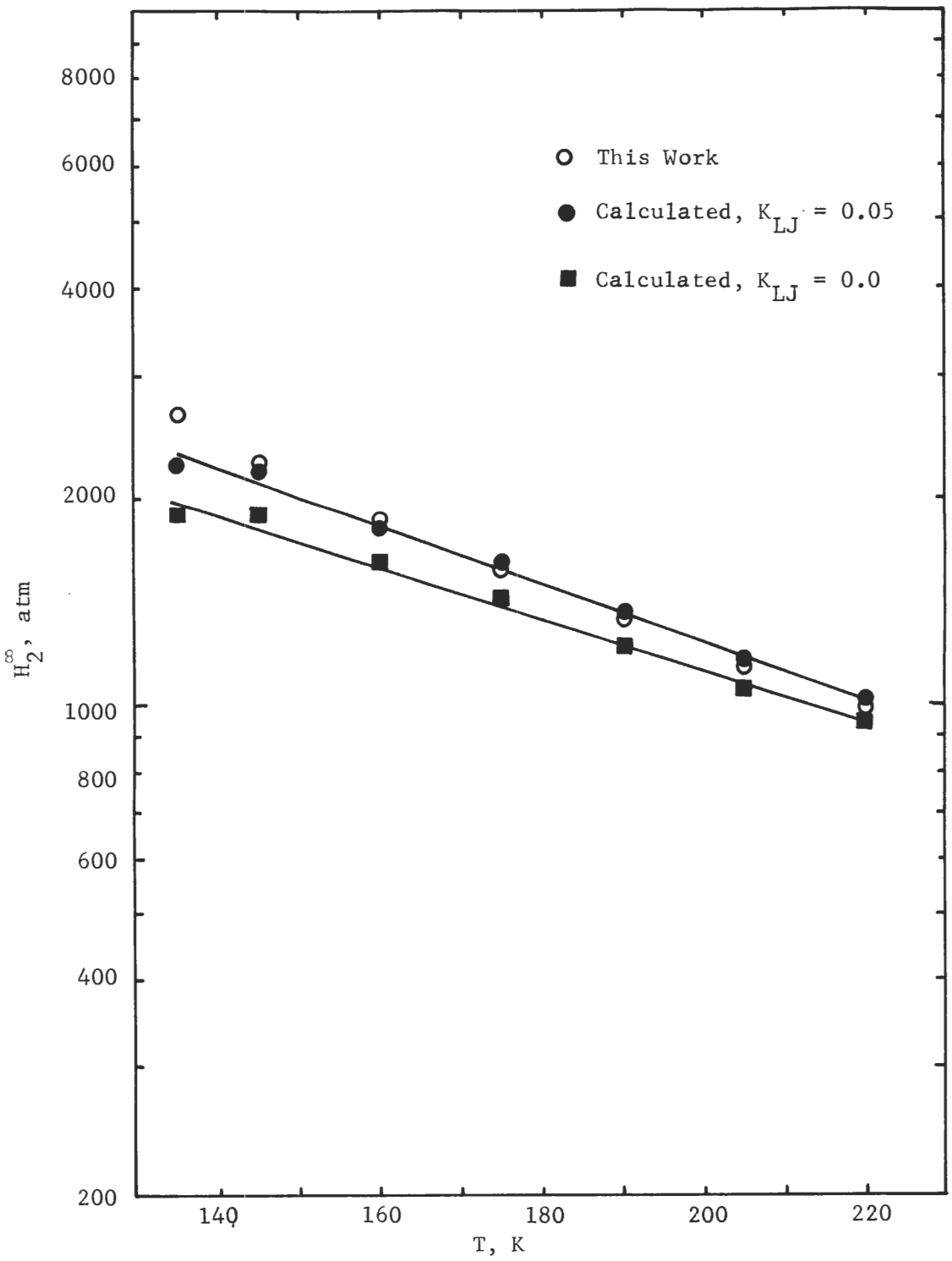

Figure 42. Comparison of Theoretical and Experimental H_2^∞ for the Hydrogen-Chlorotrifluoromethane System.

experimental value of the saturated liquid molar volume and used to calculate ΔH_2^s, positive values are obtained. The values of α_P used in this calculation are 3.02×10^{-3} and 2.47×10^{-3} K^{-1} for carbon tetrafluoride and chlorotrifluoromethane respectively, and the average values of ΔH_2^s predicted for the entire temperature range are 236 cal/gm mole and 392 cal/gm mole for the hydrogen-carbon tetrafluoride and hydrogen-chlorotrifluoromethane systems respectively. With the roughly estimated values of α_P, the ΔH_2^s values calculated from Equation (VI-28) are in good agreement with the observed values of this work. Usually, the uncertainty of the ΔH_2^s measurement is approximately ± 400 cal/gm mole for organic solvents (92).

Figures 43 and 44 show the experimental $\overline{V}_2^\infty$ values and predicted $\overline{V}_2^\infty$ values from Equations (VI-40) and (VI-41). In predicting the theoretical $\overline{V}_2^\infty$ values, the values of β_T are required for this calculation. The theoretical values of $\overline{V}_2^\infty$ have been calculated by the β_T of Equation (VI-45) and also calculated by using the isothermal compressibility shown in Tables 23 and 24 of Appendix F. The calculated curves deviate from the experimental values by ± 50 percent as shown in Figures 43 and 44.

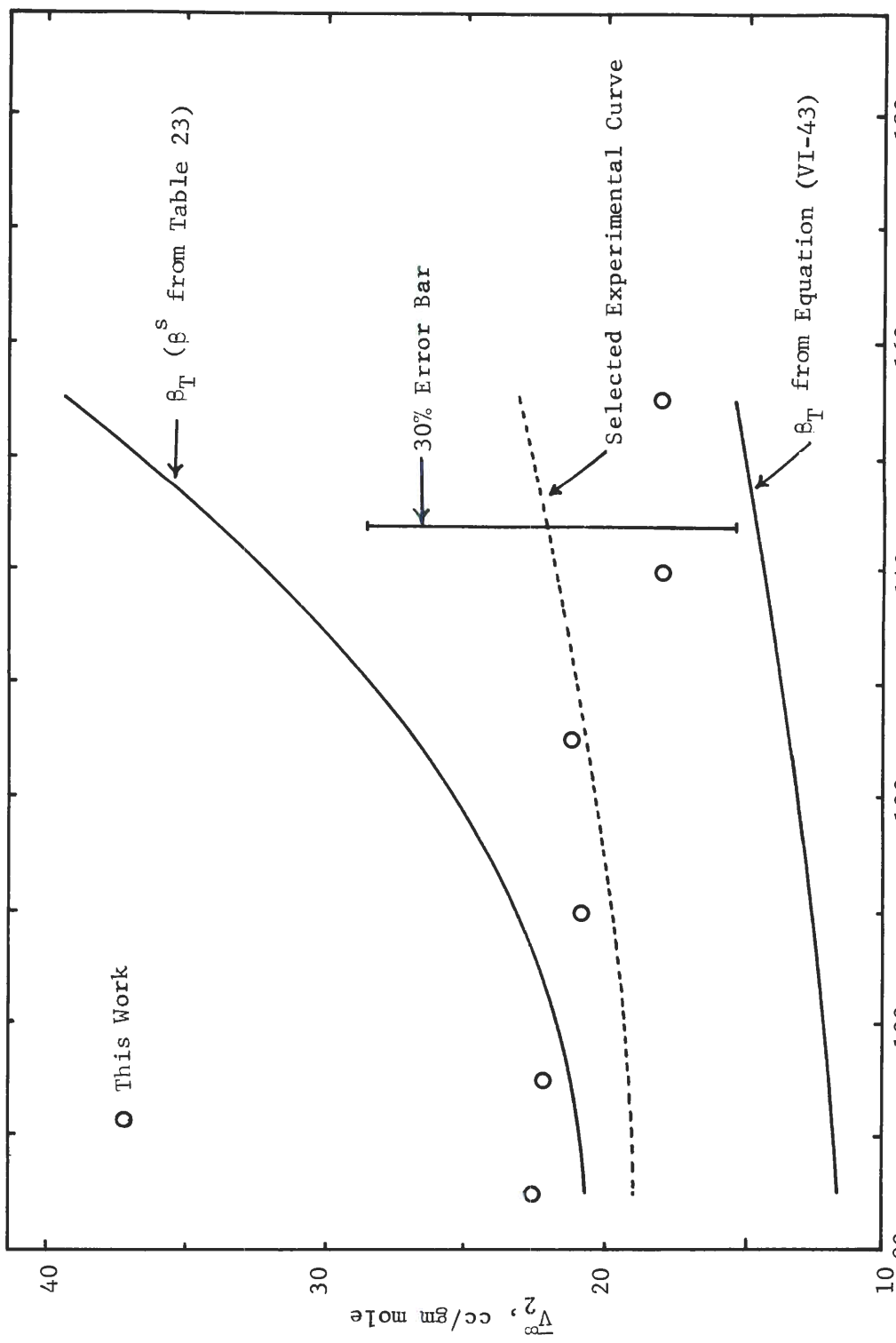

Figure 43. Comparison of Theoretical and Experimental $\overline{V}_2^\infty$ for the Hydrogen-Carbon Tetrafluoride System.

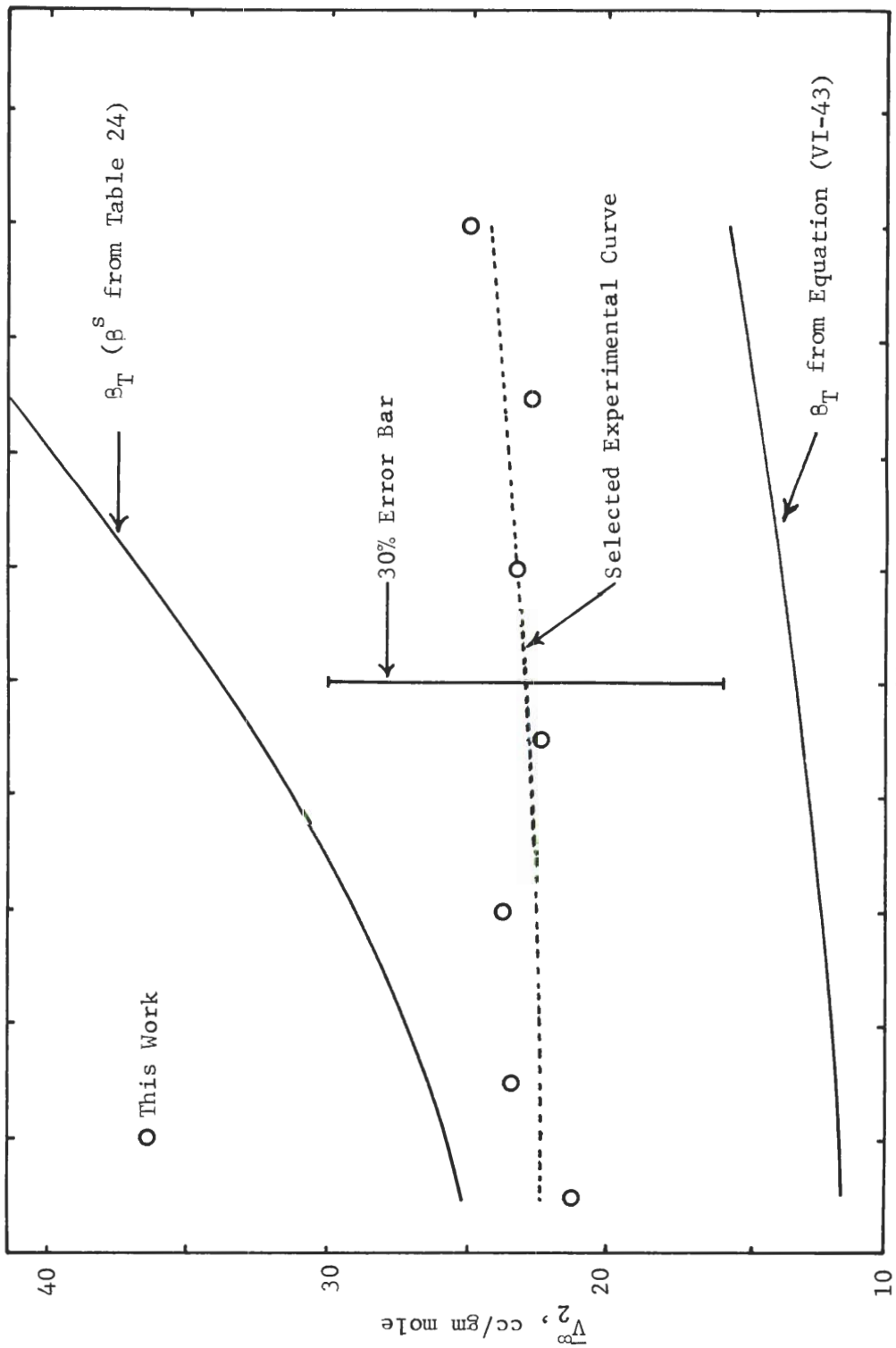

Figure 44. Comparison of Theoretical and Experimental $\overline{V}_2^\infty$ for the Hydrogen-Chlorotrifluoromethane System.

CHAPTER VII

CONCLUSIONS AND RECOMMENDATIONS

Conclusions

The equilibrium gas and liquid compositions have been measured for the hydrogen-carbon tetrafluoride system at six isotherms of 94.94, 105.01, 119.94, 135.01, 149.98 and 164.99 K. The equilibrium gas and liquid compositions for the hydrogen-chlorotrifluoromethane have been measured at seven isotherms of 134.97, 145.02, 160.02, 175.02, 189.97, 205.03 and 219.99 K. The temperature reported in this work are based upon the International Practical Temperature Scale of 1968. The compositions are measured at pressures up to 120 atmospheres at intervals of 20 atmospheres along each isotherm. The experimental enhancement factors are estimated to be accurate to $\pm$ 2.5 percent for the hydrogen-carbon tetrafluoride system and $\pm$ 3.0 percent for the hydrogen-chlorotrifluoromethane system. The liquid phase compositions for both systems are estimated to be accurate to $\pm$ 2.0 percent of the stated hydrogen composition. The uncertainties of the composition are determined by the uncertainty of the temperature measurement, the pressure measurement and the chromatographic calibration curves. In constructing the chromatographic calibration curves, a gas imperfection correction for the gas mixture of 0.4 mole percent and 1.1 mole percent has been taken into consideration for the hydrogen-carbon tetrafluoride system and the hydrogen-chlorotrifluoromethane system respectively.

Five theoretical models LJCL, KIH, KIHCK12, BWR(LORENTZ), and BWR(LINEAR) have been used to predict the theoretical values of $\emptyset$ and B_{12} for the hydrogen-carbon tetrafluoride system. Three models LJCL, KIH, and KIHCK12 were used to predict the theoretical $\emptyset$ and B_{12} of the hydrogen-chlorotrifluoromethane system. Although the theoretical models cannot represent the experimental data too well, the theoretical values follow the same trends as the experimental data.

The phase equilibrium data of the six helium systems He-X (X= Ar(87), CH_4(44), C_2H_6 (50), C_2H_4 (35,50), CF_4 (132), $CClF_3$ (132)) as well as the four hydrogen systems H_2-X (X = Ar (87), CH_4 (61), C_2H_6 (52) and C_2H_4 (51)) and the two hydrogen systems of this work were summarized for comparison. Since their theoretical models follow similar trends as the experimental data, the experimental data are compared and analyzed with the help of the theoretical models. From this comparison and analysis, it is found that the major difference between the helium and the hydrogen systems is the B_{12} values. The majority of the B_{12} values of the helium binary systems fall in the positive region while all the B_{12} values of the hydrogen binary systems fall in the negative region. If, in Equation (V-6), which is applicable at moderate pressures, the contribution of the $\ln(x_1)$ term is neglected, the equation is simplified as follows:

$$\ell n\ \emptyset = \frac{V_{o1}}{8\beta^s T}\left[\{1 + 9\beta^s (P - P_{o1})\}^{8/9} - 1\right] + \frac{2\ B_{11}}{V_{o1}} - \ell n\ Z_{o1}$$

$$- \frac{2(y_1 B_{11} + 2\ y_2\ B_{12})}{V_m} + \ell n\ Z_m \qquad \text{(VII-1)}$$

In the calculation of the enhancement factors for a hydrogen and a helium binary system with the same condensed component, all the parameters in Equation (VII-1) are the same for both systems except B_{12}. This equation is capable of predicting the following experimentally observed characteristics of the He-X and H_2-X systems discussed in this thesis:

(1) At the same temperature and pressure, the hydrogen systems always show larger enhancement factors than the corresponding helium systems.

(2) At a given pressure, the enhancement factors of the hydrogen systems always decrease as temperature increases, while the helium systems, except the He-Ar system, show an enhancement factor minimum on each of their enhancement factor isobars.

(3) At a given temperature, y_1 values of the helium systems always decrease as pressure increases, while the hydrogen systems show a y_1 minimum on each of their y_1 isotherms at low temperatures.

(4) At 20 atmosphere, the enhancement factors of the hydrogen systems always decrease as temperature increases, while many helium systems (35) show a minimum as well as a maximum on each of their 20 atm enhancement factor isobars.

(5) At a given temperature, the enhancement factors of the hydrogen systems increase with pressure more rapidly than those of the corresponding helium systems.

Therefore, the values of B_{12} are responsible for the differences exhibited by the two systems. It is expected that a hydrogen system

will behave like a helium system in the temperature region where the B_{12} values are positive.

For the liquid phase, the solubility of hydrogen is always higher than that of helium in the same condensed phase at the same temperature and pressure. This can be explained by the fact that the attractive force between the hydrogen and the condensed component molecules is greater than that between the helium and the condensed component molecules.

The method of Pierotti (92, 93, 94), which is based on the scaled particle theory (105), was used to predict the H_2^∞, $\overline{V}_2^\infty$, and ΔH_2^s values of the hydrogen-carbon tetrafluoride and hydrogen-chlorotrifluoromethane systems. The method of Pierotti predicts H_2^∞ values which are too low by a factor of 4 at low temperatures and also too low by a factor of 1.5 at high temperatures for the hydrogen-carbon tetrafluoride system. An introduction of a correction, $K_{LJ} = 0.33$, to the geometric mixing rule for the Lennard-Jones energy potential is required to bring the theoretical values within $\pm$ 20 percent into agreement with the experimental values. For the hydrogen-chlorotrifluoromethane system, the Pierotti method predicts H_2^∞ values which are approximately 10 percent lower than the experimental values except the value at the lowest temperature. The predicted H_2^∞ is approximately 30 percent lower than the experimental value at the lowest temperature. The H_2^∞ values predicted with a correction, $K_{LJ} = 0.05$, show very good agreement with the experimental values. It has been mentioned by Pierotti (92) that the prediction of H_2^∞ may be considered satisfactory if the predicted H_2^∞ are within a factor of two of the observed values. The discrepancy

between the observed and predicted H_2^{∞} is mainly caused by the uncertainty of the a_1 values, the method used to obtain the interaction energy, and the LJCL parameters used in this calculation.

The predictions of $\overline{V}_2^{\infty}$ and ΔH_2^s might show better agreement with the experimental values, if the values of β_T and α_p used were those experimentally determined.

Recommendations

(1) Run the hydrogen systems to the higher temperature region where the B_{12} values are positive. Hopefully, there will be a minimum on the isobar for the enhancement factor at higher pressure.

(2) Run the helium systems to the lower temperature region where the B_{12} values are negative to see if there is a y_1 minimum on the composition isotherm at higher pressure.

(3) Run both systems at pressures lower than the critical pressure of the condensed component to see if there is a maximum on the isobar for the enhancement factor.

(4) In the comparison of the hydrogen and the helium systems with the same condensed component, it might be interesting to compare the two systems based on the same T_{R2}.

(5) Use the values of the hard sphere diameter a_1 obtained for carbon tetrafluoride and chlorotrifluoromethane to calculate the theoretical H_2^{∞}, $\overline{V}_2^{\infty}$, and ΔH_2^s for the helium systems by using Pierotti's method. Use the values of a_1 for argon, methane, ethane, and ethylene obtained by Garber (35) to calculate the theoretical H_2^{∞}, $\overline{V}_2^{\infty}$, and ΔH_2^s for the hydrogen systems.

(6) Use some other theoretical models such as one which used the Redlich-Kwong equation of state (103) to predict the enhancement factor. Hopefully, the model can represent the experimental data not only qualitatively, but also quantitatively as well.

APPENDIX A

TEMPERATURE SCALE USED AND CORRECTIONS FOR PRESSURE GAUGES

The temperature measurements reported in this work were obtained by using a platinum resistance thermometer. The thermometer, made by Leeds and Northrup Company, serial Number 1583528, has been calibrated by the U. S. National Bureau of Standards on the International Practical Temperature Scale of 1948. All temperature measurements in this work were reported on the IPTS-68 scale. The measured temperatures were converted from IPTS-48 to IPTS-68 based on the correction given by Barber (2). Conversion of the temperature scale was made using the following relation

$$T(\text{IPTS-68}) = 273.15 + t_{48}(^{o}C) + (t_{68}(^{o}C) - t_{48}(^{o}C))$$

The uncertainty of the temperature measurement is $\pm$ 0.03 K which is estimated from the temperature gradients along the equilibrium cell and the cell temperature fluctuation.

The pressure measurements in this work were obtained from two pressure gauges. The two pressure gauges were calibrated by Kirk (61) against a dead weight tester and recently calibrated by Garber (35) using the vapor pressure of argon and carbon dioxide. Garber (35) and Yoon (132) have also checked these two pressure gauges by pressurizing the two gauges from 50 to 540 psi and then depressurizing from 540 to 0 psi. The average difference between these two pressure gauges was found to be 10.0 psi by Garber and 9.7 psi by Yoon. A similar

test was also done before taking the phase equilibrium data. The difference between the two gauges was found to be 10.4 psi. The uncertainty of the pressure measurements is $\pm$ 0.05 percent which is estimated from the uncertainty of the vapor pressure measurements done by Garber (35) and the precision in reading the pressure scales.

According to the corrections made by Garber, 10.0 psi was added to the high pressure gauge reading and 1 psi was added to the low pressure gauge reading.

APPENDIX B

HELIUM-CARBON TETRAFLUORIDE MEASUREMENT

In order to check the phase equilibrium apparatus and to acquire some operating technique, four experimental points of the helium-carbon tetrafluoride system previously obtained by Yoon (132) were rerun.

The calibration curves of the helium-carbon tetrafluoride system were checked before the phase equilibrium data were taken. The results are within the error claimed by Yoon. The experimental gas and liquid compositions found at 147.10 K are shown in Figure 45 together with Yoon's results. It can be seen that these points agreed within $\pm$ 2 percent of Yoon's curves.

These results confirm that both the operating condition of the apparatus and the operating technique used are satisfactory.

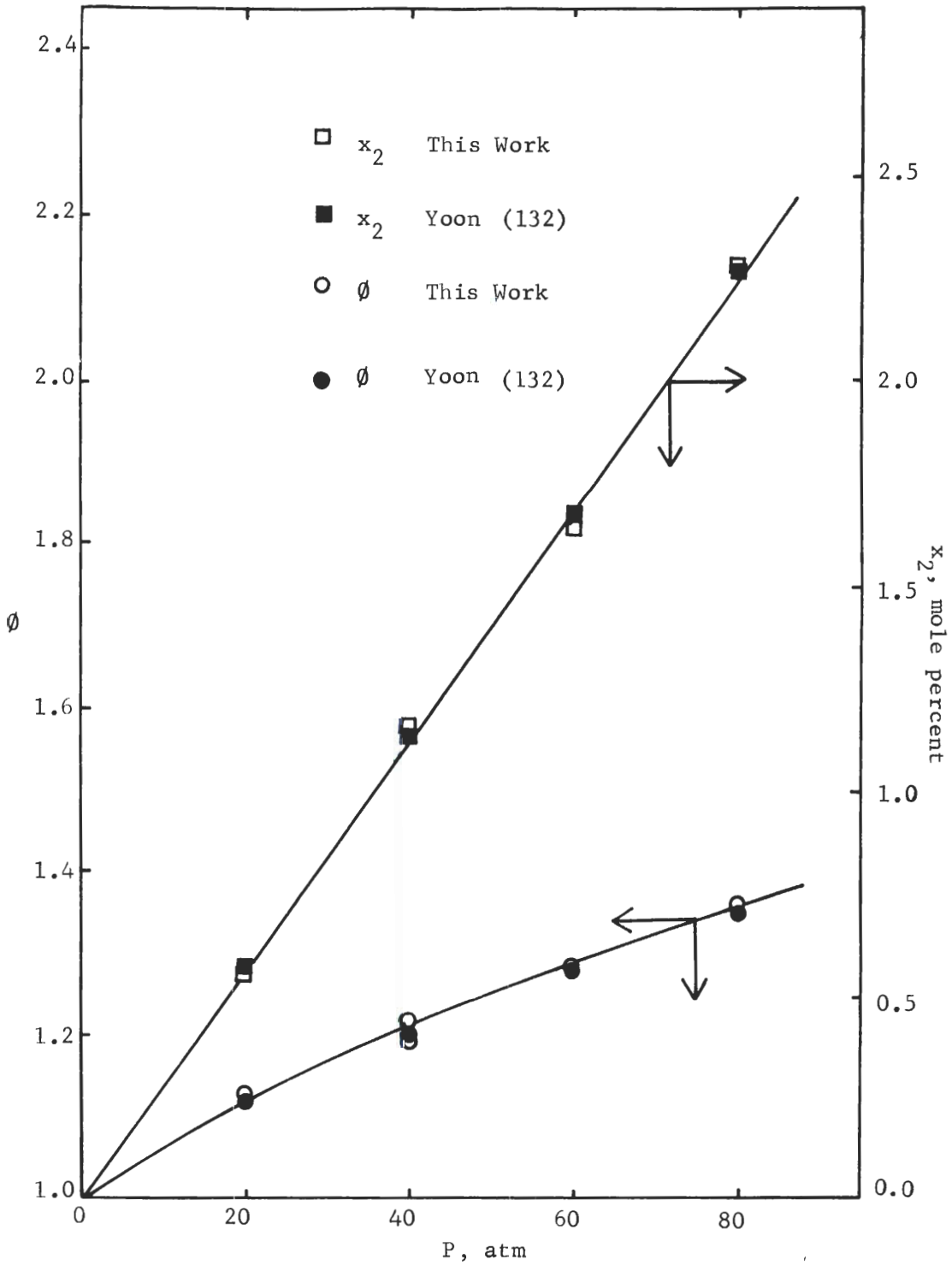

Figure 45. Experimental Enhancement Factors and Helium Solubility in Liquid for the Helium-Carbon Tetrafluoride System at 147.10 K.

APPENDIX C

CALIBRATION OF GAS CHROMATOGRAPHS

In designing the experimental runs of this investigation, the approximate range of gas phase compositions was estimated by using the LJCL model and assuming that the liquid phase is pure. The approximate range of liquid phase compositions was determined by two actual runs at 120 atm of the highest and at 20 atm of the lowest temperatures.

Prior to the calibration of the two Perkin-Elmer vapor fractometers 154B and 154D, the separation columns, the carrier gases and the operating conditions must be properly selected to obtain the best separation and the best peak of the gases to be analyzed. The selected separation columns, the carrier gases, and the operating conditions for the two chromatographs are shown in Table 10. After the optimum conditions for the calibration were obtained, a standard bottle was made for each chromatograph attenuation switch.

The composition for each standard bottle was made such that the peak height is about three-quarter of the width of the recorder chart paper. The peak heights for several standard bottles, which cover the entire composition range of the phase equilibrium measurement, were measured within two hours. The assigned peak height to each standard bottle was used to correct any drift caused by day to day variation. During the phase equilibrium measurement, the peak height of the corresponding standard bottle was measured immediately after the

Table 10. Operating Conditions of Chromatograph

	Systems of Analysis		
	H_2 in CF_4	CF_4 in H_2	$CCLF_3$ in H_2
Chromatograph	154B	154D	154D
Perkin-Elmer Column Type	Molecular Sieve 5A	Silica Gel	Silica Gel
Length, meter	1	2	1
Carrier Gas	Argon	Helium	Helium
Sample Size, cc	10	16.4	16.4
Oven Temperature, ^{o}C	30	50	75
Pressure inside Column, psig	15	13.5	10.0
Flow Rate, cc/min at Room T and Room P	135	130	172
Detector Voltage at Shunt, mv	58.50	4.65	4.65
Recorder Voltage at Shunt, mv	10.41	0.9*	0.5*
Chart Speed, inches/min	1.5	1.5	1.5

*These voltages caused a deflection of 95 divisions on the recorder chart.

unknown sample was measured. The unknown sample peak height was corrected by multiplying by the ratio of the standard peak height of the standard bottle and the measured peak height of the standard bottle. This ratio rarely differed from unity by more than 2 percent.

In constructing the calibration curves, the gas mixtures of known compositions were prepared in a gas mixing burette designed by Kirk (61). The correction for gas imperfection was taken into consideration in preparing the gas mixture of known composition. The calibration curves were constructed by plotting the values of (h.s) versus (h.s/y) on a semilog paper, where h is the corrected peak height, s is the factor of the attenuation switch, and y is the composition of the minor component of a sample.

To determine the composition of the sample gas from the equilibrium cell, the gas sample was analyzed by using the gas chromatograph. With the known value of the corrected peak height and the factor of the attenuation switch, the gas compositions were determined from the calibration curves.

Analysis of Carbon Tetrafluoride in Hydrogen

The calibration curve of the carbon tetrafluoride in hydrogen required for the determination of the gas phase composition was obtained using the 154D chromatograph. The calibration curve is shown in Figure 46. Nine standard bottles were prepared to cover the composition range from 0.05 to 20 mole percent. In this calibration the gas mixture made up in the gas burette was corrected for gas imperfection by 0.4 percent. A smooth curve was drawn through the calibration points and all points

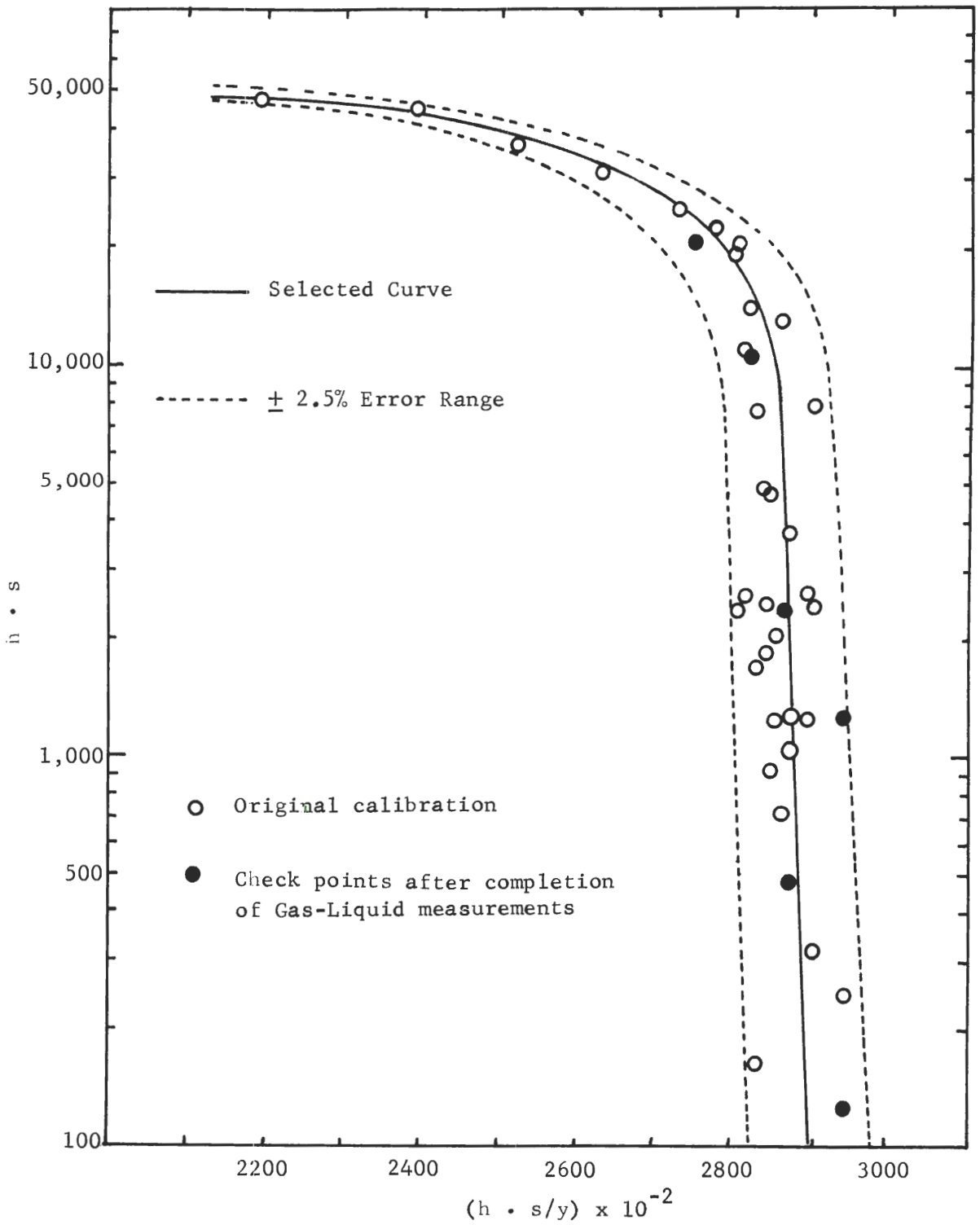

Figure 46. Calibration Curve of Carbon Tetrafluoride in Hydrogen.

fell within ± 2.5 mole percent from the selected curve. After completion of the phase equilibrium runs, six additional points were made to check the validity of the calibration curve.

Analysis of Chlorotrifluoromethane in Hydrogen

Figure 47 shows the calibration curve obtained for chlorotrifluoromethane in hydrogen using the 154D chromatograph. Nine standard bottles were prepared to cover the composition range from 0.05 to 23 mole percent of chlorotrifluoromethane. A 1.1 percent correction for gas imperfection of the gas mixture was applied in making up the standard gas mixture in the gas mixing burette. A smooth curve was drawn through the calibrated points and all points fell within ± 3.0 mole percent from the selected curve. The calibration curve was checked after completing the phase equilibrium runs for the hydrogen-chlorotrifluoromethane system. The checked points are also shown in Figure 47.

Analysis of Hydrogen in Carbon Tetrafluoride and Chlorotrifluoromethane

The 154B chromatograph was used to analyze the liquid phase samples for the composition of hydrogen in carbon tetrafluoride and in chlorotrifluoromethane. Only one calibration curve was constructed to cover the composition range of 0.45 to 9.99 mole percent of hydrogen. All of the calibration points fell within ± 2 mole percent of the selected curve. Six standard bottles were required to cover this range. The same amount of gas imperfection for the gas mixture stated earlier was also applied in making the gas mixture in the gas mixing burette. The calibration curve for the hydrogen analysis is shown

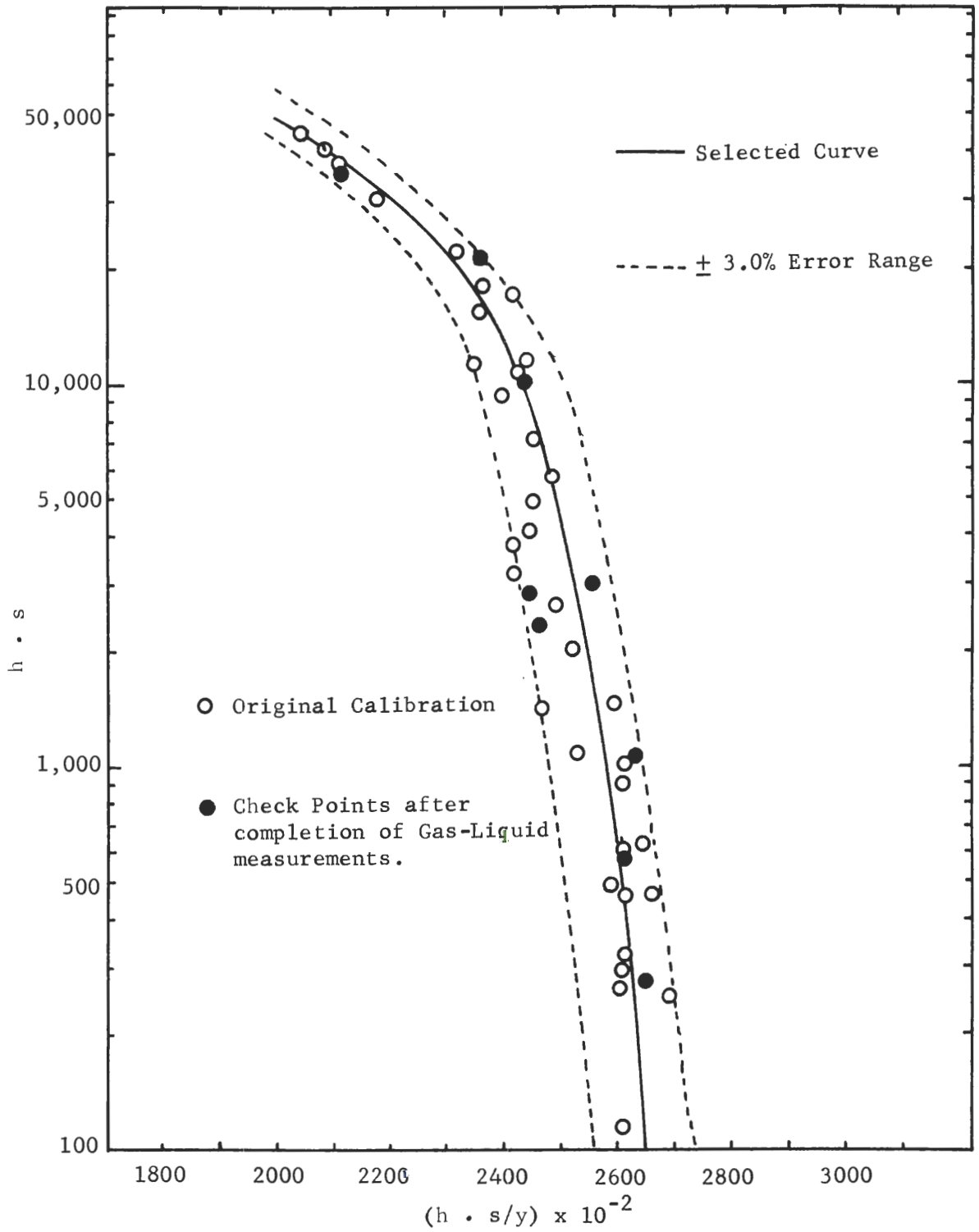

Figure 47. Calibration Curve of Chlorotrifluoromethane in Hydrogen.

in Figure 48 together with the checked points.

The 154B chromatograph had been modified by Yoon (132) for the purpose of obtaining a better separation of helium from carbon tetrafluoride or chlorotrifluoromethane. A seven foot column of silica gel (30/60 mesh) was externally installed between the sample valve and the main molecular sieve separation column. The externally installed column was also used in this work for the same purpose. Since chlorotrifluoromethane is permanently adsorbed on the molecular sieve 5A, chlorotrifluoromethane was vented to the air immediately after the hydrogen peak was measured in order to prevent this fluorocarbon from entering the main column.

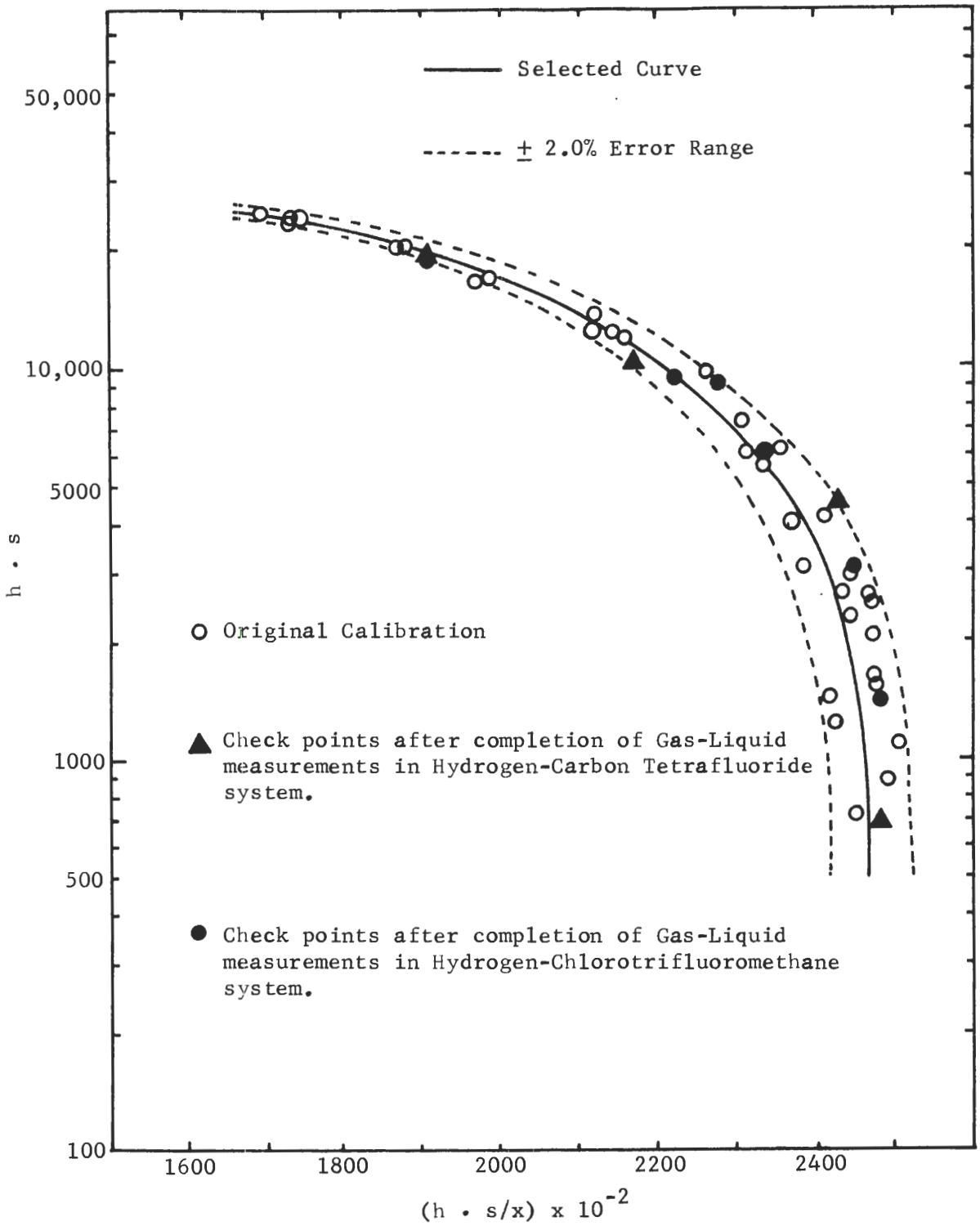

Figure 48. Calibration Curve of Hydrogen in Carbon Tetrafluoride and Chlorotrifluoromethane.

APPENDIX D

SUMMARY OF EXPERIMENTAL PHASE EQUILIBRIUM DATA FOR THE HYDROGEN-CARBON TETRAFLUORIDE AND HYDROGEN-CHLOROTRIFLUOROMETHANE SYSTEMS

The experimental phase-equilibrium data for the hydrogen-carbon tetrafluoride and hydrogen-chlorotrifluoromethane systems are presented in Tables 11 and 12. The data are presented in the order they were measured. The first column in these tables gives the code name of the sample. The first letter G or L indicates whether the sample was taken from the gas or liquid phase. The second letter represents the isotherm being measured. The first number designates the pressure setting and the second number is the sequence number of the samples taken at each pressure point.

The temperatures are reported in the (IPTS-68). The temperature of the gas and liquid samples was the average temperature indicated by the platinum resistance thermometer at the moment of withdrawal. The equilibrium cell temperature was always maintained at $\pm$ 0.03 K and temperature gradients along the equilibrium cell are always less than 0.03 K for both systems. The uncertainty of the pressure measurement is $\pm$ 0.5 percent. The pressure reading did not change significantly for each pressure setting.

The uncertainty of the gas phase composition measurement is $\pm$ 2.5

for the hydrogen-carbon tetrafluoride system and $\pm$ 3.0 percent for the hydrogen-chlorotrifluoromethane system. The uncertainty of the liquid phase composition measurement is $\pm$ 2.0 percent for both systems. With the uncertainties given above, the last number in the numerical values of y_1 and x_2 is included only for the purpose of internal consistency in the numerical calculation. The normal flow rate of these experimental points was 100 cc/hr at the cell temperature and pressure, unless specified.

Also shown in Table 11 and 12 are the equilibrium K-values, determined by the relation $K_i = y_i/x_i$.

Table 11. Experimental Gas and Liquid Phase Equilibrium Compositions in the Hydrogen-Carbon Tetrafluoride System.

Sample No.	T, K	P, atm	P_{o1}, atm	$100y_1$ mole%	Ø	$100x_2$ mole%	$K_1 \times 10^3$	K_2
L1A1	164.985	20.13				1.650		
L1A2	±0.02	20.13				1.629		
L1A3		20.13				1.652		
Selected	164.99	20.13	3.3599			1.644		
G2A3	164.985	40.30	3.3599	12.175				
G2A4	±0.014	40.30		12.194				
G2A5		40.30		12.224				
L2A1		40.30				3.540		
L2A2		40.30				3.550		
Selected	164.99	40.30	3.3599	12.197	1.463	3.545	126.5	24.77
G3A3	164.985	119.99	3.3599	7.656				
G3A4	±0.015	119.99		7.674				
G3A5		119.99		7.673				
Selected	164.99	119.99	3.3599	7.668	2.738			
G4A3	164.985	100.06	3.3599	8.019				
G4A4	±0.001	100.06		8.044				
G4A5		100.06		7.982				
L4A1		100.06				8.969		
L4A2		100.06				8.959		
Selected	164.99	100.06	3.3599	8.015	2.387	8.964	88.04	10.26

Table 11. (Continued)

Sample No.	T, K	P, atm	P_{ol}, atm	$100y_1$ mole%	Ø	$100x_2$ mole%	$K_1 \times 10^3$	K_2
G5A3	164.985	80.19	3.3599	8.547				
G5A4	±0.004	80.19		8.621				
G5A5		80.19		8.529				
L4A1		80.19				7.108		
L4A2		80.19				7.121		
Selected	164.99	80.19	3.3599	8.566	2.044	7.115	92.22	12.85
G6A3	164.985	59.91	3.3599	9.424				
G6A4	±0.017	59.91		9.388				
G6A5		59.91		9.418				
L6A1		59.91				5.439		
L6A2		59.91				5.435		
Selected	164.99	59.91	3.3599	9.410	1.678	5.437	99.51	16.66
G7A3*				12.079				
G7A4*	164.985	40.30	3.3599	12.131				
G7A5*	±0.012	40.30		12.131				
G7A6*		40.30		12.125				
L7A1*		40.30				3.518		
L7A2*		40.30				3.504		
Selected	164.99	40.30	3.3599	12.117	1.453	3.511	125.6	25.03
G8A3**		40.30		12.199				
G8A4**	164.985	40.30	3.3599	12.193				
G8A5**	±0.013	40.30		12.133				
G8A6**		40.30		12.105				
L8A1**		40.30				3.523		

Table 11. (Continued)

Sample No.	T, K	P, atm	P_{ol}, atm	$100y_1$ mole%	Ø	$100x_2$ mole%	$K_1 \times 10^3$	K_2
L8A2**		40.30				3.511		
Selected	164.99	40.30	3.3599	12.157	1.458	3.517	126.0	24.98
G9A3*		100.04		7.994				
G9A4*	164.985	100.04	3.3599	7.985				
G9A5*	±0.015	100.04		7.982				
G9A6*		100.04		7.973				
L9A1*		100.04				8.954		
L9A2*		100.04				8.995		
Selected	164.99	100.04	3.3599	7.984	2.377	8.980	87.72	10.25
G1B3	149.975	20.05	1.3903	8.695				
G1B4	±0.004	20.05		8.800				
G1B5		20.05		8.673				
G1B6		20.05		8.637				
L1B1		20.05				1.444		
L1B2		20.05				1.421		
Selected	149.98	20.05	1.3903	8.701	1.255	1.433	88.27	63.71
G2B3		40.30		5.327				
G2B4	149.975	40.30	1.3903	5.340				
G2B5	±0.002	40.30		5.342				
G2B6		40.30		5.337				
L2B1		40.30				2.926		
L2B2		40.30				2.919		

Table 11. (Continued)

Sample No.	T, K	P, atm	P_{ol}, atm	$100y_1$ mole%	ø	$100x_2$ mole%	$K_1 \times 10^3$	K_2
Selected	149.98	40.30	1.3903	5.335	1.546	2.923	54.96	32.39
G3B3		59.76	1.3903	4.296				
G3B4	149.975	59.76		4.298				
G3B5	±0.014	59.76		4.358				
G3B6		59.76		4.380				
L3B1		59.76				4.388		
L3B2		59.76				4.366		
Selected	149.98	59.76	1.3903	4.333	1.863	4.377	45.31	21.86
G4B3		80.04		3.924				
G4B4 1	149.75	80.04	1.3903	3.966				
G4B5	±0.010	80.04		3.957				
G4B6		80.04		3.923				
L4B1		80.04				5.884		
L4B2		80.04				5.892		
Selected	149.98	80.04	1.3903	3.943	2.270	5.888	41.90	16.31
G5B3		100.06		3.775				
G5B4	149.975	100.06	1.3903	3.742				
G5B5	±0.017	100.06		3.719				
G5B6		100.06		3.729				
L5B1		100.06				7.049		
L5B2						6.995		
L5B3						6.989		
Selected	149.98	100.06	1.3903	3.741	2.688	7.011	40.23	13.73

Table 11. (Continued)

Sample No.	T, K	P, atm	P_{ol}, atm	$100y_1$ mole %	Ø	$100x_2$ mole %	$K_1 \times 10^3$	K_2
G6B3		120.06		3.662				
G6B4	149.975	120.06	1.3903	3.701				
G6B5	±0.007	120.06		3.745				
G6B6		120.06		3.672				
L6B1		120.06				8.455		
L6B2		120.06				8.437		
Selected	149.98	120.06	1.3903	3.695	3.191	8.446	40.36	11.40
G1C3		120.05		1.559				
G1C4	134.010	120.05	0.4624	1.542				
G1C5	±0.016	120.05		1.574				
G1C6		120.05		1.562				
L1C1		120.05				6.272		
L1C2		120.05				6.302		
Selected	135.010	120.05	0.4624	1.559	4.048	6.287	16.64	15.66
G2C3		20.19		3.060				
G2C4	135.01	20.19	0.4624	3.056				
G2C5	±0.020	20.19		3.044				
G2C6		20.19		3.060				
L2C1		20.19				1.213		
L2C2		20.19				1.180		
Selected	135.01	20.19	0.4624	3.054	1.334	1.196	30.91	81.06
G3C3	135.010	40.30	0.4624	1.982				
G3C4	±0.016	40.30		1.977				

Table 11. (Continued)

Sample No.	T, K	P, atm	P_{ol}, atm	$100y_1$ mole%	Ø	$100x_2$ mole%	$K_1 \times 10^3$	K_2
G3C5		40.30		1.978				
G3C6		40.30		1.994				
L3C1		40.30				2.356		
L3C2		40.30				2.355		
Selected	135.010	40.30	0.4624	1.983	1.728	2.355	20.31	41.62
G4C3		60.17		1.673				
G4C4		60.17	0.4624	1.680				
G4C5	135.010	60.17		1.669				
G4C6	±0.013	60.17		1.671				
G4C7		60.17		1.686				
L4C1		60.17				3.416		
L4C2		60.17				3.383		
Selected	135.010	60.17	0.4624	1.676	2.181	3.399	17.35	28.93
G5C3		80.11		1.558				
G5C4	135.010	80.11		1.555				
G5C5	±0.015	80.11		1.551				
G5C6		80.11		1.573				
L5C1		80.11				4.465		
L5C2		80.11				4.484		
Selected	135.01	80.11	0.4624	1.559	2.701	4.475	16.32	21.99
G6C3		100.11	0.4624	1.522				
G6C4	135.01	100.11		1.540				
G6C5	±0.013	100.11		1.538				

Table 11. (Continued)

Sample No.	T, K	P, atm	P_{o1}, atm	$100y_1$ mole%	Ø	$100x_2$ mole%	$K_1 \times 10^3$	K_2
G6C6		100.11		1.536				
L6C1		100.11				5.587		
L6C2		100.11				5.570		
Selected	135.01	100.11	0.4624	1.534	3.321	5.578	16.25	17.65
G1D3		20.06		0.8136				
G1D4	119.941	20.06	0.11073	0.8092				
G1D5	±0.021	20.06		0.8026				
G1D6		20.06		0.8057		0.9072		
L1D1		20.06				0.8891		
L1D2		20.06						
Selected	119.95	20.06	0.11073	0.8078	1.463	0.8981	8.151	110.45
G2D3		40.01		0.5501				
G2D4	119.41	40.01	0.11073	0.5483				
G2D5	±0.004	40.01		0.5470				
G2D3		40.01		0.5474				
L2D1		40.01				1.752		
L2D2		40.01				1.755		
Selected	119.94	40.01	0.11073	0.5482	1.985	1.753	5.580	56.73
G3D3	119.941	60.38	0.11073	0.4944				
G3D4	±0.02	60.38		0.4988				
G3D5		60.38		0.4966				
L3D1		60.38				2.585		
L3D2		60.38				2.567		

Table 11. (Continued)

Sample No.	T, K	P, atm	P_{ol}, atm	$100y_1$ mole%	Ø	$100x_2$ mole%	$K_1 \times 10^3$	K_2
Selected	119.94	60.38	0.11073	0.4966	2.708	2.576	5.097	38.63
G4D3		79.91		0.4950				
G4D4	119.941	79.91	0.11073	0.3977				
G4D5	±0.015	79.91		0.4959				
G4D6		79.91		0.4956				
L4D1		79.91				3.213		
L4D2		79.91				2.318		
Selected	119.94	79.91	0.11073	0.4960	3.579	3.216	5.125	30.94
G5D3		100.08		0.5078				
G5D4	119.941	100.08	0.11073	0.5169				
G5D5	±0.012	100.08		0.5190				
L5D1		100.08				3.988		
L5D2		100.08				3.952		
Selected	119.94	100.08	0.11073	0.5146	4.650	3.970	5.359	25.06
G6D3		119.98		0.5424				
G6D4	119.941	119.98		0.5423				
G6D5	±0.019	119.88		0.5438				
G6D6		119.98		0.5439				
L6D1		119.98				4.651		
L6D2		119.98				4.664		
Selected	119.94	119.98	0.11073	0.5431	5.885	4.657	5.696	21.36

Table 11. (Continued)

Sample No.	T, K	P, atm	P_{ol}, atm	$100y_1$ mole%	ϕ	$100x_2$ mole%	$K_1 \times 10^3$	K_2
G1E3		20.14		0.03290				
G1E4	94.939	20.14	0.00310	0.03359				
G1E5	±0.030	20.14		0.03320				
G1E6		20.14		0.03326				
L1E1		20.14				0.4692		
L1E2		20.14				0.4660		
Selected	94.94	20.14	0.00310	0.03324	2.159	0.4676	0.3340	213.79
G2E3*		20.21		0.03429				
G2E4*	94.939	20.21	0.00310	0.03431				
G2E5*	±0.018	20.21		0.03431				
G2E6*		20.21		0.03430				
L2E1*		20.21				0.4683		
L2E2*		20.21				0.4701		
Selected	94.94	20.21	0.00310	0.03430	2.235	0.4692	0.3446	213.05
G3E3**		20.09		0.03325				
G3E4**	94.939	20.09	0.00310	0.03275				
G3E5**	±0.03	20.09		0.03305				
G3E6**		20.09		0.03209				
L3E1**		20.09				0.4705		
L3E2**		20.09				0.4650		
Selected	94.94	20.09	0.00310	0.03278	2.124	0.4682	0.3293	213.51
G4E3	94.939	40.37		0.02746				
G4E4	±0.019	40.37	0.00310	0.02757				

Table 11.(Continued)

Sample No.	T, K	P, atm	P_{ol}, atm	$100y_1$ mole%	Ø	$100x_2$ mole%	$K_1 \times 10^3$	K_2
G4E5	+0.019	40.37		0.02928				
G4E6		40.37		0.02863				
L4E1		40.37				0.8842		
L4E2		40.37				0.8821		
Selected	94.94	40.37	0.00310	0.02823	3.675	0.8833	0.2848	113.18
G5E3		60.17		0.03175				
G5E4	94.939	60.17	0.00310	0.03121				
G5E5	±0.016	60.17		0.03154				
G5E6		60.17		0.03171				
L5E1		60.17				1.261		
L5E2		60.17				1.263		
Selected	94.94	60.17	0.00310	0.03155	6.123	1.262	0.3195	79.21
G6E3		80.04		0.03715				
G6E4	94.939	80.04	0.00310	0.03699				
G6E5	±0.013	80.04		0.03681				
G6E6		80.04		0.03740				
L6E1		80.04				1.566		
L6E2		80.04				1.577		
Selected	94.94	80.04	0.00310	0.03709	9.575	1.572	0.3768	63.59
G7E3*		119.94		0.05456				
G7E4*	94.939	119.94	0.00310	0.05435				
G7E5*	±0.013	119.94		0.05429				
G7E6*		119.94		0.05409				

Table 11. (Continued)

Sample No.	T, K	P, atm	P_{ol}, atm	$100y_1$ mole%	Ø	$100x_2$ mole%	$K_1 \times 10^3$	K_2
L7E1*		119.94				2.145		
L7E2*		119.94				2.128		
Selected	94.94	119.94	0.00310	0.05432	21.012	2.136	0.5551	46.79
G8E3		100.06		0.04454				
G8E4	94.939	100.06	0.00310	0.04429				
G8E5	±0.014	100.06		0.04421				
G8E6		100.06		0.04536				
L8E1		100.06				1.853		
L8E2		100.06				1.850		
L8E3						1.837		
Selected	94.94	100.06	0.00310	0.04460	14.393	1.846	0.4544	54.15
G9E3**		119.38	0.00310	0.05319				
G9E4**	94.939	119.38		0.04374				
G9E5**	±0.007	119.38		0.05334				
G9E6**		119.38		0.05305				
L9E1**		119.38				2.120		
L9E2**		119.38				2.109		
Selected	94.94	119.38	0.00310	0.05333	20.533	2.114	0.5448	47.28
G10E3		119.38		0.05241				
G10E4	94.939	119.38	0.00310	0.05368				
G10E5	±0.028	119.38		0.05347				
G10E6		119.38		0.05388				
L10E1		119.38				2.147		

Table 11. (Continued)

Sample No.	T, K	P, atm	P_{ol}, atm	$100y_1$ mole%	Ø	$100x_2$ mole%	$K_1 \times 10^3$	K_2
L10E2		119.38				2.099		
Selected	94.94	119.38	0.00310	0.05336	20.545	2.123	0.5452	47.08
G1F3		20.07		0.1354				
G1F4	105.007	20.07	0.016644	0.1335				
G1F5	±0.030	20.07		0.1347				
G1F6		20.07		0.1345				
L1F1		20.07				0.6375		
L1F2		20.07				0.6337		
Selected	105.01	20.07	0.016644	0.1345	1.622	0.6356	1.354	157.12
G2F3		40.19		0.1097				
G2F4	105.007	40.19	0.016644	0.1093				
G2F5	±0.021	40.19		0.1101				
G2F6		40.19		0.1095				
L2F1		40.19				1.201		
L2F2		40.19				1.202		
Selected	105.01	40.19	0.016644	0.1096	2.646	1.201	1.109	83.17
G3F3		60.18		0.1092				
G3F4	105.007	60.18	0.016644	0.1086				
G3F5	±0.022	60.18		0.1102				
G3F6		60.18		0.1101				
L3F1		60.18				1.716		
L3F2		60.18				1.712		

Table 11.(Continued)

Sample No.	T, K	P, atm	P_{ol}, atm	$100y_1$ mole%	Ø	$100x_2$ mole%	$K_1 \times 10^3$	K_2
Selected	105.01	60.18	0.016684	0.1095	3.959	1.714	1.114	58.28
G4F3		79.93		0.1197				
G4F4	105.007	79.93	0.016644	0.1194				
G4F5	±0.029	79.93		0.1189				
G4F6		79.93		0.1192				
L4F1		79.93				2.182		
L4F2		79.93				2.175		
Selected	105.01	79.93	0.016644	0.1193	5.729	2.179	1.220	45.84
G5F3		99.99		0.1278				
G5F4	105.007	99.99	0.016644	0.1291				
G5F5	±0.003	89.89		0.1277				
G5F6		99.98		0.1291				
L5F1		99.99				2.590		
L5F2		99.99				2.667		
Selected	105.01	99.99	0.016644	0.1284	7.714	2.629	1.319	37.99
G6F3		120.00		0.1459				
G6F4	105.007	120.00		0.1468				
G6F5	±0.017	120.00		0.1469				
G6F6		120.00		0.1455				
L6F1		120.00				3.018		
L6F2		120.00				3.077		
Selected	105.01	120.00	0.016644	0.1463	10.548	3.048	1.509	32.76

* Flow Rate was half the normal flow rate. ** Flow rate was twice the normal flow rate.

Table 12. Experimental Gas and Liquid Phase Equilibrium Compositions in the Hydrogen-Chlorotrifluoromethane System.

Sample No.	T, K	P, atm	P_{o1}, atm	$100y_1$ mole%	Ø	$100x_2$ mole%	$K_1 \times 10^3$	K_2
G1A3	189.965	20.09	0.90822	5.519				
G1A4	±0.011	20.09		5.560				
G1A5		20.09		5.572				
L1A1		20.09				1.403		
L1A2		20.09				1.411		
Selected	189.97	20.09	0.90822	5.551	1.229	1.407	56.30	67.13
G2A3		40.16		3.270				
G2A4	189.965	40.16	0.90822	3.297				
G2A5	±0.010	40.16		3.316				
G2A6		40.16		3.288				
L2A1		40.16				2.916		
L2A2		40.16				2.924		
Selected	189.97	40.16	0.90822	3.293	1.456	2.920	33.92	33.12
G3A3		59.76		2.524				
G3A4	189.965	59.76	0.90822	2.538				
G3A5	±0.006	59.76		2.542				
G3A6		59.76		2.556				
L3A1		59.76				4.191		
L3A2		59.76				4.212		
Selected	189.97	59.76	0.90822	2.540	1.671	4.201	26.51	23.41

Table 12. (Continued)

Sample No.	T, K	P, atm	P_{ol}, atm	$100y_1$ mole%	∅	$100x_2$ mole%	$K_1 \times 10^3$	K_2
G4A3	189.965	79.90	0.90822	2.308				
G4A4	±0.005	79.90		2.285				
G4A5		79.90		2.276				
Selected	189.97	79.90	0.90822	2.290	2.015			
G5A3	189.965	80.25	0.90822	2.274				
G5A4	±0.005	80.25		2.258				
G5A5		80.25		2.297				
L5A1		80.25				5.471		
L5A2		80.25				5.488		
Selected	189.97	80.25	0.90822	2.276	2.011	5.480	24.13	17.83
G6A3		99.91		2.108				
G6A4	189.965	99.91	0.90822	2.119				
G6A5	±0.005	99.91		2.089				
G6A6		99.91		2.089				
L6A1		99.91				6.900		
L6A2		99.91				6.880		
Selected	189.97	99.91	0.90822	2.102	2.312	6.890	22.57	14.21
G7A3		119.98		2.034				
G7A4	189.965	119.98	0.90822	2.019				
G7A5	±0.005	119.98		2.028				
G7A6		119.98		2.018				
L7A1		119.98				8.138		
L7A2		119.98				8.160		

Table 12.(Continued)

Sample No.	T, K	P, atm	P_{o1}, atm	$100y_1$ mole%	∅	$100x_2$ mole%	$K_1 \times 10^3$	K_2
L7A3						8.300		
Selected	189.97	119.98	0.90822	2.024	2.674	8.200	22.05	11.95
G1B3		20.06		2.358				
G1B4	175.018	20.06	0.37095	2.348				
G1B5	±0.024	20.06		2.383				
G1B6		20.06		2.382				
L1B1		20.06				1.221		
L1B2		20.06				1.203		
Selected	175.02	20.06	0.37095	2.368	1.280	1.212	23.97	80.55
G2B3		40.37		1.372				
G2B4	175.018	40.37	0.37095	1.372				
G2B5	±0.014	40.37		1.386				
G2B6		40.37		1.382				
L2B1		40.37				2.462		
L2B2		40.37				2.433		
Selected	175.02	40.37	0.37095	1.378	1.499	2.448	14.12	40.29
G3B3		59.97		1.141				
G3B4	175.018	59.97	0.37095	1.139				
G3B5	±0.010	59.97		1.147				
G3B6		59.97		1.141				
L3B1		59.97				3.647		
L3B2		59.97				3.647		

Table 12. (Continued)

Sample No.	T, K	P, atm	P_{o1}, atm	$100y_1$ mole%	Ø	$100x_2$ mole%	$K_1 \times 10^3$	K_2
Selected	175.02	59.97	0.37095	1.142	1.847	3.647	11.85	27.14
G4B3		79.70		1.022				
G4B4	175.018	79.70		1.023				
G4B5	±0.014	79.70		1.036				
G4B6		79.70		1.032				
L4B1		79.70				4.669		
L4B2		79.70				4.677		
Selected	175.02	79.70	0.37095	1.028	2.209	4.673	10.78	21.18
G5B3		99.91		0.9785				
G5B4	175.018	99.91	0.37095	0.9794				
G5B5	±0.015	99.91		0.9783				
G5B6		99.91		0.9576				
L5B1		99.91				5.734		
L5B2		99.91				5.702		
Selected	175.02	99.91	0.37095	0.9735	2.622	5.716	10.33	17.32
G6B3		119.88		0.9481				
G6B4	175.018	119.88	0.37095	0.9651				
G6B5	±0.010	119.88		0.9670				
G6B6		119.88		0.9610				
L6B1		119.88				6.890		
L6B2		119.88				6.839		
Selected	175.02	119.88	0.37095	0.9603	3.103	6.864	10.31	14.43

Table 12. (Continued)

Sample No.	T, K	P, atm	P_{ol}, atm	$100y_1$ mole%	∅	$100x_2$ mole%	$K_1 \times 10^3$	K_2
G1C3		119.99		0.3904				
G1C4	160.018	119.99	0.12416	0.3944				
G1C5	±0.015	119.99		0.3923				
G1C6		119.99		0.3884				
L1C1		119.99				5.760		
L1C2		119.99				5.602		
Selected	160.02	119.99	0.12416	0.3913	3.782	5.681	4.149	17.53
G2C3		20.13		0.7940				
G2C4	160.018	20.13	0.12416	0.7831				
G2C5	±0.019	20.13		0.7948				
G2C6		20.13		0.7969				
L2C1		20.13				1.059		
L2C2		20.13				1.052		
Selected	160.02	20.13	0.12416	0.7922	1.284	1.055	8.006	94.04
G3C3		40.17		0.5151				
G3C4	160.018	40.17	0.12416	0.5104				
G3C5	±0.004	40.17		0.5107				
G3C6		40.17		0.5077				
L3C1		40.17				2.021		
L3C2		40.17				2.014		
Selected	160.02	40.17	0.12416	0.5110	1.653	2.018	5.215	49.30
G4C3	160.018	59.77		0.4265				
G4C4	±0.004	59.77	0.12416	0.4209				

Table 12. (Continued)

Sample No.	T, K	P, atm	P_{ol}, atm	$100y_1$ mole%	∅	$100x_2$ mole%	$K_1 \times 10^3$	K_2
G4C5		59.77		0.4265				
G4C6		59.77		0.4208				
L4C1		59.77				3.092		
L4C2		59.77				3.087		
Selected	160.02	59.77	0.12416	0.4236	2.039	3.090	4.371	32.22
G5C3		79.63		0.3957				
G5C4	160.018	79.63	0.12416	0.3903				
G5C5	±0.018	79.63		0.3869				
G5C6		79.63		0.3881				
L5C1		79.63				3.904		
L5C2		79.63				3.914		
Selected	160.02	79.63	0.12416	0.3903	2.503	3.909	4.061	25.48
G6C3		100.05		0.3775				
G6C4	160.018	100.05	0.12416	0.3830				
G6C5	±0.018	100.05		0.3786				
G6C6		100.05		0.3814				
L6C1		100.05				4.775		
L6C2		100.05				4.806		
Selected	160.02	100.05	0.12416	0.3801	3.063	4.790	3.921	20.80
G1D3		20.26		0.2175				
G1D4	145.018	20.26	0.12416	0.2169				
G1D5	±0.020	20.26		0.2177				
L1D1		20.26				0.8802		

Table 12. (Continued)

Sample No.	T, K	P, atm	P_{ol}, atm	$100y_1$ mole%	Ø	$100x_2$ mole%	$K_1 \times 10^3$	K_2
L1D1		20.26				0.8763		
Selected	145.02	20.26	0.031800	0.2164	1.379	0.8783	2.183	113.6
G2D3		40.23		1.433				
G2D4	145.018	40.23	0.031800	1.406				
G2D5	±0.010	40.23		1.418				
G2D6		40.23		1.411				
L2D1		40.23				1.667		
L2D2		40.23				1.666		
Selected	145.02	40.23	0.031800	0.1417	1.793	1.667	1.441	59.90
G3D3		59.97		0.1306				
G3D4	145.018	59.97	0.031800	0.1294				
G3D5	±0.003	59.97		0.1296				
G3D6		59.97		0.1303				
L3D1		59.97				2.442		
L3D2		59.97				2.451		
Selected	145.02	59.97	0.031800	0.1300	2.451	2.446	1.333	40.83
G4D3		79.50		0.1257				
G4D4	145.018	79.50	0.031800	0.1248				
G4D5	±0.013	79.50		0.1257				
G4D6		79.50		0.1253				
L4D1		79.50				3.190		
L4D2		79.50				3.173		

Table 12. (Continued)

Sample No.	T, K	P, atm	P_{o1}, atm	$100y_1$ mole$_1$%	Ø	$100x_2$ mole$_2$%	$K_1 \times 10^3$	K_2
Selected	145.02	79.50	0.031800	0.1254	3.135	3.182	1.295	31.39
G5D3		99.84		1.298				
G5D4	145.018	99.84	0.031800	1.289				
G5D5	±0.017	99.84		1.297				
G5D6		99.84		1.301				
L5D1		99.84				3.913		
L5D2		99.84				3.884		
Selected	145.02	99.84	0.031800	0.1296	4.069	3.899	1.349	25.61
G6D3		119.92		0.1343				
G6D4	145.018	119.92	0.031800	0.1385				
G6D5	±0.020	119.92		0.1366				
G6D6		119.92		0.1359				
L6D1		119.92				4.514		
L6D2		119.92				4.532		
Selected	145.02	119.92	0.031800	0.1363	5.140	4.553	1.428	21.93
G1E3*		120.02		0.05953				
G1E4*	135.010	120.02	0.010462	0.05903				
G1E5*	±0.013	120.02		0.05885				
G1E6*		120.02		0.05721				
L1E1*		120.02				3.905		
L1E2*		120.02				3.882		
Selected	135.01	120.02	0.010462	0.05865	6.728	3.894	0.6103	25.67

Table 12. (Continued)

Sample No.	T, K	P, atm	P_{o1}, atm	$100y_1$ mole%	∅	$100x_2$ mole%	$K_1 \times 10^3$	K_2
G2E3		119.86		0.05882				
G2E4	135.010	119.86	0.010462	0.05905				
G2E5	±0.019	119.86		0.05655				
G2E6		119.86		0.05812				
L2E1		119.86				3.888		
L2E2		119.86				3.900		
Selected	135.01	119.86	0.010462	0.05813	6.660	3.894	0.6048	25.67
G3E4**	135.010	119.91	0.010462	0.05937				
G3E5**	±0.014	119.91		0.05946				
G3E6**		119.91		0.05872				
L3E1**		119.91				3.895		
L3E2**		119.91				3.893		
Selected	135.01	119.91	0.010462	0.05917	6.782	3.894	0.6157	25.67
G4E3*				0.07479				
G4E4*	135.010	20.09	0.010462	0.07139				
G4E5*	±0.014	20.09		0.07500				
G4E6*		20.09		0.07359				
L4E1*		20.09				0.7475		
L4E2*		20.09				0.7479		
Selected	135.01	20.09	0.010462	0.07370	1.416	0.7477	0.7425	133.6
G5E3		20.06		0.07504				
G5E4	135.010	20.06	0.010462	0.07475				
G5E5	±0.021	20.06		0.07528				
G5E6		20.06		0.07456				

Table 12. (Continued)

Sample No.	T, K	P, atm	P_{ol}, atm	$100y_1$ mole%	Ø	$100x_2$ mole%	$K_1 \times 10^3$	K_2
L5E1		20.06				0.7477		
L5E2		20.06				0.7430		
Selected	135.01	20.06	0.010462	0.07491	1.436	0.7453	0.7547	134.1
G6E3**		20.06		0.07551				
G6E4**	135.010	20.06	0.010462	0.07582				
G6E5**	±0.009	20.06		0.07377				
G6E6**		20.06		0.07415				
L6E1**		20.06				0.7414		
L6E2**		20.06				0.7349		
Selected	135.01	20.06	0.010462	0.07481	1.435	0.7382	0.7537	135.4
G7E3		40.17		0.05155				
G7E4	135.010	40.17	0.010462	0.05300				
G7E5	±0.016	40.17		0.05340				
G7E6		40.17		0.05283				
L7E1		40.17				1.422		
L7E2		40.17				1.416		
Selected	135.01	40.17	0.010462	0.05270	2.023	1.419	0.5346	70.44
G8E3		59.83		0.04963				
G8E4	135.010	59.83	0.010462	0.04878				
G8E5	±0.025	59.83		0.04902				
G8E6		59.83		0.04812				
L8E1		59.83				2.045		
L8E2		59.83				2.057		

Table 12. (Continued)

Sample No.	T, K	P, atm	P_{ol}, atm	$100y_1$ mole%	ø	$100x_2$ mole%	$K_1 \times 10^3$	K_2
Selected	135.01	59.83	0.010462	0.04889	2.796	2.051	0.4991	48.73
G9E3		79.63		0.05095				
G9E4	135.010	79.63		0.04980				
G9E5	±0.023	79.63		0.05075				
G9E6		79.63		0.04966				
L9E1		79.63				2.670		
L9E2		79.63				2.678		
Selected	135.01	79.63	0.010462	0.05029	3.828	2.674	0.5167	37.38
G10E3		99.84		0.05386				
G10E4	135.010	99.84	0.010462	0.05329				
G10E5	±0.019	99.84		0.05372				
G10E6		99.84		0.05379				
L10E1		99.84				3.334		
L10E2		99.84				3.289		
Selected	135.01	99.84	0.010462	0.05367	5.122	3.311	0.5551	30.19
G1F3		20.20		21.823				
G1F4	219.994	20.20	3.656	21.551				
G1F5	±0.015	20.20		21.529				
G1F6		20.20		21.771				
L1F1		20.20				1.634		
L1F2		20.20				1.625		
Selected	219.99	20.20	3.656	21.668	1.197	1.630	220.3	48.06

Table 12. (Continued)

Sample No.	T, K	P, atm	P_{ol}, atm	$100y_1$ mole%	ø	$100x_2$ mole%	$K_1 \times 10^3$	K_2
G2F3*		20.67		21.414				
G2F4*	219.994	20.67	3.656	21.516				
G2F5*	±0.007	20.67		21.508				
G2F6*		20.67		21.550				
L2F1*		20.67				1.619		
L2F2*		20.67				1.620		
Selected	219.99	20.67	3.656	21.497	1.192	1.620	218.5	48.46
G3F3**	219.994	20.06	3.656	21.851				
G3F4**	±0.015	20.06		21.903				
G3F5**		20.06		21.914				
L3F1**		20.06				1.610		
L3F2**		20.06				1.621		
Selected	219.99	20.06	3.656	21.889	1.202	1.616	222.5	48.34
G4F3		39.90		12.422				
G4F4	219.994	39.90	3.656	12.376				
G4F5	±0.010	38.90		12.410				
G4F6		39.90		12.467				
L4F1		39.90				3.499		
L4F2		39.90				3.463		
Selected	219.99	39.90	3.656	12.419	1.355	3.481	128.7	25.16
G5F3		59.90		9.728				
G5F4	219.994	59.90	3.656	9.805				
G5F5	±0.014	59.90		9.860				

Table 12. (Continued)

Sample No.	T, K	P, atm	P_{o1}, atm	$100y_1$ mole%	ø	$100x_2$ mole%	$K_1 \times 10^3$	K_2
G5F6		59.90		9.759				
L5F1		59.90				5.344		
L5F2		59.90				5.336		
Selected	219.99	59.90	3.656	9.801	1.606	5.340	103.5	15.02
G6F3		79.91		8.201				
G6F4	219.994	79.91	3.656	8.138				
G6F5	±0.013	79.91		8.141				
G6F6		79.91		8.141				
L6F1		79.91				7.219		
L6F2						7.206		
Selected	219.99	79.91	3.656	8.155	1.782	7.213	87.89	12.73
G7F3		99.98		7.336				
G7F4	219.94	99.98		7.396				
G7F5	±0.009	99.98		7.389				
G7F6		99.98		7.294				
L7F1		99.98				8.986		
L7F2		99.98				8.982		
Selected	219.99	99.98	3.656	7.354	2.011	8.984	80.80	10.31
G8F3*		119.99		6.793				
G8F4*	219.994	119.99	3.656	6.748				
G8F5*	±0.012	119.99		6.742				
G8F6*		119.99		6.766				
L8F1*		119.99				10.529		

Table 12. (Continued)

Sample No.	T, K	P, atm	P_{ol}, atm	$100y_1$ mole%	ø	$100x_2$ mole%	$K_1 \times 10^3$	K_2
L8F2*		119.99				10.445		
Selected	219.99	119.99	3.656	6.762	2.219	10.487	75.54	8.891
G9F3		119.99		6.744				
G9F4	219.994	119.99		6.737				
G9F5	±0.011	119.99		6.708				
G9F6		119.99		6.744				
L9F1		119.99				10.584		
L9F2		119.99				10.586		
Selected	219.99	119.99	3.656	6.733	2.210	10.585	75.30	8.811
G1G3		120.02		3.898				
G1G4	205.031	120.02	1.9312	3.907				
G1G5	±0.012	120.02		3.901				
G1G6		120.02		3.823				
L1G1		120.02				9.360		
L1G2		120.02				9.371		
Selected	205.03	120.02	1.9312	3.883	2.413	9.365	42.84	10.26
G2G3		100.15		4.123				
G2G4	205.031	100.15	1.9312	4.076				
G2G5	±0.017	100.15		4.097				
G2G6		100.15		4.113				
L2G1		100.15				7.883		
L2G2		100.15				7.855		

Table 12. (Continued)

Sample No.	T, K	P, atm	P_{o1}, atm	$100y_1$ mole%	Ø	$100x_2$ mole%	$K_1 \times 10^3$	K_2
Selected	205.03	100.15	1.9312	4.102	2.127	7.869	44.52	12.19
G3G3		79.91		4.336				
G3G4	205.031	79.91	1.9312	4.529				
G3G5	±0.018	79.91		4.499				
G3G6		79.91		4.484				
L3G1		79.91				6.434		
L3G2		79.91				6.390		
Selected	205.03	79.91	1.9312	4.462	1.846	6.412	47.70	14.90
G4G3		59.90		5.084				
G4G4	205.031	59.90	1.9312	5.162				
G4G5	±0.011	59.90		5.183				
G4G6		59.90		5.129				
L4G1		59.90				4.780		
L4G2		59.90				4.767		
Selected	205.03	59.90	1.9312	5.139	1.594	4.773	53.97	19.87
G5G3		40.10		6.812				
G5G4	205.031	40.10	1.9312	6.809				
G5G5	±0.011	40.10		6.833				
G5G6		40.10		6.825				
L5G1		40.10				3.209		
L5G2		40.10				3.217		
Selected	205.03	40.10	1.9312	6.820	1.416	3.213	70.46	29.00

Table 12. (Continued)

Sample No.	T, K	P, atm	P_{ol}, atm	$100y_1$ mole%	Ø	$100x_2$ mole%	$K_1 \times 10^3$	K_2
G6G3		20.20		11.298				
G6G4	205.031	20.20	1.9312	11.248				
G6G5	±0.007	20.20		11.407				
G6G6		20.20		11.171				
L6G1		20.20				1.546		
L6G2		20.20				1.542		
Selected	205.03	20.20	1.9312	11.280	1.180	1.544	114.6	57.46

* Flow rate was half the normal flow rate

** Flow rate was twice the normal flow rate

APPENDIX E

SMOOTHED EXPERIMENTAL AND THEORETICAL ENHANCEMENT FACTORS AND SMOOTHED EXPERIMENTAL SOLUBILITY OF HYDROGEN

The phase equilibrium data of the hydrogen-carbon tetrafluoride and hydrogen-chlorotrifluoromethane systems have been smoothed by using a least squares fitting program. The experimental data on each isotherm expressed as $\emptyset$ or x_2 were fitted to polynomials of order 1 up to order 4. The best fitted polynomial was selected to calculate these quantitites at smoothed pressures. The deviations of the experimental value from the smoothed value are always less than 2 percent. The smoothed experimental values, together with values of $\emptyset$ calculated from the theoretical models, are shown in Tables 13 and 14.

The theoretical enhancement factors of the hydrogen-carbon tetrafluoride system were calculated from five different theoretical models for the gas phase. These five models are the Lennard-Jones (6-12) classical (LJCL); the Kihara core model (KIH); the Kihara core model (KIHCK12) with K_{12} calculated from Equation (V-5); the BWR equation with $(B_o)_{12}$ calculated using a linear average (BWR(LINEAR)), and the BWR equation with $(B_o)_{12}$ calculated using the Lorentz average (BWR(LORENTZ)). Only three models (LJCL), (KIH), (KIHCK12) were calculated for the hydrogen-chlorotrifluoromethane system, since the constants of the BWR equation for chlorotrifluoromethane are not available.

The theoretical enhancement factors and the smoothed experimental data in the gas-liquid region of the hydrogen-argon (87), hydrogen-methane (61), hydrogen-ethane (52), and hydrogen-ethylene (51) systems are also presented in Table 15 through Table 18. Five theoretical models (LJCL), (KIH), (KIHCK12), BWR(LINEAR) and BWR(LORENTZ) were calculated for the hydrogen-methane (61) and hydrogen-ethane (52) systems. Besides these models, the (KIHEK12) model was also calculated for the hydrogen-ethylene system (51). The (KIHEK12) model is calculated by using the experimental K_{12} value shown in Table 2 of Chapter V. Three theroetical models (LJCL), (KIH), and BWR(LORENTZ) calculated for the hydrogen-argon system are taken directly from those presented by Mullins (87).

Table 13. Smoothed Experimental and Theoretical Enhancement Factors of Carbon Tetrafluoride in Hydrogen, and the Smoothed Experimental Solubility of Hydrogen in Liquid Carbon Tetrafluoride.

P atm	Ø exp	Ø LJCL	Ø KIH	Ø KIHCK12	Ø BWR(a)	Ø BWR(b)	$100x_2$
			..... 94.94 K				
20	2.165	1.878	1.870	1.863	1.938	1.911	0.4653
40	3.640	3.447	3.382	3.360	3.603	3.503	0.8768
60	6.092	6.141	5.869	5.813	6.372	6.112	1.257
80	9.581	10.571	9.739	9.617	10.679	10.111	1.574
100	14.36	17.543	15.456	15.220	16.959	15.860	1.844
120	20.86	28.053	23.521	23.102	25.568	23.631	2.132
			..... 105.01 K				
20	1.652	1.634	1.626	1.622	1.630	1.610	0.6334
40	2.606	2.614	2.571	2.559	2.577	2.512	1.197
60	4.002	4.084	3.947	3.919	3.946	3.799	1.708
80	5.679	6.221	5.875	5.819	5.843	5.559	2.182
100	7.743	9.235	8.482	8.385	8.367	7.867	2.628
120	10.54	13.370	11.911	11.750	11.600	10.784	3.048
			..... 119.94 K				
20	1.462	1.429	1.426	1.423	1.411	1.395	0.8935
40	1.982	2.006	1.989	1.982	1.937	1.894	1.760
60	2.693	2.769	2.725	2.710	2.614	2.527	2.534
80	3.583	3.761	3.665	3.640	3.466	3.312	3.252
100	4.646	5.025	4.844	4.803	4.514	4.265	3.949
120	5.886	6.608	6.299	6.236	5.777	5.396	4.662
			..... 135.01 K				
20	1.330	1.318	1.322	1.321	1.319	1.306	1.182
40	1.723	1.704	1.709	1.704	1.677	1.642	2.345
60	2.175	2.181	2.186	2.177	2.112	2.045	3.379
80	2.700	2.755	2.762	2.747	2.631	2.519	4.480
100	3.316	3.443	3.456	3.433	3.249	3.073	5.567
120	4.046	4.277	4.307	4.272	3.992	3.729	6.287

Table 13. (Continued)

P atm	Ø exp	Ø LJCL	Ø KIH	Ø KIHCK12	Ø BWR(a)	Ø BWR(b)	$100x_2$
			..... 149.98 K				
20	1.255	1.256	1.270	1.269	1.291	1.280	1.436
40	1.537	1.544	1.569	1.566	1.579	1.548	2.871
60	1.876	1.877	1.921	1.915	1.915	1.856	4.450
80	2.260	2.267	2.343	2.332	2.319	2.218	5.832
100	2.691	2.722	2.852	2.835	2.807	2.646	7.034
120	3.189	3.235	3.453	3.428	3.389	3.141	8.435
			.....164.99 K				
20		1.218	1.242	1.241	1.292	1.282	1.627
40	1.452	1.451	1.499	1.497	1.585	1.535	3.496
60	1.698	1.709	1.797	1.792	1.885	1.824	5.445
80	2.022	2.005	2.159	2.150	2.289	2.175	7.100
100	2.386	2.330	2.591	2.577	2.815	2.609	8.966
120	2.736	2.692	3.137	3.113	3.609	3.187	10.80*

a LORENTZ

b LINEAR

* Extrapolated Value

Table 14. Smoothed Experimental and Theoretical Enhancement Factors of Chlorotrifluoromethane in Hydrogen, and the Smoothed Experimental Solubility of Hydrogen in Liquid Chlorotrifluoromethane.

P atm	Ø exp	Ø LJCL	Ø KIH	Ø KIHCK12	$100x_2$
		.... 134.97 K			
20	1.428	1.500	1.461	1.418	0.7404
40	2.013	2.197	2.089	1.970	1.413
60	2.811	3.144	2.923	2.682	2.058
80	3.842	4.400	4.003	3.581	2.694
100	5.137	6.027	5.374	4.691	3.317
120	6.729	8.091	7.082	6.043	3.896
		.... 145.02 K			
20	1.373	1.403	1.376	1.342	0.8682
40	1.800	1.930	1.859	1.769	1.658
60	2.426	2.600	2.467	2.295	2.447
80	3.181	3.443	3.222	2.933	3.021
100	4.064	4.482	4.144	3.695	3.904
120	5.147	5.745	5.256	4.595	4.556
		.... 160.02 K			
20	1.282	1.306	1.292	1.267	1.046
40	1.647	1.673	1.641	1.578	2.030
60	2.049	2.113	2.056	1.941	3.060
80	2.507	2.634	2.550	2.363	3.965
100	3.064	3.245	3.131	2.855	4.768
120	3.782	3.944	3.802	3.409	5.686
		.... 175.02 K			
20	1.271	1.246	1.243	1.223	1.207
40	1.496	1.519	1.511	1.464	2.432
60	1.841	1.832	1.820	1.736	3.629
80	2.221	2.188	2.178	2.046	4.703
100	2.621	2.589	2.587	2.395	5.714
120	3.107	3.030	3.047	2.778	6.874

Table 14. (Continued)

P atm	Ø exp	Ø LJCL	Ø KIH	Ø KIHCK12	$100x_2$
		.... 189.97 K			
20	1.225	1.210	1.215	1.200	1.396
40	1.449	1.423	1.433	1.396	2.923
60	1.706	1.663	1.682	1.617	4.190
80	1.966	1.924	1.962	1.860	5.490
100	2.320	2.206	2.274	2.126	6.883
120	2.677	2.511	2.623	2.420	8.204
		.... 205.03 K			
20	1.177	1.191	1.203	1.191	1.532
40	1.416	1.369	1.394	1.363	3.186
60	1.594	1.557	1.604	1.549	4.819
80	1.824	1.759	1.838	1.654	6.382
100	2.124	1.975	2.101	1.979	7.877
120	2.413	2.202	2.394	2.225	9.360
		.... 219.99 K			
20	1.195	1.182	1.199	1.190	1.606
40	1.378	1.338	1.378	1.352	3.487
60	1.583	1.496	1.570	1.523	5.356
80	1.799	1.659	1.782	1.708	7.215
100	2.014	1.829	2.020	1.911	8.989
120	2.217	2.010	2.300	2.141	10.54

Table 15. Smoothed Experimental and Theoretical Enhancement Factors of Ethane in Hydrogen, and the Smoothed Experimental Solubility of Hydrogen in Liquid Ethane.

P atm	ø exp	ø LJCL	ø KIH	ø KIHCK12	ø BWR(a)	ø BWR(b)	$100x_2$
				•••• 108.00 K ••••			
20	1.869	1.900	1.770	1.621	1.787	1.757	0.4169*
40	3.074	3.504	3.035	2.552	3.093	2.991	0.7478*
60	5.017	6.237	5.010	3.888	5.155	4.907	1.131
80	8.086	10.708	7.694	5.733	8.263	7.748	1.457
100	12.46	17.721	12.196	8.145	12.73	11.770	1.740
120	18.38	28.294	18.030	11.339	18.88	17.223	1.995
				•••• 122.00 K ••••			
20	1.545	1.601	1.524	1.430	1.511	1.489	0.5498*
40	2.364	2.502	2.266	2.002	2.235	2.170	1.007
60	3.485	3.811	3.284	2.740	3.228	3.090	1.474
80	4.849	5.657	4.639	3.670	4.550	4.298	1.921
100	6.647	8.191	6.395	4.813	6.262	5.840	2.331
120	9.117	11.583	8.616	6.191	8.423	7.759	2.699
				•••• 130.00 K ••••			
20	1.392	1.493	1.435	1.360	1.417	1.398	0.6063*
40	1.991	2.180	2.014	1.813	1.970	1.916	1.253
60	2.770	3.118	2.771	2.377	2.689	2.582	1.770
80	3.761	4.366	3.737	3.062	3.605	3.417	2.235
100	4.962	5.990	4.940	3.878	4.741	4.439	2.707
120	6.425	8.057	6.410	4.834	6.122	5.665	3.182
				•••• 149.60 K ••••			
20		1.328	1.300	1.252	1.280	1.265	0.7866
40	1.683	1.732	1.660	1.541	1.613	1.574	1.519
60	2.171	2.225	2.092	1.876	2.008	1.937	2.283
80	2.730	2.819	2.604	2.258	2.473	2.359	2.998
100	3.338	3.529	3.206	2.693	3.015	2.844	3.618
120	4.029	4.364	3.907	3.182	3.639	3.396	4.170

Table 15. (Continued)

P atm	Ø exp	Ø LJCL	Ø KIH	Ø KIHCK12	Ø BWR(a)	Ø BWR(b)	$100x_2$
				•••• 169.40 K ••••			
40	1.516	1.510	1.486	1.405	1.446	1.415	1.921
60	1.853	1.818	1.777	1.636	1.708	1.653	2.811
80	2.215	2.168	2.109	1.890	2.003	1.918	3.716
100	2.622	2.564	2.485	2.171	2.335	2.213	4.519
120	3.116	3.019	2.922	2.489	2.714	2.546	4.947
				•••• 189.57 K ••••			
40	1.441	1.392	1.396	1.338	1.366	1.339	2.335
60	1.658	1.605	1.614	1.512	1.560	1.515	3.534
80	1.896	1.839	1.857	1.701	1.776	1.706	4.643
100	2.164	2.094	2.130	1.908	2.014	1.914	5.634
120	2.470	2.371	2.435	2.132	2.276	2.141	6.561

a LORENTZ

b LINEAR

* Extrapolated Value

Table 16. Smoothed Experimental and Theoretical Enhancement Factors of Ethylene in Hydrogen, and the Smoothed Experimental Solubility of Hydrogen in Liquid Ethylene.

P atm	Ø exp	Ø LJCL	Ø KIH	Ø KIHCK12	Ø KIHEK12	Ø BWR(a)	Ø BWR(b)	$100x_2$
				.... 112.00 K				
20	1.550	1.700	1.587	1.429	1.474	1.588	1.569	0.0**
40	2.367	2.795	2.454	1.999	2.123	2.560	2.402	0.0**
60	3.529	4.438	3.688	2.734	2.985	3.705	3.576	0.0**
80	5.124	6.803	5.383	3.655	4.094	5.419	5.173	0.0**
100	7.192	10.072	7.635	4.778	5.481	7.696	7.272	0.0**
120	9.706	14.429	10.545	6.118	7.174	10.622	9.938	0.0**
				.... 122.00 K				
20	1.376	1.523	1.452	1.335	1.369	1.440	1.424	0.4042*
40	1.953	2.252	2.063	1.750	1.837	2.030	1.986	0.8809
60	2.688	3.240	2.867	2.255	2.420	2.806	2.716	1.324
80	3.678	4.536	3.902	2.857	3.132	3.799	3.641	1.735
100	4.827	6.186	5.197	3.562	3.982	5.040	4.783	2.118
120	6.255	8.230	6.791	4.374	4.980	6.555	6.163	2.478
				.... 130.00 K				
40	1.783	1.982	1.864	1.620	1.689	1.822	1.784	1.117
60	2.384	2.693	2.478	2.018	2.144	2.399	2.327	1.605
80	3.092	3.577	3.239	2.479	2.683	3.110	2.987	2.067
100	3.909	4.648	4.161	3.005	3.309	3.965	3.774	2.554
120	4.891	5.918	5.264	3.600	4.028	4.979	4.696	3.023
				.... 149.70 K				
40	1.456	1.607	1.582	1.431	1.475	1.540	1.512	1.478
60	1.825	1.980	1.950	1.680	1.756	1.874	1.823	2.264
80	2.294	2.403	2.378	1.957	2.073	2.258	2.179	3.012
100	2.809	2.879	2.878	2.264	2.431	2.702	2.584	3.577
120	3.301	3.408	3.455	2.603	2.831	3.207	3.041	4.041

Table 16. (Continued)

P atm	Ø exp	Ø LJCL	Ø KIH	Ø KIHCK12	Ø KIHEK12	Ø BWR(a)	Ø BWR(b)	$100x_2$
				•••• 169.75 K ••••				
40	1.336	1.424	1.443	1.339	1.369	1.412	1.390	1.948
60	1.577	1.652	1.700	1.518	1.570	1.643	1.602	2.988
80	1.862	1.894	1.990	1.710	1.789	1.899	1.837	3.994
100	2.148	2.152	2.317	1.919	2.029	2.185	2.096	4.900
120	2.442	2.422	2.686	2.144	2.291	2.503	2.380	5.734

a LORENTZ

b LINEAR

* Extrapolated Value

** No experimental values are available

x_2 = 0.0 was used in the theoretical calculation.

Table 17. Smoothed Experimental and Theoretical Enhancement Factors of Methane in Hydrogen, and the Smoothed Experimental Solubility of Hydrogen in Liquid Methane.

P atm	ø exp	ø LJCL	ø KIH	ø KIHCK12	ø BWR(a)	ø BWR(b)	$100x_2$
				•••• 90.74 K ••••			
20	1.621	1.669	1.634	1.574	1.614	1.603	1.427
40	2.592	2.740	2.620	2.428	2.543	2.507	2.742
60	4.026	4.411	4.102	3.661	3.894	3.812	3.927
80	6.018	6.940	6.257	5.376	5.773	5.609	5.015
100	8.649	10.662	9.303	7.682	8.264	7.971	6.120
120	11.98	16.011	13.531	10.700	11.421	10.934	7.360
				•••• 103.07 K ••••			
20	1.427	1.457	1.448	1.409	1.410	1.401	1.693
40	2.048	2.084	2.062	1.951	1.947	1.923	3.294
60	2.863	2.938	2.898	2.664	2.646	2.596	4.800
80	3.875	4.074	4.018	3.584	3.528	3.438	6.330
100	5.165	5.557	5.507	4.753	4.612	4.464	7.870
120	6.883	7.483	7.522	6.247	5.924	5.693	9.273*
				•••• 109.98 K ••••			
20	1.391	1.384	1.383	1.352	1.350	1.343	1.827
40	1.881	1.880	1.885	1.798	1.786	1.765	3.614
60	2.502	2.521	2.546	2.366	2.334	2.292	5.309
80	3.033	3.332	3.409	3.081	3.007	2.933	7.033
100	4.323	4.343	4.540	3.976	3.820	3.701	8.788
120	5.482	5.597	6.070	5.110	4.793	4.608	10.45
				•••• 116.53 K ••••			
20	1.345	1.334	1.338	1.313	1.309	1.303	1.904
40	1.752	1.745	1.768	1.696	1.681	1.662	3.807
60	2.216	2.253	2.320	2.173	2.134	2.097	5.747
80	2.884	2.872	3.030	2.764	2.681	2.617	7.720
100	3.640	3.617	3.963	3.501	3.338	3.235	9.670
120	4.525	4.512	5.259	4.445	4.123	3.964	11.49

a LORENTZ

b LINEAR

* Extrapolated Value

Table 18. Smoothed Experimental and Theoretical Enhancement Factors of Argon in Hydrogen, and the Smoothed Experimental Solubility of Hydrogen in Liquid Argon.

P atm	Ø exp	Ø LJCL	Ø KIH	Ø BWR(a)	$100x_2$
			.... 86.95 K		
20	1.475	1.444	1.463	1.436	2.144
40	2.171	2.104	2.162	2.057	4.285
60	3.148	3.093	3.231	2.918	6.353
80	4.493	4.619	4.954	4.072	8.470
100	6.261	7.249	8.424	5.565	10.22
120	8.483			7.434	11.61*
			.... 94.21 K		
20	1.378	1.356	1.372	1.354	2.285
40	1.906	1.860	1.908	1.834	4.735
60	2.617	2.567	2.679	2.466	7.199
80	3.567	3.597	3.859	3.275	9.621
100	4.801	5.275		4.283	12.03
120	6.350			5.503	14.54
			.... 99.95 K		
20	1.320	1.301	1.315	1.302	2.308
40	1.768	1.724	1.766	1.708	5.060
60	2.351	2.296	2.392	2.223	7.797
80	3.115	3.100	3.331	2.863	10.58
100	4.097	4.393		3.635	13.46
120	5.328			4.534	16.48
			.... 105.01 K		
20	1.265	1.258	1.270	1.259	2.449*
40	1.674	1.630	1.667	1.618	5.360*
60	2.117	2.177	2.206	2.058	8.302*
80	2.818	2.792	3.006	2.590	11.39
100	3.644			3.212	14.69
120	4.705			3.906	18.08

a LORENTZ

* Extrapolated Value

APPENDIX F

SELECTION OF PHYSICAL PROPERTY DATA FOR PURE COMPONENTS

In the calculation of the theoretical enhancement factor and in the extraction of the experimental values of B_{12}, Henry's law constant, and partial molar volume from phase equilibrium data, the following physical property data for the pure components are required:

1. The Lennard Jones (6-12) classical and the Kihara core model potential parameters.
2. Second and third virial coefficient data.
3. Parameters for the BWR equation.
4. Vapor pressure data for the condensed components.
5. Critical constants, saturated liquid molar volume, and the isothermal compressibility of the saturated liquid for the condensed components.

Usually the Lennard-Jones (6-12) classical and the Kihara core model potential parameters are extracted using the experimental values of the second virial coefficient. Two good summaries of available virial coefficient data are presented by David and Hamann (22) and Dymond and Smith (30). The potential parameters selected for use in this work are summarized in Table 19. The available BWR parameters for the components of interest in this work are summarized in Table 20. The source of the second virial coefficient data used to extract the potential parameters and the source of the P-V-T data used to extract

Table 19. Intermolecular Potential Parameters

Parameters	H_2	CF_4	$CClF_3$	Ar	CH_4	C_2H_6	C_2H_4
LJCL (6-12)							
Reference	(This Work)	(110)	(132)	(71)	(137)	(135)	(121)
ϵ/k, K	31.68	151.5	185.8	11.93	114.39	194.14	150.76
b_o, cc/gm mole	32.73	134.7	220.2	50.91	126.4	179.42	227.06
σ, $\AA$	2.96	4.74	5.59	3.43	4.64	5.22	5.65
KIH							
Reference	(98)	(110)	(132)	(98)	(98)	(98)	(133)
U_o/k, K	46.00	289.7	404.4	146.10	194.00	453.00	383.00
ρ_o, $\AA$	2.808	3.232	3.367	3.328	3.535	2.840	2.950
M_o, $\AA$	2.33	9.048	10.21	2.199	3.405	10.17	8.800
S_o, $\AA^2$	0.00	6.514	8.302	0.3848	0.611	5.770	3.480
V_o, $\AA^3$	0.00	1.564	2.250	0.02245	0.0247	0.653	0.0
M gm/gm mole	2.01594	88.005	104.47	39.948	16.04303	28.0549	30.0708

Table 20. BWR Equation of State Parameters
(Unit: liter-atm-K-gm mole)

Ref.	H_2 (86)	CF_4 (28)	Ar (87)	CH_4 (5)	C_2H_6 (7)	C_2H_4 (7)
A_o	1.5516336(-1)*	1.86000	1.2874358	1.85500	4.15556	3.33958
B_o	2.0846541(-2)	5.52000(-2)	3.7352552(-2)	4.26000(-2)	6.27724(-2)	5.56833(-2)
C_o	1.8415239(+2)	1.54500(+5)	**	2.25700(+4)@	1.79592(+5)	1.31140(+5)
a	1.6321985(-3)	3.98530(-1)	1.7373414(-2)	4.94000(-2)	3.45160(-1)	2.59000(-1)
b	***	1.21147(-2)	1.9170501(-3)	3.38004(-3)	1.11220(-2)	8.60000(-3)
c	7.2714507	2.43300(+4)	6.6467852(+2)	2.54500(+3)	3.27670(+4)	2.11200(+4)
α	1.1655988(-4)	2.50000(-4)	5.9791362(-5)	1.24359(-4)	2.43389(-4)	1.78000(-4)
γ	3.5073692(-3)	1.25000(-2)	3.6000000(-3)	6.00000(-3)	1.18000(-2)	9.23000(-3)

* Number in parentheses indicates power of 10.

** $C_o = (1-7.5175635(T_c-T) \times 10^{-4} + 5.3958077(T_c-T)^2 \times 10^{-5} - 1.2521827(T_c-T)^3 \times 10^{-6} + 7.3843279(T_c-T)^4 \times 10^{-9}) \times 6505.1649$ for $T \leq 150.86$ K

*** $b = 3.3834422 \times 10^{-4} + 2 \times 1.6321985 \times 10^{-3}/(R \times T)$

@ $C_o = 26717.1-594645/(T-7.27238)$ for 100 K $\leq T \leq$ 172 K

the BWR parameters will be described separately for each component.

In the prediction of the theoretical enhancement factor, the Lennard-Jones (6-12) model and the method of Chueh and Prausnitz (16) were used to calculate the third virial coefficients. The parameter used for the Lennard-Jones (6-12) model are those shown in Table 19. The parameters needed for the method of Chueh and Prausnitz (16) are given in Table 22. The method of Chueh and Prausnitz was used only for calculating the third virial coefficients above $T_{Ri} = 0.8$ as recommended by Chueh and Prausnitz. The critical constants shown in Table 21 are used for calculations made with Equation (IV-11) and Equation (IV-64).

Hydrogen

A good summary of virial coefficients of hydrogen was given by Dymond and Smith (30). Hirschelder et al. (48) obtained the classical Lennard-Jones parameters by fitting the second virial coefficient data of Michels et al. (81) from 273.15 K to 423.15 K. Kirk (61) obtained the parameters by fitting the second virial coefficient data of White and Johnston (128) over the range of 60 K to 125 K. These two sets of parameters do not cover the temperature range of interest in this work. A set of parameters was obtained by a least squares program to fit the second virial coefficient data of White and Johnston (128) over the range 90.04 K to 249.99 K and the data of Michels, de Graaff and Seldam (81) over the range 98.15 K to 248.15 K. The resulting classical values, $\varepsilon/k = 31.68$ K and $b_o = 32.73$ cc/gm mole were used in this work.

Table 21. Input Parameters for the Calculation of Isothermal Compressibility, β^S, using the Method of Chueh and Prausnitz (19).

Component	T_c, K	V_c, cc/gm mole	P_c, atm
CF_4	227.53 (14)	140.65 (14)	36.96 (14)
$CClF_3$	302.00 (1)	180.81 (1)	38.19 (1)
CH_4	191.1 (67)	99.0 (67)	45.8 (67)
C_2H_6	305.5 (22)	148.0 (22)	48.3 (67)
C_2H_4	282.4 (22)	129.0 (22)	50.2 (67)

Table 22. Input Parameters for the Calculation of Third Virial Coefficients Using the Method of Chueh and Prausnitz (16).

Component	T_c, K	V_c, cc/gm mole	d_1	d_{12}	M_{12}
H_2	43.6 (16)	51.5 (16)	0.0 (16)		
CF_4	227.53 (14)	140.65 (14)	0.8 (132)	0.4	3.9416
$CClF_3$	302.00 (1)	180.81 (1)	0.6 (132)	0.3	3.9556
Ar	150.86 (82)	74.56 (82)	0.0 (16)	0.0	3.8382
CH_4	191.1 (67)	99.0 (67)	0.5 (35)	0.25	3.5814
C_2H_6	305.5 (22)	148.0 (22)	1.2 (35)	0.60	3.7786
C_2H_4	282.4 (22)	129.0 (22)	1.4 (35)	0.70	3.7616

Two sets of Kihara core parameters (59, 98) were found in the literature. The Kihara core parameters with quantum corrections obtained by Prausnitz and Myers (98) by fitting the second virial coefficient data of Michels, de Graaff and Seldam (81) over the range of 98 K to 423 K were selected for use in this work.

Several sets of BWR parameters for hydrogen have been found in the literature (32, 74, 86). Four sets of BWR parameters presented by Motar and Organick (86) were determined from the P-V-T data of Woolley et al.(131) for temperatures between 116.3 K to 200.0 K. Among the various sets of BWR parameters found in the literature, the second set of Motar and Organick (86) fits the experimental second virial coefficients best and was selected for use in this work. The experimental second virial coefficients together with those calculated from various theoretical models are shown in Figure 49.

Figure 50 shows the third virial coefficient data of Goodwin (36), White and Johnston (128), and Michels et al. (81) together with the value predicted from various theoretical methods. The method of Chueh and Prausnitz (16) and the BWR equation best represent the data of Goodwin et al.(36) and Michels et al.(81). The Lennard-Jones (6-12) model fits the data of White and Johnston (128) better. Both methods were used in this work to calculate the third virial coefficients.

Carbon Tetrafluoride

The second virial coefficients of carbon tetrafluoride have been experimentally measured by many investigators (28, 53, 56, 70, 75). No experimental second virial coefficients are available in the tempera-

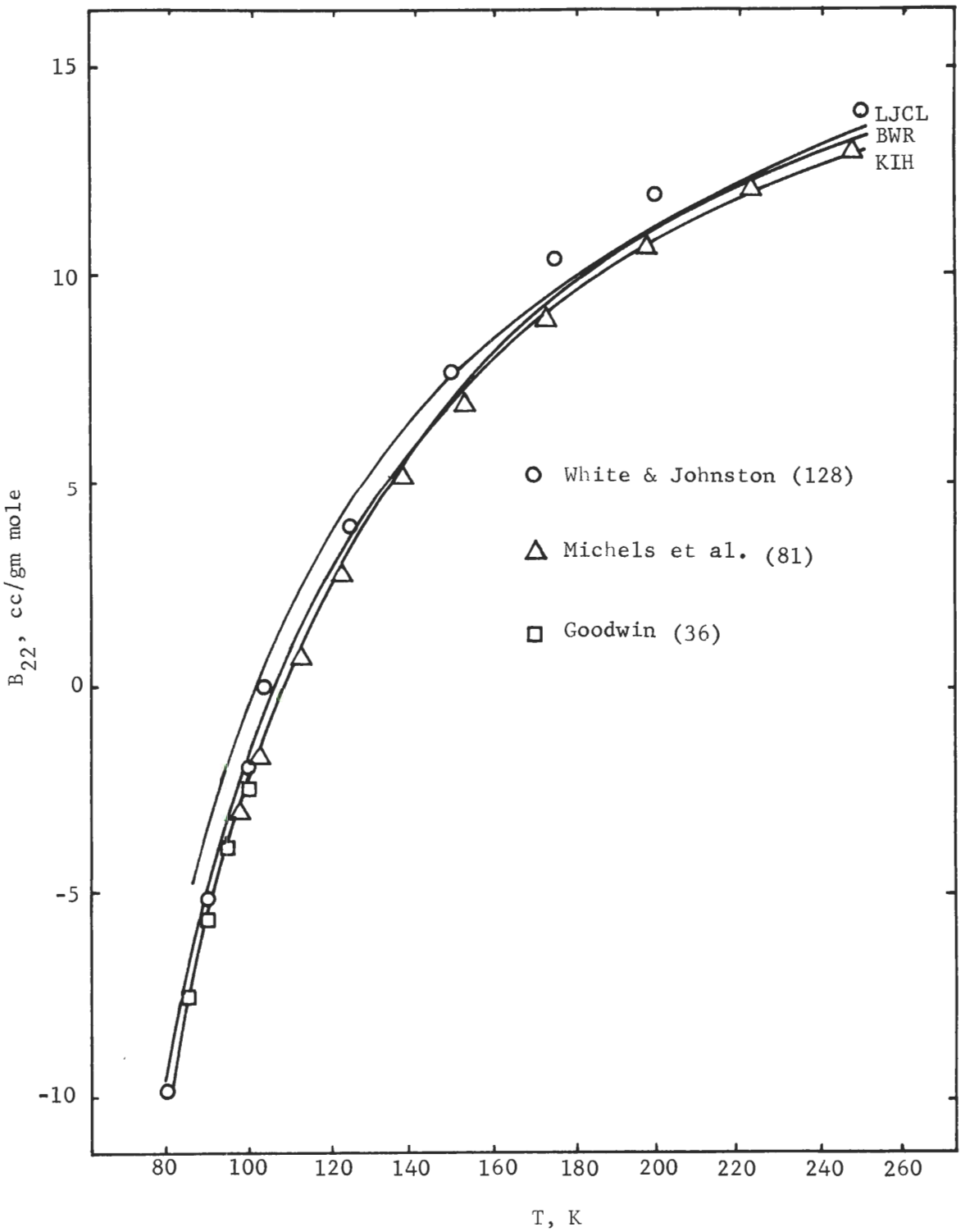

Figure 49. Second Virial Coefficients of Hydrogen.

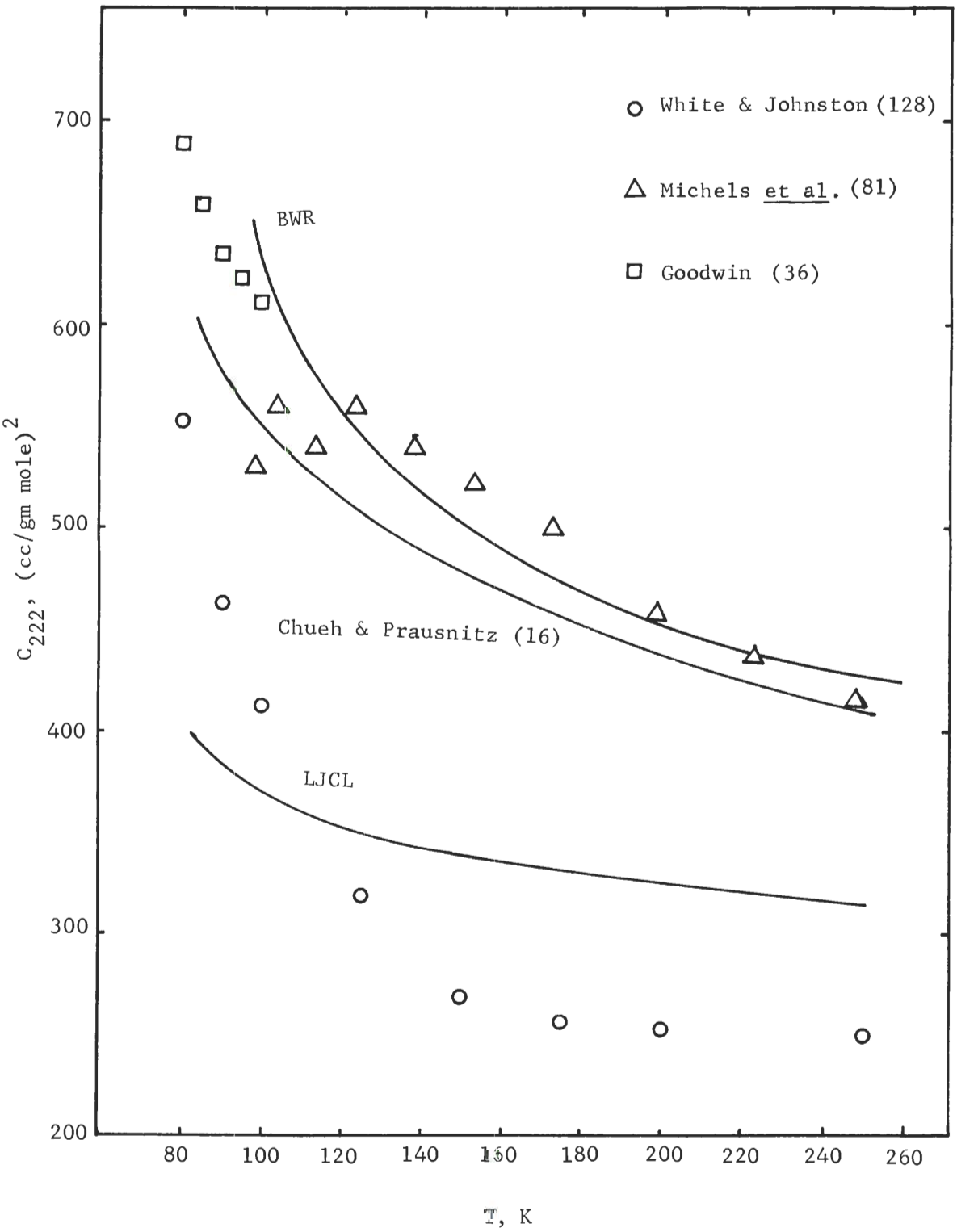

Figure 50. Third Virial Coefficients of Hydrogen.

ture range interest in this work. However, two sets of Lennard-Jones and Kihara core parameters (28, 110) were extracted from the P-V-T data of Douslin et al. (28) in the temperature range of 0^{o} C to 350^{o}C. Yoon (132) has demonstrated that the parameters of Sherwood and Prausnitz (110) fit the second virial coefficients better at lower temperature ranges. Therefore, the LJCL and KIH parameters extracted by Sherwood and Prausnitz were adopted in Yoon's and also in this work to calculate the second virial coefficients in the temperature range of interest. Douslin et al.(28) also extracted a set of BWR parameters from the same P-V-T data mentioned above. Of the three models, the Kihara model represents the experimental second virial coefficients best, the Lennard-Jones model tends to predict too high values and the BWR model predicts too low values at lower temperatures.

Among the experimental third virial coefficients found in the literature (28, 70, 75), no data are available below 200 K. Both the LJCL and BWR models fail to represent adequately the experimental third virial coefficients. The method of Chueh and Prausnitz (16) fits the data quite well for $T_R > 0.8$.

The vapor pressure has been measured by a number of investigators (14, 80, 112, 115). The equation given by Simon et al. (112) was selected for use in this work. The equation is given as follows:

$$\log P \text{ (torr)} = 6.8368405 - 511.69474/(T - 15.7744) \qquad \text{(F-1)}$$

This equation was selected because it fits both the experimental data of

Simon et al. (112) and Chari (14) within 0.5 percent up to 5 atm.

The saturated molar volumes of liquid carbon tetrafluoride have been measured by several investigators (14, 65, 122). The equation given by Terry et al.(122) covers the entire temperature range of this work and represents the experimental data within an average deviation of 0.017 cc/mole. The equation shown below was selected for use in this work to calculate the saturated molar volumes of liquid carbon-tetrafluoride.

$$v(cm^3/gm\ mole) = 46.9166 + 1.26579 \cdot 10^{-1} \times (T - 89.569) - 0.400011 \cdot 10^{-3} (T - 89.569)^2 + 2.32262 \cdot 10^{-5} (T - 89.569)^3 - 2.71815 \cdot 10^{-7} \times (T - 89.569)^4 + 1.47465 \cdot 10^{-9} (T - 89.569)^5 \qquad (F\text{-}2)$$

Table 23 shows the vapor pressures calculated from Equation (F-1), the molar volumes and the isotherm compressibilities of the saturated liquid calculated from Equations (F-2) and (IV-11) respectively. All calculations were based on the IPTS-48 temperature scale. The temperatures shown in Table 23 have been corrected to IPTS-68 scale.

The equations selected here were also selected for use by Yoon (132).

Chlorotrifluoromethane

Two sets of LJCL parameters for chlorotrifluoromethane were found in the literature (11, 40), but neither of them can satisfactorily represent the experimental second virial coefficients available in the

Table 23. Physical Properties of Saturated Liquid Carbon Tetrafluoride

T, (K)	P_{ol}, (atm)	v_{ol},(liter/gm mole)	β^s, (atm^{-1})
94.94	3.101(-3)*	4.759(-2)	1.004(-4)
105.01	1.664(-2)	4.885(-2)	1.097(-4)
119.94	1.107(-1)	5.085(-2)	1.388(-4)
135.01	4.624(-1)	5.315(-2)	1.883(-4)
149.98	1.390(+0)	5.579(-2)	2.642(-4)
164.99	3.360(+0)	5.895(-2)	3.872(-4)

* Number in parentheses indicates power of 10.

literature (40, 41, 69, 83). The LJCL and KIH parameters used in this work are those extracted by Yoon (132) from the experimental second virial coefficients of Kunz and Kapner (69) and Michels et al. (83). The only available experimental third virial coefficients, those given by Michel et al. (83), have been compared with the predicted values. The LJCL (6-12) model failed to represent the experimental data adequately. The experimental data are better described by the method of Chueh and Prausnitz (16).

The vapor pressure and liquid density have been measured by several investigators (1, 29, 33). The equation of vapor pressure and the equation of saturated liquid density presented by Albright and Martin (1) were selected for use in this work, since the equation of vapor pressure represents their experimental data within 0.08 percent and the equation of saturated liquid density represents their experimental data within 0.09 percent for temperatures between 144 K and 247 K. The equation for the vapor pressure is

$$\log P = 36.76130 - 2623.988/T - 11.80586 \log T + 5.71495 \cdot 10^{-3} T \qquad (F\text{-}3)$$

where P is pressure in psi and T is temperature in R.

The equation for the saturated liquid density is

$$d = 36.07 + 0.01566\,(83.93 - t) + 1.110 \times (83.93 - t)^{\frac{1}{2}} + 6.665 \times (83.93 - t)^{1/3} + 3.245 \times 10^{-5}\,(83.93 - t)^{2} \qquad (F\text{-}4)$$

where d is density in pounds per cubic feet and t is temperature in ^{o}F.

Table 24 shows the vapor pressure calculated from Equation (F-3), the saturated molar volume from Equation (F-4), and the isothermal compressibility from Equation (V-11). All calculations are based on the IPTS-48 temperature scale; the temperatures shown in Table 24 have been corrected to IPTS-68 scale. The equations used here were also selected for use by Yoon (132).

Table 24. Physical Properties of Saturated Liquid Chlorotrifluoromethane

T, (K)	P_{ol}, (atm)	v_{ol}, (liter/gm mole)	β^{s}, (atm^{-1})
134.97	1.046(-2)*	6.061(-2)	1.033(-4)
145.02	3.180(-2)	6.183(-2)	1.135(-4)
160.02	1.242(-1)	6.379(-2)	1.372(-4)
175.02	3.709(-1)	6.596(-2)	1.719(-4)
189.97	9.082(-1)	6.836(-2)	2.200(-4)
205.03	1.931(+0)	7.111(-2)	2.876(-4)
219.99	3.651(+0)	7.427(-2)	3.862(-4)

Argon, Methane, Ethane, and Ethylene

An extensive literature search of the physical properties for each of the following substances, argon, methane, ethane, and ethylene has been made by Ziegler et al. (133, 135, 136, 137). The property

* Number in parentheses indicates power of 10.

data required for the phase equilibrium calculation have been carefully selected for use by Kirk (61), Mullins (87), Liu (73), and Garber (35). The property data of argon, methane, ethane and ethylene used in this work were taken directly from those selected by Mullins (87) and Liu (73), Kirk (61) and Liu (73) and Garber (35), respectively. The compressibility coefficients used in this work were calculated by the method of Chueh and Prausnitz (16). The selected data are shown in Table 25 through Table 28.

Table 25. Physical Properties of Saturated Liquid Ethane

T, (K)	P_{ol}, (atm)	v_{ol}, (liter/gm mole)	β^s, (atm^{-1})
122.00	4.530(-3)*	4.846(-2)	8.961(-5)
130.00	1.254(-2)	4.915(-2)	9.165(-5)
149.62	9.158(-2)	5.098(-2)	1.083(-4)
169.40	4.059(-1)	5.341(-2)	1.413(-4)
189.57	1.306(+0)	5.583(-2)	1.947(-4)

Table 26. Physical Properties of Saturated Liquid Ethylene

T, (K)	P_{ol}, (atm)	v_{ol}, (liter/gm mole)	β^s, (atm^{-1})
112.00	4.442(-3)*	4.382(-2)	8.613(-5)
122.00	1.735(-2)	4.455(-2)	8.904(-5)

*Number in parentheses indicates power of 10.

Table 26. (Continued)

T, (K)	P_{ol}, (atm)	v_{ol}, (liter/gm mole)	β^s, (atm^{-1})
130.00	4.358(-2)*	4.516(-2)	9.492(-5)
149.70	2.633(-1)	4.706(-2)	1.220(-4)
169.75	1.021	4.939(-2)	1.697(-4)

Table 27. Physical Properties of Saturated Liquid Methane

T, (K)	P_{ol}, (atm)	v_{ol}, (liter/gm mole)	β^s, (atm^{-1})
90.74	1.166(-1)*	3.557(-2)	1.390(-4)
103.07	4.630(-1)	3.680(-2)	1.781(-4)
109.98	8.689(-1)	3.762(-2)	2.102(-4)
116.53	1.471(+0)	3.852(-2)	2.486(-4)

Table 28. Physical Properties of Saturated Liquid Argon

T, (K)	P_{ol}, (atm)
86.95	0.9632
94.21	1.9715
99.95	3.2005
105.01	4.6860

*Number in parentheses indicates power of 10.

APPENDIX G

PURITY OF GASES USED

The hydrogen gas used in this work was supplied by Airco Inc. It had a quoted purity of 99.97 percent.

The argon, helium, carbon tetrafluoride and chlorotrifluoromethane were the same as that used by Yoon (132). The sources of supply and the quoted purity of the gases were as follows:

Gas	Purity	Source of Supply
Argon	99.999	American Cryogenics, Inc.
Helium	99.997	Air Reduction Company
Carbon tetrafluoride	99.9	E.I. duPont de Nemours & Co.
Chlorotrifluoromethane	99.9	E.I. duPont de Nemours & Co.

All gases were used without further purification.

APPENDIX H

COMMENTS ON THE ASSUMPTION OF AN IDEAL SOLUTION MODEL FOR THE LIQUID PHASES

For the six hydrogen systems H_2-X(X=Ar (87), CH_4 (61), C_2H_6 (52), C_2H_4 (51), CF_4, $CClF_3$) summarized in this work, the values of H_2^{∞} and $\overline{V}_2^{\infty}$ were obtained by using the least squares method to fit the experimental $\ell n \left(\frac{f_2^G}{x_2}\right)$ and $(P-P_{o1})$ to a straight line according to Equation (VI-12), and the maximum deviation of the experimental $\ell n \left(\frac{f_2^G}{x_2}\right)$ from the calculated $\ell n \left(\frac{f_2^G}{x_2}\right)$ is $\pm$ 0.39 percent. If the elimination of the term $\ell n\ \gamma_2'$ in Equation (VI-12) were responsible for this deviation, the uncertainty of the value of γ_2' would have been $\pm$ 3.0 percent. Therefore, the value of γ_2' is 1 ± 0.03 for these systems and the assumption of an ideal solution, $\gamma_2' = 1$ in these calculations seems to be satisfactory for the liquid phases considered in this work.

Now γ_1' and γ_2' for the liquid phase must satisfy the Gibbs-Duhem relation which for a binary solution at constant temperature is

$$x_1 \left(\frac{\partial\ \ell n\ \gamma_1'}{\partial\ x_1}\right)_T + x_2 \left(\frac{\partial\ \ell n\ \gamma_2'}{\partial\ x_1}\right)_T = \frac{\Delta V^m}{RT} \left(\frac{\partial P}{\partial x_1}\right)_T \qquad \text{(H-1)}$$

If we assume the quantity on the right-hand side of Equation (H-1) is quite small (the usual case), the relation becomes

$$x_1\left(\frac{\partial \ln \gamma_1'}{\partial x_1}\right)_T + x_2\left(\frac{\partial \ln \gamma_2'}{\partial x_1}\right)_T = 0 \qquad \text{(H-2)}$$

Now the experimental solubility data suggest that γ_2' is very nearly equal to unity i.e., 1 ± 0.03 over the solubility range $0 \leq x \leq (x_2)_{max} \approx 0.1$. Since $\gamma_1' = 1$ when $x_2 = 0$ it follows from Equation (H-2) that γ_1' is very nearly one over this same composition range, that is, the solution may be assumed to be ideal with good accuracy. This is the assumption made in Chapter IV in computing the enhancement factor.

BIBLIOGRAPHY

1. Albright, L. F. and Martin, J. J., "Thermodynamic Properties of Chlorotrifluoromethane," Industrial and Engineering Chemistry 44, 188-198 (1952).

2. Barber, C. R., "The International Practical Temperature Scale of 1968," Metrologia 5, No. 2, 35-44 (1969).

3. Beattie, J. A. and Bridgeman, O. C., "A New Equation of State for Fluids," Proceedings of the American Academy of Arts and Sciences 63, 230-308 (1928).

4. Beattie, J. A. and Stockmayer, W. H., "The Thermodynamics and Statistical Mechanics of Real Gases, "A Treatise on Physical Chemistry 2, States of Matter, 3rd edition, D. Van Nostrand Company, New York, New York (1951).

5. Benedict, M., Webb, G. B. and Rubin, L. C., "An Empirical Equation for Thermodynamic Properties of Light Hydrocarbons and Their Mixtures," Journal of Chemical Physics 8, 334-345 (1939).

6. Benedict, M., Webb, G. B., and Rubin, L. C., "An Empirical Equation for Thermodynamic Properties of Light Hydrocarbons and Their Mixtures. II. Mixtures of Methane, Ethane, Propane and n-Butane," Journal of Chemical Physics 10, 747-758 (1942).

7. Benedict, M., Webb, G. B., and Rubin, L. C., "An Empirical Equation for Thermodynamic Properties of Light Hydrocarbons and their Mixtures," Chemical Engineering Progress 47, No. 8, 419, 422 (1951).

8. Benham, A. L. and Donald, L. K., "Vapor-Liquid Equilibrium for Hydrogen-Light-Hydrocarbon Systems at Low Temperatures," American Institute of Chemical Engineers Journal 3, No. 1, 33-36 (1957).

9. Bergeon, M. R., "Le Troisie'me Coefficient du Viriel Pour un Potentiel Intermole'culaire avec Force Re'pulsive en r^{-a}," Acade'mie des Sciences. Comptes Rendus (Paris) 234B, 1039-1041 (1952).

10. Bird, R. B., Spotz, E. L., and Hirschfelder, J. O., "The Third Virial Coefficient for Non-Polar Gases," Journal of Chemical Physics 18, 1395-1402 (1950).

11. Brandt, W., "Calculation of Intermolecular Force Constants from Polarizabilities," Journal of Chemical Physics 24, 501-506 (1956).

12. Brewer, J. and Vaughn, G. W., "Measurement and Correlation of Some Interaction Second Virial Coefficients from -125 to 50°C," Journal of Chemical Physics 50, No.7, 2960-2968 (1969).

13. Burnett, E. S., "Compressibility Determination Without Volume Measurements," Journal of Applied Mechanics 3, A136-140 (1936).

14. Chari, N. C. S., Thermodynamic Properties of Carbon Tetrafluoride, Sc. D. Thesis, University of Michigan (1960).

15. Chiu, C. -h. and Canfield, F. B., "Thermodynamic Analysis of Vapor-Liquid and Vapor-Solid Equilibria Data to Obtain Interaction Second Virial Coefficients," Advances in Cryogenic Engineering 12, 741-753 (1967).

16. Chueh, P. L. and Prausnitz, J. M., "Third Virial Coefficients of Nonpolar Gases and Their Mixtures," American Institute of Chemical Engineers Journal 13, No. 5, 896-902 (1967).

17. Chueh, P. L. and Prausnitz, J. M., "Vapor-Liquid Equilibria at High Pressures. Vapor-Phase Fugacity Coefficients in Non-polar and Quantum Gas Mixtures," Industrial Engineering Chemistry Fundamentals 6, No. 4, 492-498 (1967).

18. Chueh, P. L. and Prausnitz, J. M., "Vapor-Liquid Equilibria at High Pressures. Calculation of Partial Molar Volumes in Nonpolar Liquid Mixtures," American Institute of Chemical Engineers Journal 13, No. 6, 1099-1107 (1967).

19. Chueh, P. L. and Prausnitz, J. M., "A Generalized Correlation for the Compressibilities of Normal Liquids," American Institute of Chemical Engineers Journal 15, No. 3, 471-472 (1969).

20. Correia, Bon P., Schafer, K., and Schneider, M., "Bestimmung der zwischenmolekularen Krafte aus Ultraschalldispersionsmessungen in Gasgemischen," Berichte der Bunsengesellschaft fur Physikalische Chemie 73, No. 6, 507-513 (1969).

21. Dantzler, E. M., Knobler, C. M., and Windsor, M. L., "Second Virial Coefficients of Some Argon-Hydrocarbon Mixtures and Their Comparison with Chromatographic Values," Journal of Chromatography 32, 433-438 (1968).

22. David, H. G. and Hamann, S. D., "The Gas Imperfections of Hydrocarbons," Proceedings of the Joint Conference in Thermodynamics and Transport Properties of Fluids, London, 74-78 (1957).

23. Davidson, N., Statistical Mechanics, McGraw-Hill, Inc., New York, New York (1962).

24. De Boer, J. and Michels, A., "Contributions to the Quantum-Mechanical Theory of the Equation of State and the Law of Corresponding States. Determination of the Law of Force of Helium," Physica 5, 945-957 (1938).

25. De Boer, J. and Michels, A., "The Influence of the Interaction of More than Two Molecules on the Molecular Distribution-Function in Compressed Gases," Physica 6, 97-114 (1939).

26. Dokoupil, Z., "Some Solid-Gas Equilibria at Low Temperatures," Progress in Low Temperature Physics, Vol. III, Edited by C. J. Gorter, North-Holland Publishing Company, Amsterdam, Interscience Publishing, Inc., New York 454-480 (1961).

27. Dokoupil, Z., Van Soest, G., and Swenker, M. D. P., "On the Equilibrium Between the Solid Phase and the Gas Phase of the Systems Hydrogen-Nitrogen,Hydrogen-Carbon Monoxide, and Hydrogen-Nitrogen-Carbon Dioxide," Applied Scientific Research A5, 182-240 (1955).

28. Douslin, D. R., Harrison, R. H., Moor, R. T., and McCullough, J. P., "Tetrafluoromethane: P-V-T and Intermolecular Potential Energy Relations," Journal of Chemical Physics 35, 1357-1366 (1961).

29. DuPont de Nemours & Co., E. I., Thermodynamic Properties of Freon 13 Refrigerant, Bulletin T13 (1959).

30. Dymond, J. H. and Smith, E. B., The Virial Coefficients of Gases, Clarendon Press, Oxford (1969).

31. Eckert, C. H., Renon, H., and Prausnitz, J. M., "Molecular Thermodynamics of Simple Fluid Mixtures," Industrial and Engineering Chemistry. Fundamentals 6, No. 1, 58-67 (1967).

32. Eubanks, L. S., Vapor-Liquid Equilibrium in the System Hydrogen-Nitrogen-Carbon Monoxide, Ph.D. Thesis, Rice Institute, Houston, Texas (1957).

33. Fiske, D. L., "Low Temperature Freon Refrigerants," Refrigerating Engineering 53, 336-339 (1949).

34. Fowler, R. and Graben, H. W., "Nonadditive Third Virial Coefficient for Intermolecular Potentials with Hard-Sphere Cores," Journal of Chemical Physics 50, No. 10, 4347-4351 (1969).

35. Garber, J. D., Gas-Liquid Phase Equilibrium in the Helium-Ethylene and Helium-Propylene Systems Below 260°K and 120 Atmospheres, Ph.D. Thesis, Georgia Institute of Technology, Atlanta, Georgia (1970).

36. Goodwin, Robert D., "Apparatus for Determination of Pressure-Density-Temperature Relations and Specific Heats of Hydrogen to 350 Atmospheres at Temperatures above 14°K," Journal of Research of the National Bureau of Standards 65C, 231-43 (1961).

37. Graben, H. W. and Present, R. D.,"Evidence of Three-Body Forces From Third Virial Coefficient," Physical Review Letters 9, 247-248 (1962).

38. Graben, H. W. and Present, R. D., McCulloch, R. D., "Intermolecular Three-Body Forces and Third Virial Coefficients," Physical Review 144, No. 1, 140-142 (1966).

39. Gunn, R. D., Chueh, P. L. and Prausnitz, J. M., "Prediction of Thermodynamic Properties of Dense Gas Mixture Containing One or More of the Quantum Gases" American Institute of Chemical Engineers Journal 12, 937-940 (1966).

40. Hajjar, R. F. and MacWood, G. E., "Second Virial Coefficients and the Force Constants, ϵ_o and r_o, of Six Halogen-Substituted Methanes," Journal of Chemical Physics 49, 4567-4570 (1968).

41. Hajjar, R. F. and MacWood, G. E.,"Determination of the Second Virial Coefficients of Six Fluorochloromethanes by a Gas Balance Method in the Range 40 to 130°C," Journal of Chemical and Engineering Data 15, No. 1, 3-6 (1970).

42. Hanley, H. J. M. and Klein, M., "On the Selection of the Intermolecular Potential Function: Application of Statistical Mechanical Theory to Experiment," National Bureau of Standards Technical Note 360, 82 pages (1967).

43. Heck, C. K., Jr., Experimental and Theoretical Liquid-Vapor Equilibrium in Some Binary Systems, Ph.D. Thesis, University of Colorado, Denver, Colorado (1968).

44. Heck, C. K. and Hiza, M. J., "Liquid-Vapor Equilibrium in the System Helium-Methane," American Institute of Chemical Engineers Journal 13, 593-599 (1967).

45. Herring, R. N. and Barrick, P. L., "Gas-Liquid Equilibrium Solubilities for the Helium-Oxygen System," Advances in Cryogenic Engineering 10, 151-159 (1965).

46. Hildebrand, J. H. and Scott,R. L., Regular Solutions Prentice-Hall Inc., New Jersey (1962).

47. Hirschfelder, J. O., Buehler, R. J., McGee, H. A. and Sutton, J. R., "Generalized Equation of State for Gases and Liquids," Industrial and Engineering Chemistry 50, No. 3, 375-385 (1958).

48. Hirschfelder, J. O., Curtiss, C. J., and Bird, R. B., Molecular Theory of Gases and Liquids, John Wiley & Sons, Inc., New York (1964).

49. Hiza, M. J., "Solid-Vapor Equilibria Research on Systems of Interest in Cryogenics," Cryogenics 10, No. 2, 106-115 (1970).

50. Hiza, M. J. and Duncan, A. G., "Equilibrium Gas-Phase Compositions of Ethane and Ethylene in Binary Mixtures with Helium and Neon Below 150°K and a Correlation for Deviations from the Geometric Mean Combining Rule," Advances in Cryogenic Engineering 14, 30-40 (1968).

51. Hiza, M. J., Heck, C. K., and Kidnay, A. J., "Liquid-Vapor and Solid-Vapor Equilibrium in the System Hydrogen-Ethylene," Chemical Engineering Progress Symposium Series No. 88, 57-65 (1968).

52. Hiza, M. J., Heck, C. K., and Kidnay, A. J., "Liquid-Vapor and Solid-Vapor Equilibrium in the System Hydrogen-Ethane," Advances in Cryogenic Engineering 13, 343-356 (1968).

53. Hoover, A. E., Canfield, F. B., Kobayashi, R., and Leland, T. W., Jr., "Determination of Virial Coefficients by the Burnett Method," Journal of Chemical and Engineering Data 9, No. 4, 568-573 (1964).

54. Hudson, G. H. and McCoubrey, J. C., "Intermolecular Forces Between Unlike Molecules," Transactions of the Faraday Society 56, 761-766 (1960).

55. Huff, J. A. and Reed, T. M., "Second Virial Coefficients of Mixtures of Nonpolar Molecules from Correlations on Pure Components," Journal of Chemical and Engineering Data 8, No. 3, 306-311 (1963).

56. Kalfoglou, N. K. and Miller, J. G., "Compressibility of Gases. V. Mixtures of Spherically Symmetric Molecules at Higher Temperatures. The Helium-Argon and Helium-Tetrafluoromethane Systems," The Journal of Physical Chemistry 71, No. 5, 1256-1264 (1967).

57. Kihara, T., "Determination of Intermolecular Forces from the Equation of State of Gases," Journal Physical Society Japan 3, 265-268 (1948).

58. Kihara, T., "Determination of Intermolecular Forces from the Equation of State of Gases, Journal Physical Society Japan 6, 184-188 (1951).

59. Kihara, T., "Virial Coefficients and Models of Molecules in Gases," Reviews of Modern Physics 25, No. 4, 831-843 (1953).

60. Kihara, T., "Virial Coefficients and Models of Molecules in Gases B," Reviews of Modern Physics 27, No. 4, 412-423 (1955).

61. Kirk, B. S., Predicted and Experimental Gas Phase Compositions in Pressurized Binary Systems Containing an Essentially Pure Condensed Phase. Phase Equilibrium Data for the Methane-Hydrogen System from 66.88 to 116.53°K and Up to 125 Atmospheres, Ph.D. Thesis, Georgia Institute of Technology, Atlanta, Georgia (1964).

62. Kirk, B. S. and Ziegler, W. T., "A Phase Equilibrium Apparatus for Gas-Liquid Systems and the Gas Phase of Gas-Solid System. Application of Methane-Hydrogen from 66.88 to 116.53°K and Up to 125 Atmospheres," Advances in Cryogenic Engineering 10, 160-170 (1965).

63. Kirk, B. S., Ziegler, W. T., and Mullins, J. C., "A Comparison of Methods of Predicting Equilibrium Gas Phase Compositions in Pressurized Binary Systems Containing an Essentially Pure Condensed Phase," Advances in Cryogenic Engineering 6, 413-427 (1961).

64. Kiser, R. W. and Hobrock, D. L., "The Ionization Potential of Carbon Tetrafluoride," Journal of American Chemical Society 87, 922-923 (1965).

65. Knobler, C. M. and Pings, C. J., "Saturated Liquid Density of Carbon Tetrafluoride from 90 to 150°K," Journal of Chemical and Engineering Data 10, No. 2, 129-130 (1965).

66. Kobatake Y. and Alder B. J., "Cell Potentials and Gas Solubility," Journal of Physical Chemistry 66, 645-654 (1962).

67. Kobe, K. A. and Lynn, R. E., "The Critical Properties of Elements and Compounds," Chemical Reviews 52, 117-236 (1953).

68. Krichevsky, I. R. and Kasarnovsky, J. S., "Thermodynamical Calculations of Solubilities of Nitrogen and Hydrogen in Water at High Pressures," Journal of the American Chemical Society 57, 2168-2171 (1935).

69. Kunz, R. G. and Kapner, R. S., "Second Virial Coefficients from Tabulated P-V-T Data. Results for $CClF_3$, CCl_2F_2, CCl_3F, and $B(OCH_3)_3$," Journal of Chemical and Engineering Data 14, No. 2, 190-191 (1969).

70. Lange, H. B., Jr. and Stein, F. P., "Volumetric Behavior of Polar-Nonpolar Gas Mixtures: Trifluoromethane-Tetrafluoromethane," Journal of Chemical and Engineering Data 15, 56-61 (1970).

71. Levelt, J. M. H., "The Reduced Equation of State, Internal Energy and Entropy of Argon and Xenon," Physica 26, 361-377 (1960).

72. Lin, H. -M. and Robinson, R. L., Jr., "Uncertainties in Intermolecular Pair Potential Parameters Determined from Macroscopic Property Data. I. Virial Coefficients," Journal of Chemical Physics 52, No. 7. 3727-3731 (1970).

73. Liu, K. F., Phase Equilibria in the Helium-Carbon Dioxide,-Argon, -Methane,-Nitrogen, and -Oxygen Systems, Ph. D. Thesis, Georgia Institute of Technology, Atlanta, Georgia (1969).

74. Low Temperature Heavy Water Plant, Final Report to the U.S.A.E.C. by Hydrocarbon Research, Inc., Contract No. AT(30-1)810 NYO-889, March 16, 1951, pages 90-104.

75. MacCormack, K. E. and Schneider, W. G., "Compressibility of Gases at Pressures up to 50 atmospheres. V. Carbon-Tetrafluoride in the Temperature range 0-400°C. VI. Sulfur Hexafluoride in the Temperature range 0-250°C," Journal of Chemical Physics 19, 845-848 (1951).

76. Martin, J. J. and Hou, Y. C., "Development of an Equation of State for Gases," American Institute of Chemical Engineers Journal 1, No. 2, 142-145 (1955).

77. Mayer, J. E., "Statistical Mechanics of Condensing Systems. V Two Component Systems," Journal of Physical Chemistry 43, 71-95 (1939).

78. Mayer, J. E. and Mayer, M. G., Statistical Mechanics John Willey and Sons, Inc., New York, 1940.

79. McCain, W. D., Jr., Vapor-Liquid Phase Equilibria of the Binary System Argon-Helium, Ph.D. Thesis, Georgia Institute of Technology, Atlanta, Georgia (1964).

80. Menzel, V. W. and Mohry, F., "Die Dampfducke des CF_4 abd NF_3 und der Tripelpunkt des CF_4, Zeitschrift fur Anorganische und allgememeine Chemie, 210, 257-263 (1933).

81. Michels, A., De Graaff, W., and Ten Seldam, C. A., "Virial Coefficients of Hydrogen and Deuterium at Temperatures Between -175° and +150°C. Conclusions from the Second Virial Coefficient with Regards to the Intermolecular Potential," Physica 26, 393-408 (1960).

82. Michels, A., Levelt, J. M. and De Graaff, W., "Compressibility Isotherms of Argon at Temperatures Between -25°C and -155°C, and at Densities up to 640 Amagat (Pressures up to 1050 Atmospheres)," Physica 24, 659-671 (1958).

83. Michels, A., Wassenaar, T., Wolkers, G. J., Prins, C., and Klunkert, L.v.d., "P-V-T Data and Thermodynamical Properties of Freon 12 (CCl_2F_2) and Freon 13($CClF_3$) Fluorocarbons at Temperatures between 0 and 150°C and at pressures up to 400 atm.," Journal of Chemical and Engineering Data 11, No. 4, 449-452 (1966).

84. Miller, R. C. and Prausnitz, J. M., "Statistical Thermodynamics of Simple Liquid Mixtures," Industrial and Engineering Chemistry Fundamentals 8, No. 3, 449-452 (1969).

85. Montroll, E. W. and Mayer, J. E., "Statistical Mechanics of Imperfect Gases," Journal of Chemical Physics 9, 626-637 (1941).

86. Motard, R. L. and Organick, E. I., "Thermodynamic Behavior of Hydrogen-Hydrocarbon Mixtures," AIChE Journal 6, 39-43 (1960).

87. Mullins, J. C., Phase Equilibria in the Argon-Helium and Argon-Hydrogen Systems, Ph.D. Thesis, Georgia Institute of Technology, Atlanta, Georgia (1965).

88. Mullins, J. C. and Ziegler, W. T., "Phase Equilibrium in the Argon-Helium and Argon-Hydrogen Systems from 68 to 108°K and Pressures up to 120 Atmospheres," Advances in Cryogenic Engineering 10, 171-181 (1965).

89. Nakahara T. and Hirata M., "The Prediction of Henry's Constants for Hydrogen-Hydrocarbon Systems," Journal of Chemical Engineering of Japan 2, No. 2, 137-142 (1969).

90. O'Connell, J. P. and Prausnitz, J. M., "Applications of the Kihara Potential to Thermodynamic and Transport Properties of Gases," Symposium Thermophysical Properties, Papers, 3rd, Lafayette, Indiana, 19-31 (1965).

91. Orentlicher, M. and Prausnitz, J. M., "Thermodynamics of Hydrogen Solubility in Cryogenic Solvents at High Pressures," Chemical Engineering Science, 19, 775-782 (1964).

92. Pierotti, R. A., "The Solubility of Gases in Liquids," Journal of Physical Chemistry 67, 1840-1845 (1963).

93. Pierotti, R. A., "Aqueous Solutions of Nonpolar Gases," Journal of Physical Chemistry 69, No. 1, 281-288 (1965).

94. Pierotti, R. A., "On the Scaled-Particle Theory of Dilute Aqueous Solutions," Journal of Physical Chemistry 71, 2366-2367 (1967).

95. Prausnitz, J. M., Molecular Thermodynamics of Fluid-Phase Equilibria, Prentice-Hall, Inc., Englewood Cliffs, New Jersey (1969).

96. Prausnitz, J. M. and Chueh, P. L., Computer Calculations for High Pressure Vapor-Liquid Equilibrium, Prentice-Hall, Inc., Englewood Cliffs, New Jersey (1968).

97. Prausnitz, J. M., Eckert, C. A., Orye, R. V. and O'Connell, J. P., Computer Calculations for Multi-Component Vapor-Liquid Equilibria, Prentice-Hall, Inc., Englewood Cliffs, New Jersey (1968).

98. Prausnitz, J. M. and Myers, A. L., "Kihara Parameters and Second Virial Coefficients for Cryogenic Fluids and Their Mixtures," American Institute of Chemical Engineers Journal 9, No. 1, 5-11 (1963).

99. Prausnitz, J. M. and Shair, F. H., "A Thermodynamic Correlation of Gas Solubilities," American Institute of Chemical Engineers Journal 7, No. 4, 682-686 (1961).

100. Preston, G. T. and Prausnitz, J. M., "A Generalized Correlation for Henry's Law Constants in Nonpolar Systems," Industrial and Engineering Chemistry Fundamentals 10, No. 3, 389-397 (1971).

101. Prigogine, I., The Molecular Theory of Solutions, North-Holland Publishing Company, Amsterdam (1957).

102. Prigogine, I. and Mathot, V., "Application of the Cell Method to the Statistical Thermodynamics of Solutions," Journal of Chemical Physics 20, 49-57 (1952).

103. Reddlich, O. and Kwong, J. N. S., "On the Thermodynamics of Solutions. V An Equation of State. Fugacities of Gaseous Solutions," Chemical Reviews 44, 233-244 (1949).

104. Reed, R. I., Ion Production by Electron Impact, Academic Press, New York, (1962).

105. Reiss, H., "Scaled Particle Methods in the Statistical Thermodynamics of Fluids," Advances in Chemical Physics IX, 1-84 (1965).

106. Reuss, J. and Beenakker, J. J. M., "Determination of the Second Virial Coefficient B_{12} of Gas Mixtures," Physica 22, 869-879 (1956).

107. Rowlinson, J. S., Summer, F. H., and Sutton, J. T., "The Virial Coefficients of a Gas Mixture," Transactions of the Faraday Society 50, 1-8 (1954).

108. Sherwood, A. E., Derocco, A. G., and Mason, E. A., "Nonadditivity of Intermolecular Forces: Effects on the Third Virial Coefficient," Journal of Chemical Physics 44, No. 8, 2984-2994 (1966).

109. Sherwood, A. E. and Prausnitz, J. M., "Third Virial Coefficient for the Kihara, Exp-6, and Square-Well Potentials," Journal of Chemical Physics 41, No. 2, 413-428 (1964).

110. Sherwood, A. E. and Prausnitz, J. M., "Intermolecular Potential Functions and the Second and Third Virial Coefficients," Journal of Chemical Physics 41, No. 2, 429-437 (1964).

111. Sikora, P. T., "Combining Rules for Spherically Symmetric Intermolecular Potentials," Journal of Physics B: Atomic and Molecular Physics 3, 1475-1482 (1970).

112. Simon, M., Knobler, C. M., and Duncan, A. G., "The Vapor Pressure of Carbon Tetrafluoromethane from 86 to 146°K," Cryogenics 7, No. 6, 138-140 (1967).

113. Sinor, J. E. and Kurata, F., "The Liquid Phase Volumetric Behavior of the Helium-Methane System," Journal of Chemical and Engineering Data 11, 1-6 (1966).

114. Sinor, J. E., Schindler, D. L., and Kurata, F., "Vapor-Liquid Phase Behavior of the Helium-Methane System," American Institute of Chemical Engineers Journal 12, No. 2, 353-357 (1966).

115. Smith, J. H. and Pace, E. L., "The Thermodynamic Properties of Carbon Tetrafluoride from 12 K to Its Boiling Point. The Significance of Parameter ν", Journal Physical Chemistry 73, 4232-4236 (1969).

116. Smith, G. E., Sonntag, R. E. and Van Wylen, G. J., "Analysis of the Solid-Vapor E uilibrium System Carbon Dioxide-Nitrogen," Advances in Cryogenic Engineering 8, 162-173 (1963).

117. Smith, G. E., Sonntag, R. E. and Van Wylen, G. J., "Solid-Vapor Equilibrium of the Carbon Dioxide-Nitrogen System at Pressures to 200 Atmospheres" Advances in Cryogenic Engineering 9, 197- 206 (1964).

118. Snider, N. S. and Herrington, T. M., "Hard Sphere Model of Binary Liquid Mixture," Journal of Chemical Physics 47, No. 7, 2248-2255 (1967).

119. Solen, K. A., Chueh, P. L. and Prausnitz, J. M.,"Thermodynamics of Helium Solubility in Cryogenic Solvents at High Pressures," Industrial and Engineering Chemistry Process Design and Development 9, No. 2, 310-317 (1970).

120. Stockbridge, T. R., "Thermodynamic Properties of Nitrogen from 14 to 300 K between 0.1 and 200 Atmospheres," U.S. National Bureau of Standards Technical Note No. 129 (1962).

121. Tee, L. S., Gotoh, S., and Stewart, W. E., "Molecular Parameters for Normal Fluids," Industrial and Engineering Chemistry Fundamentals 5, No. 3, 356-363 (1966).

122. Terry, M. J., Lunch, J. T., Bunclark, M., Mansell, K. R., and Staveley, A. L.K., "The Densities of Liquid Argon, Krypton, Xenon, Osyten, Nitrogen, Carbon Monoxide, Methane, and Carbon Tetrafluoride along the Orthobaric Liquid Curve," Journal of Chemical Thermodynamics 1, 413-424 (1969).

123. Trust, D. B. and Kurata, F., "Vapor-Liquid Behavior of the Hydrogen-Propane and Hydrogen-Carbon Monoxide-Propane Systems" American Institute of Chemical Engineers Journal 17, 86-91 (1971).

124. Tsonopoulos, C. and Prausnitz, J. M., "Equation of State: A Review for Engineering Applications," Cryogenics 9, No. 10, 315-327 (1969).

125. Van Itterbeck, A. and Van Doninck, W., "Measurements on the Velocity of Sound in Mixtures of Hydrogen, Helium, Oxygen, Nitrogen and Carbon Dioxide at Low Temperature," Proceedings of the Physical Society (London 62B, 62-69 (1949).

126. Volk, H. and Halsey, G. D., Jr., "Solubility of Hydrogen and Deuterium in Liquid Argon," The Journal of Chemical Physics 33, 1132-39 (1960).

127. Watanabe, K., Nakayama, T., and Mottl, J., "Ionization Potentials of Some Molecules," Journal of Quantative Spectroscopy & Radiating Transfer 2, 369-382 (1962).

128. White, D. and Johnston, H. L., The Thermodynamic Properties of Gaseous Hydrogen from Experimental Data of State, Tech. Report No. 26, Project RF-264, Cryogenic Laboratory, Department of Chemistry, The Ohio State University, Columbus, Ohio, November, 1953 (ASTIA AD No. 27-622) page 2. See also, Friedman, A. S., "Pressure-Volume-Temperature Relationships of Gases. Virial Coefficients," American Institute of Physics Handbook, ed. by D. E. Gray, New York: McGraw-Hill Book Co., 1957,Section 4i, Table 4i-8.

129. White, David, Rubin, Thor, Camky, Paul, and Johnston, H. L., "The Virial Coefficients of Helium from 20 to 300°K," Journal of Physical Chemistry 64, 1607-12 (1960).

130. Williams, R. B. and Katz D. L., "Vapor Liquid Equilibria in Binary Systems," Industrial and Engineering Chemistry 46, No. 12 2512-2520 (1964).

131. Woolley, H. W., Scott, R. B., and F. G. Brickwedde, "Compilation of Thermal Properties of Hydrogen in its Various Isotopic and Ortho-Para Modifications," Journal of Research National Bureau of Standards 41, 379-475 (1948).

132. Yoon, Y. K., Gas-Liquid Phase Equilibria in the Helium-Carbon Tetrafluoride and Helium-Chlorotrifluoromethane Systems at Low Temperatures and 20-120 Atmospheres, Ph.D. Thesis, Georgia Institute of Technology, Atlanta, Georgia (1971).

133. Ziegler, W. T., Kirk, B. S., Mullins, J. C. and Berguist, A. R., Calculation of the Vapor Pressure and Heats of Vaporization and Sublimation of Liquids and Solids Below one Atmosphere. VII. Ethane. Technical Report No. 2, Project A-764, Engineering Experiment Station, Georgia Institute of Technology, Atlanta, Georgia, December 31, 1964 (Contract No. CST-1154, National Bureau of Standards, Boulder, Colorado.)

134. Ziegler, W. T. and Mullins, J. C., Calculation of the Vapor Pressure and Heats of Vaporization and Sublimation of Liquids and Solids, Especially Below One Atmosphere. IV. Nitrogen and Fluorine. Technical Report No. 1, Project A-663, Engineering Experiment Station, Georgia Institute of Technology, Atlanta, Georgia, April 15, 1963 (Contract No. CST-7404, National Bureau of Standards, Boulder, Colorado).

135. Ziegler, W. T., Mullins, J. C., and Kirk, B. S., Calculation of the Vapor Pressure and Heats of Vaporization and Sublimation of Liquids and Solids, Especially Below One Atmosphere Pressure. I. Ethylene. Technical Report No. 1, Project A-460, Engineering Experiment Station, Georgia Institute of Technology, Atlanta, Georgia, June 2, 1962 (Contract No. CST - 7238, National Bureau of Standards, Boulder, Colorado).

136. Ziegler, W. T., Mullins, J. C., and Kirk, B. S., Calculation of the Vapor Pressure and Heats of Vaporization and Sublimation of Liquids and Solids, Especially Below One Atmosphere Pressure. II. Argon. Technical Report No. 2, Project No. A-460, Engineering Experiment Station, Georgia Institute of Technology, Atlanta, Georgia, June 15, 1962 (Contract No. CST-7238, National Bureau of Standards, Boulder, Colorado).

137. Ziegler, W. T., Mullins, J. C., and Kirk, B. S., Calculation of the Vapor Pressure and Heats of Vaporization and Sublimation of Liquids and Solids, Especially Below One Atmosphere Pressure. III. Methane. Technical Report No. 3, Project No. A-460, Engineering Experiment Station, Georgia Institute of Technology, Atlanta, Georgia, August 31, 1962 (Contract No. CST-7238, National Bureau of Standards, Boulder, Colorado).

VITA

Ju Fu Shiau was born January 3, 1941,in Taipei, Taiwan, to Cheng Lin Shiau and Chia Tong Shiau. He graduated from the High School of Taiwan National Normal University in 1959. He received his Bachelor of Science degree in Chemical Engineering from Chung Yuan College of Science and Engineering, Taiwan, in 1963. After one year of service in the Chinese Army, he was employed by Yeng Fong Chemical Company as an engineer.

In September, 1967 he entered Tennessee Technological University where he received the Master of Science in Chemical Engineering in September, 1969. From September, 1969 when he enrolled in the Georgia Institute of Technology to the present time, he has been employed as a graduate teaching assistant in the School of Chemical Engineering.

He is an associate member of Sigma Xi.